The Dissertation Committee for Joonkyoung Han certifies that this is the approved version of the following dissertation:

A Unified Approach for Modeling the Variable Reactivity of Goethite: Surface Complexation Modeling of Proton, Alkaline Earth Metal Ion, and Transition Metal Ion Adsorption

Committee:

Lynn E. Katz, Supervisor

Desmond F. Lawler

Charles J. Werth

Navid Saleh

Philip C. Bennett

A Unified Approach for Modeling the Variable Reactivity of Goethite: Surface Complexation Modeling of Proton, Alkaline Earth Metal Ion, and Transition Metal Ion Adsorption

by

Joonkyoung Han

Dissertation

Presented to the Faculty of the Graduate School of

The University of Texas at Austin

in Partial Fulfillment

of the Requirements

for the Degree of

Doctor of Philosophy

The University of Texas at Austin

August 2018

Dedication

To my beloved wife, Dong Yerp Sung, who is always right.

I thank you for all the love and support.

Acknowledgements

I want to express my gratitude to my supervisor, Dr. Lynn Katz, for all her help and guidance over the past six years. She has been the perfect mentor to me who has provided wisdom and encouragement when they were most needed. I would have never accomplished this much without her assistance. I feel extremely fortunate to have had the chance to work together with her. More importantly, I thank her for being a great friend who has made my life in the United States much more enjoyable.

I would like to thank my colleagues who have helped me through out my Ph.D. research. Michael Sherer, Seung Hwan Chun, Luis Anaya and Sheik Nomaan, a.k.a the Glovebox boys, thank you for working with me on this project. The work you have done has become an essential part of this research. I also deeply thank Justin Davis, James Grundy, Farith Diaz, and Celina Dozier who worked together with me in the Katz Lab (and Bryant Chambers who visited us all the time) and gave me strength to proceed in the darkest moments of my Ph.D. life. I also thank all the EWRE professors and students for their help and support.

Finally, I would like to thank the U.S. Department of Energy Office of Basic Energy Sciences Grant No. DE-FG02-04ER15496 for funding this work.

A Unified Approach for Modeling the Variable Reactivity of Goethite: Surface Complexation Modeling of Proton, Alkaline Earth Metal Ion, and Transition Metal Ion Adsorption

Joonkyoung Han, Ph.D.

The University of Texas at Austin, 2018

Supervisor: Lynn E. Katz

Developing tools to predict the fate and transport of contaminants in the environment has been the focus of many environmental studies. Among these efforts, surface complexation models (SCM) have been suggested as a promising tool for simulating the adsorption behavior of hazardous metal cations and oxyanions onto metal oxide surfaces. However, the predictive capability of SCMs is often limited to system conditions over which the modeling parameters were estimated, and hence, a self-consistent model capable of making accurate predictions over a wide range of solution and surface conditions observed in natural environments is still lacking. The goal of this study was to develop a modeling approach that broadens the predictive capability and applicability of SCMs. To achieve this goal, two issues related to the complex interactions among the constituents of the mineral-water interfacial system were addressed and investigated: 1) variable reactivity of metal oxide surfaces, and 2) interactions between alkaline earth metal ions and the surface. The scope of this study is limited to goethite. The selection of goethite was based on the fact that it is one of the most important minerals

that controls adsorption of ions in common natural soils and has been extensively investigated as a sorbent mineral in many previous SCM studies.

In the current research, the variation of surface reactivities observed for different goethite morphologies was captured in a charge distribution – multisite complexation (CD-MUSIC) model by incorporating established relationships between crystal face contribution (CFC), inner-Helmholtz capacitance (C_1), and protonation constants (pK_a's) with the specific surface area (SSA) of goethites. By using the surface parameters estimated by these relationships, CD-MUSIC model was able to predict proton, Cd^{2+}, and SeO_3^{2-} adsorption onto a wide range of different goethite morphologies (21 – 105 m^2/g SSA) using data obtained in our laboratory and reported in the literature.

The adsorption behavior of alkaline earth metal (AEM) ions was also investigated. Experimental results showed that adsorption of AEM cations of weaker affinity onto goethite was more highly impacted by the types and concentrations of background electrolytes. It is suggested that the electrolyte effect (i.e., reduction in extent of adsorption) is due to the combined effect of competitive adsorption and aqueous complexation with electrolyte cations and anions, respectively. This result indicates background electrolytes should not be indiscriminately assumed inert or indifferent, especially when assessing the adsorptive behavior of weakly sorbing solutes. Specifically, discrete effects of electrolytes must be considered and accounted for when determining equilibrium constants of other ions using experimental data.

Finally, surface complex model species and equilibrium constants of AEM ions ($^{int}K_{Me}$) were determined by calibrating adsorption binding constants using selected data sets and validating the model with a larger range of data. It was proven that with these modeling parameters, a CD-MUSIC model was capable of accurately predicting AEM

adsorption onto three preparations of goethite (50 m^2/g, 64.5 m2/g, and 73 m^2/g SSA) over a range of solution conditions (i.e., pH 5-11, ionic strength 0.01M – 0.7M, various background electrolytes). In addition, the model was also able to predict the impact of high concentrations of Mg^{2+} on Cd^{2+} adsorption, and the impact of Cd^{2+} on Mg^{2+} adsorption. Despite the fact that both ions were considered to form inner-sphere complexes with goethite, the presence of both solutes showed no effect on adsorption of either ion.

The results of this study demonstrate that the suggested modeling approach could greatly improve the predictability of a CD-MUSIC surface complexation model; the SSA values of pure synthetic goethites were able to capture the change of CFC, capacitance and pK_a, and accurate predictions have been made for proton, AEM ions, Cd^{2+} and SeO_3^{2-} adsorption onto various preparations of goethite over a wide range of solution conditions.

Table of Contents

List of Tables

List of Figures

Chapter 1. Introduction

1.1. Background

The ability to accurately predict the fate and transport of contaminants in natural and engineered systems can greatly enhance the capabilities of engineers and scientists to establish pollution management strategies. Therefore, development of predictive models that simulate the interactions of contaminants within various environmental media has been the aim of many environmental research investigations. In particular, adsorption reactions occurring at the soil-water interface have attracted the attention of many researchers due to their crucial role in controlling the migration of contaminants [1]–[5]. Hence, various adsorption models have been developed and proposed over the past century [6]–[14].

Among these adsorption models, surface complexation models (SCMs) have shown great potential as a tool for predicting the adsorption of metal cations and oxyanions onto mineral surfaces [15]–[19]. SCMs utilize the same thermodynamic approaches as those applied in solution chemistry; these include chemical reactions with associated equilibrium constants, stoichiometry to describe the ion adsorption onto functional groups on mineral surfaces, and mass balances to ensure conservation of molecular species and surface functional groups [18], [20]–[23]. This unique feature allows SCMs to have a distinct advantage over the empirical partitioning coefficient approach with respect to predicting adsorption across varying solution conditions (i.e., pH, ionic strength) assuming that the correct modeling parameters are provided [15], [24]–[26]. Therefore, properly describing the mineral surface functionality, the type of surface complex species formed, and the equilibrium constants of the surface complexation reactions has been considered as a major goal for many SCM studies.

While SCMs have been used to simulate the adsorption processes of ions on various metal oxides and clays, goethite has been one of the most commonly investigated sorbents. Goethite is an iron oxyhyroxide mineral (α-FeOOH), which is abundant, ubiquitous, and stable in soil environments, and has relatively large surface area [1], [2], [34]–[36], [3], [27]–[33]. Therefore, it is known to play an important role in the migration of metal cations and oxyanions in natural soil environments [1], [2], [23], [33], [37]–[42]. Moreover, its relatively well-characterized crystalline structure and well-established protocol for synthesis has made goethite an ideal mineral for adsorption studies [31]. In fact, these features have allowed synthetic preparations of goethite to serve as a reference for the development of many of the SCMs [43].

Despite numerous studies on SCMs that were conducted over the past several decades, we still lack the ability to make accurate predictions in complex systems that are typical of natural environments [44], [45]. In this regard, this study focuses on addressing two issues that remain unresolved with respect to our understanding of the complex interactions between constituents of a goethite-water interfacial system and prevent the application of a self-consistent model capable of predicting adsorption over a wide range of system conditions. The two issues examined in this study include 1) variation of goethite surface reactivity, and 2) adsorption behavior of alkaline earth metal ions onto goethite in the presence of varying background electrolytes. The current limitations of SCMs associated with these issues are discussed in the following section (Chapter 1.2.).

1.2. PROBLEM STATEMENT

1.2.1. Variable surface reactivity of goethite

Previous studies have shown that the surface properties of goethite vary among different preparations; these properties appear to be correlated with the specific surface area (SSA) of goethite samples but cannot be directly normalized to surface area [2], [31], [46]–[53]. Therefore, the SSA has been commonly used as a metric to distinguish different preparations of goethite in many previous studies. It is documented in literature that the SSA of goethite typically varies between 10 – 110 m^2/g depending on its preparation method. Some of these varying surface properties are assumed to strongly affect the reactivity of the goethite particles, and studies have experimentally shown that the affinity of goethite surfaces towards specific ions can be significantly different among different preparations of goethite. Figure 1-1 shows an example of such variable reactivity among different preparations of goethite by comparing potentiometric titration data conducted at a single ionic strength. The plot indicates that at a given pH the amount of protons adsorbed onto a unit surface area may vary depending on the preparation of goethite which is represented by SSA. One hypothesis for this phenomenon is that the distribution of crystal faces varies systematically with SSA and specific faces vary in reactivity.

Many adsorption modeling studies have not considered such variation of goethite surface properties, and thus, their predictive capability is limited to only certain goethite preparations [31], [49]–[51]. A generalized strategy for accounting for the difference in goethite surface properties is required for developing a single self-consistent model capable of predicting adsorption for any goethite sample.

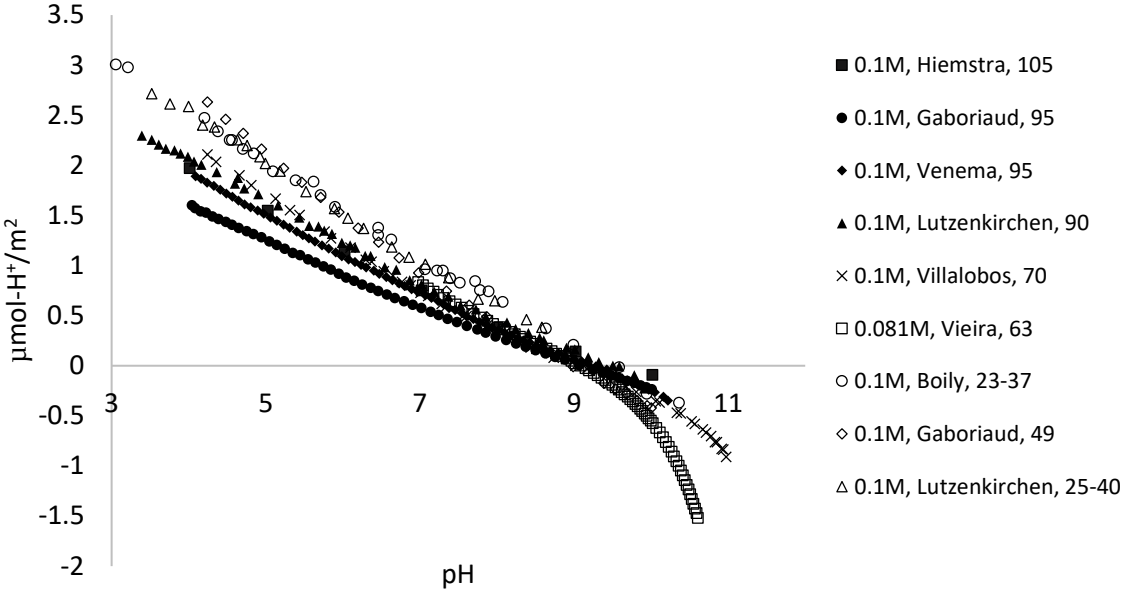

Figure 1-1. Comparison of the titration data for different goethites in 0.081 M - 0.1 M $NaNO_3$ solution. (Numbers on the legend indicate the SSA (m^2/g) of goethite used in each study)

1.2.2. Alkaline earth metal ions

Alkaline earth metal ions are abundant in natural and engineered waters, and often are present in high concentrations relative to regulated contaminants of concern [45], [54]–[61]. While the importance of understanding the fate and transport of alkaline earth metal ions is often overlooked, their presence at high concentrations can have significant impacts on the fate of toxic metal ions, oxyanions, radionuclides and even organic contaminants [44], [45], [56], [57], [61], [62]. In particular, extremely high concentrations (e.g., 3,000 – 30,000 mg/L of Ca) of these metals are commonly found in ground waters, produced waters, recycled fracking waters, and wastewaters from soil remediation sites [45], [54]–[60]. While alkaline earth metal ions such as Mg^{2+} and Ca^{2+} are generally considered to

be weakly adsorbed to common soil minerals such as iron oxides, accurate modeling of their adsorption is required for predicting the adsorption of other weakly and strongly adsorbing solutes [44], [45], [56], [57], [61], [62].

Although numerous studies have elucidated the adsorption behavior of alkaline earth metal ions, agreement is still lacking on many adsorption characteristics of these metals; including, but not limited to, the mode of adsorption (inner- or outer-sphere), complex structure (monodentate, bidentate or tetradentate complexes) and surface affinity [44], [61], [71]–[80], [63], [81], [64]–[70]. This lack of agreement has been partially due to the lack of molecular modeling and/or spectroscopic data identifying the structure of surface complexes for the dominant alkaline earth metal ions (e.g., Ca^{2+} and Mg^{2+}). Another reason for the limited understanding of alkaline earth metal ion adsorption is the common assumption that alkali metal ions and strong acid anions (e.g., NO_3^-, Cl^-) are considered inert or indifferent background electrolytes [44], [45]. Most macroscopic studies have conducted experiments using simple monovalent electrolyte systems, such as NaCl, $NaNO_3$, $NaClO_4$, and KNO_3 because the ions associated with these salts are considered indifferent. In other words, even when surface complexation reactions for these ions are included in surface complexation modeling, there is little to no difference in the types of surface complexes formed or the value of the surface complexation constants. However, recent studies have started to investigate potential impacts of the interaction between the background electrolytes, sorbed ions, and surfaces at the mineral-water interface. As an example, recent molecular modeling studies have suggested that alkali metal ions such as Na^+ form inner-sphere surface complexes which suggests that their impact on strongly sorbing transition metal ions may be more significant than originally thought (Unpublished study by Criscenti et al.). Hence, studies examining adsorption in

various electrolyte systems is critical for isolating the impacts of specific electrolytes on adsorption behavior of alkaline earth metal ions.

1.3. OBJECTIVES

The main goal of this study is to develop a modeling approach that is capable of predicting the effect of variable reactivity between different morphologies of goethite and the adsorption behavior of alkaline earth metal ions (Mg^{2+}, Ca^{2+}, Sr^{2+} and Ba^{2+}) onto goethite over an extensive range of solution conditions, including a wide range of pH and ionic strengths, various anionic (Cl^-, NO_3^-, ClO_4^-) and cationic species (Na^+, K^+, Rb^+, Cs^+, Mg^{2+}, Ca^{2+}) as background electrolytes, and the presence of transition metals (e.g., Cd^{2+}) in the solution. This study utilizes the surface complexation modeling (SCM) framework, in which sorption processes are described by assuming that metal ions adsorb at the surface in a manner analogous to aqueous complexation reactions [12], [18], [82]–[88]. The CD-MUSIC version of the surface complexation models is selected because it closely represents adsorption to different crystallographic faces of goethite by including surface heterogeneity on each goethite and a detailed description of the charge-potential relationships within the interfacial region [14], [53], [82], [84], [85], [89], [90]. In previous studies within our laboratories, the CD-MUSIC description of the surface-water interface provided successful modeling of Cd^{2+}, Pb^{2+}, and SeO_3^{2-} adsorption onto goethite in single and bi-solute systems [89]. Refinement of alkaline earth metal ion adsorption into these pre-developed models will enhance our capability to predict adsorption of both alkaline earth metals and toxic metal ions across the range of complexity of natural systems that include a range of background electrolytes. The primary objectives of this study are:

1. Establish an approach to account for the effect of goethite morphology (specifically, the crystal face distribution) on surface properties and the associated impact of these properties on ion adsorption in a CD-MUSIC model

2. Evaluate effects of different background electrolytes on alkaline earth metal ion adsorption onto goethite

3. Utilize a surface complexation model to describe and predict alkaline earth metal ion adsorption onto goethite under a wide range of solution conditions

1.4. DISSERTATION OUTLINE

This dissertation is made up of six chapters. The motivation and objectives of this research has been described in Chapter 1. In Chapter 2, a literature review presents the theory and features of more commonly used surface complexation models.

In Chapter 3, a novel approach for capturing the variable reactivity of goethites within a CD-MUSIC model is presented. Methods used to establish relationships between surface parameters (i.e., crystal face contribution, capacitance, and protonation constants) and the specific surface area of goethite are described and followed by a description of the CD-MUSIC model utilized in this study. The model optimization procedure with the utilization of FITEQL [91], a nonlinear least squares optimization program, is also discussed in detail. Finally, model predictions are presented for a wide range and variety of macroscopic adsorption experimental data reported in the literature in order to verify the predictive capability of the new approach developed within this research.

Chapter 4 provides experimental data for adsorption of alkaline earth metals onto goethite over a range of solution conditions (i.e., pH, ionic strength, and background electrolytes). Experimental and analytical procedures are described in detail, and the effect of background electrolytes on alkaline earth metal ion adsorption is highlighted through comparison of experimental results to macroscopic adsorption data.

Chapter 5 presents the approach and results of the surface complexation modeling of alkaline earth metal ions on goethite. The procedures for determination of surface complex species and equilibrium constants are discussed. Also, predictions of alkaline earth metal ion and cadmium adsorption are evaluated respect to the model capabilities.

Chapter 6 provides the conclusions of this research followed by a discussion regarding implications of the current study with respect to the utility of the findings, applications of the findings to the field, and future research needs. Finally, the Appendix includes additional modeling results which were not included in the main chapters, descriptions of the input files used for the FITEQL software, and descriptions of a coded program which was developed to automate iterative calculations.

Chapter 2. Review of Surface Complexation Models

2.1. Empirical vs. Thermodynamic Approaches

The prediction of adsorption behavior of hazardous ions in natural and engineered environment has been commonly conducted through an empirical approach in which linear isotherms and associated partition coefficients (K_d) are used to describe the mass distribution of a specific ion between solid and aqueous phases [72], [92]. Despite their simplicity and capability for directly estimating the partitioning of ions in a specific solution, the application of these methods is limited to solution conditions from which their parameters were evaluated, and therefore, are not capable of predicting adsorption outside of the conditions of the specific site [15], [72], [93]–[96].

To overcome this drawback associated with empirical approaches, surface complexation models (SCMs) that employ a thermodynamic approach which describes adsorption as a series of specific reactions between dissolved ions and surface sites have been developed and implemented over the past several decades [15], [72], [97]. The thermodynamic constants that are used in the SCM enable the prediction of adsorption in various solution conditions with a single set of parameters [15], [24]–[26], [72]. Many previous studies have demonstrated successful simulation of ion adsorption over a range of pH, ionic strength, solute concentration, and multi-component systems, hence proving that SCMs can be a viable alternative to empirical methods [15], [16], [18], [24], [83], [84], [93], [98]. However, the application of SCMs is currently constrained by the lack of a coherent thermodynamic complexation database for a wide range of ions and solids found in natural waters [18], [72], [99]–[102]. Overcoming the difficulties associated with collecting critical information of the functional groups, electrostatic profiles of the mineral

surfaces, and the structure and reaction of surface complex species has been the main challenge in the field of SCM [89].

2.2. SURFACE COMPLEXATION THEORY

The chemical reactions used in SCMs are analogous to the formation of solution-phase complexes that can be described by mass law equations with associated stoichiometry and equilibrium constants between solutes and surface sites [18], [20]–[23]. Similar to the metal – ligand complexation reaction in an aqueous system, reactive surface sites on the adsorbent mineral can be treated as aqueous species which can undergo complexation with solute ions [18], [20]–[23]. However, surface complexation differs from aqueous complexation in two aspects; 1) the electrostatic contribution of the surface is taken into account by incorporating a correction term in the equilibrium constants of surface chemical reactions [18], [84], [93], which is derived from electric double layer (EDL) theory, and 2) the effect of immobility of surface sites is reflected in the stoichiometry and preferential use of a mole fraction standard state to multidentate complex species [24], [86], [103].

The electrostatic contribution results from charge variation of the surface due to sorption/desorption of protons and ions, since the electrical potential produced from such surface charge impacts the free energy associated with these formation reactions [23], [93]. As a result, in surface complexation theory the free energy of an adsorption/desorption reaction is comprised of two components, chemical (intrinsic) and electrostatic, which can be theoretically separated as in Eq. 2-1.

Eq. 2-1) $$\Delta G^{o}_{total} = \Delta G^{o}_{intrinsic} + \Delta G^{o}_{electrostatic}$$

where ΔG^o_{total} is the total free energy of the adsorption/desorption reaction at standard state, $\Delta G^o_{intrinsic}$ is the intrinsic free energy of reaction which reflects the chemical energy change due to reaction of the adsorbing ion with a surface functional group, and $\Delta G^o_{electrostatic}$ is the electrostatic free energy which represents the energy required to move the ion from bulk solution to a surface with an electrostatic potential different from the bulk solution.

The intrinsic energy term, $\Delta G^o_{intrinsic}$, can be written as Eq. 2-2:

Eq. 2-2) $$\Delta G^o_{intrinsic} = \Delta G^o_{chem} + RTln\Pi_i a_i^{n_i}$$

where ΔG^o_{chem} is the Gibbs chemical free energy of reaction at standard state conditions, R is the universal gas constant (8.314 J/mol·K), T is the temperature of the system in Kelvin, Π_i is the mathematical symbol for the product of all *i* terms, and a_i and n_i are the activity and stoichiometric coefficient of the i^{th} species in the reaction, respectively. Such expression of intrinsic energy is identical to the free energy equation of chemical reactions among aqueous species where no electrostatic energy is accounted for because the electrostatic potential remains constant.

The electrostatic term, $\Delta G^o_{electrostatic}$, can be expanded into Eq. 2-3:

Eq. 2-3) $$\Delta G^o_{electrostatic} = \Sigma_k \Delta Z_k F \psi_k$$

where ΔZ_k is the change in charge at the k^{th} electrostatic plane in units of moles of charge, F is Faraday's constant (96,485 C/mol), and ψ_k is the electric potential of the k^{th} electrostatic plane in Joules per coulomb (J/C).

By combining Eq. 2-1 – Eq. 2-3, the total free energy ΔG^o_{total} can be rewritten as Eq. 2-4.

Eq. 2-4) $$\Delta G^{o}_{total} = \Delta G^{o}_{chem} + RTln\Pi_i a_i^{n_i} + \Sigma_k \Delta Z_k F \psi_k$$

At equilibrium, $\Delta G^{o}_{total} = 0$, the equation simplifies to Eq. 2-5.

Eq. 2-5) $$K_{app} = K_{int} exp(\Sigma_k \Delta Z_k F \psi_k)$$

where K_{app} is the apparent surface adsorption equilibrium constant, K_{int} is the intrinsic equilibrium constant, and the exponential term is the coulombic correction factor [5], [83], [85], [104]. In surface complexation modeling, the coulombic correction factor is calculated based on the charge associated with sorbed ions located on each electrostatic plane, whereas K_{int} is obtained through optimization to best fit experimental data or theoretical considerations.

2.3. SURFACE COMPLEXATION MODELS

Various types of SCMs have been developed over the past years. The most frequently used SCMs include the diffuse layer model (DLM) [12], [18], the constant capacitance model (CCM) [16], [22], [105]–[107], the triple layer model (TLM) [108], the triple plane model (TPM) [104], and the charge distribution – multisite complexation model (CD-MUSIC) [83]. These models differ from each other in formulation of the surface reaction (e.g., structure and distribution of ions in the interfacial region and representation of surface sites) and/or in the description of the electric double layer [33], [83].

The complexity of SCMs also varies among models depending on the number of "adjustable" parameters required to apply the model to describe potentiometric titration data or solute adsorption data. Models with more adjustable parameters are likely to fit

experimental data more closely. However, the relatively large number of parameters that must be determined can make the model impractical for many applications. Hence, a tradeoff between predictability and practicality must be considered when selecting the appropriate model to be used in modeling adsorption.

2.3.1. Diffuse layer model (DLM)

The DLM considers only two layers of charges; a surface layer (0-plane) and diffuse layer (d-plane) of counterions in solution [12], [18] (See Figure 2-1). All specifically sorbed ions are considered to be located on the surface layer, while all non-specifically sorbed ions are placed on the diffused layer [89]. Hence, it is assumed that all complexes are inner-sphere and no ion-pairing occurs on the surface. The relationship between the surface charge density of the diffuse plane (σ_d) and its electrostatic potential (ψ_d) is described using the Gouy-Chapman theory, which is constrained to symmetrical 1:1 electrolytes [97], [109]–[111]. The DLM has usually been restricted to modeling low ionic strength conditions because it has been found to significantly over-predict the diffuse-layer potential at high ionic strengths [18]. It is considered one of the simplest models since it only needs four parameters, two surface protolysis constants, K^+, K^-, affinity constant for the adsorbing metal, K, and the total number of surface sites, N_t. The original model proposed by Stumm et al. (1970) [12] assumed only 1 type of surface site, but later Benjamin and Leckie (1981) [112] expanded the model to account for multiple binding sites and Dzombak and Morel (1990) [18] also modified the model to have high and low affinity sites in order to improve the predictions for cation adsorption. Another modification of the model is the work proposed by Farley et al. (1985) [113] which

extended the predictive capability of the model to solutions with high sorbate/sorbent ratios and accounted for surface precipitation of the sorbates.

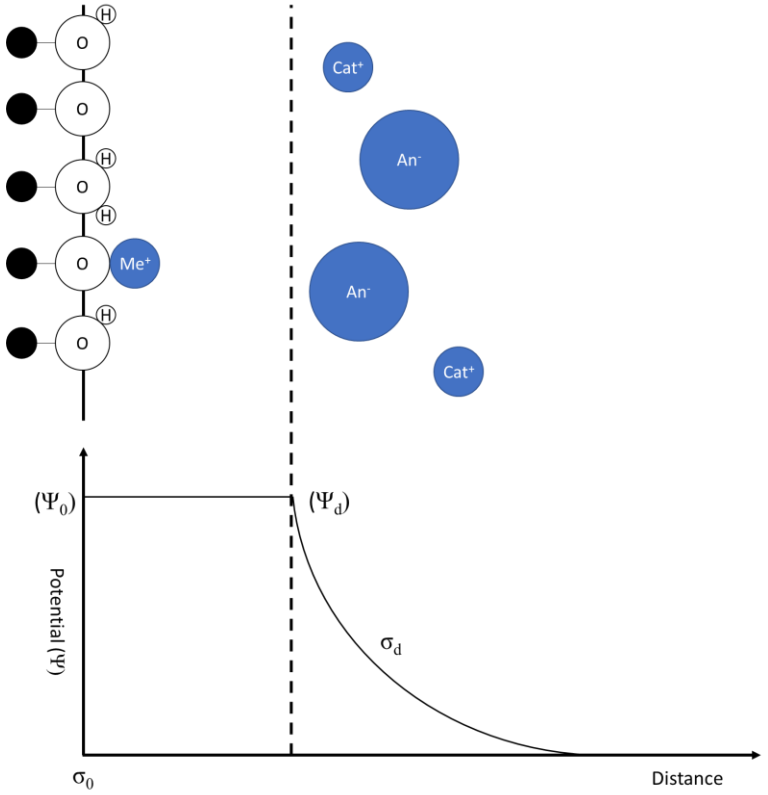

Figure 2-1. Schematic of the electric double layer (EDL) used in the diffuse layer model. Figure adapted from Hayes et al. (1991). The 0-plane lies on the surface oxygen groups.

2.3.2. Constant capacitance model (CCM)

The CCM assumes that a layer of constant capacitance isolates the bulk solution from the charged surface sites [16], [22], [105]–[107] (See Figure 2-2). The model is based on the idea that the electric double layer can be approximated as a parallel plate capacitor

in high ionic strength solution [93]. Hence, an additional fitting term that represents the constant capacitance layer (C_1) is required, resulting in 5 adjustable parameters in total [15]. Similar to the DLM, all complexes are considered to be placed on the 0-plane as inner-sphere complexes, and no ion-pairing occurs. The CCM is restricted to constant ionic strength conditions [15]. This restriction is due to the form of the charge-potential relationship, which for the CCM is given by $\sigma_0 = C_1\psi_0$. Because of this, a different set of CCM surface constants is required for each set of ionic strength conditions to be modeled [15].

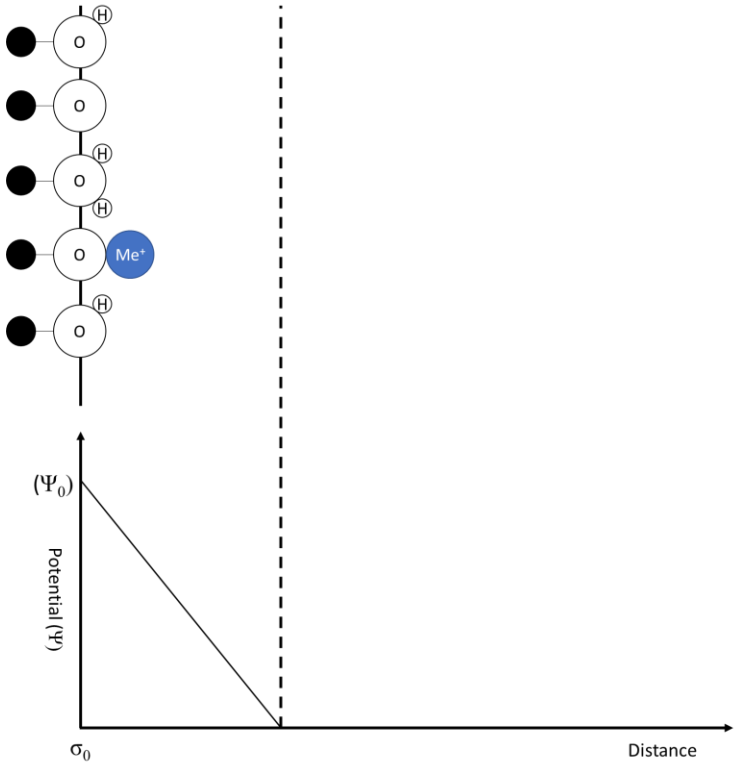

Figure 2-2. Schematic of the electric double layer (EDL) used in the constant capacitance model. Figure adapted from Hayes et al. (1991)

2.3.3. Triple layer model (TLM)

As the name indicates, the TLM assumes three electrostatic layers on the surface (i.e., 0-plane, β-plane, and d-plane) [108] (See Figure 2-3). Allowing surface reactions between the background electrolyte ions and surface hydroxide sites is a unique feature of the TLM compared to the simpler SCMs [15]. Specific adsorption is placed on the 0-plane and ions that form outer-sphere complexes (ion-pair electrolytes) are placed in the β- plane [114]. In the absence of specifically adsorbing ions, the TLM simplifies to the basic stern model (BSM) because the mid-plane does not contain any charge [83]. The TLM is applicable to systems with ionic strengths from near zero to the upper limit of applicability of the Davies equation [15]. The TLM has eight adjustable parameters in total; two surface protolysis constants, K^+, K^- (2-pKa), two capacitance parameters, C_1, C_2, surface affinity constant, K, total site concentration, N_t, and two electrolyte surface-binding constants, K_{An} and K_{cat}[15].

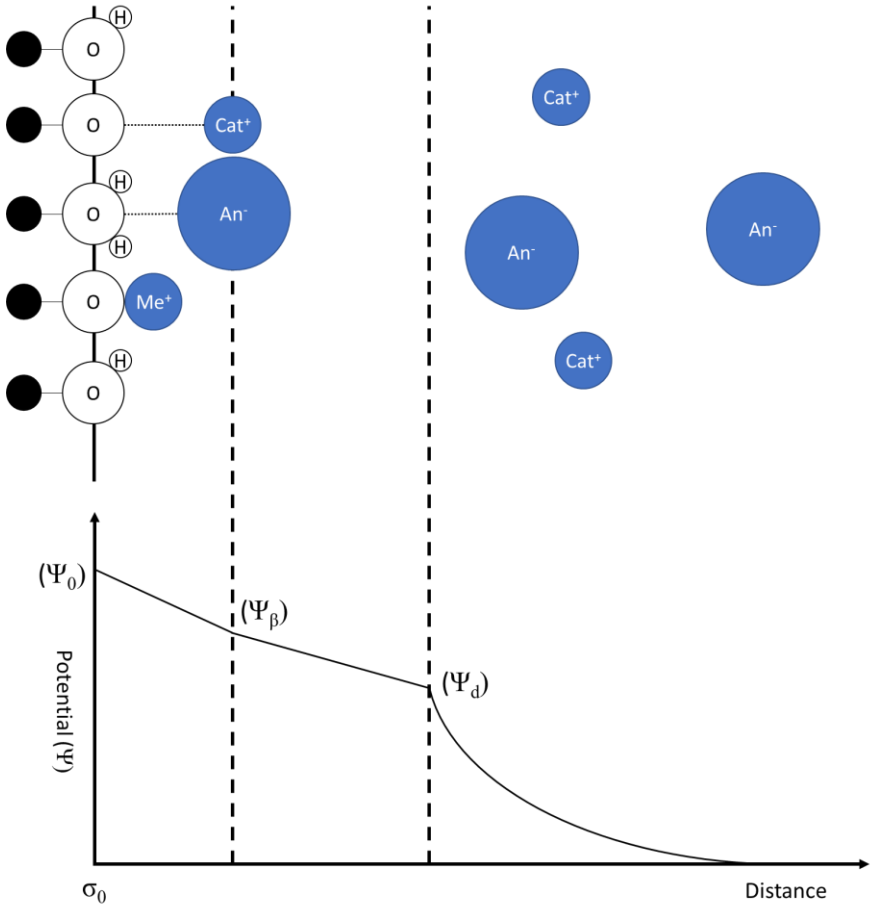

Figure 2-3. Schematic of the electric double layer (EDL) used in the triple layer model. Figure adapted from Hayes et al. (1991)

2.3.4. Charge distribution multisite complexation model (CD-MUSIC)

The CD-MUSIC model defines EDL identical to the TLM, but uses crystallographic information to describe surface acidity and reactive site density of specific minerals [83] (See Figure 2-4). The CD-MUSIC model differs from other widely used SCMs in three principal ways; 1) representation of surface acidity, 2) placement of ions and charge in the EDL, and 3) representation of reactive surface adsorption sites [83], [84].

This model emphasizes the importance of the surface structure and of charge distribution within interfaces [115]. Apportionment of certain types of ionic charge to more than one electrostatic plane is a unique feature of the CD- MUSIC model. In the absence of surface complex formation, the compact part of the double layer between the surface and the diffuse double layer does not contain any ions and the model becomes identical with the basic Stern layer approach [115]. Unlike other SCMs, the total number of parameters can vary depending on the number of crystal faces and coordinated reactive sites considered. However, the type of parameters that are required includes those used in the TLM, including protonation constants, capacitance values, affinity constants of sorbing ions, ion-pair constants, and total reactive site densities.

The unique features of the CD-MUSIC surface complexation model were essential for conducting the current study. By allowing different distances between the sorbed ions and the surface, which is accounted through the apportion of ion charges onto two different electrostatic planes, the model was able to simulate the subtle differences in surface affinity between inner-sphere surface complexes. Moreover, accounting for the heterogeneity of the goethite surface sites and distribution of sites on different crystal faces was crucial for capturing the variable reactivity of different morphologies of goethite; these factors were assumed to be the main cause for the variation in reactivity with SSA.

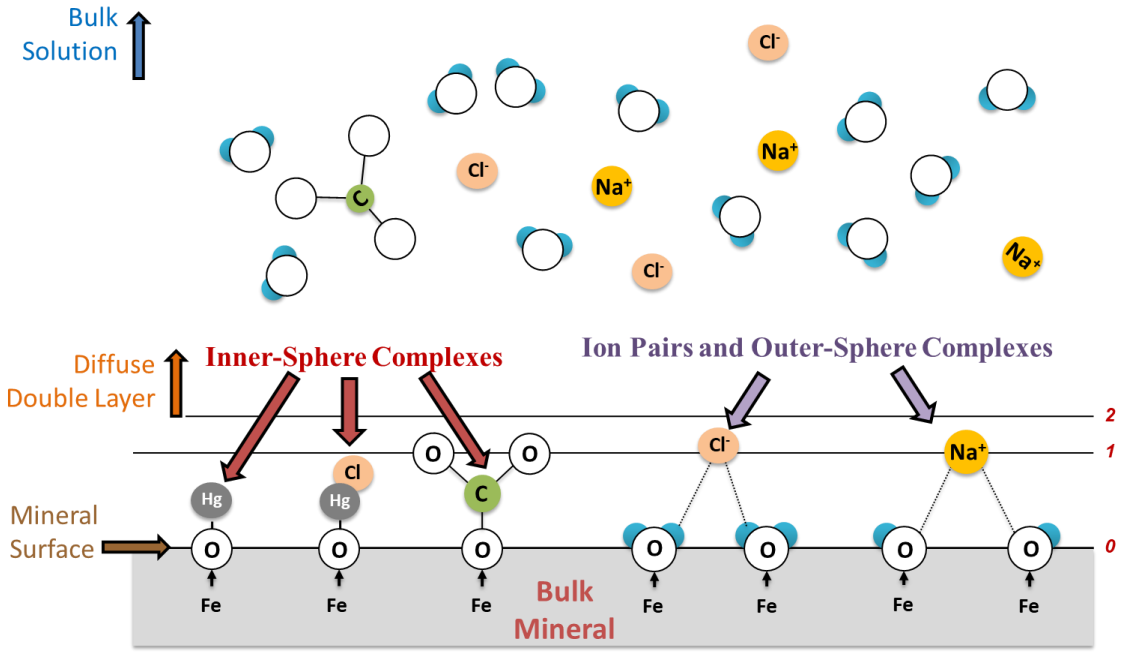

Figure 2-4. Schematic of the mineral – water interface as described in CD-MUSIC model. Figure adapted from Mangold (2013)

Chapter 3. Capturing the Variable Reactivity of Goethites Within the CD-MUSIC Model

3.1. INTRODUCTION

Goethite is one of the most abundant and stable iron oxyhydroxide minerals in soils and sediments [2], [3], [34], [35], [46], and due to its high surface area [1], [27], [28], [36], it has been shown to play an important role in the migration of aqueous ions and species [2], [23], [39], [40], [47]. For this reason, characterization of goethite surfaces has been a focus of many adsorption studies, especially in the research field of surface complexation modeling (SCM) [2], [31], [43], [116]. However, despite the extensive amount of research focused on characterization and modeling of the goethite-water interface, a consistent model and parameter set that is capable of predicting adsorption over a wide range of background water characteristics and goethite morphologies are still lacking. One possible explanation for this deficiency is that the surface reactivity of goethite for specific ions varies depending on the synthesis and preparation of the goethite [2], [31], [33], [46], and the cause and extent of such variation has not yet been fully elucidated.

One of the properties of goethite that varies depending on the preparation method is the specific surface area (SSA) obtained through Brunauer–Emmett–Teller (BET) gas adsorption analysis. Hence, the BET-SSA has become a common metric to distinguish different preparations of synthetic goethites in numerous studies. Using SSA as a metric for distinguishing goethites is justified by the fact that synthetic goethite particles all show one basic acicular shape regardless of their size and preparation method [29], [117], [118]. The acicular shape of goethites have been seen through microscopic images presented in the literature [32], [33], [47], [119]. In addition, thermodynamic nano-morphology model analysis has shown that goethite crystals can only form in a limited number of forms.

As displayed in Table 3-1, a number of surface properties, such as the crystal size, surface roughness, crystal face contribution (CFC), capacitance values, surface charge density, and proton affinity have been observed to correlate with SSA [31], [33], [89], [116], [118], [120]–[124], [34], [43], [47]–[52]. Therefore, establishing relationships among these surface properties and goethite SSA may provide a viable approach for generalizing the variation of surface reactivity in adsorption models, and consequently expanding SCM predictive capabilities across a range of different goethites. Figure 3-1 highlights the extensive range of specific surface areas of goethite samples that have been employed across 104 previous adsorption studies. The variation in morphology (CFC) associated with these different goethites provides a potential explanation for the inconsistency in modeling parameters among goethite studies; the variability also emphasizes the need for an approach that can incorporate the variation of surface properties of different goethites into a single model.

Table 3-1. Observed trends in goethite surface properties with specific surface area (SSA)

	Lower SSA goethite	↔	**Higher SSA goethite**	**References**
Crystal Size	Larger	↔	Smaller	[31], [33], [43]
Surface roughness	Rougher	↔	Smoother	[49], [118]
Crystal face contribution	Higher portion of capping face	↔	Lower portion of capping face	[43], [116], [118]
Capacitance	Larger	↔	Smaller	[31], [33], [48], [49], [51], [64], [116], [118]
Surface charge density	Higher	↔	Lower	[31], [33], [49], [120], [121], [123]
Proton affinity	Higher	↔	Lower	[31], [43], [48], [52]

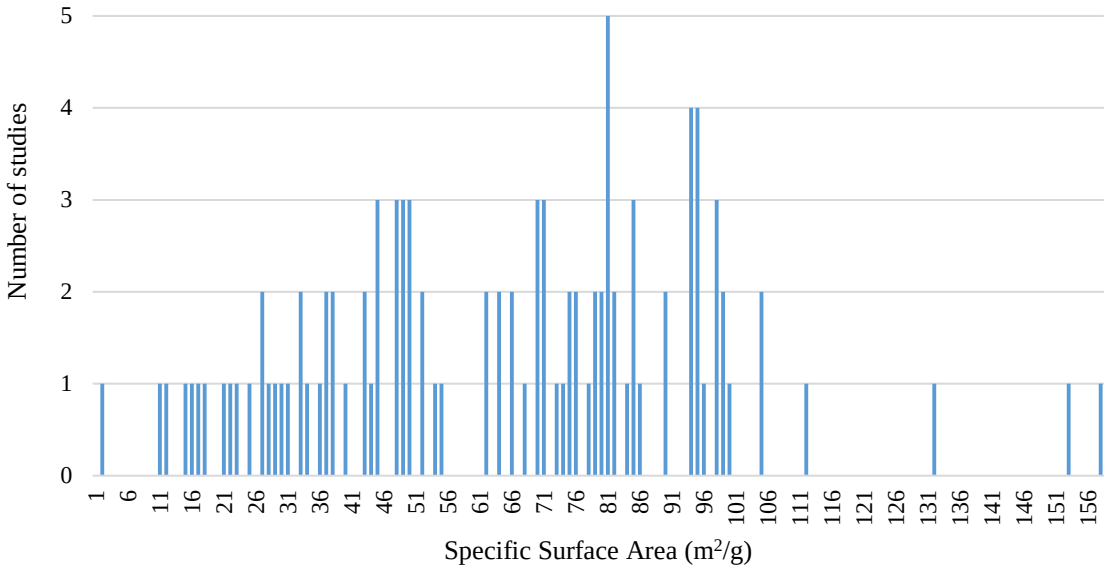

Figure 3-1. Number of adsorption studies per type of goethite

Although several studies have proposed methods to capture the variable properties of goethite within particular SCMs, none have put forth a model that is capable of predicting surface properties across a range of goethite preparations solely based on the SSA. In many of these studies, additional experimental data were required for each goethite morphology in order to obtain surface parameters independent of the SSA; such data are often limited to the experimental conditions tested and only applicable to specific goethite characteristics. A series of studies by Villalobos and collaborators [31], [43], [116], [118] has promoted the hypothesis that variation in surface reactivity of goethites can be attributed primarily to differences in surface site density resulting from varying crystal face contributions (CFCs) of different goethites. Based on this hypothesis, maximum ion adsorption capacity and proton adsorption data were used to estimate the reactive site densities and CFC for each goethite morphology individually.

Utilizing the hypothesis set forth by Villalobos and coworkers, Mangold (2014) [125] used data from Salazar-Camacho and Villalobos (2010) [116] to develop a CD-MUSIC model for which goethite CFCs could be estimated based on a quasi-linear relationship between SSA and proton reactive site density (N_H). Although the model was capable of making accurate predictions of Hg^{2+} adsorption on three different goethite morphologies (i.e., 76 m^2/g, 70 m^2/g, 15 m^2/g SSA) in various solution conditions, the validity of the result obtained by this approach was limited as numerous combinations of CFC values could be derived from a single value of reactive site density (N_H). Also, the capacitance values for each goethite were selected arbitrarily to obtain the best fit to the potentiometric titration data, which indicates that this approach also requires proton adsorption data for goethites of varying SSA.

Several studies have suggested methods to model the variation in proton affinity between different goethites by changing one or two parameters in the SCM. These studies, however, have failed to establish approaches to estimate the parameters over a range of different goethite characteristics, since only two goethites were investigated in each study and the models were not tested over a range of SSA goethites. In addition, these studies were also limited by the fact that the assumed CFC values were not consistent with the microscopic and/or crystallographic data reported in literature. Boily et al. (2001) [48] were able to predict proton adsorption data for 23 – 37 m^2/g and 85 m^2/g SSA goethites by changing the capacitance values for different goethites while keeping the CFC, surface site densities, and proton affinity identical. Similarly, Lützenkirchen et al. (2008) [49] proposed a model for proton adsorption which accounted for changes in capacitance values and electrolyte affinity constants for the 25 – 40 m^2/g and 90 m^2/g SSA goethites. Both of these studies assumed that the CFC for all goethites used were identical and composed of

90% main faces (i.e., (101) and (001) face) and 10% capping faces (i.e., (210) and (010) face). These CFC values, however, are not consistent with microscopic observations [126], where different shapes and morphologies were observed for different goethite preparations. In a study by Gaboriaud and Ehrhardt (2003) [33] , the relationship between proton affinity and CFC was investigated for the 49 m^2/g and 95 m^2/g SSA goethites. Atomic force microscopy (AFM) images were used to determine the surface contribution of (101) and (001) faces. Although this study accounts for the variation of CFC between different preparations of goethite, the contribution of the capping faces was assumed to be negligible. This assumption conflicts with recent microscopic observations that suggest that the contribution of capping faces on low SSA goethites can be considerably high [126].

The goal of this current study was to develop an approach for predicting adsorption data for a range of different goethites using SSA correlations for SCM parameters impacted by variable crystal face reactivity. Specifically, our objective was to correlate the CFC, capacitance values, and protonation constants of goethites based on their SSAs within a CD-MUSIC model and then employ these correlations to predict proton and ion adsorption behavior to various preparations of goethite. To achieve the objective, the current study was conducted using the four-step scheme shown in Figure 3-2. First, the relationship between CFC and goethite SSA was established based on reported trends, microscopic and macroscopic data, and modeling analyses collected from either literature or experiments. Then, the established CFC-SSA relationship and a CD-MUSIC model that was developed based on data from Vieira (2007) [127] and modeling by Mangold (2013) [89] were utilized to optimize capacitance values and protonation constants of potentiometric titration data from four different goethites. The optimized parameters then served as the basis for establishing relationships between capacitance and protonation constants and goethite SSA.

Finally, the model was tested to assess whether it could accurately predict proton, SeO_3^{2-} and Cd^{2+} adsorption on a wider range of goethites.

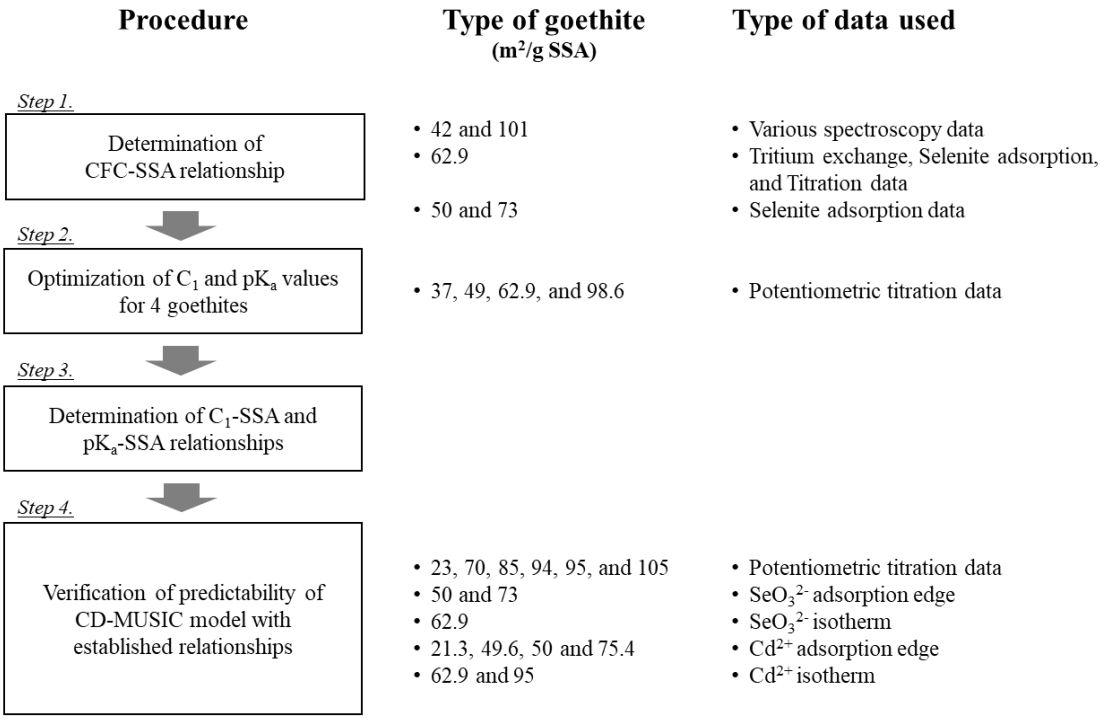

Figure 3-2. Scheme used to develop and verify estimation approach for SCM parameters for different goethite morphologies (SSAs)

3.2. MODEL DESCRIPTION

3.2.1. CD-MUSIC model

The CD-MUSIC surface complexation model was used in this study to describe and predict surface reactions related to proton and ion adsorption. The CD-MUSIC model is an incorporation of the CD model with the MUSIC model [83] and describes the mineral-water interface with three electrostatic planes (the 0-, 1-, and 2-plane) as in the case of the triple layer model (TLM) (see Figure 3-3). One of the main features of the CD model is that it accounts for the physical size of sorbed ions by distributing the charge over multiple planes [83]. This interpretation of surface complexation enables the model to account for subtle differences in ion-surface reactivity by incorporating the apportioned ion charge into the electrostatic calculations [50], [83], [98]. The MUSIC model utilizes crystallographic information to describe protonation and reactive site densities of specific surface sites of adsorbent minerals [83], [84]. Metal oxide surfaces commonly consist of multiple types of surface binding sites that have distinctive surface charge, proton affinity, reactivity, and densities. The capability to account for such surface heterogeneity is one of the advantages of the MUSIC model [14], [33], [48], [83], [128].

Previous studies have shown that CD-MUSIC is capable of making accurate predictions of adsorption of various metal cations and oxyanions on goethite. Proponents of this model purport that the unique features of CD-MUSIC enable the model to employ surface complexes in closer agreement with molecular scale analyses (i.e., spectroscopic data and computational molecular modeling simulations) than other SCMs [89]. For this study in particular, the CD model was helpful for describing the Cd^{2+} and SeO_3^{2-} surface complex species, and the MUSIC model representation of the mineral-water interface

facilitated the incorporation of heterogeneity which is presumed to be one of the primary causes of variation in surface reactivity of goethites [43], [116], [118].

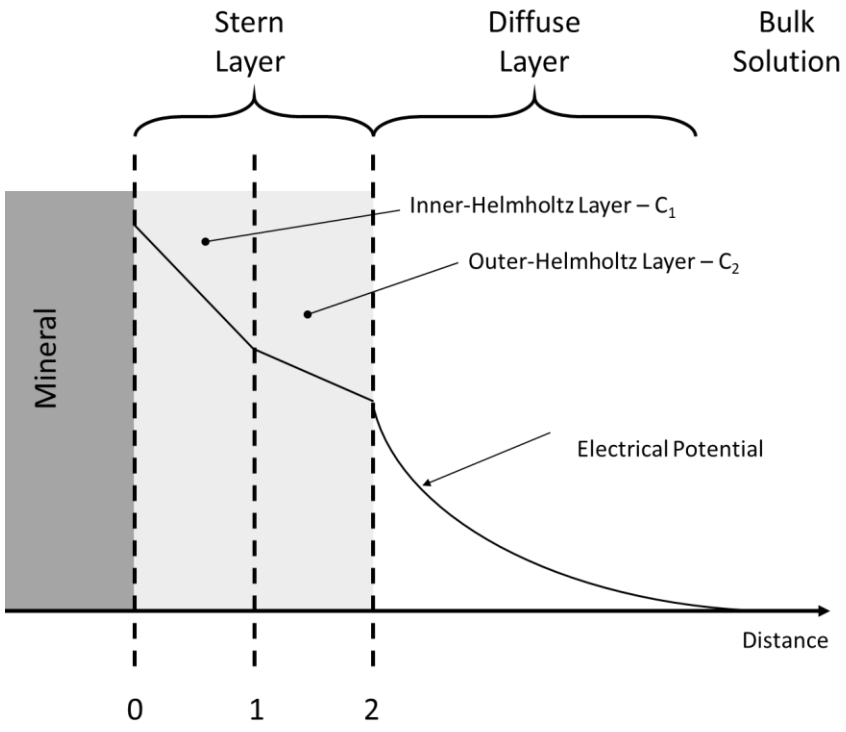

Figure 3-3. Schematic representation of the surface-water interface with three electrostatic planes. (Image adapted from Tadanier and Eick, 2002 [84])

3.2.2. Crystal face contribution (CFC)

Crystal face contribution is the percent of a crystal face contributing to the total surface area of the crystal. Accurately describing the CFC of minerals is important for SCMs since it provides the basis for determining surface site densities (N_s). On goethite, three types of surface oxygens exist on the crystal faces which are termed singly, doubly,

and triply coordinated oxygen groups depending on the number of iron atoms to which they are bound [48], [83]. The density and reactivity of these surface oxygen groups vary on each crystal face [129]–[132]. As the CFC of a goethite crystal changes, the total number and composition of adsorption sites (i.e., surface oxygens) may also change, resulting in variable adsorption behavior. Figure 3-4 presents schematic images of the crystal structure of goethite at the (101) and (001) planes, along with the location and distribution of singly-, doubly-, and triply-coordinated surface oxygens (Fe_1O, Fe_2O, and Fe_3O, respectively) with respect to underlying Fe^{3+} atoms. The subscripted Roman numbers (i.e., I and II) are used to distinguish oxygens with strong (O_I) and weak (O_{II}) affinities. Descriptions of different surface oxygen groups will be discussed in more detail in later sections (i.e., Section 3.2.4 and 3.3.2).

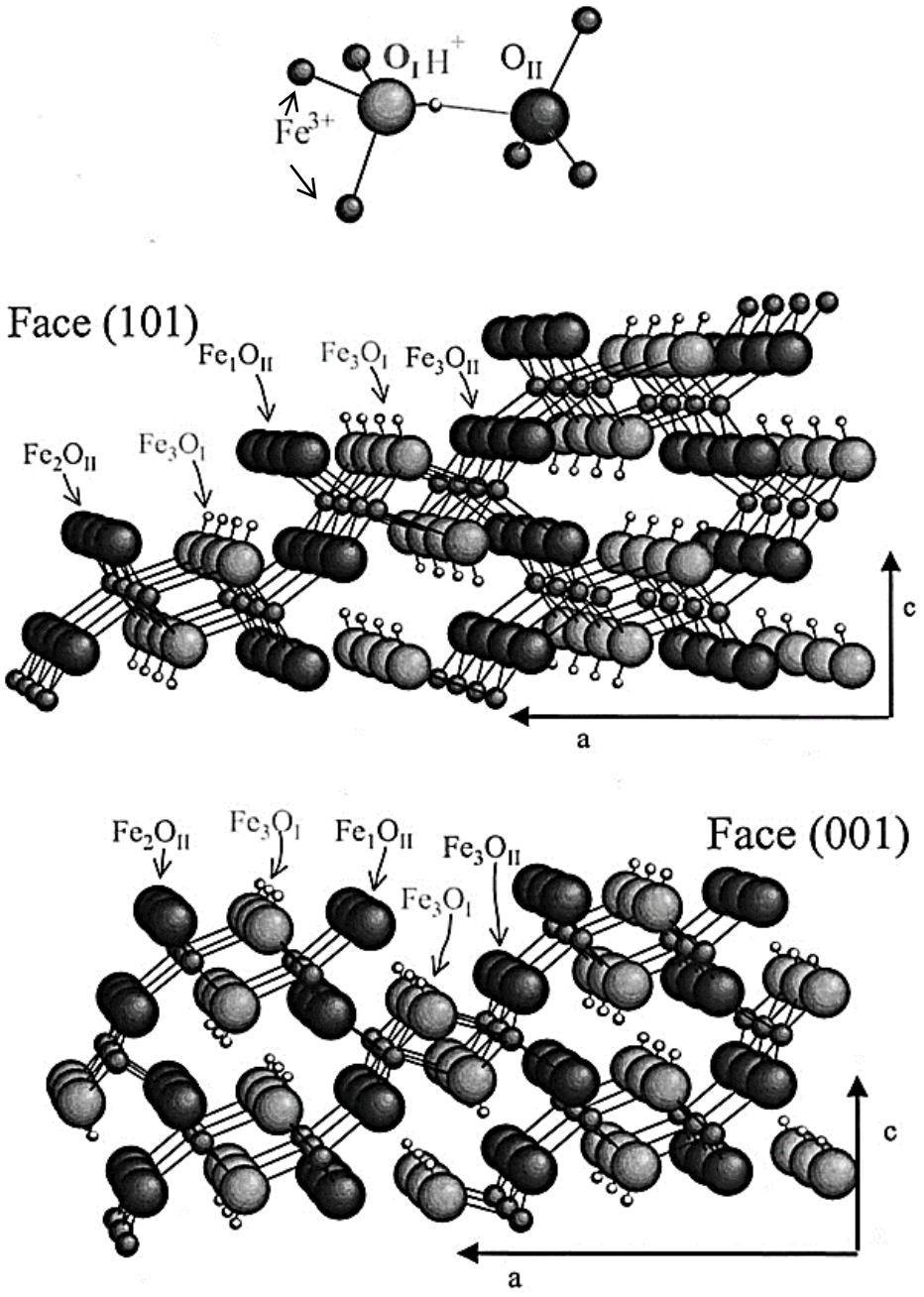

Figure 3-4. Schematic representation of the (101) and (001) plane of goethite surfaces (Image adopted from Gaboriaud and Ehrhardt (2003) [33]). The strong and weak affinity oxygens are drawn as large circles with light and dark shading, respectively. Mid-size circles represent Fe atoms, and small empty circles indicate protons (i.e., H^+ ions). The c-axis is in the direction along the stacking of crystal layers, and hence, the arrows are pointing from the inside toward the outside (surface) of the goethite crystal.

Goethites are typically considered to consist of four principal crystal faces. In addition to the (101) and (001) faces shown in Figure 3-5, (210) and (010) faces are also presented in *Pnma* settings (Figure 3-5) [33], [43], [133]. Various microscopic techniques including scanning electron microscopy (SEM), transmission electron microscopy (TEM), deflection mode atomic force microscopy (AFM), and deflection mode scanning force microscopy (SFM) have identified the (101) and (001) faces as the dominant faces comprising the longitudinal planes of the acicular shaped goethite crystals; and the (210) and (010) faces as the capping faces at the crystal ends [2], [48], [115], [128], [134]–[138].

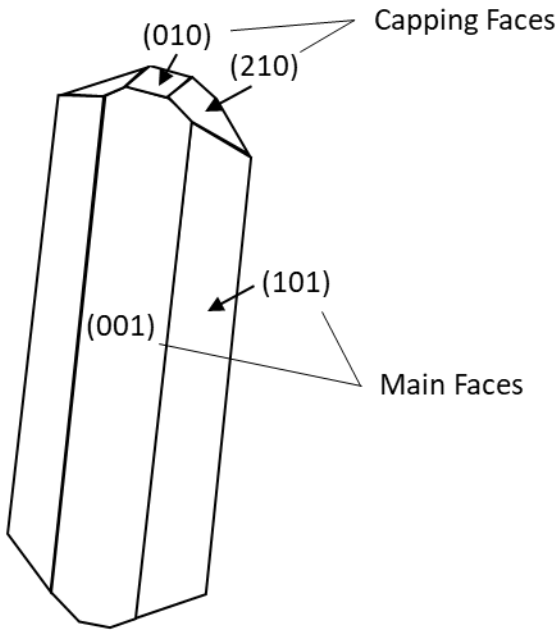

Figure 3-5. Simplified model of goethite crystal faces

It has been documented that the CFCs of these faces change as synthetic goethite crystals grow in size, presumably due to the difference in growth rates of each plane and the crystal growth patterns [43], [118], [139]. A study by Weidler et al. (1996) [139] showed, with multiple spectroscopic techniques, that goethite crystals undergo step-like growth on the (101) and (001) faces which causes notable increases in the capping face contribution and changes in the CFC of each plane as growth proceeds. The step-like crystal growth can be observed in a AFM image (Figure 3-6) provided by Villalobos et al. (2009) [118]. Since SSA varies inversely with crystal size, a correlation between CFC and SSA is expected.

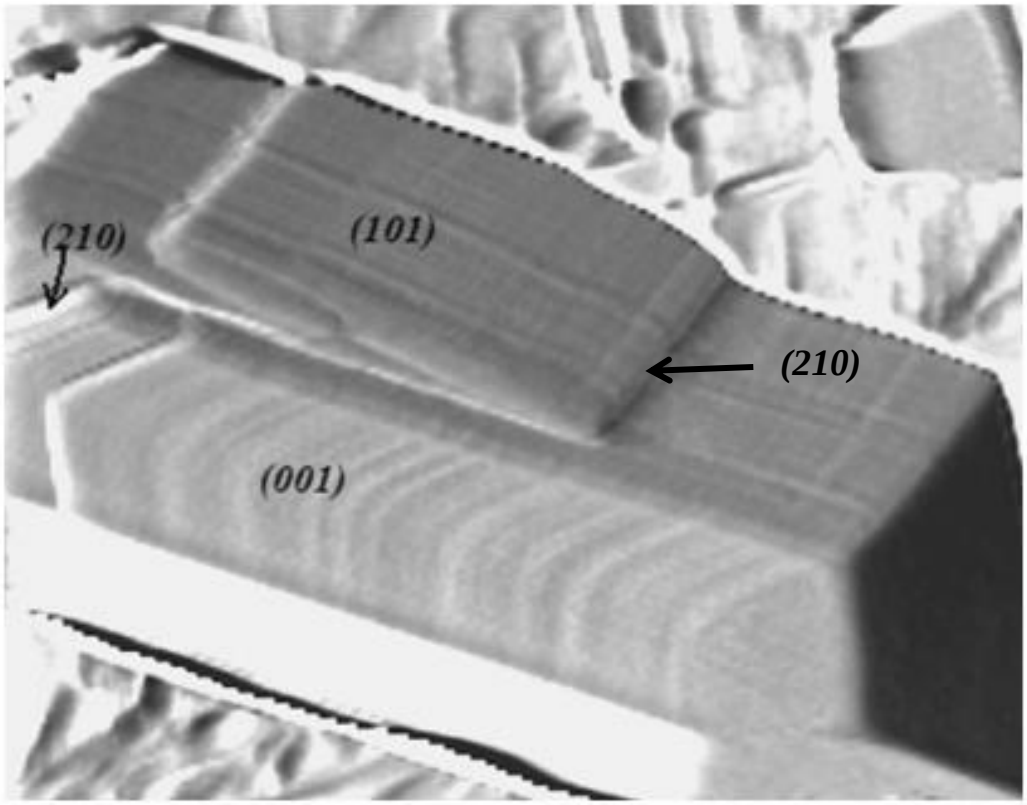

Figure 3-6. AFM (deflection mode) image of a goethite crystal showing the growth face (210) at kinks and steps (Image adopted from Villalobos et al. (2009) [118])

Previous studies have indeed suggested that there are apparent trends related to CFC and SSA, as listed in Table 3-2. Several spectroscopic studies have observed that the fraction of (101) faces is greater than the fraction of (001) faces on high SSA goethites. The opposite trend appears as SSA is reduced which is presumably due to the difference in growth rate between the two faces [33], [49], [140]. Growth rates of capping faces have been observed to be higher than the main faces, resulting in an increase in the contribution of capping faces as the crystal grows and the SSA decreases [43], [116], [118], [126]. For the (010) face, however, there are conflicting views between studies. Cornell et al. (1974) [136] suggested that the (010) face contribution is lower on low SSA goethite based on electron microscope images, while Salazar-Camacho and Villalobos (2010) [116] concluded that the opposite is true based on experimental analyses of surface site densities (Note that the (210) face was not included in their study). A very recent microscopic study by Livi et al. (2017) [126] concluded that the contribution of the (010) face on both low and high SSA goethites was less than 0.5%, which suggest that in practice the (010) face can be disregarded.

Table 3-2. Trends relating (high and low) SSA and goethite crystal face contribution

Low SSA Goethite	**High SSA Goethite**	**Reference**
High (001) face, Low (101) face	Low (001) face, High (101) face	[33], [49], [140]
Higher contribution of capping face	Lower contribution of capping face	[43], [116], [118], [126]
Best represented by (210)/(101) or (010)/(101) face combination	Best represented by (101)/(001) face combination	[43], [116], [118]
Low contribution of (010) face	High contribution of (010) face	[136]
Higher contribution of (010) face	Lower contribution of (010) face	[116]

3.2.3. Capacitance

The capacitance is a surface parameter that describes the Stern layer's ability to store electric charge at a given electrostatic potential difference between two hypothetical interfacial planes. The parameter originates from the representation of the interfacial region as a solid-state parallel plate capacitor, where two surfaces separated by a fixed distance hold a certain amount of electric charge, and no charge exists in, or passes through the space between the surfaces [141]. Although the capacitance value was originally defined to be proportional to the charged area, it is common in the field of geochemistry to use the term to refer to 'area normalized capacitance', which is independent of the area and expressed in units of F/m^2 instead of F (i.e., farad). This convention is followed throughout this thesis.

Capacitance plays an important role in describing the electrostatic effects of surface complexes in SCMs. Since the potential difference between electrostatic surfaces cannot be directly measured, capacitance values are employed to estimate the drop in electric potential based on the charge placed on each electrostatic plane [51]. Mathematically, the capacitance can be described as Eq. 3-1;

Eq. 3-1) $$C = \frac{\sigma}{\Psi_1 - \Psi_2} = \frac{\epsilon_0 \epsilon}{d}$$

where C is the capacitance in units of F/m^2, σ is the surface charge density (i.e., charge normalized by area) on the electrostatic planes expressed in C/m^2, Ψ_1 and Ψ_2 are electrical potentials on the first and second plane respectively, ϵ_0 and ϵ are the absolute (8.85×10^{-12} C/V·m) and relative permeability constants for the interfacial medium, respectively, and d is the distance between the two electrostatic planes. The above equation indicates that the capacitance is solely determined by the distance between charged planes and is independent of the amount of charge present on each plane. In theory, the distance between planes is determined by the minimum distance of approach of ions; therefore, capacitance values are often regarded to be dependent on the type and concentration of ions in solution. While it is reasonable to assume that capacitance values will also vary among different crystal faces [50], [51], [142], [143], variable field effects are generally not included in SCMs for simplicity, and capacitance values are assumed to be constant [122].

In 3-plane SCMs, such as the triple layer model (TLM) and MUSIC model, the Stern layer can be separated into inner- and outer-Helmholtz layers based on the form and location of ion complexes with surface ligands [115]. The two layers may act as separate

capacitors arranged in series yielding two different capacitance values: C_1 and C_2 [144]. In early studies, the C_2 value was commonly assumed to be a fixed value of 0.2 F/m^2 in the triple layer model (TLM), based on direct measurements of the AgI-electrolyte interface [15], [145]. However, more recent studies have pointed out that the assumption that AgI could be used as a surrogate for oxide minerals was based on a misinterpretation of the relationship between the double layer properties of AgI and that of metal (hydr)oxides [82], [83], [121], [122]. Thus, modeling studies now often use the approximation that C_2 is equal to C_1 [146]–[149]. Hiemstra and Van Riemsdijk (2006) [122] and Sverjensky (2005) [51] were able to accurately simulate proton adsorption using this assumption as it yielded reasonable predictions of the zeta potential (ζ) (calculated assuming $\zeta=\psi_d$) at pH values within about 2 units of the isoelectric point for goethite, rutile and hematite. The effect of C_2, in fact, is known to be minimal in simulating potentiometric titration data, while C_1 directly impacts the surface charge calculation [51]. Thus, for proton adsorption, the objective in SCM parameter estimation is generally focused on the determination of C_1.

3.2.4. Protonation constants

Protonation/deprotonation reactions are an essential part of models for ion adsorption on metal oxides [51], [64], [82], [150], [151], primarily because the interaction of protons with surface oxygens determines the surface charge of oxide surfaces which consequently controls ion adsorption behavior [93], [152], [153]. Hence, it is crucial in SCMs to properly estimate pK_a values for protonation reactions of reactive surface groups.

In classical site binding models, the titration behavior of oxide surfaces is commonly described by assuming protonation reactions on only one type of reactive site which is modeled using either a single (1-pK model) or two consecutive protonation

reactions (2-pK model) [14], [15], [31], [34], [48], [49], [51], [154]. Typically, the pK_a for the 1-pK model would coincide with the point-of-zero-charge (pH_{pzc}) of the oxide, whereas for the 2-pK model, pK_{a1} and pK_{a2} would equally deviate from the pH_{pzc} (i.e., $pH_{pzc} = 0.5 \times (pK_{a2} + pK_{a1})$). The pK_a values in these models are assumed to reflect the empirically "averaged" protonation behavior of all the reactive surface sites rather than the actual protonation reaction. Such simplification of the protonation behavior of metal oxides has been observed to yield reasonable predictions of titration data in many studies. However, the predictive capability of these models is constrained to a very narrow range of solution and surface conditions where the parameters are estimated.

An ideal way to describe protonation reactions in SCMs is to separately incorporate individual protonation reactions for each type of surface site. For the case of goethite, as an example, multiple surface oxygen groups undergo protonation and each type of surface functional group may have different proton affinities; thus, multiple pK_a values can exist. The problem with a multiple proton reactive site model, however, arises from the fact that discrete pK_a values for each individual surface oxygen group cannot be readily obtained via experimental methods, since the surface charging behavior of minerals (e.g., pH_{pzc}, titration curve) results from the combined action of multiple surface groups which overshadow the individual contribution [155]. Rather, theoretical approaches have been applied as a means to estimate the intrinsic proton affinity of individual goethite surface oxygen groups. One of the most successful methods for pK_a estimation was proposed by Hiemstra and colleagues [14], [83], [115], [156]; this method utilizes bond-valence theory and Fe-O bond lengths taken from crystallographic studies for the calculation of proton affinity of each type of surface oxygen. This method, which is often referred as the bond-valence method, assumes that the proton affinity of an oxygen originates from

undersaturation of the oxygen valence. Table 3-3 lists the pK_a values of each surface oxygen type obtained through this method. A number of studies have been able to successfully describe surface charge predictions using this method [14], [115], [157]–[162]. However, limitations of the bond-valence approach are associated with its strong sensitivity to slight variations in hydrogen bond strengths and Fe-O bond lengths as pointed out in several studies [48], [151], [163], [164].

Table 3-3. Proton affinity constant (pK_a) values calculated for each surface oxygen group and goethite crystal face based on the MUSIC approach [33], [156]. Surface relaxation was not considered in the calculations.

Surface oxygen group[1)]	(101) face[2)]		(001) face[3)]		(210) face[2)]	
	log K_{a1}	Log K_{a2}	log K_{a1}	Log K_{a2}	log K_{a1}	Log K_{a2}
Fe_1O_I					23.8	11.9
Fe_1O_{II}	19.6	7.7	19.9	8.0	20.0	8.1
Fe_2O_I					19.6	7.7
Fe_2O_{II}	12.3	0.4	11.5	-0.4	11.9	0.0
Fe_3O_I	11.7		11.7			
Fe_3O_{II}	-0.2		-0.2			

[1)] O_I and O_{II} indicate surface oxygen groups with strong and weak reactivity, respectively
[2)] Obtained from Venema et al. (1998) [156]
[3)] Obtained from Gaboriaud and Ehrhardt (2003) [33]

Different approaches to overcome these drawbacks associated with the bond-valence method have been suggested in several studies. A molecular dynamic study by Boily (2012) [164] estimated the effect of relaxed surface Fe-O and H-acceptor distances and populations, while Leung and Criscenti (2012) [151] applied *ab initio* molecular dynamics (AIMD) to calculate the pK_a values of a singly-coordinated oxygen group on the (101) surface. Despite such attempts to estimate the intrinsic pK_a values of individual

surface group types on goethite, agreement on the correct values for the protonation constants is still lacking as they depend heavily on the assumptions made.

An alternative approach to model protonation on metal oxide surfaces is to partition surface oxygens into several groups and estimate the "average" pK_a of each group through model optimization to titration data; the key is to constrain the selection of proton reactive oxygen groups using crystallographic information obtained from bond-valence calculations. This approach incorporates features of both the classical single site model and the bond-valence method. Similar to the single-site model, this approach incorporates a surface averaging approach in which protonation reactions occurring on all proton reactive sites of a metal oxide surface are expressed by a limited number of "averaged" protonation reactions. However, it yields a more reasonable representation of the surface compared to the classical single site model since the surface oxygens are subdivided into groups based on their similarity with respect to protonation. Also, information regarding crystal structure and chemical bonds are used to constrain the selection of effective protonation sites and the range of pK_a values. As an example for goethite, many SCM studies that applied the MUSIC model have assumed that two types of proton reactive oxygen groups exist: singly- and triply-coordinated oxygens that go through only the second and first protonation reaction in the pH range of natural waters (i.e., pH 2 – 12), respectively [48], [50], [61], [82], [118], [155], [156], [165]. The reduced number of protonation reactions compared to the bond-valence approach makes model application more practical, and because pK_a values are estimated via objective curve fitting, it is not necessary to accurately determine the chemical bond lengths and molecular structure in the interfacial region. In the current study, this simplified multi-site protonation model, which

assumes one protonation reaction each for singly- and triply-coordinated surface oxygens, was used to simulate the surface charging behavior of goethites.

3.3. Experimental and Modeling Approach

3.3.1. Batch adsorption experiments

As shown in Figure 3-2, various adsorption data from a number of sources were collected and used to establish the relationships between CFC, capacitance, and pK_a with goethite SSA and verify the accuracy of the parameterized model. While most of the adsorption data were obtained from literature, two different goethites were synthesized and evaluated as part of this work in order to obtain additional adsorption data that were not available from previous studies. The goethites were synthesized according to the method described by Schwertmann et al. (1985) [46] and Peak et al. (1999) [166], where $Fe(NO_3)_3$ was used as the precursor and aged for 14 days in a KOH solution at 25 °C. The $Fe(NO_3)_3$ and KOH solutions were mixed at two different rates (i.e., fast and slow mixing) in order to obtain two different goethite morphologies. During the synthesis process, contact with CO_2 and use of glassware were avoided to prevent possible contamination by carbonate [33], [43], [50] and silicon [50], [83], respectively. Multi-point N_2 BET results showed that the SSA of the synthesized goethites were 50 m^2/g and 73 m^2/g. X-ray diffraction (Philips Vertical Scanning Diffractometer, PANalytical) was also conducted to verify the crystallography and purity of the goethite samples.

Cadmium and selenite adsorption data collected in the laboratory included adsorption edge (constant initial concentrations of metal and goethite, variable pH) and isotherm data (variable initial concentrations, constant pH). Batch reactors for the

adsorption of Cd^{2+} and SeO_3^{2-} were prepared in 15 mL polypropylene centrifuge vials. High purity $NaNO_3$, $Cd(NO_3)_2$ and Na_2SeO_3 salts (i.e., Puratronic® by Alfa Aesar^{TM}) were used to make stock solutions, and 0.1N HNO_3 and 0.1N NaOH standard solutions were used to adjust the pH of the reactors. For the cadmium adsorption experiment, 3.5×10^{-5} M of Cd^{2+} and 1.72 g/L of the 50 m^2/g SSA goethite were injected into each reactor, and adsorption edge data were collected for two different ionic strengths, 0.01 M and 0.7 M. The selenite adsorption experiments were conducted on both 50 m^2/g and 73 m^2/g SSA goethites with three different concentrations of SeO_3^{2-} for each type of goethite (i.e. 1.0×10^{-4} M, 3.75×10^{-4} M, and 1.5×10^{-3} M for the 50 m^2/g SSA goethite; and 1.0×10^{-4} M, 5.0×10^{-4} M, and 1.65×10^{-3} M for the 73 m^2/g SSA goethite). The goethite concentrations in the reactors were 2.87 g/L and 1.84 g/L for the 50 m^2/g and 73 m^2/g SSA goethites, respectively; ionic strength was adjusted to 0.05M for all selenite adsorption tests. After preparation, the reactors were placed in a rotating tumbler for 24 hours to reach equilibrium, and then filtered with a polyethersulfone (PES) syringe filter (0.2 µm pore size). Inductively coupled plasma - optical emission spectrometry (ICP-OES, 710 Agilent Technologies, Santa Clara, CA) was used to analyze Cd^{2+} and SeO_3^{2-} concentrations in the filtrate, and pH was measured for the remaining solution using a combination pH electrode (Thermo Scientific Orion ROSS Ultra®) in a CO_2-free glovebox. The pH electrode was calibrated in the glovebox with three commercial buffer solutions (pH 4, 7 and 10) at the beginning of each experiment and after every ten measurements. A previous study by Wiesner et al. (2006) has documented that the impact of electrolyte concentration on the pH measurement in $NaNO_3$ solution is negligible up to 1.0 M; thus, ionic strength corrected buffers were not used for this study. The pH was recorded when the potential drift was less than 0.01 mV/min.

3.3.2. CD-MUSIC formulation

The basic formulation for the CD-MUSIC model used in this study was largely based on the work conducted by Mangold (2013) [89], which parameterized the model based on adsorption data for Cd^{2+}, Pb^{2+}, and SeO_3^{2-} on a 62.9 m^2/g SSA goethite. The reactive surface site densities (N_s) of singly-, doubly-, and triply-coordinated sites on each crystal face are listed in Table 3-4, which were determined by using values reported from previous crystallographic studies on goethite. In order to reduce the number of parameters in the model, it was further assumed that reactivities of surface sites are identical between the same type of sites (i.e., singly- and triply-coordinated oxygen groups) on (101) and (001) faces, and also between the sites on the (210) and (010) faces. As a result, the number of surface site types that were considered in the model was reduced to four: singly- and triply-coordinated sites on the main faces, and singly- and doubly-coordinated sites on the capping faces. The surface site concentration of each site, expressed in units of mol/L, that were used in the model were calculated by combining the site density values in Table 3-4, CFC values, SSA, and solid concentration (C_s) of each goethite as described by Eq. 3-2.

Eq. 3-2)
$$[Surface\ Site]_i \left(\frac{mol}{L}\right) = \sum_k \left(N_{s,i,j} \times \%CFC_j\right) \times SSA \times C_s \times 10^{18} \times 6.023 \times 10^{23}$$

where, $[Surface\ site]_i$ is the concentration of the i^{th} surface site, $N_{s,i,j}$ is the site density of the i^{th} surface site type on the j^{th} crystal face, $\%CFC_j$ is the % contribution of the j^{th} crystal face, k is the total number of crystal faces, SSA is the specific surface area of the goethite, C_s is the goethite concentration in solution in units of g/L, 10^{18} is the conversion factor from nm^2 to m^2, and 6.023×10^{23} is Avogadro's number.

Table 3-4. Surface site densities of singly-, doubly- and triply-coordinated surface sites on each goethite crystal face

Site type	Crystal Faces (sites/nm^2)			
	(101)	(001)	(210)	(010)
Singly	3.03	3.34	7.5	9.1
Doubly	0	0	3.75	4.55
Triply	3.03	3.34	0	0

Source: (101) & (001) Gaboriaud and Ehrhardt (2003) [33], *Lützenkirchen et al. (2008)* [49]*; (210) & (010) Lützenkirchen et al. (2008)* [49], *Venema et al. (1996)* [82]

A simplified 1-pK multi-site protonation model which assumes two types of proton reactive sites (i.e., singly- and triply-coordinated surface oxygens) was applied to describe the protonation behavior of goethites. This approach has been used in many previous studies which successfully predicted adsorption of protons, numerous metal cations and oxyanions on goethite [48], [50], [61], [82], [118], [156], [165]. While the goethite structure includes six different surface oxygen sites with different protonation affinities as listed in Table 3-3 (i.e., singly-, doubly-, and triply-coordinated surface oxygens with either strong (O_I) or weak (O_{II}) reactivities), only a few of the potential protonation reactions occur in the pH range of natural waters (i.e., pH 2 - 12). According to density functional theory [167] and bond-valence calculations [14], [33], [115], [156], [168], the non-protonated singly-coordinated sites, $\equiv FeO_{(I\ \&\ II)}^{-3/2}$, are highly unstable and are always protonated in aqueous systems (i.e., $\equiv FeO_{(I\ \&\ II)}H^{-1/2}$) [167], [169]. However, the transformation to $\equiv FeO_{(I\ \&\ II)}H_2^{+1/2}$ via a second protonation is considered operative in the pH range of natural environments. Thus, the non-protonated form of singly-coordinated sites was neglected and only one pK_a was determined for the singly-coordinated surface sites. By the same reasoning, doubly-coordinated sites were assumed to be non-reactive; and therefore, only exist as $\equiv Fe_2OH$ in the pH range tested (i.e., pH 3 -11) [50], [82]. For

triply-coordinated sites (i.e., $\equiv Fe_3O_I^{-1/2}$ and $\equiv Fe_3O_{II}^{-1/2}$), the surface sites with O_I oxygen, $\equiv Fe_3O_I^{-1/2}$, are generally protonated over a wide range of pH values due to their high affinity for protons, whereas the lower proton affinity surface oxygens (i.e., O_{II}) are non-protonated [48], [50]. In this study, only higher proton affinity triply-coordinated oxygen sites (i.e., $\equiv Fe_3O_I^{-1/2}$) were considered since the surface density of these sites is assumed to be twice that of the lower affinity oxygen sites, and the charge of the dominant higher and lower proton affinity sites (i.e., +0.5 and -0.5 v.u., respectively) cancel each other one-to-one. Hence, only one protonation reaction constant was required for the triply-coordinated sites. The two protonation reactions considered in this study are represented by Eq. 3-3 and Eq. 3-4.

Eq. 3-3) $$\equiv FeO_{(I\,\&\,II)}H^{-1/2} + H^+ \leftrightarrow \equiv FeO_{(I\,\&\,II)}H_2{}^{+1/2}$$

Eq. 3-4) $$\equiv Fe_3O_I{}^{-1/2} + H^+ \leftrightarrow \equiv Fe_3O_IH^{+1/2}$$

The charge from protonation or deprotonation of surface sites was all attributed to the 0-plane, while the charge from inner-sphere complexes were distributed between 0- and 1-planes. For outer-sphere complexes and ion-pairs, the charges were placed on the 1-plane. In many previous CD-MUSIC studies, the charge of outer-sphere complexes is located on the 2-plane which designates the beginning of the diffuse layer [82], [84]. However, a study from Rahnemaie et al. (2006a) [50] has revealed that charge separation between the minimum distance of approach of the ion-pairs and the beginning of the diffuse layer exists. Due to this finding, current SCM studies that utilize CD-MUSIC place outer-sphere complex charge and ion-pair charge on the 1-plane [122], [146]–[149], [155], [170]. The charge distribution values and equilibrium constants for the ion-pair reactions between

background electrolyte and surface sites are listed in Table 3-5. Monovalent ions, such as Na^+ and NO_3^-, are normally assumed to be adsorbed as outer-sphere monodentate complexes on oxide surfaces [50], [64], [98], [114], [171], [172]. Hence, the charge of Na^+ and NO_3^- ions were both located at the 1-plane in this study.

Equilibrium constants of the ion-pair complexes were set equal to the values determined by Mangold (2013) [89] who optimized the parameters by fitting potentiometric titration data of 62.9 m^2/g SSA goethite for three different concentrations of $NaNO_3$ with the same surface complexes listed in Table 3-5. Equilibrium constants of aqueous species were obtained from NIST Standard Reference Database 46 [173] and are listed in Table 3-6.

Table 3-5. Equilibrium constants and charge distribution values for ion-pairs and protonation reactions on singly-, doubly-, and triply-coordinated surface oxygen sites

Surface Species	Equilibrium constant (log K)[1)]	Charge Distribution[2)]		
		Δz_0	Δz_1	Δz_2
$\equiv FeOH^{-1/2}$	0	0	0	0
$\equiv FeOH_2^{+1/2}$	$pK_{a2,singly}$	1	0	0
$\equiv FeOH_2\_NO_3^{-1/2}$	$pK_{a2,singly} - 0.5$	1	-1	0
$\equiv FeOH\_Na^{+1/2}$	0.1	0	1	0
$\equiv Fe_2OH^0$	0	0	0	0
$\equiv Fe_3O^{-1/2}$	0	0	0	0
$\equiv Fe_3OH^{+1/2}$	$pK_{a1,triply}$ (=11.7)	1	0	0
$\equiv Fe_3OH\_NO_3^{-1/2}$	$pK_{a1,triply} - 0.5$ (=11.2)	1	-1	0
$\equiv Fe_3O\_Na^{+1/2}$	0.1	0	1	0

[1)] *Source: Mangold (2013)* [89]
[2)] *Source: Mangold (2013)* [89], *Stachowicz et al. (2008)* [61], *Weng et al. (2008)* [66], *Rahnemaie et al. (2007)* [148], *and Talebi Atouei et al. (2016)* [165]

Table 3-6. Equilibrium formation constants of aqueous species used in the CD-MUSIC model

Aqueous Species	Equilibrium Constant	Reference
H_2O	13.997	[173]
NaOH (aq)	-13.897	[173]
$NaNO_3$(aq)	-0.55	[173]
$CdOH^+$	-10.097	[173]
$Cd(OH)_2$ (aq)	-20.294	[173]
$Cd(OH)_3^-$	-33.3	[174]
$Cd(OH)_4^{2-}$	-47.288	[173]
Cd_2OH^{3+}	-9.397	[173]
$CdNO_3^+$	0.5	[173]
$Cd(NO_3)_2$ (aq)	0.2	[173]
$HSeO_3^-$	8.4	[173]
H_2SeO_3 (aq)	11.03	[173]

Modeling parameters for the adsorption of Cd^{2+} and SeO_3^{2-}, such as the surface complex species, equilibrium constants, and charge distribution values, were obtained through a separate study extended from Mangold (2013) [89]. Details are as listed in Table 3-7. In the original study, the selection of surface species was based on information gathered from various literature sources that provided evidence for the structure of the species by EXAFS spectroscopy [130], [131], [175], density function theory calculations [131], [176], pressure-jump relaxation techniques [177], and model optimization [82], [146]. The relative contribution of each surface complex species and their equilibrium constants were further refined by fitting adsorption edges for each ion, which was conducted on a 62.9 m^2/g SSA goethite, with the CD-MUSIC model. The charge distributions, Δz_0 and Δz_1, of the surface complexes were determined by an approach

similar to the one described by Hiemstra et al. (2007b) [146] which utilizes the cation - surface oxygen bond lengths for the calculation of charge apportion. With these parameters, Mangold (2013) [89] was successful in predicting the isotherm data of both ions.

Table 3-7. Surface complex species and modeling parameters for Cd^{2+} and SeO_3^{2-}

Adsorbate	Crystal Face	Surface Complex	Linkage Type	Δz_0 [1]	Δz_1 [1]	Log K_{in} [2]
Cd^{2+}	(101) & (001)	$2(\equiv FeOH^{-1/2}) + Cd^{2+} \rightarrow (\equiv FeOH)_2\text{-}Cd$	Corner	0.82	1.18	5.978
		$\equiv FeOH^{-1/2} + Cd^{2+} + 2H_2O \rightarrow (\equiv FeOH)\text{-}Cd(OH)_2 + 2H^+$	Vertex	0.41	-0.41	-11.960
	(210)	$2(\equiv FeOH^{-1/2}) + \equiv Fe_2OH^0 + Cd^{2+} \rightarrow (\equiv FeOH)_2\text{-}Cd\text{-}(\equiv Fe_2OH)$	Edge	1.15	0.85	6.311
		$2(\equiv FeOH^{-1/2}) + \equiv Fe_2OH^0 + Cd^{2+} \rightarrow (\equiv FeOH)_2\text{-}Cd\text{-}(\equiv Fe_2O) + H^+$	Edge	0.32	0.68	-0.903
SeO_3^{2-}	(101) & (001)	$2(\equiv FeOH^{-1/2}) + SeO_3^{2-} + 2H^+ \rightarrow (\equiv FeO)_2\text{-}SeO + 2H_2O$	Corner	0.75	-0.75	22.849
	(210)	$2(\equiv FeOH^{-1/2}) + SeO_3^{2-} + 2H^+ \rightarrow (\equiv FeO)_2\text{-}SeO + 2H_2O$	Corner	0.67	-0.67	23.926
		$2(\equiv FeOH^{-1/2}) + SeO_3^{2-} + 3H^+ \rightarrow (\equiv FeO)_2\text{-}SeOH + 2H_2O$	Corner	0.67	0.33	29.831

[1] Δz_0 and Δz_1 represents the charge distribution of the adsorbed ion on to 0- and 1-plane, respectively
[2] Log of intrinsic equilibrium constants which utilizes mole fraction standard states

3.3.3. Evaluation of model results

The accuracy of the model predictions for adsorption data was quantified by calculating the weighted sum of squares divided by the degrees of freedom (WSOS/DF). The difference between experimental and calculated concentrations of adsorbate at each data point was weighted with estimated absolute and relative error values to account for the uncertainties involved in the experimental data. For this study, the absolute and relative error estimates presented by Dzombak and Morel (1990) [18] were employed (Table 3-8). These values were established through extensive modeling analysis and literature review on cation and anion adsorption to ferrihydrite. Since WSOS/DF values between 0.1 and

20 are commonly considered satisfactory model fits to experimental data [178] for these error estimates, this criterion was also used in this study.

Table 3-8. Error estimates used in CD-MUSIC modeling. Adopted from Dzombak and Morel (1990)

Measurement [a]	s[rel] [b]	s[abs] [c]
$X_{H\text{-sorption}}$	0.05	0.0
$X_{H\text{-titration}}$	0.10	0.0
T_H	0.01	0.01 × min T_H
X_M	0.05	0.0
T_M	0.01	0.01 × min T_M
X_A	0.05	0.0
T_A	0.01	0.01 × min T_A

[a] H: Hydrogen ion, M: Metal cation, T: Total concentration, X: Free concentration
[b] Relative experimental error
[c] Absolute experimental error

3.4. ESTABLISHMENT OF PARAMETER RELATIONSHIPS

3.4.1. Crystal face contribution (CFC) and SSA relationship

The relationship between CFC and SSA of the goethites used in this study was determined based on the documented CFC-SSA trends described in the previous section (Table 3-2), and macroscopic and microscopic data from previous studies. Previous work by Mangold (2013) [89] proposed a method to compute the CFC of goethite by simultaneously fitting tritium exchange, maximum selenite adsorption, and potentiometric titration data. With this method, values for CFCs of 31% for the (101) face, 55% for the (001) face, and 14% for the (210) face were derived for their 62.9 m^2/g SSA goethite. Multiple microscopic methods used in research by Livi et al. (2017) [126] specified the

CFC of a 42 m^2/g and a 101 m^2/g SSA goethite. In their study, the step-like crystal formation, which develops on the (101) face and contributes to the increase in capping faces with goethite crystal growth, was used for to quantify the total contribution of the (210) face; the results yielded a 36% and a 14% contribution on the 42 m^2/g and 101 m^2/g SSA goethite, respectively. In addition, AFM images from Gaboriaud and Ehrhardt (2003) [33] showed the ratios between the contribution of (101) and (001) faces were 70/30 and 30/70 for 95 and 49 m^2/g SSA goethites, respectively. Although their assumption that the contribution of capping faces was negligible (and thus disregarded in their work) is disputable, the relative ratios obtained between the two main faces can still be considered valid regardless of the contribution of the capping faces.

A CFC-SSA relationship was established from the findings of these previous studies as summarized in Table 3-9. The CFC values of the capping faces (i.e., (210) and (010)) for the 42 m^2/g, 63 m^2/g, and 101 m^2/g SSA goethite were adopted from literature [89], [126], and adjustments were made to the distribution of the main faces (i.e., (101) and (001)) for the 42 m^2/g and 101 m^2/g SSA goethite to incorporate the CFC ratios suggested by Gaboriaud and Ehrhardt (2003) [33]. Since the SSAs of goethites used in Gaboriaud and Ehrhardt (2003) [33] and Livi et al. (2017) [126] are not very different, it was assumed that the morphologies of goethites used in both studies were very similar. The resulting CFC values for the (101) and (001) faces on the 42 m^2/g and 101 m^2/g goethites were recalculated to be 19%/45% and 60%/26%, respectively. This adjustment resulted in approximately 7.0% and 3.0% increases in reactive surface oxygen site densities on the main faces of the 42 m^2/g and 101 m^2/g SSA goethites, respectively; this had minimal effect on ion or proton adsorption. The contribution from the (010) face was assumed to be

negligible on all three goethites which is consistent with the findings of Livi et al. (2017) [126] and Mangold (2013) [89].

Table 3-9. CFC values obtained from literature for each goethite morphology

Reference		Mangold (2013)	Livi et al. (2017) & Gaboriaud and Ehrhardt (2003)[1)]		Current study[2)]	
SSA of goethites		62.9 m^2/g	42 m^2/g	101 m^2/g	50 m^2/g	73 m^2/g
CFC values	(101)	33%	19% [3)]	60% [4)]		
	(001)	55%	45% [3)]	26% [4)]		
	(210)	14%	36%	14%	36%	14%
	(010)	-	-	-	-	-

[1)] CFC of (101) face reported in Livi et al. (2017) [126] *were distributed into (101) and (001) faces based on the findings from Gaboriaud and Ehrhardt (2003)* [33]*. The morphology of the 42 m^2/g and 101 m^2/g SSA goethites were assumed to be similar to 49 m^2/g and 95 m^2/g SSA goethites, respectively.*
[2)] Values obtained from maximum selenite adsorption
[3)] Adjusted from 64% (101) by applying 30/70 ratio between (101) and (001) faces
[4)] Adjusted from 86% (101) by applying 70/30 ratio between (101) and (001) faces

Maximum selenite ion adsorption data for two different goethites with SSAs of 50 m^2/g and 73 m^2/g were also used to establish the CFC-SSA relationship. These two goethites were specifically selected to obtain more information on mid-range SSA goethites (i.e., between 42 m^2/g and 62.9 m^2/g, and 62.9 m^2/g and 101 m^2/g). Several studies, including an early EXAFS study by Hayes et al. (1987) [175], suggested that selenite ion adsorption to the goethite surface occurs through formation of an inner-sphere bidentate complex species with singly-coordinated oxygens [146], [175], [177]. Hence, by combining selenite saturation data and information quantifying singly-coordinated oxygen

site densities on each crystal face, the CFC of a goethite sample was estimated using Eq. 3-5.

Eq. 3-5) $$\Gamma_{Se,Max} = \frac{\Sigma_k[(\%CFC)_i \times (N_{s,\equiv FeOH})_i]}{2} \times \frac{10^{18}}{N_A} \times 10^6$$

where $\Gamma_{Se,Max}$ is the saturation density of selenite on the goethite expressed in units of μmol/m^2, k is the total number of crystal faces, $(\%CFC)_i$ is the CFC value for the i^{th} crystal face, $(N_{s,\equiv FeOH})_i$ is the density of singly coordinated sites present on the i^{th} crystal face in units of sites/nm^2, N_A is Avogadro's number (i.e., 6.023×10^{23}), 2 is the number of singly coordinated oxygens occupied by a single SeO_3^{2-} molecule adsorbed for a bi-dentate surface complex, and 10^{18} and 10^6 are the conversion factors from nm^2 to m^2 and mol to μmol, respectively.

It should be noted, however, that the maximum number of surface sites occupied by selenite cannot be assumed to be equal to the total number of singly-coordinated surface oxygens on a goethite sample due to competition with protons and electrolytes. Regardless, the selenite saturation data can provide a good approximation of the minimum number of singly-coordinated reactive surface sites on goethites. According to a CD-MUSIC based selenite adsorption model developed and documented by Mangold (2013) [89], more than 90% of the singly coordinated oxygens were shown to be complexed with the selenite ion when saturated. Therefore, in the current study, the surface site density obtained from selenite adsorption data represented a lower bound on the surface site density. Estimation of the CFC was constrained by selenite surface saturation at low pH and the CFC-SSA trends described previously. The maximum selenite adsorption density for the 50 m^2/g SSA goethite was 3.76 μmol/m^2, which corresponds to 4.53 sites/nm^2 of singly coordinated

oxygens. For this site density value, the contribution of the (210) face was required to be at least 33.6%. For the 73 m^2/g SSA goethite, the maximum selenite adsorption yielded only 3.71 sites/nm^2 of occupied singly coordinated sites which led to a (210) face contribution of at least 12.0%. The lower bound of CFC values of the (210) face on the 50 m^2/g and 73 m^2/g SSA goethites obtained with selenite saturation data (i.e., 33.6% and 12.0% respectively) were very similar (but slightly less) than the values obtained by microscopy for the 42 m^2/g and 101 m^2/g SSA goethites (which were 36% and 14%, respectively [126]). Since the CFC-SSA trends should be consistent across the range of SSA goethites, the CFCs of the (210) face on the 50 m^2/g and 73 m^2/g SSA goethites were adjusted to 36% and 14%, respectively. This adjustment was consistent with our argument that the selenite saturation data provides a lower limit of reactive surface site density.

3.4.2. Capacitance value and SSA relationship

Capacitance values are commonly determined through objective curve fitting of potentiometric titration datasets which relate the surface charge (σ_0) to the solution pH [15], [82]–[84]. The current study also employed an optimization procedure using potentiometric titration data to determine C_1 (i.e., the inner-Helmholtz capacitance) values of four different goethites. Using the previously determined CFC values and the described CD-MUSIC model, the capacitance values and protonation constants were simultaneously optimized. Details of the optimization process are described in section 3.4.4. After the capacitance values of the four goethites were determined, the values were plotted against goethite SSA, and it was assumed that the C_1-SSA relationship could be established by finding the linear trend line of the four points.

The capacitance values (C_1) that were selected to fit proton adsorption data were constrained to maintain consistency with trends from the literature that suggest a quasi-linear, inverse relationship between SSA and inner-layer capacitance (C_1) for goethites [31], [33], [43], [48]–[51], [116], [118]. It has been proposed that trends in increasing capacitance with decreasing SSA are related to surface roughness [48]. The basis for this hypothesis is that rough surfaces provide greater surface oxygen site densities resulting in higher potential for stabilizing counter-ions in the electrostatic plane of the surface-water interface and smaller average distances of approach [48], [49], [51], [52]. In addition, some studies suggest that capacitance values must be constrained within a feasible range regardless of the estimation method. This suggestion is based on the fact that capacitance values are theoretically related to the distance of approach of the ions to the surface which is determined by solution chemistry and the dimensions of the interfacial region [50], [121], [122]. Hence, the selection of C_1 for each goethite was constrained to a range of values reported in previous studies (i.e., 0.6 – 1.45 F/m^2) which focused on developing relationships between SSA and capacitance values [31], [33], [48], [49], [51], [116], [118].

3.4.3. Protonation constants and SSA relationship

The pK_a values were determined simultaneously with the capacitance values by fitting titration data under a number of constraints (details in section 3.4.4.). For the singly-coordinated oxygen groups, the Fe-O bond lengths may vary depending on where the oxygen is located within the octahedral crystal chain, and thus the pK_a value calculated by bond-valence theory varies between oxygen groups on different crystal faces (i.e., (101), (001), and (210) faces) as well as within the same crystal face (i.e., FeO_I and FeO_{II}). Table 3-3 shows that estimated pK_a values of the second protonation reaction of singly-

coordinated surface oxygens may range from 7.7 to 11.9 when calculated through bond-valence theory. Thus, the pK_a was constrained to fall in this range during the optimization process. In addition, since the pK_a values estimated by bond-valence theory vary among crystal faces, it is expected that the overall "average" pK_a of the singly-coordinated oxygen groups will be affected by the change of CFC. With the expectation that relative values of pK_a will be higher on sites on the (001) and (210) faces compared to the (101) face, it is reasonable to assume that the "average" pK_a of singly coordinated oxygens would increase as the goethite SSA decreases based on the previous CFC-SSA trends described. A molecular dynamic study by Rustad and Felmy (2005) [179] provides evidence for an inverse relationship between goethite pK_a and SSA. They have found that greater proton charging occurs at acute angles between crystal faces; they attributed this behavior to dielectric effects from improved water solvation at such locations. Using the same reasoning, they have suggested that rougher surfaces would provide more favorable conditions for proton accumulation. Since it is known that lower SSA goethites have greater surface roughness [49], [118], [126], it is possible to predict that the apparent pK_a would increase as SSA decreases. This trend was incorporated into the optimization procedure for the pK_a of singly-coordinated surface oxygens of different SSA goethites. The triply coordinated oxygens, on the other hand, showed consistent pK_a values of 11.7 for all crystal faces, and thus, were held constant at that value.

3.4.4. Data-fitting: optimization of C_1 and $pK_{a2,singly}$

The assumptions and constraints described above were used to fit titration data to simultaneously optimize the inner-Helmholtz capacitance value (C_1) and the second protonation constant of singly-coordinated sites ($pK_{a2,singly}$) as a function of goethite SSA.

Titration data from four different goethite preparations collected from literature were used for parameter optimization. The SSAs of the goethites used in the collected data were 37 m^2/g, 49 m^2/g, 62.9 m^2/g and 98.6 m^2/g (obtained from Boily et al. (2001) [48], Gaboriaud and Ehrhardt (2003) [33], Vieira (2007) [127], and Rahnemaie et al. (2006) [50], respectively). All titrations were reported to be performed in CO_2-free environments, with $NaNO_3$ as electrolytes, and with pH_{pzc} values for goethite of 9.1±0.3. Descriptions of the titration data sets and the goethite used in the studies are listed in Table 3-10.

Each set of titration data was extracted from published graphs using an image digitizing software application (WebPlotDigitizer [180]), and the conversion of pH values into log concentration of H^+ was conducted utilizing a chemical equilibrium modeling software package, Visual MINTEQ [181]. For the calculation of activity coefficients in Visual MINTEQ, the Davies equation with the B parameter set to 0.3 was applied. The mass balance equations were calculated differently depending on whether the titration data were reported in terms of TOTH or net proton adsorption (NPA), as shown in Eq. 3-6 and Eq. 3-7 below.

Eq. 3-6)
$$TOTH = [H^+] - [OH^-] - [NaOH] + \frac{1}{2}\Big(\left[\equiv FeOH_2^{+1/2}\right] - \left[\equiv FeOH^{-1/2}\right] + \left[\equiv FeOH_{2_{An}}\right] - \left[\equiv FeOH_{Cat}\right] + \left[\equiv Fe_3OH^{+1/2}\right] - \left[\equiv Fe_3O^{-1/2}\right] + \left[\equiv Fe_3OH_{An}\right] - \left[\equiv Fe_3O_{Cat}\right]\Big)$$

Eq. 3-7)
$$NPA = \frac{1}{2}\Big(\left[\equiv FeOH_2^{+1/2}\right] - \left[\equiv FeOH^{-1/2}\right] + [\equiv FeOH_2\_An] - [\equiv FeOH\_Cat] + \left[\equiv Fe_3OH^{+1/2}\right] - \left[\equiv Fe_3O^{-1/2}\right] + [\equiv Fe_3OH\_An] - [\equiv Fe_3O\_Cat]\Big)$$

The optimization of C_1 and $pK_{a2,singly}$ values was conducted by manually testing hundreds of combinations of the two parameters within the range of 0.70 – 1.20 F/m^2 with increments of 0.05 and 7.5 – 9.5 log units with increments of 0.1 for capacitance and protonation constants, respectively. Among the combinations which model predictions resulted in WSOS/DF values below 20, ones that satisfied the general trends of C_1-SSA and pK_a-SSA, and also, returned the best fit to the data were selected as the optimum C_1 and pK_a values for each goethite.

Table 3-10. Description of potentiometric titration data sets selected from the literature

Literature	SSA (m^2/g)	Solid conc. (g/L)	pH_{pzc}	Electrolyte conc. (M)	Temp (°C)	Surface charge expression
Rahnemaie et al. (2006) [50]	98.6	16.52	9.0	0.015M, 0.05M, 0.2M	20±0.1	μmol-H$^+$/m^2 (NPA)[3)]
Vieira (2007) [127]	62.9	10	9.1	0.01M, 0.081M, 0.31M	25±0.5	mol-H$^+$/L (TOTH)
Gaboriaud and Ehrhardt (2003) [33] [1)]	49	22 – 23 [2)]	9.0	0.01M, 0.05M, 0.1M, 0.5M	25	mol-H$^+$/L (TOTH)
Boily et al. (2001) [48]	37	10	9.4	0.01M, 0.1M, 0.05M, 0.6M[4)]	25±0.5	C/m^2 (NPA) [3)]

[1)] Raw data reported in terms of Cb-Ca (mol/L) was used.

[2)] Solid concentrations were not specified in the original literature. The concentrations were therefore back-calculated using reported raw titration data and converted surface charge data.

[3)] NPA: Net proton adsorption

[4)] Titration data conducted in a 2 M ionic strength solution which was originally included in the study was excluded from the optimization process since results obtained by FITEQL 4.0 are questionable outside of the ionic strength range of the Davies equation [182] *(i.e., >0.5M ionic strength)*

3.5. Application of SSA Relationships for Parameter Estimation

3.5.1. CFC and SSA relationship

The CFC-SSA relationship established by the proposed method is plotted in Figure 3-7. The results show that there is a clear difference in the capping face contribution between goethite groups with SSAs lower than 50 m^2/g and higher than 62.9 m^2/g, where the %CFCs of the (210) face are 36% and 14%, respectively. The current result is consistent with many studies which reported relatively greater surface reactivity for goethites of SSA below ca. 60 m^2/g [31], [33], [184], [48], [53], [83], [120], [121], [154], [169], [183] which can be explained by an increase in contribution of the more reactive capping faces, such as the (210) face. The steep shift in surface site density between the 50 m^2/g and 62.9 m^2/g SSA goethites, shown with a dotted line in Figure 3-7, is similar to the observation made by Villalobos and Pérez-Gallegos (2008) [43], which suggested that there may be two categories of goethites; those with higher average reactive sites densities corresponding to SSAs below 60 – 70 m^2/g and those that have lower average reactive site densities corresponding to higher SSAs (above 70 m^2/g).

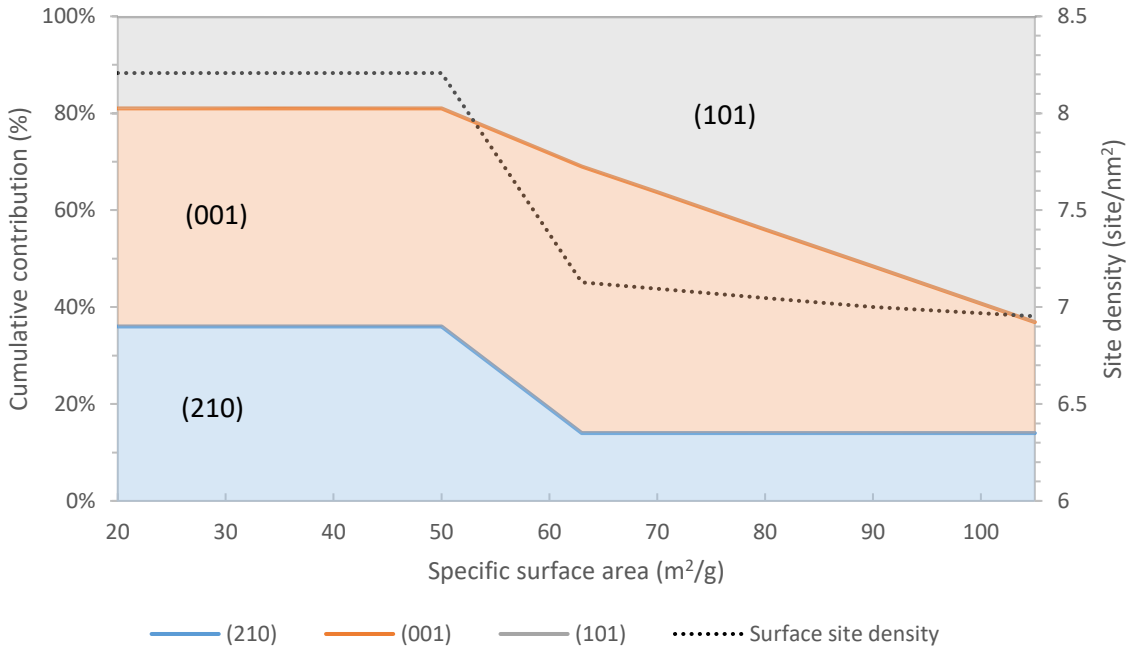

Figure 3-7. The established CFC-SSA relationship and surface site density of goethites. The percent contribution of each crystal face is stacked to visualize its contribution relative to the total surface.

The current results are also in agreement with many previous modeling studies that have specified the CFC of goethites used in their models. Previous SCM studies have commonly used CFC values of 90% for the (101) face and 10% for the (210) face (or (010) face) for all goethites regardless of their SSA. These values were mainly assumed based on microscopic image analysis from Schwertmann (1984) [134] and/or Schwertmann and Cornell (1991) [135] where the (101) face was determined to be the dominant crystal face of acicular goethite particles, and Weidler et al. (1996) [139] or Boily et al. (2001) [48], where the (210) and (010) faces were proposed as the terminal face, respectively. The assumption of 90% (101) face / 10% (210) or (010) face contribution has been shown to be successful in obtaining accurate prediction results with reasonable surface parameters

for various goethites with SSA above ca. 60 m^2/g (e.g., 66 m^2/g [84], 78 m^2/g [185], 85 m^2/g [48], [148], 95 m^2/g [82], [186], 96.4 m^2/g [187], 98 m^2/g [165] and 98.6 m^2/g [50], [64]). Remarkably, CFC values of these goethites are only marginally different from our result for goethites above SSA of 62.9 m^2/g which distributes 86 % of the CFC to main faces (i.e., (101) and (001)) and 14% to the 210 face.

Hiemstra and van Riemsdijk (1996) [83] conducted electron microscopy for a 105±5 m^2/g SSA goethite and determined that the capping face contributes about 5% of the surface, which is considerably lower than our result for the 101 m^2/g SSA goethite (i.e., 14%). The value obtained by Hiemstra and van Riemsdijk (1996) [83], however, does not include the contribution of the step-wise formation that grows on the main crystal faces. Thus, the actual CFC value of the capping faces must be higher when calculated using the procedure described in the current study. Livi et al. (2017) [126] has documented that the CFC of the capping face of the 101 m^2/g SSA goethite is 9.4% instead of 14% when the step formations are not considered. Therefore, if the same CFC estimation method is used, our results are only slightly different (i.e., 5% vs. 9.4%) from the microscopic observations made by Hiemstra and van Riemsdijk (1996) [83].

3.5.2. Model optimization results

Titration curve simulations displayed in Figure 3-8 show that the model parameters determined using the established CFC-SSA correlation and parameter optimization procedure described above are capable of describing proton adsorption on the four SSA goethites used to develop the correlations at various ionic strengths; capacitance and protonation constant values obtained from the optimization process are listed in Table 3-11.

Table 3-11. CFC profile and optimization results of selected goethites

Literature	SSA (m^2/g)	Crystal Face Contribution[1)] (101)	(001)	(210)	Capacitance[2)] (F/m^2)	$pK_{a2,singly}$[2)]
Rahnemaie et al. (2006) [50]	98.6	58.2%	27.8%	14%	0.80	8.5
Vieira (2007) [127]	62.9	31%	55%	14%	1.05	8.5
Gaboriaud and Ehrhardt (2003) [33]	49	19%	45%	36%	1.10	8.9
Boily et al. (2001) [48]	37	19%	45%	36%	1.10	8.9

[1)] Determined by established CFC-SSA relationship in current study
[2)] Obtained by optimizing with potentiometric titration data

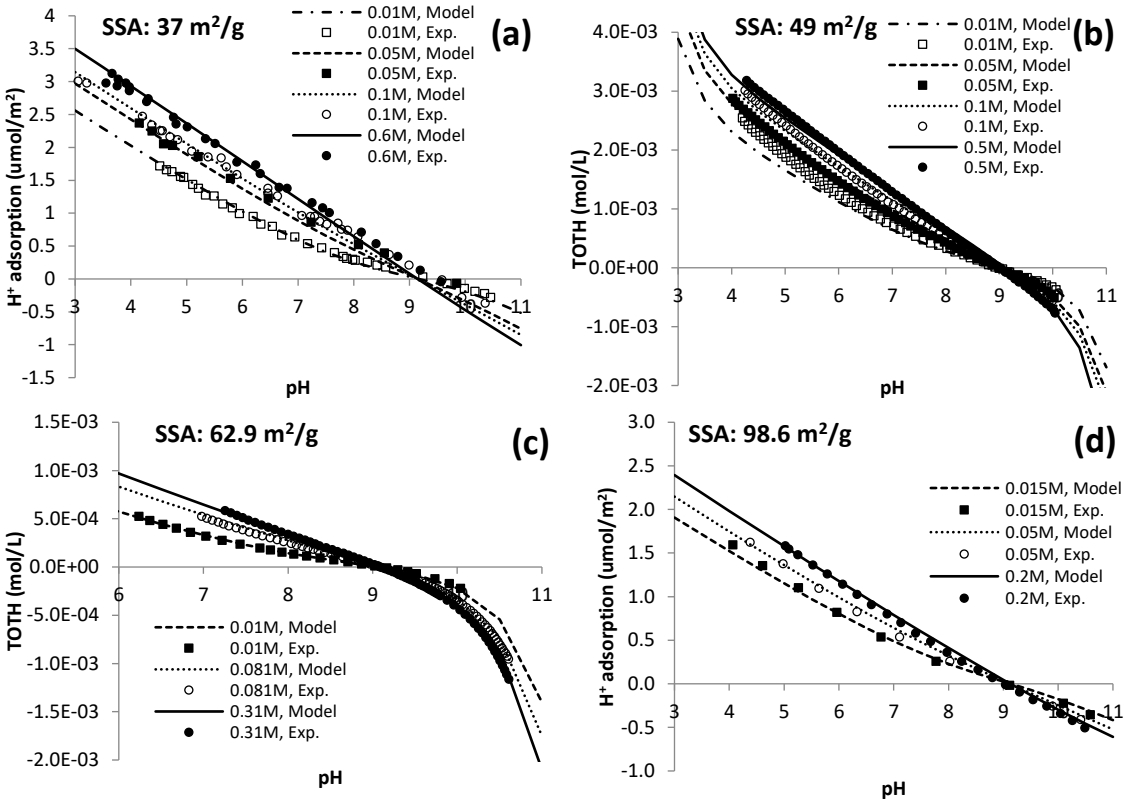

Figure 3-8. Potentiometric titration data from four different synthetic goethite preparations in various ionic strength solutions collected from literature and compared with optimized model predictions

3.5.3. Capacitance values and SSA relationship

The estimated capacitance values determined from the optimization are consistent with results from other previous studies (see Figure 3-9) which utilized various SCMs to establish capacitance-SSA relationships [31], [33], [43], [49], [51], [116], [118]. This supports the idea that capacitance values should be constrained within physically reasonable values regardless of the estimation method [15], [31], [51]. Description of these previous studies including the type of SCM used are listed in Table 3-12.

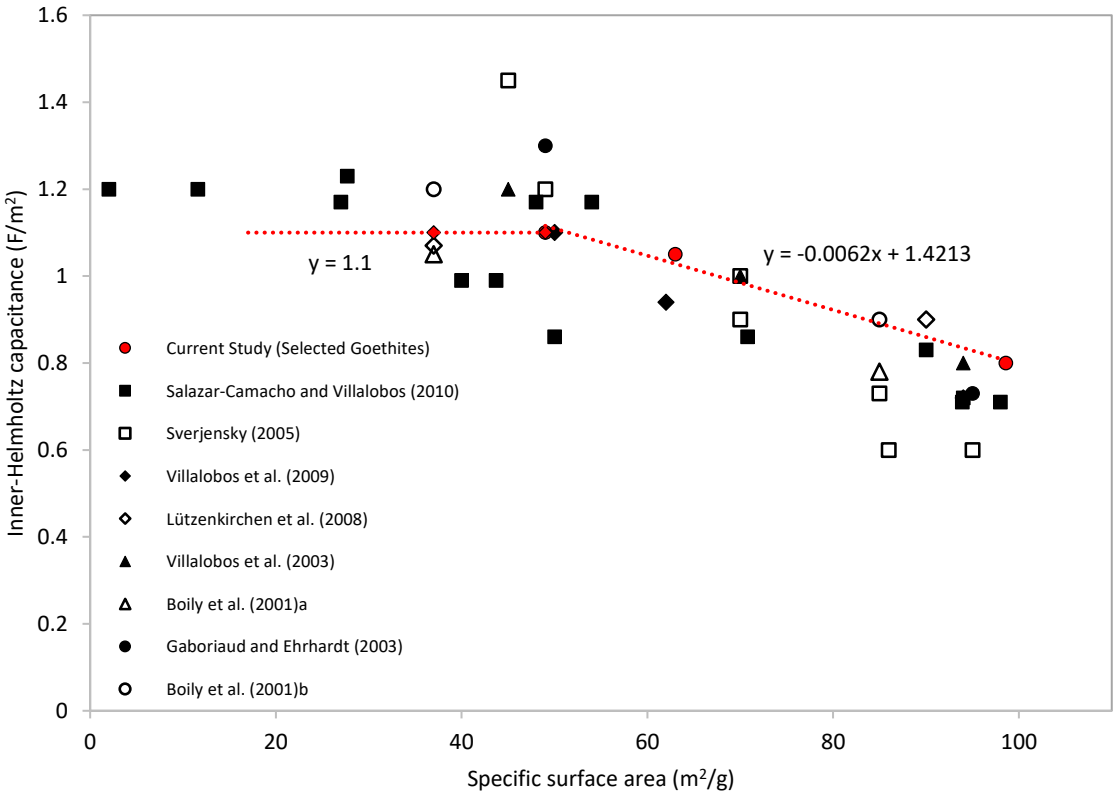

Figure 3-9. Comparison among optimized inner-layer capacitance values (C_1) of four selected goethite preparations (37, 49, 62.9, 98.6 m^2/g SSAs) and values reported in the literature for other goethites. Dash lines represent the relationship established in this research between inner-layer capacitance values (C_1) and SSAs of the selected goethites used to develop the relationship. Optimization was conducted by simultaneously adjusting C_1 and the protonation constant ($pK_{a2,singly}$) to fit titration data for each goethite.

Table 3-12. Description of SCMs and number of data points used to establish C_1-SSA relationships in other studies

Reference	SCM	Site and Protonation Description	# of Data Points
Current Study	CD-MUSIC	3-site, 1-pK_a for each singly- and triply-coordinated sites	4
Salazar-Camacho and Villalobos (2010) [116]	TLM+MUSIC	3-site, 2-pK_a for each singly- and triply-coordinated sites	13
Villalobos et al. (2009) [118]	TLM+MUSIC	3-site, 1-pK_a for each singly- and triply-coordinated sites	3
Villalobos et al. (2003) [31]	TLM	1-site, 2-pK_a	3
Sverjensky (2005) [51]	Modified TLM	1-site, 2-pK_a	7
Lützenkirchen et al. (2008) [49]	BSM	1-site, 1-pK_a	2
Boily et al. (2001)a [48] 1)	BSM	3-site, 1-pK_a	2
Boily et al. (2001)b [48] 1)	BSM	3-site, 1-pK_a for each singly- and triply-coordinated sites	2
Gaboriaud and Ehrhardt (2003) [33]	BSM	1-site, 1-pK_a	2

1) *Two types of model were suggested in the study*

Many previous studies have identified that capacitance values are inversely correlated with the SSA of goethites using simple linear relationships. Our results, however, show that the capacitance-SSA relationship may differ between high (ca. > 50 m^2/g) and low (ca. <50 m^2/g) SSA goethites, as plotted with dotted lines in Figure 3-9. In the low SSA range, a constant capacitance value of 1.1 F/m^2 appears to be independent of SSA, whereas an inverse linear relationship between capacitance and goethite SSA is apparent for higher SSA goethites. Regression of data from Table 3-11 indicates the slope of the linear relationship can be expressed as Eq. 3-8 on goethites with SSAs above 50 m^2/g:

Eq. 3-8) $C_1 = -0.0062 \times SSA + 1.4213$ *(when SSA > 50 m^2/g)*

A two-stage relationship between capacitance and SSA of goethite, as suggested in this study, has not been reported in previous studies. One possible reason for this might be the fact that most of the previous studies investigated only two or three goethite morphologies and only one or none had SSA below 50 m^2/g. As seen in Figure 3-9, only Salazar-Camacho and Villalobos (2010) [116] investigated a sufficient number of goethites less than 50 m^2/g to establish a trend. This study proposed a simple linear capacitance-SSA relationship over the entire SSA range studied. However, the similarities in capacitance values estimated for the goethites of SSA below 30 m^2/g suggest that capacitance may in fact be constant for low SSA goethites.

Interestingly, as seen in Figure 3-10, the resulting capacitance from our study closely correlates with the change in %CFC of the (101) crystal face on goethites. Considering that goethite crystals undergo step-wise growth on the (101) crystal face, it is expected that surface roughness (and consequently the capacitance) increases while the contribution of the (101) face decreases with crystal growth. Thus, our results suggest that the established capacitance-SSA relationship is also consistent with the estimated CFC of goethite.

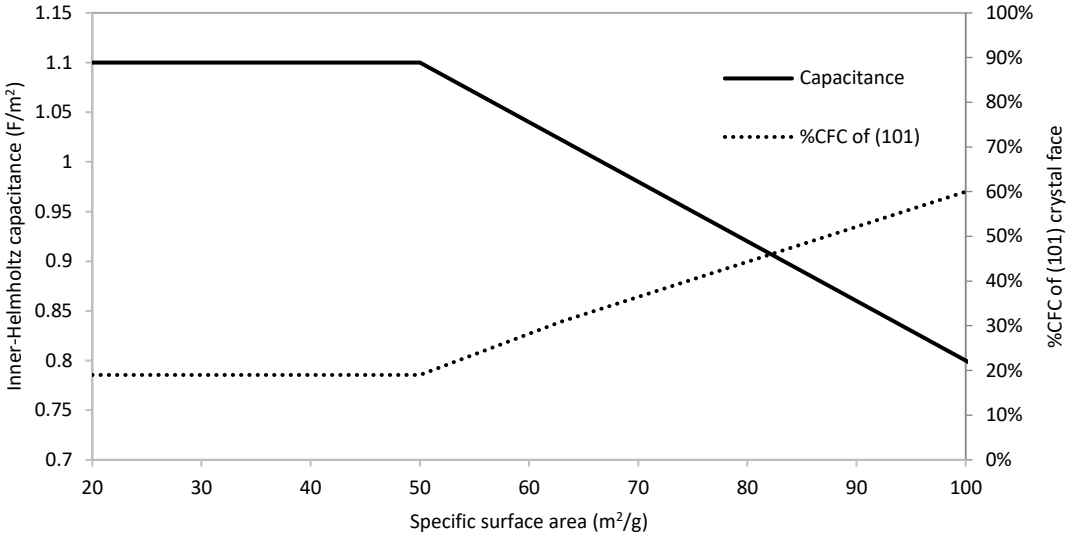

Figure 3-10. Inverse correlation between inner-Helmholtz capacitance (C_1) values and % CFC of the (101) crystal face dependent to SSA of goethite

3.5.4. Protonation constants and SSA relationship

The optimized value for the second protonation constant of the singly-coordinated surface oxygen ($pK_{a2,singly}$) for the 37 m^2/g, 49 m^2/g, 62.9 m^2/g, and 98.6 m^2/g SSA goethites were 8.9, 8.9, 8.5, and 8.5, respectively, which indicates a clear division between goethites with SSA below and above ca. 50 – 60 m^2/g. According to calculations made using the bond-valence method, singly-coordinated oxygens on the (210) face have considerably higher pK_a values than surface oxygens with the same coordination number on other faces. Therefore, it is expected that the "average" pK_a of singly-coordinated sites will closely correlate with the %CFC of the (210) face. The optimized $pK_{a2,singly}$ values obtained from this study follow this trend, and hence, the $pK_{a2,singly}$ – SSA relationship was established based on this expectation as seen in Figure 3-11.

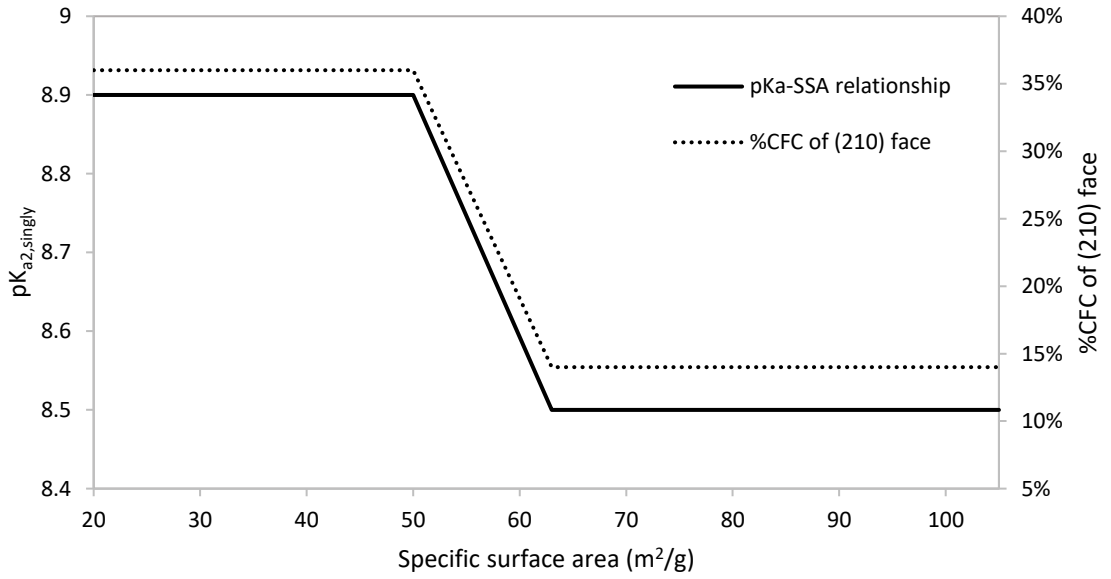

Figure 3-11. Established relationship between protonation constants of singly-coordinated surface oxygens ($pK_{a2,singly}$) and goethite SSA, and its correlation with the % CFC of (210) crystal face

3.6. VERIFICATION OF THE MODELING APPROACH

3.6.1. Methods

Once the relationships for SSA and CFC, capacitance and pK_a were established and CD-MUSIC parameters were determined, the parameterized model was used to predict proton, SeO_3^{2-}, and Cd^{2+} adsorption for a range of different goethite SSAs and solution conditions. For this, a variety of adsorption data, including potentiometric titration, adsorption edge (pH vs. % adsorbed at fixed initial concentration and goethite dose), and isotherm data (fixed pH) were obtained from literature data or experimental results. In order to minimize complicating factors in the model, only adsorption data obtained from solutions with $NaNO_3$ as the background electrolyte were selected in this study except for

two sets of Cd^{2+} adsorption data which were conducted with KNO_3 concentrations below 0.01 M. Potentiometric titration data were further screened to exclude datasets with point-of-zero-salt-effect (pH_{pzse}) values outside the range of 8.8 – 9.5, since this is an indication of possible contamination of goethite by carbonate or electrolytes. A pH_{pzc} value of 9.15 was used for all titration data which was the median value for the goethites used in this study. Simulations were conducted with the FITEQL 4.0 program without using the optimization function. Adjustments were made on the mass-balance expression of the 0-plane and equilibrium constants (log K) of multi-dentate species to account for non-zero charge reference state and improper representation of surface species in the original FITEQL4 code, respectively, as described by Tadanier and Eick (2002) [84] and Gustafsson (2003) [188]. Table 3-13 shows the resulting parameter values (i.e., CFC, capacitance, and pK_a) for each goethite SSA used in this study. The resulting goodness of fit values (WSOS/DF) for all predictions made by the model are listed in Table 3-14.

Table 3-13. CFC, capacitance, and pK_a values for each goethite obtained through the established approach

SSA (m^2/g)	Crystal Face Contribution			Capacitance (F/m^2)	$pK_{a2,singly}$	Adsorbate	Data from
	(101)	(001)	(210)				
21.3	19%	45%	36%	1.10	8.9	Cd^{2+}	Hoins et al. (1993) [189]
23	19%	45%	36%	1.10	8.9	H^+	Boily et al. (2001) [48]
49.6	19%	45%	36%	1.10	8.9	Cd^{2+}	Angove et al. (1999) [190]
50	19%	45%	36%	1.10	8.9	SeO_3^{2-}, Cd^{2+}	Current Study
62.9	31%	55%	14%	1.05	8.5	SeO_3^{2-}, Cd^{2+}	Vieira (2007) [127]
70	36.3 %	49.7 %	14%	0.99	8.5	H^+	Villalobos and Leckie (2001) [191]
73	38.6 %	47.4 %	14%	0.97	8.5	SeO_3^{2-}	Current Study
75.4	40.5 %	45.5 %	14%	0.95	8.5	Cd^{2+}	Theis et al. (1988) [192]
85	47.8 %	38.2 %	14%	0.90	8.5	H^+	Boily et al. (2001) [48]
94	54.7 %	31.3 %	14%	0.84	8.5	H^+	Villalobos et al. (2003) [31]
95	55.4 %	30.6 %	14%	0.83	8.5	H^+, Cd^{2+}	Venema et al. (1996) [82], Gaboriaud and Ehrhardt (2003) [33]
105±5	63.1 %	22.9 %	14%	0.77	8.5	H^+	Hiemstra and van Riemsdijk (1996) [83]

Table 3-14. Goodness of fit values (WSOS/DF) for all proton, SeO_3^{2-}, and Cd^{2+} adsorption data sets investigated for model verification

SSA (m^2/g)	Ionic Strength (M)	Model Fit (WSOS/DF)	SSA (m^2/g)	Surface Loading or pH ($\mu mol/m^2$)	Model Fit (WSOS/DF)
Proton Adsorption (Titration)			***Selenite Adsorption Edge***		
23	0.01 M	4.4	50	0.70	1.9
	0.05 M	10.3		2.61	10.7
	0.1 M	10.0		10.45	10.6
	0.6 M	15.0	73	0.75	7.3
70	0.015 M	22.4		3.73	5.9
	0.05 M	8.6		12.31	3.4
	0.1 M	14.0			
85 [1)]	0.003 M	6.2	***Cadmium Adsorption Edge***		
	0.01 M	6.6	21.3	0.011	7.8
	0.05 M	7.5		0.026	38.5
	0.1 M	5.9		0.11	86.5
94	0.015 M	20.8	49.6	0.53	30.8
	0.24 M	7.3	50	0.41 (at 0.01M IS)	8.4
95	0.005 M	15.7		0.41 (at 0.7M IS)	1.4
	0.01 M	7.6	75.4	0.22	42.1
	0.1 M	2.5			
95	0.01M	132.5	***Selenite Isotherm***		
	0.05M	93.4	62.9 [2)]	9.89	13.2
	0.1M	94.4			
	0.5M	40.4	***Cadmium Isotherm***		
105±5	0.005 M	10.4	62.9 [2)]	6.89	12.2
	0.01 M	14.3	95	5	52.9
	0.1 M	12.5		9	302.9

[1)] Titration data of the 85 m^2/g SSA goethite reported in Boily et al. (2001) [48] *is identical to that of 90 m^2/g SSA goethite reported in Lützenkirchen et al. (2008)* [49]. *Regardless of whether 85 m^2/g or 90 m^2/g is considered as the SSA of the goethite, the model predictions provided similar fit to the titration data in our study.*
[2)] Model prediction previously published in Mangold (2013) [89]

3.6.2. Prediction of proton adsorption

The modeling results for proton adsorption on various goethites are plotted in Figure 3-12-(a) – (g). The model was able to provide satisfactory predictions ($0.1 <$ WSOS/DF < 20) of most data sets that were consistent with the pre-documented trend in which lower SSA goethites yield greater proton reactivity (i.e., steeper slope). Figure 3-12-(h) demonstrates how the model prediction changes for different SSA goethites at a given ionic strength (i.e., 0.1M $NaNO_3$ solution) when utilizing the parameters determined in this study.

Gaboriaud and Ehrhardt (2003) [33] and Venema et al. (1996) [82] both conducted titrations on 95 m^2/g SSA goethite, but their results deviated considerably from each other. The cause for the difference in proton adsorption behavior of the 95 m^2/g SSA goethites between these studies was not identified. Our model was able to make satisfactory predictions for the data of Venema et al (1996) [82] (Figure 3-12-(e)), but returned WSOS/DF values larger than 40 for all four titration data sets of Gaboriaud and Ehrhardt (2003) [33] (Figure 3-12-(g)). Since the estimation of model parameters is solely based on SSA, it is not surprising that our model can only fit one of the two data sets when the SSA of the goethites used for the titration are identical. Further investigation is required to fully understand the cause of the discrepancy between the two data sets. However, it is worth noting that Venema's data matches more closely with that of Villalobos et al. (2003) [31] where a 94 m^2/g SSA goethite was used, while Gaboriaud and Ehrhardt's data showed relatively lower proton reactivities compared to other data including those of Hiemstra and van Riemsdijk (1996) [83] which used 105 m^2/g SSA goethites.

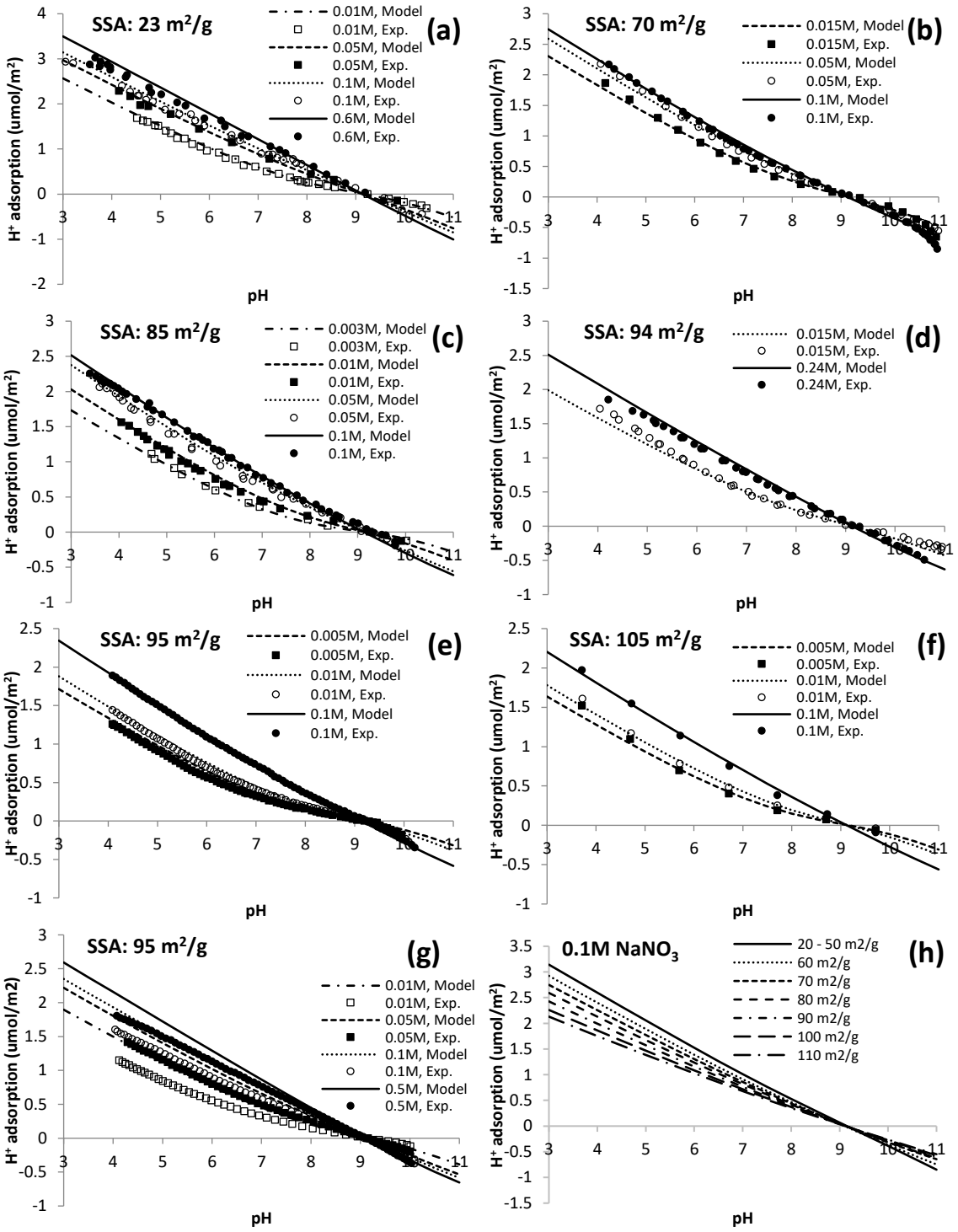

Figure 3-12. Model prediction results in comparison with proton adsorption experimental data collected from literature; Circle symbols represent experimental data and solid lines represent model predictions

3.6.3. Prediction of selenite adsorption

Figure 3-13 shows model predictions for selenite adsorption on three goethites made by utilizing surface complex species and equilibrium constants determined by Mangold (2013) [89]. The model predictions show good agreement (WSOS/DF < 20) with the adsorption edge data at three different maximum surface loadings for goethites of 50 m^2/g and 73 m^2/g SSA (Figure 3-13-(a) and (b)). Maximum surface loading is defined as the total moles of adsorbate added to the system per unit area of adsorbent surface (m^2). The isotherm data and modeling results for the 62.9 m^2/g SSA goethite (Figure 3-13-(c)) were published previously in Mangold (2013) [89], which utilized identical modeling parameters as used in this study. Although slight overprediction was obtained in the high range of aqueous selenite concentration, the model was capable of providing accurate predictions for data with selenite concentrations less than 1.0×10^{-4} M.

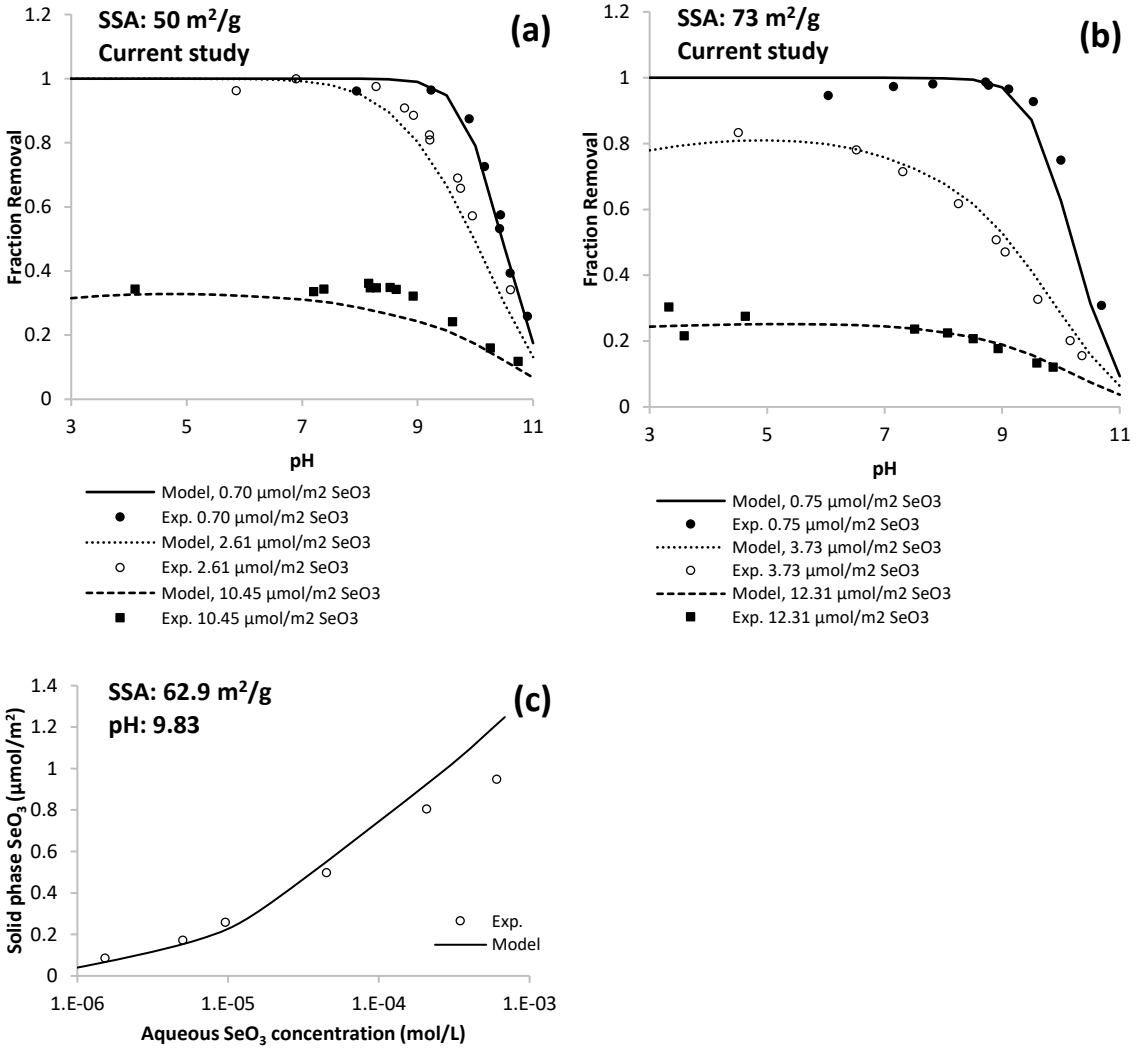

Figure 3-13. Model predictions of SeO_3^{2-} adsorption edge data and isotherm data collected from experiments and literature, respectively; Symbols represent experimental data and solid lines represent model predictions. The SSA of goethite used in each study are, (a) 50 m^2/g, (b) 73 m^2/g, and (c) 62.9 m^2/g [89]

3.6.4. Prediction of cadmium adsorption

Predictions of four Cd^{2+} adsorption edges and two isotherms were made as shown in Figure 3-14 by utilizing the Cd surface complex species and the equilibrium constants

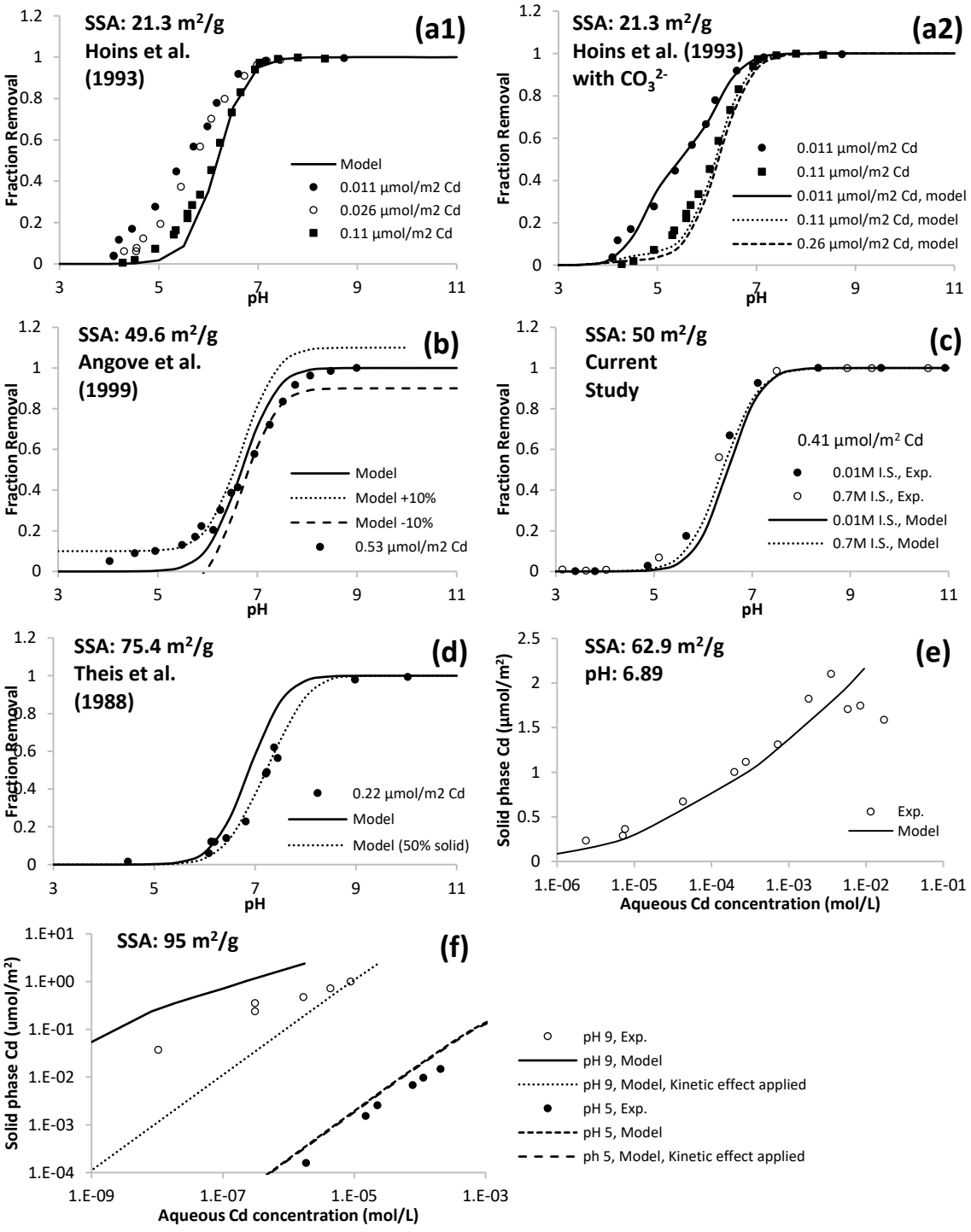

Figure 3-14. Model predictions of Cd^{2+} adsorption edge and isotherm data collected from literature or experiments conducted as part of this study; Symbols represent experimental data and lines (solid, dotted, and dashed) represent model predictions

employed by Mangold (2013) [89]. These data were collected over a range of maximum surface loading from 0.011 μmol/m^2 to 0.53 μmol/m^2.

Typically, at moderate surface loadings, a larger fraction of Cd adsorbs onto the goethite surface at a given pH as surface loading decreases. This trend is also observed in the data of Hoins et al. (1993) [189] (Figure 3-14-(a1)) for Cd adsorption experiments conducted with three different maximum surface loadings ranging between 0.011 μmol/m^2 and 0.11 μmol/m^2 on a 21.3 m^2/g SSA goethite. However, while our model satisfactory predicted the 0.11 μmol/m^2 Cd loading data, it failed to capture the trend of increasing fractional removal for smaller surface loadings; in fact, the model predicted no change in fractional adsorption with decreasing surface coverage. Previous research by Benjamin (1981) documented that fractional adsorption of Cd may not be affected by surface loadings when loadings are low [112]. In their study, fractional removal of Cd onto amorphous iron oxyhydroxide (i.e., $Fe_2O_3 \cdot H_2O$(am)) was not impacted by surface loading when the Fe:Cd ratio was in the range of 2×10^{-5} - 2×10^{-6}. This range of Cd loading is similar to that of Hoins et al. (1993) [189] when the number of reactive sites per Fe on amorphous iron oxyhydroxide for Cd adsorption is assumed to be in the range of 0.001 – 0.005 mol/mol Fe as reported in literature [18], [193], [194]. The increased fractional removal at lower Cd loadings observed in data of Hoins et al. (1993) [189] may have been due to intrusion of carbonate in the system. A relatively low pH_{pzc} (i.e., pH 7.8) was reported for the goethite in their study, which is commonly regarded as an indication of carbonate contamination [195], [196]. Carbonate ions may adsorb onto goethite and lower the surface charge, which would lead to increased metal cation adsorption proportional to the amount of carbonate adsorbed. This would result in greater increase in fractional removal of metal cations for lower surface loading. This effect can be simulated by using carbonate CD-MUSIC

parameters suggested by Rahnemaie et al. (2007) [147], and including a Cd-CO_3 ternary complex. As in Figure 3-14-(a2), the model results show that fractional removal of Cd can increase when surface loading is lowered due to interaction with carbonate; fractional removal is negligibly impacted when surface loading is raised ($[CO_3]_T$ was optimized to 1.5×10^{-6} M).

The model predictions made for adsorption data of Angove et al. (1999) [190] (Figure 3-14-(b)) yielded a WSOS/DF value of 30.8, slightly exceeding the criterion for a satisfactory fit (WSOS/DF < 20). However, the results were within a ±10% error range as shown in the dotted and dashed lines. Adsorption tests with similar SSA goethite and Cd loadings to Angove et al. (1999) [190] were conducted in the current study for two different ionic strengths; 0.01M and 0.7M by $NaNO_3$. The modeling results are shown in Figure 3-14-(c). The model provided accurate fits to both sets of adsorption data (WSOS/DF < 20) and no significant ionic strength effect was observed in the experiment or in the model predictions.

For the adsorption data of Theis et al. (1988) [192], model results returned approximately 20% higher fractional removal of Cd in the pH range of 6 – 8 (Figure 3-14-(d)). The cause of such discrepancy is unclear. The model provided better fit to the data when the goethite concentration was reduced. The goethite concentration reported in the study was 0.6 g/L which is approximately an order magnitude lower than used in typical adsorption studies. Dzombak and Morel (1990) [18] documented that loss of sorbent to vessel walls can be significant when solid concentrations are in this lower range. Also, the study used glass containers for reactors which generally leads to more adhesion of high pH_{pzc} oxide minerals, such as goethite, compared to plastic containers.

The model was also capable of predicting Cd^{2+} adsorption isotherms (Figure 3-14-(e) and (f)). It should be noted that the isotherm prediction for the 62.9 m^2/g SSA goethite (Figure 3-14-(e)) was originally published by Mangold (2013) [89]. Slight overprediction was made for the two isotherms on the 95 m^2/g SSA goethite, for which experimental data were provided by Venema et al. (1996) [82] (Figure 3-14-(f)). Although the deviation between the experimental data and modeling results seems large for the pH 9 isotherm, the differences in percent Cd^{2+} removal between data and predictions are less than 2%p for all data points. In fact, the data are based on a 4 hour equilibration time, and Venema et al. (1996) [82] reported approximately 2.1%p difference in percent Cd^{2+} removal between 4 and 100 hour of equilibration times in various experimental conditions as part of a kinetic study. The dotted line in Figure 3-14-(f) shows how the modeling result changes when predictions are lowered by 2.1%p. Moreover, considering the fact that experimental and analytical error can be larger than 2.1%, our modeling results for the pH 9 isotherm appear reasonable.

3.7. CONCLUSIONS

The results from this study suggest that a generic method to predict the CFC, capacitance, and pK_a of goethites based on its BET-SSA can be established by combining information for the goethite surface-water interface obtained from a number of different studies and measures, including microscopic investigation, theoretical calculations, modeling analysis, and macroscopic adsorption experiments. With the established relationships between surface parameters and the SSA of goethites, a CD-MUSIC model was capable of predicting proton, SeO_3^{2-} (oxyanion), and Cd^{2+} (metal cation) adsorption

for a range of different goethite morphologies (i.e., 20 – 105 m^2/g SSA) and solution chemistries (i.e., pH 3 – 11, various ionic strengths and surface loadings).

The significance of this study arises from its convenience in modeling the variable reactivity of goethites where only a single parameter, the BET-SSA, is required; which is relatively easy to obtain with precision. It is also meaningful that the relationships developed between goethite SSA and CFC, capacitance, and pK_a are all consistent with most surface property trends found in the literature. Moreover, the surface reactivity model developed can serve as a basis for parameterizing self-consistent SCMs for other aqueous ions and can be used to link results between studies which use different goethite morphologies. Thus, it will be possible to develop a comprehensive SCM database for goethite. It is also possible that the approach can be extended to other well-crystallized minerals.

It should be noted that obtaining accurate measurements of BET-SSA values is crucial for the current approach, since error in SSA values may impact the modeling results. This is particularly a concern for goethites with SSAs ranging between 50 – 63 m^2/g; the CFC and proton affinity constants of these goethites are assumed to shift sharply as the SSA changes, which results in high sensitivity of the model towards SSA. However, modeling results of goethites with SSAs below 50 m^2/g and above 63 m^2/g are relatively insensitive to the SSA value.

Chapter 4. Impact of Background Electrolyte Ions on the Adsorption of Alkaline Earth Metal Ions onto Goethite

4.1. INTRODUCTION

Background electrolytes, most commonly Na^+, K^+, Mg^{2+}, Ca^{2+}, Cl^-, NO_3^-, and SO_4^{2-}, are ubiquitous in natural waters and are known to affect adsorption of other ions on mineral surfaces [4], [86], [98], [197]. Generally, electrolytes present at relatively high concentrations have adverse impacts on metal ion adsorption, either through competition between ions for surface sites, effects on the electrical double layer properties, or interactions with adsorbing ions [45], [50], [64], [74], [89], [112], [165], [186], [198], [199]. Reduced adsorption is often more significant with increasing electrolyte concentration [72], [74], [198]–[200].; however the degree of impact of electrolytes on adsorption strongly depends on the type of electrolyte, adsorbing metal ion, and mineral surfaces that are present in system [72], [74], [98], [197].

Many hazardous metal ions that are of interest to environmental systems possess high affinity for oxide surfaces, and therefore electrolyte effects are only evident when background electrolytes are present at high concentrations (i.e., >0.1M ionic strength). The adsorption of weakly adsorbing alkaline earth metal ions, however, is known to be more sensitive to background electrolytes compared to strongly sorbing transition metal ions due to their low charge densities [18]. Thus, alkaline earth metal ions represent ideal probes for investigating electrolyte effects on metal ion adsorption. The major downside of employing alkaline earth metal ions for this purpose is the lack of spectroscopic tools that extend across this periodic group. Nevertheless, it is possible to isolate and identify the effects of electrolytes on alkaline earth metal ion adsorption utilizing macroscopic

adsorption studies, molecular dynamics and surface complexation modeling. Understanding the impact of background electrolytes as well as the trends in alkaline earth metal ion adsorption can further enhance our capability to predict adsorption of more hazardous metal ions onto oxide surface in saline solutions.

The objective of this study was to evaluate the effect of different electrolytes on alkaline earth metal ion (i.e., Mg^{2+}, Ca^{2+}, Sr^{2+} and Ba^{2+}) adsorption onto goethite by conducting macroscopic adsorption experiments over a range of solution conditions. The underlying hypothesis is that the impact of electrolytes on adsorption of metal ions to oxide surface is a combined effect of competitive adsorption (with cationic electrolytes) and aqueous complexation (with anionic electrolytes); such effects will be clearly observable in macroscopic studies of alkaline earth metal ion adsorption on oxide minerals.

4.2. MATERIALS AND METHODS

4.2.1. Goethite preparation

Goethite, the selected adsorbent for this study, was synthesized in the laboratory. Goethite was prepared according to the method described by Schwertmann et al. (1985) [46], Peak et al. (1999) [166] and further refined by Vieira (2007) [127], where $Fe(NO_3)_3$ was used as the precursor and aged for 14 days in a KOH solution at 25°C. The entire synthesis process was performed inside a N_2 gas-filled glove box (Protector®, Labconco, Kansas City, MO) in order to minimize potential contamination of CO_2, and degassed CO_2-free ultrapure water of 18.2MΩ-cm resistivity (Barnstead™ Nanopure™, Thermo Fisher Scientific, Waltham, MA) was used to wash out impurities remaining on the solids. Use

of glassware was avoided during the entire synthesis process due to risk of silica contamination.

Characterization of solids was conducted using N_2-BET (Quantachrome Instruments, Boynton Beach, FL) and x-ray diffraction (XRD, Philips Analytical, Amsterdam, Netherlands). The pH_{pzse} of goethite was determined by potentiometric titration [23]. For the BET analysis, the goethite samples were freeze-dried prior to being weighed and degassed at room temperature for at least 24 hours to ensure stable measurement of surface area while avoiding errors associated with phase transformation to non-stoichiometric hematite [201]; approximately 0.3 – 0.5 g of dried goethite was used for each measurements. Three different types of goethite were prepared, with specific surface area (BET-SSA) values of 50 m^2/g, 64.5 m^2/g, and 73 m^2/g. The SSA values of the goethites were similar to values reported in previous studies using the same preparation method [89], [127]. The pH_{pzse} of 9.1 was also within the range of 9.0 – 9.5 which has been documented in many studies that have minimized CO_2 contamination [31], [48], [49], [202], [203].

4.2.2. Batch adsorption experiments

Adsorption of alkaline earth metal ions (i.e., Mg^{2+}, Ca^{2+}, Sr^{2+}, and Ba^{2+}) on goethite was investigated by conducting a series of batch adsorption experiments to obtain adsorption edges for each adsorbate over a range of various solution conditions. Batch reactors were prepared in 15 mL polypropylene vials. Stock solutions containing adsorbent media particles (goethite), alkaline earth metal ions and background electrolyte were also prepared and stored in polypropylene bottles. To eliminate possible contamination in vials and bottles, all vessels were soaked in a nitric acid bath for at least 8 hours and rinsed with

ultrapure water prior to use. After rinsing, purified compressed air was used to blow out any remaining water droplets from the vessels. Degassed CO_2-free ultrapure water and high purity salts (> 99.999%, Puratronic® by Alfa Aesar) were used to prepare stock solutions in order to minimize contamination of unwanted ions in the solution. The alkaline earth metal ion stock solutions were made from nitrate salts of each metal ion at a concentration range of 10^{-5} – 10^{-3} M and were acidified to 0.318 N nitric acid (Trace metal grade, Fisher Scientific) for preservation. The electrolyte stock solutions were made from high purity $NaNO_3$, NaCl, $NaClO_4$, KNO_3, $RbNO_3$, and $CsNO_3$ salts at multiple concentrations ranging from 0.01 M to 0.7 M. Goethite slurries were prepared in concentrations ranging from 1 g/L – 9.4 g/L. The whole process of preparing the stock solutions and batch reactors was performed inside an N_2 gas-filled glovebox to avoid introduction of carbonates.

Once the contents of the batch reactors were added, pH was adjusted using either 0.1N HNO_3, 0.1N HCl or 0.1N NaOH depending on the electrolyte composition and target pH. Reactors were then placed on a shaker in a 25°C temperature-controlled room for equilibration. Equilibration time was set to 24 hours, based on results of a preliminary test which compared Sr^{2+} fractional removal between 24 and 90 hours of equilibration time; the test was conducted in 0.1M $NaNO_3$ solution with pH ranging between 8 – 11. Many previous adsorption studies conducted with goethite have also documented that equilibrium in batch adsorption reactors can be reached within 4 – 20 hours of reaction [50], [73], [83], [98], [165]. After equilibration, samples were centrifuged at 3,500 rpm in a JA-20 fixed-angle rotor (Beckman Coulter®), which was equivalent to relative centrifugal field of approximately ×1,000 g. The supernatants were taken out of the reactors with a non-rubber plunger syringe and filtered with 0.45 μm polyethersulfone (PES) membrane syringe filters

for analysis. Rubber plunger syringes and cellulose acetate and polypropylene membranes were avoided since it was found that a considerable amount of Ca^{2+} may leach from these materials into samples at low pH (i.e., below pH 4.5). In addition, blank tests (i.e., reactors without goethite) conducted on Mg^{2+}, Ca^{2+}, and Sr^{2+} have confirmed that the loss of these cations onto vial walls and membranes is minimal.

For every experimental set, 6 types of blanks were prepared in triplicates to ensure accurate analysis and identify possible contamination in each stock solutions. The composition of each blank was as listed below (pH was not adjusted) :

- Blank 1: Millipore water (MPW) only
- Blank 2: Millipore water + 2% vol/vol nitric acid
- Blank 3: Alkaline earth metal stock solution + MPW
- Blank 4: Electrolyte stock solution + MPW
- Blank 5: Goethite + MPW
- Blank 6: Goethite + Electrolyte stock solution + MPW

4.2.3. Analysis

The metal cation composition of each filtered sample was analyzed by inductively coupled plasma - optical emission spectrometry (ICP-OES) (ICP 710, Agilent Technologies, Santa Clara, CA). To minimize the impact of solution matrix, samples were diluted by a factor of 20, and an internal standard prepared with scandium was used for quality control. The dilution factor of 20 was determined after conducting preliminary tests with Mg^{2+}, Ca^{2+} and Sr^{2+}; no matrix effects were observed among different solution matrices with electrolyte concentrations between 0.01 M – 0.3 M when samples were

diluted by a factor of 20. The minimal matrix effect was due to the fact that the nitric acid, which was used for acidification of all samples and standards, became the dominating constituent in all samples after the dilution (i.e., the NO_3^- concentration contributed by nitric acid preservation was approximately 0.32 M). However, matrix effects were still observable for the 0.7 M ionic strength samples even after the 1/20 dilution. The dilution factor had to be at least 50 to reduce the matrix effect in 0.7 M ionic strength samples to a negligible level. However, with such high dilution factor, the error associated with the dilution procedure was considered to be comparable to the matrix effect, and thus, the dilution factor was compromised to 20. For the 0.7 M ionic strength samples, a separate set of standards was prepared in solution matrices identical to the samples. Matrix spiking was conducted to verify the validity of the established sample preparation protocols.

Standards were prepared by diluting commercial metal cation standard solutions. All four alkaline earth metals and cadmium were in a single set of standards, with the lowest concentration at 0.5 µg/L. Matrix spiking was conducted to assure 0.5 µg/L was above the detection limit for all target cations. In most of the experiments 0.5 µg/L was less than 0.5% of the total injected concentration of the targeted cation, and thus, any measurements below 0.5 µg/L were regarded as 100% adsorption; this simplification had minimal impact on the subsequent modeling analysis. In cases where 0.5 µg/L corresponded to more than 0.5% of the total injected concentration, a lower dilution factor was applied to the sample and a separate set of standards that match the matrices of the samples were used for the analysis.

The pH of each reactor was measured in a N_2-filled glovebox at 25°C, with a Thermo Orion® ROSS® combination pH electrode (8103BNUWP). Depending on the pH range of the sample set, either 2 or 3 buffer solutions among pH 4, 7, and 10 standard buffer

solutions were used to calibrate the pH probe. Measurements were only used when the potential-pH correlation was above 98.5% and potential drift at pH 7 was less than ±20 mV.

4.3. RESULTS AND DISCUSSIONS

4.3.1. Affinity trends for alkaline earth metal ion sorption onto metal oxide surfaces

The trend in surface affinity of alkaline earth metal ions on goethite is clearly observable through the comparison of adsorption test results. Metal ion adsorption onto surfaces is commonly expressed in terms of fractional removal of the ion as a function of pH, which is called the adsorption edge [83]. As shown in Figure 4-1, the adsorption edges on goethite are shifted toward lower pH range as the radius of non-hydrated alkaline earth metal ions become smaller ($Mg^{2+} < Ca^{2+} < Sr^{2+} < Ba^{2+}$). The observed adsorption trend of alkaline earth metal ions is consistent with previous research indicating that smaller cations are more favorably adsorbed on goethite. [44], [64], [165], [204].

The inverse relationship between intrinsic adsorption constants and ionic radii of divalent metal ions can be explained in various ways as done by previous researchers. Stumm et al. (1976), Schindler et al. (1976) and Schindler (1985) [16], [17], [21] suggested that the relationship is correlated to the first hydrolysis constant (Ka_1) of the alkaline earth metal ion, since adsorption to a mineral surface hydroxyl group is thermodynamically analogous to hydrolysis reactions as both involve complexation with an oxygen atom. Also, Zhang et al. (2004) [77] has correlated the trend to the distance between the specifically adsorbed ion and the surface oxygen, while Rahnemaie et al. (2006) [64] suggests that it is a result of different binding mechanisms of alkaline earth metal ions on goethite (i.e., Mg^{2+}

as inner-sphere, Ca^{2+} as combination of inner- and outer-sphere, and Sr^{2+} as an outer-sphere complex).

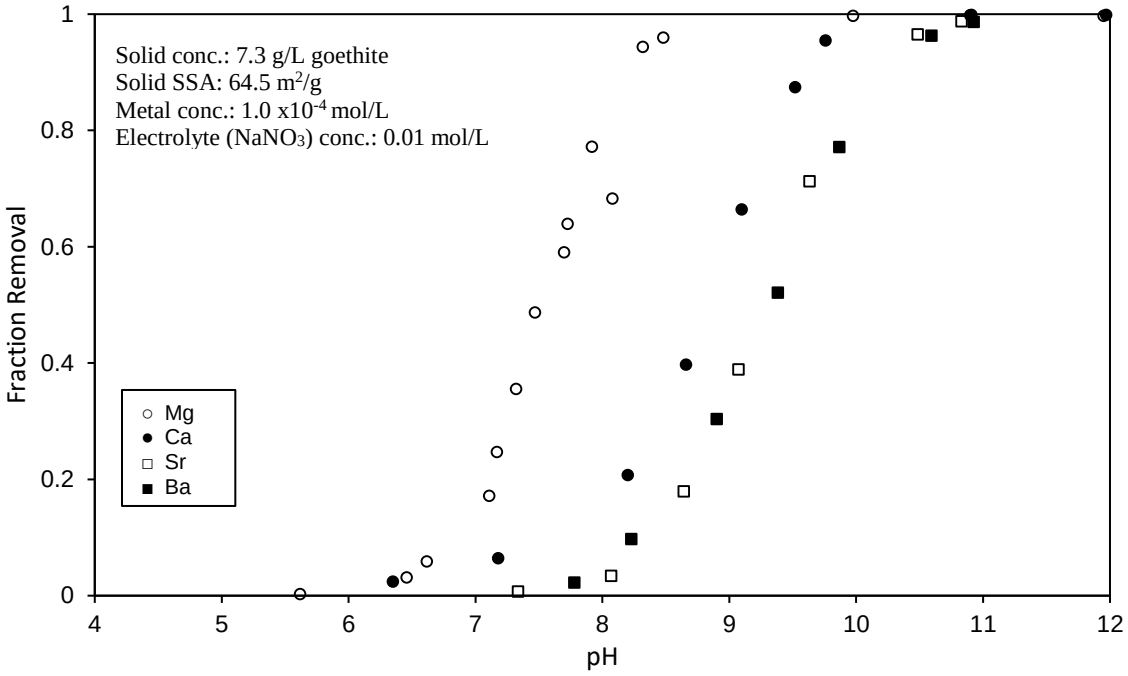

Figure 4-1. Trends in adsorption edges of alkaline earth metal ions on goethite

By adopting the Born solvation and crystal-chemical theory, Sverjensky (2006) [44] was able to predict the adsorption constants of alkaline earth metal ions on various oxide minerals and relate the adsorption behavior to the dielectric constant of the mineral. It was suggested that for high dielectric constant solids (e.g., rutile, magnetite, manganese dioxide), where there is essentially no opposing solvation energy involved, ion adsorption correlates with crystal radius (i.e., $Ba^{2+} > Sr^{2+} > Ca^{2+} > Mg^{2+}$). In contrast, in low dielectric constant solids (e.g., hematite, gibbsite, goethite and silica), the trend is reversed as observed in our present study.

4.3.2. Impact of the presence of additional alkaline earth metal ions

Competition between alkaline earth metal ions for adsorption sites may occur when more than one metal cation is present in solution. Figure 4-2-(a) and Figure 4-2-(b) show the adsorption edges of Mg^{2+} and Ca^{2+} on goethite, respectively, and compare the adsorption of each ion with and without the presence of the other ion in solution. The presence of Ca^{2+} had little or no impact on the adsorption of Mg^{2+}, while the presence of Mg^{2+} significantly reduced the adsorption of Ca^{2+}.

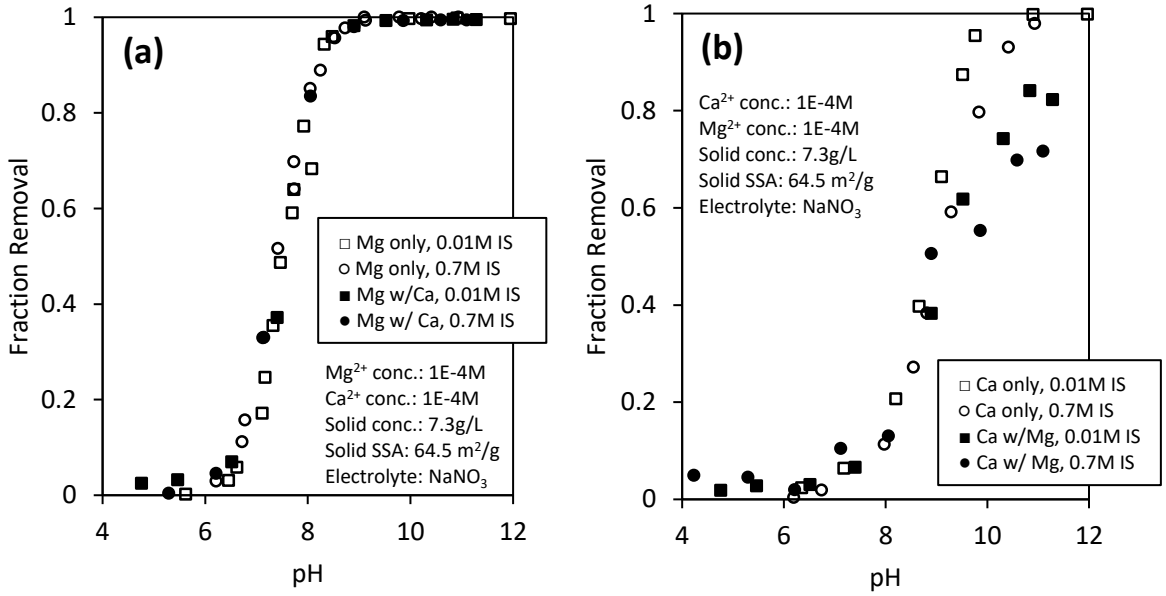

Figure 4-2. Adsorption edges for (a) Mg^{2+} and (b) Ca^{2+} on goethite with and without the presence of the other metal cations in two different $NaNO_3$ solutions (i.e., 0.01M and 0.7M)

4.3.3. Impact of electrolyte concentration

Figure 4-3 displays the effect of raising the $NaNO_3$ background electrolyte concentration. The electrolyte concentration inversely impacts the adsorption of alkaline

earth metal ions, and the degree of impact becomes greater for ions with less affinity to the surface. Reduced adsorption in high concentration electrolyte solutions has been commonly observed in many adsorption studies. It is assumed that background electrolytes may affect the adsorption of ions by varying the surface charge of minerals, competing with ions for surface sites, and/or by directly interacting with adsorbing ions [18], [50], [199], [200], [64], [73], [74], [86], [98], [165], [197], [198].

The degree of impact was shown to follow the order $Ba^{2+} > Sr^{2+} > Ca^{2+} > Mg^{2+}$. For Mg^{2+}, the effect of $NaNO_3$ as background electrolyte is almost negligible in the concentration range of 0.01M – 0.7M. This agrees with findings from Talebi Atouei et al. (2016) [165] where no significant effect on Mg^{2+} adsorption on goethite was observed in 0.01M - 0.3M NaCl solutions. Our Ca^{2+} test results are also similar with Talebi Atouei et al. (2016) [165], where it is reported that Ca^{2+} adsorption is not affected by ionic strength in the range of 0.01M – 0.1M. However, our study shows that when ionic strength is further raised (e.g., 0.7M), the adsorption of Ca^{2+} is reduced. The effect of increased electrolyte was significantly greater for adsorption of Sr^{2+} and Ba^{2+} in our study, similar to results reported for Sr^{2+} adsorption on various mineral surfaces [72], [198], [199].

The results from the experiment suggest that the competition between the alkaline earth metal cations and the electrolyte cation, which is in this case Na^{+}, reduces divalent cation adsorption. Divalent cations generally have stronger attraction to the mineral surface than monovalent ions [64], [205]–[209]. However, the weak complexing power of monovalent alkali ions can be outweighed by their high concentration, and thus, influence the adsorption of stronger complexing metal ions [57]. Therefore, higher concentration and/or greater adsorption affinity of electrolyte cation (e.g., Na^{+}) will result in greater competition with alkaline earth metal ions for adsorption to oxide surfaces. In the case of

Mg^{2+}, no electrolyte effects were observed which is presumably due to the relatively high affinity of these metal cations to the surface. However, it is still possible that the adsorption of Mg^{2+} maybe reduced when the Na^{+} concentration is raised higher than 0.7M.

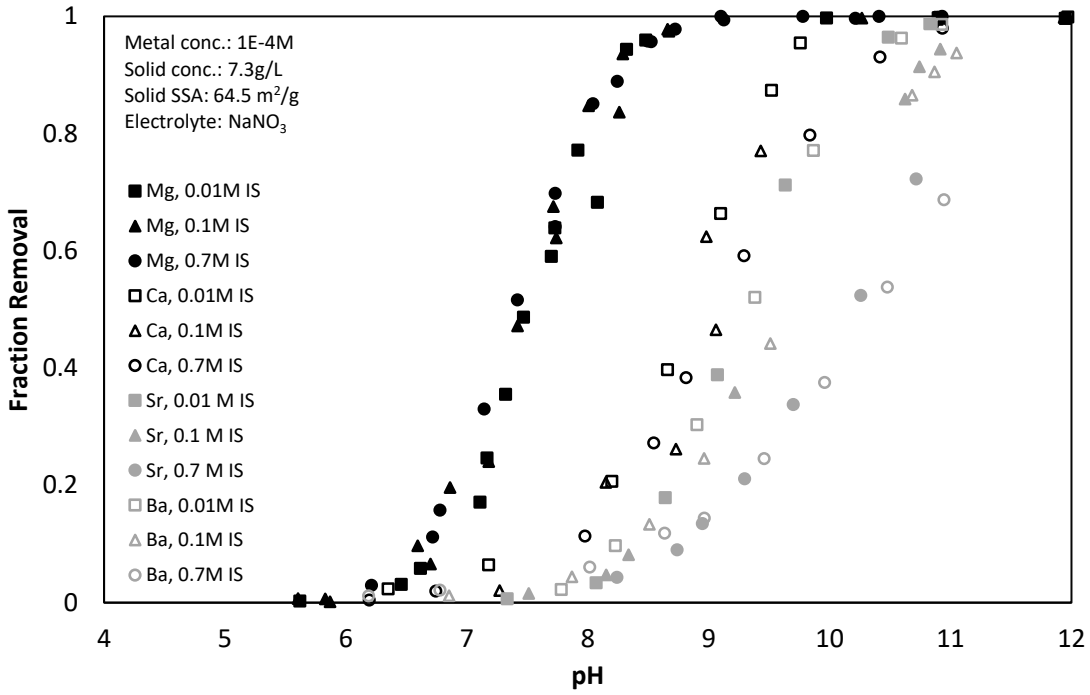

Figure 4-3. Adsorption edges for alkaline earth metal ions on goethite under various $NaNO_3$ concentrations. Clear trends in affinity with the surface is observed which is in the order of $Mg^{2+} > Ca^{2+} > Sr^{2+} > Ba^{2+}$

4.3.4. Impact of electrolyte cations

All of the previous results utilized sodium as the background cation. Sodium and potassium are the most commonly used background electrolytes in adsorption studies in large part due to their widespread occurrence in natural waters. Figure 4-4-(a) examines

differences in Ba^{2+} adsorption on goethite for $NaNO_3$, $RbNO_3$, and $CsNO_3$ solutions. More Ba^{2+} is adsorbed on goethite as the non-hydrated radii of the cationic electrolyte in solution increases (i.e., $Cs^+ > Rb^+ > Na^+$). These results can be explained by the difference in surface affinities of Na^+, Rb^+ and Cs^+, and their competition for surface sites with Ba^{2+}. In other words, as the surface affinity of the cationic background electrolyte decreases, more Ba^{2+} is able to adsorb onto goethite due to reduced competition. The relationship between the size of cationic electrolytes and their affinity to goethite is based on the assumption that the trends for adsorption of the alkali metal ions are the same as the alkaline earth metal ions where larger ionic radius results in lower affinity as described in Sverjensky (2006) [44]. This assumption is further supported by the study of Rahnemaie et al. (2006) [64] which suggested that Na^+ must be located closer to the goethite surface than K^+ and Cs^+, based on fitting titration data for goethite in different electrolyte solutions using a CD-MUSIC model.

In contrast to Ba^{2+} adsorption, no notable differences in Mg^{2+} adsorption were observed between experiments with KNO_3, $RbNO_3$ and $CsNO_3$ as electrolytes (Figure 4-4-(b)). The minimal impact of electrolytes on the adsorption of Mg^{2+} is presumably due to the strong surface affinity of Mg^{2+} which diminished the effect of the alkali metal electrolytes at concentrations of 0.7M. Both test results further substantiate one of our assertions, which has been illustrated previously in this study, that competition between cations for adsorption sites is a major factor that determines the electrolyte effect on alkaline earth metal ion adsorption.

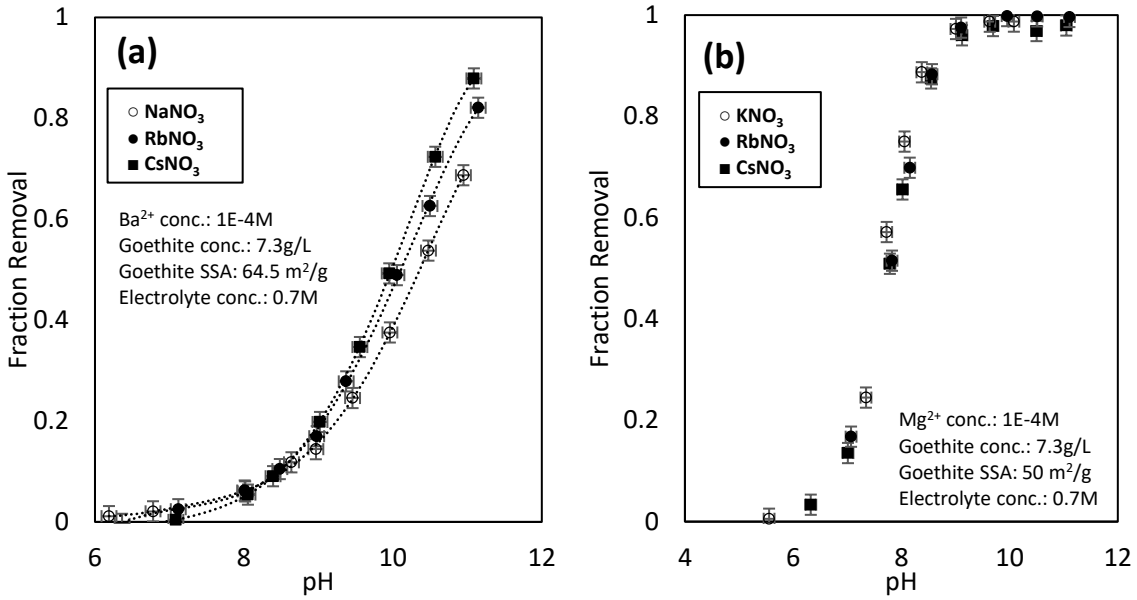

Figure 4-4. Adsorption edges for (a) Ba^{2+} on goethite in Na^{+}, Rb^{+} and Cs^{+} cationic electrolyte solutions, and (b) Mg^{2+} on goethite in K^{+}, Rb^{+} and Cs^{+} cationic electrolyte solutions. Error bars indicate ± 0.1 pH unit (x-axis) and ± 2%p error in fraction removal of solute (y-axis)

4.3.5. Impact of electrolyte anions

At concentrations of background electrolytes that are high relative to the concentrations of alkaline earth metal ions in solution, a considerable fraction of the alkaline earth metal ion may form aqueous complexes with the anionic electrolytes. Figure 4-5-(a) and (b) show how the concentration of free alkaline earth metal ions would change when the concentration of $NaNO_3$ and NaCl as background electrolyte increases, respectively. The plots in Figure 4-5 were obtained using *Visual MINTEQ* ver. 3.1, a chemical equilibrium model software package [181], utilizing equilibrium constants from the NIST 46.7 database [173]. Table 4-1 displays the equilibrium constants used in this study. As seen in Figure 4-5-(a), free metal ion concentrations decrease as the

concentration of the background electrolyte (i.e., $NaNO_3$) increases, showing a clear trend in the degree of reduction in percent adsorbed across the pH range in the order $Ba^{2+} > Sr^{2+} > Ca^{2+}$ (Note that the equilibrium constant for $MgNO_3^+$ was not found in the literature). However, the trend is completely reversed when NaCl is used as background electrolyte (Figure 4-5-(b)). For example, the concentration of free Ba^{2+} is higher in a NaCl solution compared to a $NaNO_3$ solution at high electrolyte concentrations when total Ba concentrations are identical. It is, however, important to note that the constants used for this study may vary among different sources since they depend on the method used for determination. Therefore, the distribution of alkaline earth metal ions obtained with the constants from the NIST database should not be considered definitive; the focus should be limited to trends observed experimentally among alkaline earth metal ions.

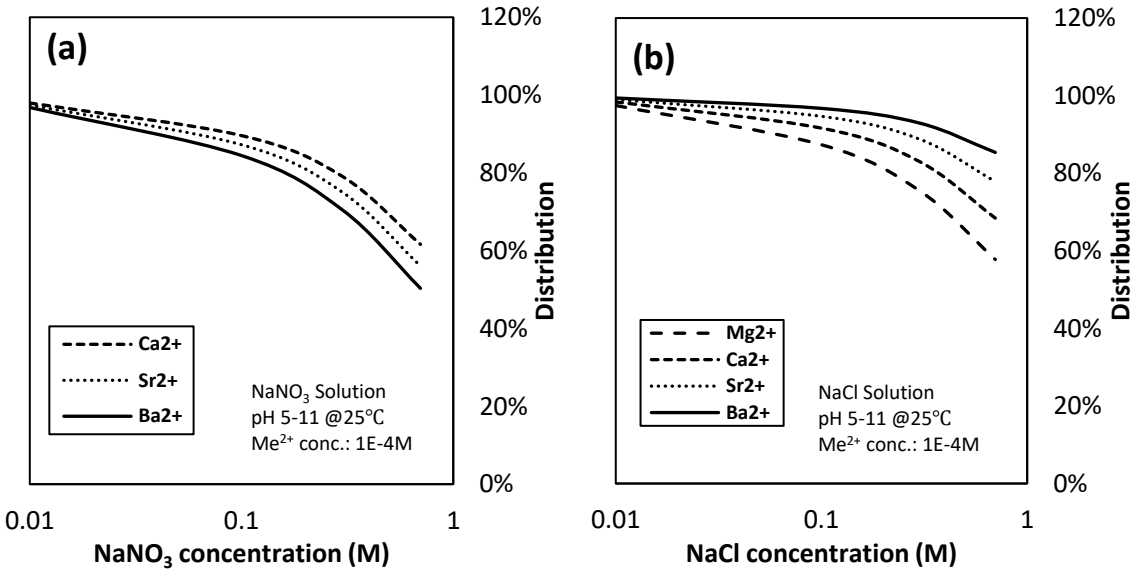

Figure 4-5. Fraction of free Me^{2+} for alkaline earth metal ions in (a) $NaNO_3$ and (b) NaCl solutions at electrolyte concentrations ranging from 0.01M to 0.7M. Alkaline earth metal ion concentrations are 10^{-4} M and pH is in the range of 5 – 11.

When Ba^{2+} adsorption in $NaNO_3$ and NaCl solutions are compared, as seen in Figure 4-6-(a), the adsorption is slightly higher in NaCl solutions compared to $NaNO_3$ solutions; this observation is also consistent with the trends for the expected free metal ion fractions calculated from visual MINTEQ. The correlation between the fraction of free Ba^{2+} ion in solution and fraction adsorbed on goethite indicates that aqueous complexation of Ba^{2+} with anionic electrolytes has a significant impact on its adsorption, and thus implies that electrolyte anions play an important role in adsorption of metal ions in saline solutions. For the case of Mg^{2+} (Figure 4-6-(b)) no difference is apparent between adsorption in $NaNO_3$ and NaCl solutions. The minimal effect of electrolytes is presumably due to the strong affinity of Mg^{2+} to goethite which reduces the impact of electrolytes compared to Ba^{2+}.

Table 4-1. Equilibrium constants for aqueous complexes used in the study (NIST 46.7)

NO_3^- complex species	**log K**	**Cl^- complex species**	**log K**
$Mg^{2+} + NO_3^- \rightarrow MgNO_3^+$	-[a)]	$Mg^{2+} + Cl^- \rightarrow MgCl^+$	0.6
$Ca^{2+} + NO_3^- \rightarrow CaNO_3^+$	0.5	$Ca^{2+} + Cl^- \rightarrow CaCl^+$	0.4
$Sr^{2+} + NO_3^- \rightarrow SrNO_3^+$	0.6	$Sr^{2+} + Cl^- \rightarrow SrCl^+$	0.19
$Ba^{2+} + NO_3^- \rightarrow BaNO_3^+$	0.7	$Ba^{2+} + Cl^- \rightarrow BaCl^+$	-0.03

[a)] *Equilibrium constant not available*

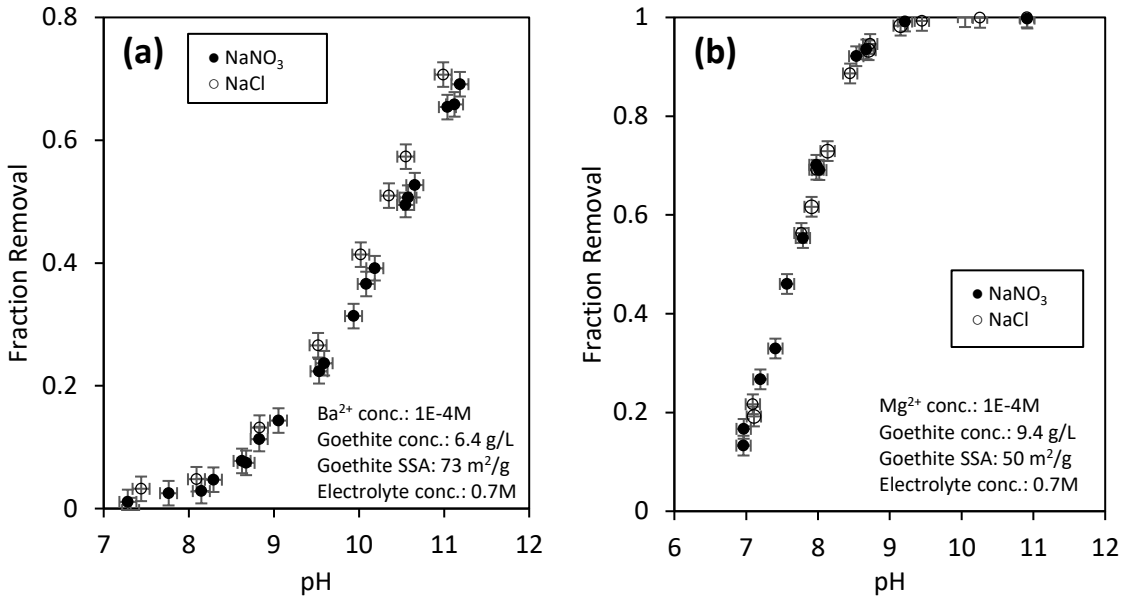

Figure 4-6. Adsorption edges for (a) Ba^{2+} and (b) Mg^{2+} on goethite in 0.7M $NaNO_3$ and NaCl solutions. Error bars indicate ± 0.1 pH unit (x-axis) and ± 2%p error in fraction removal of solute (y-axis)

4.4. CONCLUSIONS

The results from adsorption experiments with alkaline earth metal ions on goethite highlight the importance of considering background electrolytes in solution; at least two different mechanisms are operative. First, the effect of the electrolyte will depend on the relative affinity of cations to the surface. Adsorption of cations with higher affinity is minimally affected by cations of lower affinity, but the impact is significant for the opposite case. This is assumed to be due to competition between cations for adsorption sites. Another important factor related to electrolyte effects is the formation of aqueous complexes of alkaline earth metal ions with anionic electrolytes. It was shown in this study that altering the anionic electrolyte affects the adsorption of alkaline earth metal ions by changing the fraction of free metal ions in solutions. In other words, a decrease in the

availability of free metal ions results in reduced total adsorption to the surface suggesting that ion pairs have lower affinity. Regardless of the mechanisms responsible for the impact of background electrolytes on alkaline earth metal ion adsorption, the concentration of electrolyte plays an important role. Generally, background electrolytes have weak complexing power which is why they are commonly considered inert in many adsorption studies. However, high concentrations of these electrolytes can compensate for their weak reactivity, and their effect on metal adsorption can be significant.

The findings from this study indicate that accurately identifying the type and extent of electrolyte interaction can be important in cases where adsorption occurs in highly saline solutions or/and when adsorbing metal ions have low affinity for the adsorbent surface (e.g., alkaline earth metal ions on goethite). Hence, it is crucial to incorporate reactions regarding surface complexation and aqueous complex formation of electrolytes in the SCMs for metal ion adsorption in such cases.

The extensive adsorption data collected from this study is crucial for isolating individual electrolyte effects on alkaline earth metal ion adsorption. Combined with molecular dynamics, spectroscopy and/or surface complexation modeling, macroscopic results can serve as a basis for accurately determining the surface complex species of alkaline earth metal ions and goethite hydroxyl sites.

Chapter 5. Prediction of Alkaline Earth Metal Ion Adsorption on Goethite for Various Background Electrolytes

5.1. INTRODUCTION

Alkaline earth metal ions are abundant in natural systems and crucially impact the chemical behavior of other ions and their interactions with surfaces. Hence, understanding the adsorption of alkaline earth metal ions on mineral surfaces is important for predicting and characterizing adsorption behavior of transition metals and other ions [44], [56], [62], [165]. Although numerous studies have elucidated the adsorption behavior of alkaline earth metal ions (Table 5-1 and Table 5-2), agreement is still lacking on many adsorption characteristics of these metals including, but not limited to, the mode of adsorption (inner- or outer-sphere), surface complex stoichiometry and surface affinity [44], [61], [64], [165]. The disagreements have been partially due to the lack of molecular modeling and/or spectroscopic data identifying the structure of surface complexes for most of the alkaline earth metal ions (i.e., Mg^{2+}, Ca^{2+} and Ba^{2+}).

The effect of electrolytes on alkaline earth metal ion adsorption must also be fully identified in order to completely understand their adsorption behaviors. Elucidating the effect of different electrolytes is particularly important for alkaline earth metal ions due to their relatively week affinity to mineral surfaces, which results in greater impact of electrolytes [18]. Most experimental studies, however, have focused on experiments using only a few simple electrolyte systems, such as NaCl, $NaNO_3$, $NaClO_4$ and KNO_3, which makes it difficult to isolate and identify the influence of individual electrolytes, and hence, limits the effectiveness of predicting adsorption in diverse electrolyte conditions which are seen in natural and engineered waters [44].

This study was conducted in order to develop a model that could predict alkaline earth metal cation (Mg^{2+}, Ca^{2+}, Sr^{2+} and Ba^{2+}) adsorption onto goethite under an extensive range of background electrolyte conditions, including a large range of ionic strength, pH, and various anionic (Cl^-, NO_3^-) and cationic species (Na^+, Rb^+, Cs^+) that serve as background electrolytes and control ionic strength. Moreover, this study focused on establishing a surface complexation model capable of predicting adsorption with multiple background electrolytes as well as adsorption of a transition metal ion, Cd^{2+}, in saline waters containing high concentrations of Na^+ and Mg^{2+} by combining the alkaline earth metal ion adsorption model parameters with a pre-developed Cd^{2+} adsorption model [89].

5.1.1. Surface complexes for alkaline earth metal ion adsorption

A number of previous studies have targeted elucidating the structure and stoichiometry of surface complexes containing alkaline earth metal ions. These studies utilized various methods for the task, including surface complexation modeling (SCM), molecular dynamic simulations, and spectroscopic approaches. It must be noted that no single method is sufficient by itself for the determination of surface complexation species, and hence, different methods must be used together to provide guidance and/or validation.

Table 5-1 and Table 5-2 list the results from studies focused on goethite and other minerals, respectively. As can be seen in these tables, except for a Sr-complex species on the rutile surface (i.e., inner-sphere, tetra-dentate), consistent agreement is lacking for the type of dominant surface complexes among different studies. Table 5-1 and Table 5-2 highlight the range of surface complexes employed and indicate whether spectroscopic or molecular modeling information was used to guide the selection of surface complexes. These results were also used to guide the selection of surface complexes in this study.

Table 5-1. Suggested structures of surface complex species of alkaline earth metal ions on goethite documented in literature

Mg	Ca	Sr	Ba	Spectroscopy	Ref.
Inner- / Bi-	Inner- / Mono- (high pH) Outer- / Mono- (low pH)				[165]
Inner- / Bi-	Inner- / Mono- Outer- / Mono-				[61]
Inner- / Bi-	Inner- / Mono- Inner- / Bi-	Outer / Mono-			[64]
Outer- / Mono- Outer- / Tetra-	Outer- / Mono- (pH > 11) Outer- / Tetra- (pH < 10)		Outer- / Tetra-		[44]
	Inner- / Mono- Inner- / Bi-				[67]
	Inner- / Bi- Outer- / Mono-				[65]
	Inner- / Mono-				[68]
	Inner- / Mono- (high pH) Outer- / Mono- (low pH)				[66]
		Outer- / Mono-		XAS	[71]
		Inner- / Bi-		EXAFS	[69]
		Outer- / (ND)		EXAFS	[70]
		Outer- / Mono- Outer- /Tetra-		EXAFS	[72]
		Outer- / (ND) (neutral pH) Inner- / (ND) (high pH)		EXAFS	[198]
			Inner- / Tetra-		[63]

ND: Not Determined

Table 5-2. Suggested structures of surface complex species of alkaline earth metal ions on non-goethite mineral surfaces documented in literature

Mineral	Mg	Ca	Sr	Ba	Spectroscopy	Ref.
Kaolinite, Calcite			Outer- / (ND)		SEM/EDS, XANES, EXAFS	[81]
Kaolinite, Illite, Hectorite, Montmorillonite			Outer- / Mono-		XAS	[80]
Quartz			Outer- / (ND)		XAS	[74]
Cassiterite			Inner- / (ND)			[76]
Gibbsite	Outer- / (ND)	Outer- / (ND) Inner- / (ND)	Outer- / (ND) Inner- / (ND)	Inner- / (ND)	MD	[73]
Rutile			Inner- / Tetra-		XSW	[75]
Rutile			Inner- / Tetra-			[77]
Rutile		Inner- / Tetra-	Inner- / Tetra-		MD	[78]
Rutile		Inner- / Tetra-	Inner- / Tetra-			[210]
Rutile		Inner- / Bi- (neutral pH) Inner- / Tetra- (high pH)				[79]
Rutile			Inner- / Tetra-		XSW, MD	[76]

ND: Not Determined

5.2. METHODS

5.2.1. CD-MUSIC formulation

The CD-MUSIC surface complexation model was formulated as described in Chapter 3. The relationships between specific surface area (SSA) and goethite surface properties, which were established in Chapter 3, were incorporated into the model to predict adsorption on different preparations of goethite. Surface site densities for singly-, doubly-, and triply-coordinated surface oxygens of goethite were determined as described in Chapter 3. Two protonation constants, one each on singly- and triply-coordinated surface sites, were assumed, and all ion-pair complexes were considered to be located on the 1-plane (see Figure 5-1-(c)). The charge distribution (CD) values of alkaline earth metal surface complex species and ion-pairs were determined by Pauling's bond theory [211]. The negative charge of the hydroxyl ligand (OH^-) on the metal cation was considered to be located on the 1-plane for both inner- and outer-sphere complex species as illustrated in Figure 5-1-(b) and (d).

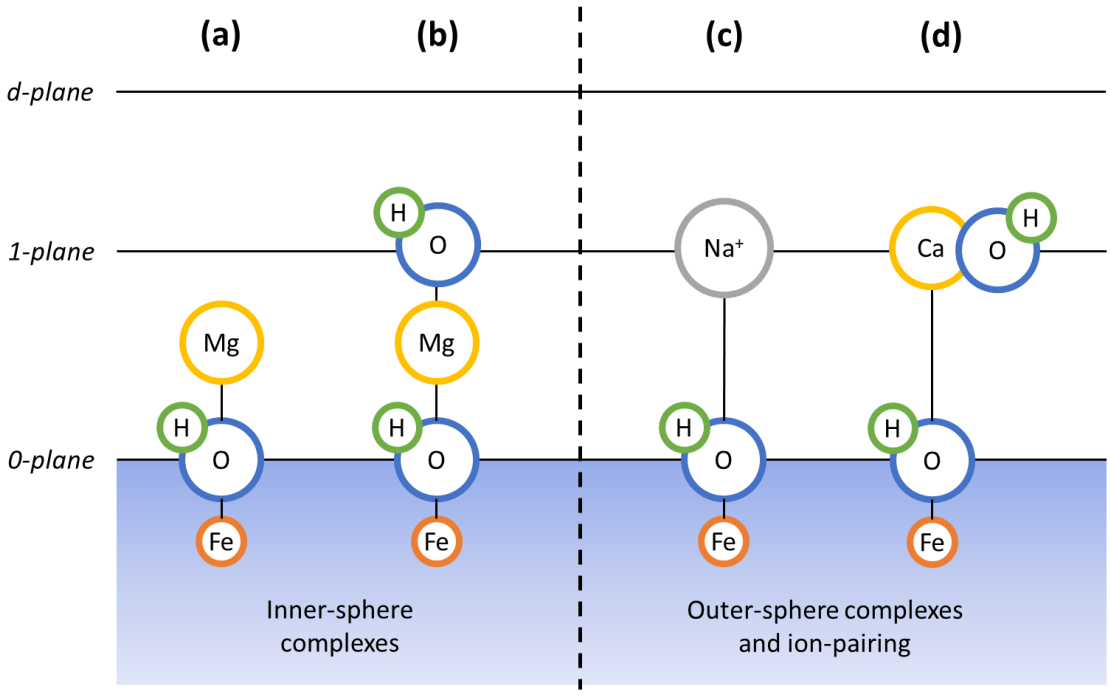

Figure 5-1. Schematic of the CD-MUSIC representation of the goethite-water interface; (a) inner-sphere complex, (b) hydrolyzed inner-sphere complex, (c) outer-sphere complex and electrolyte ion-pair, and (d) hydrolyzed outer-sphere complex

5.2.2. Model optimization

Experimental adsorption data were collected through a series of batch adsorption experiments as described in previous chapters. The experimental data were plotted as fractional removal of metal ions as a function of solution pH to obtain adsorption edges. For each alkaline earth metal (i.e., Mg, Ca, Sr and Ba), two adsorption data sets were used to select the surface complex species and optimize surface complexation equilibrium constants (i.e., log K). The specifications of the two adsorption data sets selected for the optimization process are described in Table 5-3. The values reported in the previous chapter for ion-pair equilibrium constants, equilibrium constants for aqueous complexation

reactions, protonation constants, and capacitance were all regarded as fixed values and not adjusted during the optimization process. Data fitting was conducted by using a non-linear least squares optimization program, FITEQL 4.0 [18], [91], [178], [212]. An example of an input file used in FITEQL 4.0 is presented in Appendix A.

Table 5-3. Description of adsorption experiments used to optimize model parameters

Test description	Adsorption test 1	Adsorption test 2
Electrolyte concentrations	0.01 M	0.7 M
Solutes	Mg^{2+}, Ca^{2+}, Sr^{2+}, Ba^{2+}	
Electrolytes	$NaNO_3$	
Goethite SSA[1)]	64.5 m^2/g	
Goethite concentration	7.3 g/L	
Initial metal ion concentration	1.0×10^{-4} M	
Equilibration time	24 hrs	
Temperature	25 °C	

1) SSA: Specific Surface Area

The number of dominant surface complex species for each alkaline earth metal ion was limited to two, which is consistent with most previous studies as shown in Table 5-1 and Table 5-2. In other words, it was assumed that adsorption of each alkaline earth metal ion in various solution conditions could be simulated with just two surface complexation reactions. Forty-four types of surface complex species as listed in Table 5-4 were considered as possible species. Hence, a total of 946 (= 44 × 43 / 2) combinations of surface species were tested in the optimization process to find all pairs that returned satisfactory fits (i.e., WSOS/DF < 20) to the adsorption test data.

Table 5-4. List of all types of surface complex species for alkaline earth metal ion adsorption onto goethite that were considered during the model optimization process

No.	Mode	Structure	Non-hydrolyzed vs. Hydrolyzed	Sorption site (Oxygen group)	Crystal face	Formula
1	Outer-	Mono-	Non-hydrolyzed	Singly-	(101) & (001)	$FeOH\_Me^{2+}$
2					(210)	$FeOH\_Me^{2+}$
3				Triply-	(101) & (001)	$Fe_3O\_Me^{2+}$
4			Hydrolyzed	Singly-	(101) & (001)	$FeOH\_MeOH^{+}$
5					(210)	$FeOH\_MeOH^{+}$
6				Triply-	(101) & (001)	$Fe_3O\_MeOH^{+}$
7		Bi-	Non-hydrolyzed	Singly-	(101) & (001)	$2(FeOH)\_Me^{2+}$
8					(210)	$2(FeOH)\_Me^{2+}$
9				Triply-	(101) & (001)	$2(Fe_3O)\_Me^{2+}$
10				Singly- & Triply-	(101) & (001)	$(FeOH)(Fe_3O)\_Me^{2+}$
11			Hydrolyzed	Singly-	(101) & (001)	$2(FeOH)\_MeOH^{+}$
12					(210)	$2(FeOH)\_MeOH^{+}$
13				Triply-	(101) & (001)	$2(Fe_3O)\_MeOH^{+}$
14				Singly- & Triply-	(101) & (001)	$(FeOH)(Fe_3O)\_MeOH^{+}$
15		Tetra-	Non-hydrolyzed	Singly-	(101) & (001)	$4(FeOH)\_Me^{2+}$
16					(210)	$4(FeOH)\_Me^{2+}$
17				Triply-	(101) & (001)	$4(Fe_3O)\_Me^{2+}$
18				Singly- & Triply-	(101) & (001)	$2(FeOH)2(Fe_3O)\_Me^{2+}$
19			Hydrolyzed	Singly-	(101) & (001)	$4(FeOH)\_MeOH^{+}$
20					(210)	$4(FeOH)\_MeOH^{+}$
21				Triply-	(101) & (001)	$4(Fe_3O)\_MeOH^{+}$
22				Singly- & Triply-	(101) & (001)	$2(FeOH)2(Fe_3O)\_MeOH^{+}$
23	Inner-	Mono-	Non-hydrolyzed	Singly-	(101) & (001)	$FeOHMe^{2+}$
24					(210)	$FeOHMe^{2+}$
25				Triply-	(101) & (001)	Fe_3OMe^{2+}
26			Hydrolyzed	Singly-	(101) & (001)	$FeOHMeOH^{+}$
27					(210)	$FeOHMeOH^{+}$
28				Triply-	(101) & (001)	Fe_3OMeOH^{+}
29		Bi-	Non-hydrolyzed	Singly-	(101) & (001)	$2(FeOH)Me^{2+}$
30					(210)	$2(FeOH)Me^{2+}$
31				Triply-	(101) & (001)	$2(Fe_3O)Me^{2+}$
32				Singly- & Triply-	(101) & (001)	$(FeOH)(Fe_3O)Me^{2+}$
33			Hydrolyzed	Singly-	(101) & (001)	$2(FeOH)MeOH^{+}$
34					(210)	$2(FeOH)MeOH^{+}$
35				Triply-	(101) & (001)	$2(Fe_3O)MeOH^{+}$
36				Singly- & Triply-	(101) & (001)	$(FeOH)(Fe_3O)MeOH^{+}$
37		Tetra-	Non-hydrolyzed	Singly-	(101) & (001)	$4(FeOH)Me^{2+}$
38					(210)	$4(FeOH)Me^{2+}$
39				Triply-	(101) & (001)	$4(Fe_3O)Me^{2+}$
40				Singly- & Triply-	(101) & (001)	$2(FeOH)2(Fe_3O)Me^{2+}$
41			Hydrolyzed	Singly-	(101) & (001)	$4(FeOH)MeOH^{+}$
42					(210)	$4(FeOH)MeOH^{+}$
43				Triply-	(101) & (001)	$4(Fe_3O)MeOH^{+}$
44				Singly- & Triply-	(101) & (001)	$2(FeOH)2(Fe_3O)MeOH^{+}$

An automation program was coded and utilized to assist and accelerate the iterative calculations. The program was coded in AutoHotkey (AHK) language, which is a free, open-source custom scripting language for Microsoft Windows™, and specifically developed for building software that can automate repetitive tasks [213]. Details of the developed program, actual codes, and user tips are presented in Appendix B. A simplified algorithm sequence of the program is described below:

Step 1. Choose a combination (pair of surface species) to test (e.g., FeOH_Me^{2+} and FeO_3_$MeOH^+$); return the name of first and second surface species as constants 'Sp1' and 'Sp2', respectively.

Step 2. Find equilibrium constant (i.e., logK value) of Sp1 that gives the lowest WSOS/DF toward the adsorption data (Sp2 is excluded in this step); return the logK value as constant 'K1_opt'.

Step 3. Repeat Step 2 with Sp2; return the logK value as constant 'K2_opt'.

Step 4. Set scanning range of logK for both Sp1 and Sp2.

- Start point: K_n_opt - 2
- End point: K_n_opt + 0.5

(Example: if K1_opt was 9.4, the scanning range for Sp1 is 7.4 – 9.9)

Step 5. Start scanning.

- Log K of Sp1 and Sp2 both start from their initial points
- Run model with the log K values and record the resulting WSOS/DF
- Increase log K value by 0.1 increments and repeat scanning
- Abort scanning when log K equal the end points of the scanning range

Step 6. Return to Step 1 and repeat with the next combination.

As described in the simplified algorithm, the automation program scans a range of log K values for a given pair of surface species and records the WSOS/DF values obtained from each set of the log K values used. Since the deviation between the start and end points of the scanning range is 2.5 and the scanning is processed with a step increment of 0.1, 625 iterations were conducted for each pair of surface species which resulted in 591,250 iterations to complete all 946 combinations.

5.2.3. Surface species determination

A number of surface species combinations returned satisfactory fits (WSOS/DF < 20) to the adsorption data during the model optimization process, and hence, further screening of surface species of alkaline earth metal ions was conducted based on extensive review of previous SCM, molecular modeling, and spectroscopic studies as listed in Table 5-1 and Table 5-2 in the previous section of this chapter. Identifying the structure of Sr-surface complexes was the starting point for selecting the other alkaline earth metal ion surface complexes since Sr is the most extensively studied alkaline earth metal ion and various methods have been employed; moreover, the species that were identified in the literature were relatively consistent among studies (i.e., outer-sphere mono-dentate and tetra-dentate). Thus, identification of Mg, Ca and Ba species were extended from the findings for Sr-complexes and studies for the individual ions. Surface species identified with spectroscopic methods were given more weight compared to those determined via model analysis.

5.2.4. Model verification

Once the surface complex species and equilibrium constants of the alkaline earth metal ion surface complexation reactions were determined, predictions were made using additional experimental data collected in $NaNO_3$ solutions. After validating the surface complexation reactions and their associated equilibrium constants, the model was used to simulate adsorption in other background electrolyte systems. The equilibrium constants for ion-pair complexes for electrolyte systems other than those containing Na^+ and NO_3^- (i.e., Rb^+, Cs^+, and Cl^-) were determined through an additional model calibration process. In this step, Ba^{2+} adsorption data collected from $RbNO_3$, $CsNO_3$, and NaCl electrolyte systems were used for the calibration of electrolyte surface complexation constants. Since the constants for Na^+ and NO_3^- were predetermined, only one parameter, which is the electrolyte surface complexation constant of either the cation or anion electrolyte, was adjusted to fit the adsorption data.

Finally, predictions were made for alkaline earth metal ion adsorption on different preparations of goethite in various solution conditions and in mixed electrolyte systems using data collected from experiments conducted as part of this study and from various literature. Table 5-5 lists the surface parameters of goethites and type of adsorbates used in the current study for verification of the calibrated model. The CFC, capacitance and pK_a values of different preparations of goethite were estimated with the pre-established relationships between these parameters and SSA as described in Chapter 3.

The accuracy of the model predictions was quantified with the weighted sum of squares divided by the degrees of freedom (WSOS/DF). Detailed description of this quantification method is presented in Chapter 3. Values of WSOS/DF between 0.1 – 20 were considered satisfactory model fits.

Table 5-5. CFC, capacitance and pK_a values of goethites and types of adsorbate used for model verification

SSA (m^2/g)	Crystal Face Contribution			Capacitance (F/m^2)	$pK_{a2,singly}$	Adsorbate	Data from
	(101)	(001)	(210)				
37.8	19%	45%	36%	1.10	8.9	Sr^{2+}	Carroll et al. (2008) [72]
50	19%	45%	36%	1.10	8.9	Mg^{2+}, Ca^{2+}, Sr^{2+}, Ba^{2+}	Current Study
51.8	20.7%	46.4%	32.9%	1.10	8.8	Mg^{2+}	Balistrieri and Murray (1981) [214]
64.5	32.1%	53.9%	14%	1.05	8.5	Mg^{2+}, Ca^{2+}, Sr^{2+}, Ba^{2+}	Current Study
73	38.6%	47.4%	14%	0.97	8.5	Mg^{2+}, Ca^{2+}, Sr^{2+}, Ba^{2+}	Current Study
79.4	43.5%	42.5%	14%	0.93	8.5	Ca^{2+}	Ali and Dzombak (1996) [67]
93.9	54.6%	31.4%	14%	0.84	8.5	Ca^{2+}	Weng et al. (2005) [68]

5.3. RESULTS AND DISCUSSION

5.3.1. Surface complex species and electrolyte surface complexation constants

The model calibration results are presented in Figure 5-2 and resulting surface complexation reaction constants for each alkaline earth metal ion determined from the model calibration process are listed in Table 5-6. Two surface species were determined for each of the alkaline earth metal ions. For Ca^{2+}, Sr^{2+} and Ba^{2+}, only outer-sphere species were required to fit experimental data, whereas for Mg^{2+}, an inner-sphere species was required. This is consistent with the observed trend from our adsorption batch experiments where Mg^{2+} exhibited the highest affinity for the goethite surface compared to other alkaline earth metal cations. Adsorption of $MeOH^+$ species were required to fit the adsorption at high pH ranges for all alkaline earth metal ions which is not surprising given the dominance of these aqueous species at high pH. Also, as suggested by spectroscopic

and molecular dynamic data, outer-sphere tetradentate and monodentate species were the dominant species for Sr and Ba adsorption [70]–[72], [198].

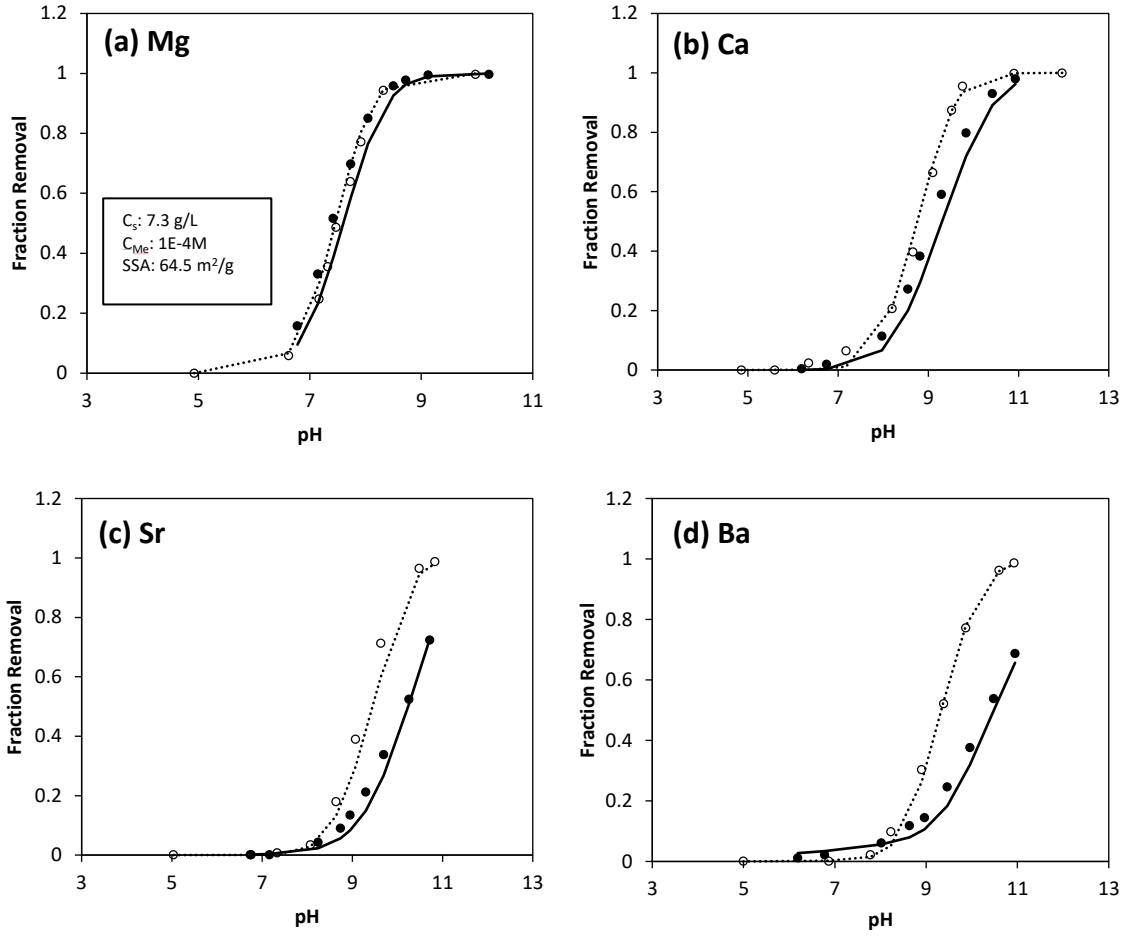

Figure 5-2. Model calibration results for alkaline earth metal ions. Symbols and lines represent experimental data and modeling results, respectively. 0.7 M I.S. results are presented in filled circles and solid lines, and 0.01M I.S. results in empty circles and dotted lines.

Table 5-6. Surface complexes and associated surface complexation equilibrium constants for alkaline earth metal ion adsorption to goethite determined by FITEQL model optimization

Surface Complex Species			Charge Distribution			log K			
Formula	**Description**	**Location (crystal face)**	**Δz_0**	**Δz_1**	**Δz_2**	**Mg**	**Ca**	**Sr**	**Ba**
≡(FeOH)MeOH	Inner-, Mono-	(210)	0.33	0.67	0	-4.700			
≡2(FeOH)2(Fe_3O)_MeOH	Outer-, Tetra-	(101), (001)	0	1	0	1.658			
≡2(FeOH)_MeOH	Outer, Bi-	(101), (001)	0	1	0		-6.712		
≡4(FeOH)_MeOH	Outer, Tetra-	(210)	0	1	0		-4.333		-5.596
≡FeOH_MeOH	Outer-, Mono-	(210)	0	1	0			-6.827	
≡4(Fe_3O)_Me	Outer-, Tetra-	(101), (001)	0	2	0			12.916	
≡2(FeOH)_Me	Outer, Bi-	(101), (001)	0	2	0				2.854

Figure 5-3 displays possible locations of outer-sphere tetradentate species within the water-goethite surface interface. Two types of the outer-sphere tetradentate species (i.e., 2(FeOH)-Me-2(Fe_3O) and 4(Fe_3O)-Me) were assumed on the main faces (i.e., (101) and (001)), and another (i.e., 4(FeOH)-Me) on the capping faces (i.e., (210) and (010)). As illustrated in arrow lines in Figure 5-3, these surface complexes are bound to four singly- and/or triply-coordinated surface oxygen sites on the goethite surface.

The electrolyte surface complexation constants obtained through model calibration are presented in Table 5-7. The results show a clear trend in equilibrium constants. As discuss in Chapter 4, the affinity of alkali metal ions to goethite is inversely correlated with ionic radii, and a similar trend is also observed among anionic electrolytes; these results are consistent with previous studies [51], [98], [203], [215].

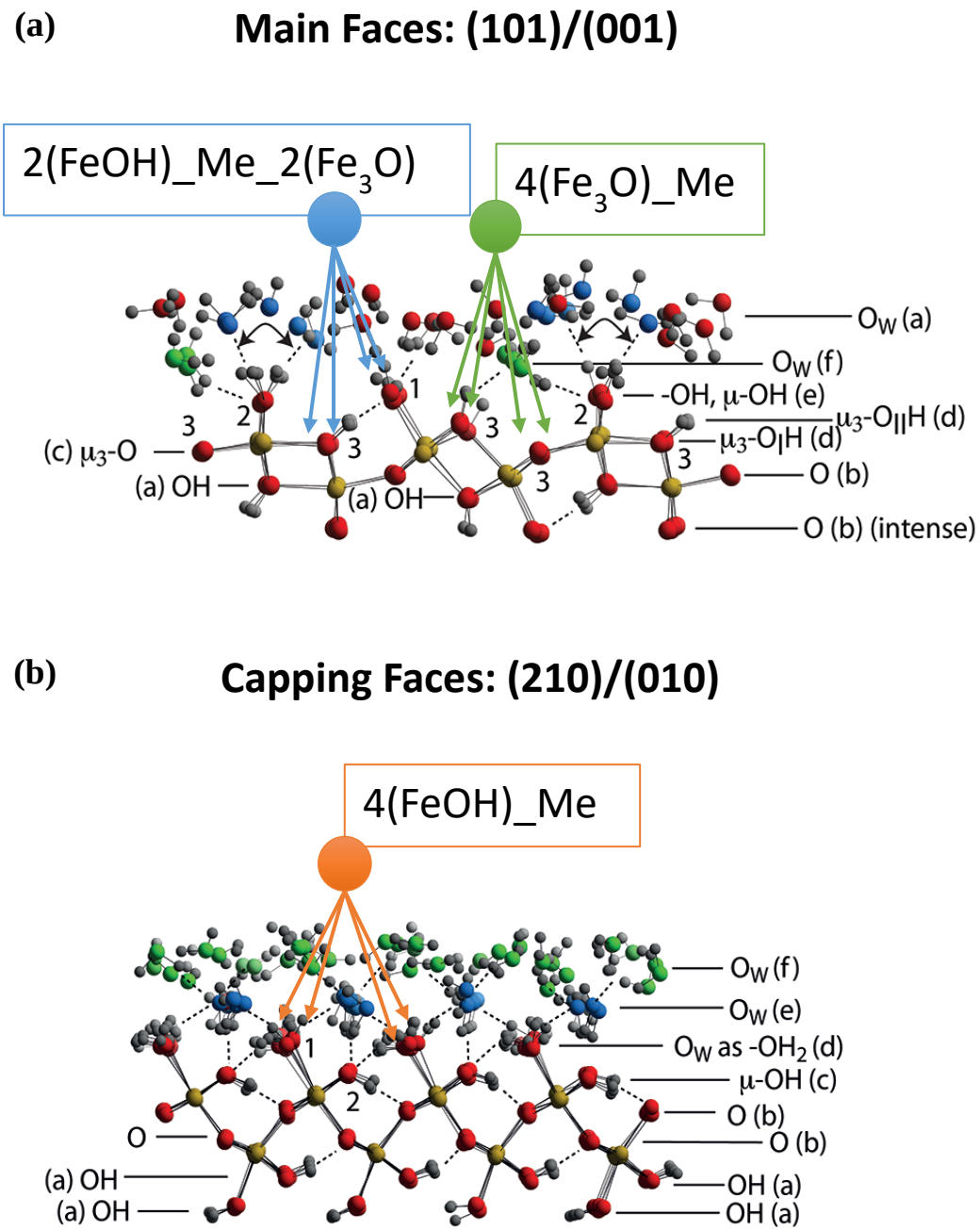

Figure 5-3. Illustration of possible locations of outer-sphere tetra-dentate surface species at (a) the (101) and (001) faces, and (b) the (210) face (goethite figure adopted from Boily (2012) [164]

Table 5-7. Electrolyte surface complexation constants for each electrolyte

	Ion-pairing reaction	Type of electrolyte	Equilibrium constant (log K)[1)]
Electrolyte Cations	$\equiv FeOH^{-1/2} + Cat^{+} \rightarrow \equiv FeOH\_Cat^{+1/2}$ $\equiv Fe_3O^{-1/2} + Cat^{+} \rightarrow \equiv Fe_3O\_Cat^{+1/2}$	Na^{+}	0.1
		K^{+}	0.03
		Rb^{+}	-0.15
		Cs^{+}	-0.3
Electrolyte Anions	$\equiv FeOH_2^{+1/2} + An^{-} \rightarrow \equiv FeOH_2\_An^{-1/2}$ $\equiv Fe_3OH^{+1/2} + An^{-} \rightarrow \equiv Fe_3OH\_An^{-1/2}$	Cl^{-}	-0.4
		NO_3^{-}	-0.5

5.3.2. Model predictions

Predictions were made for adsorption data collected in various solution conditions to verify the accuracy of the developed model. The resulting WSOS/DF values for all predictions made by the model are listed in Table 5-8. All WSOS/DF values were lower than 20, which is regarded as the criteria for satisfactory fit with the error estimates employed by Dzombak and Morel [18].

Table 5-8. Model fits (WSOS/DF) for all alkaline earth metal ion adsorption data sets investigated

Metal Ion	SSA (m^2/g)	Solid Conc. (g/L)	Metal Conc. (M)	I.S. (M)	Electrolyte	WSOS/DF	Remarks
Datasets used for model optimization							
Mg^{2+}	64.5	7.3	1.00E-04	0.01	$NaNO_3$	**3.2**	
	64.5	7.3	1.00E-04	0.7	$NaNO_3$	**17.3**	
Ca^{2+}	64.5	7.3	1.00E-04	0.01	$NaNO_3$	**3.8**	
	64.5	7.3	1.00E-04	0.7	$NaNO_3$	**12.9**	
Sr^{2+}	64.5	7.3	1.00E-04	0.01	$NaNO_3$	**8.8**	
	64.5	7.3	1.00E-04	0.7	$NaNO_3$	**8.3**	

Table 5-8, cont.

Metal Ion	SSA (m^2/g)	Solid Conc. (g/L)	Metal Conc. (M)	I.S. (M)	Electrolyte	WSOS/DF	Remarks
Ba^{2+}	64.5	7.3	1.00E-04	0.01	$NaNO_3$	**2.6**	
	64.5	7.3	1.00E-04	0.7	$NaNO_3$	**6.6**	
Datasets used for model verification							
Mg^{2+}	50	9.4	1.00E-04	0.7	$NaNO_3$	**0.48**	
	50	9.4	1.00E-04	0.7	NaCl	**5.6**	
	50	1.7	2.50E-04	0.01	$NaNO_3$	**2.5**	
	50	1.7	2.50E-04	0.01	$NaNO_3$	**3.5**	With 3.5e-5M Cd^{2+}
	50	1.7	2.50E-04	0.01	$NaNO_3$	**2.5**	With 3.5e-5M Cd^{2+}
	64.5	1.2	9.75E-05	0.01	$NaNO_3$	**5.4**	
	64.5	1.2	9.75E-05	0.1	$NaNO_3$	**9.4**	
	64.5	1.2	9.75E-05	0.3	$NaNO_3$	**12.3**	
	64.5	1.2	9.75E-05	0.7	$NaNO_3$	**19.7**	
	64.5	0.1	1.00E-04	0.01	$NaNO_3$	**2.4**	
	64.5	0.1	1.00E-04	0.1	$NaNO_3$	**2.7**	
	64.5	0.1	1.00E-04	0.3	$NaNO_3$	**12.5**	
	64.5	0.1	1.00E-04	0.7	$NaNO_3$	**15.1**	
	64.5	0.5	1.00E-04	0.01	$NaNO_3$	**10.4**	
	64.5	0.5	1.00E-04	0.1	$NaNO_3$	**19.8**	
	64.5	0.5	1.00E-04	0.3	$NaNO_3$	**17.7**	
	64.5	0.5	1.00E-04	0.7	$NaNO_3$	**11.8**	
	64.5	7.3	1.00E-04	0.1	$NaNO_3$	**1.8**	
	64.5	7.3	1.00E-04	0.3	$NaNO_3$	**0.4**	
	64.5	7.3	1.00E-04	0.01	NaCl	**6.2**	
	64.5	7.3	1.00E-04	0.1	NaCl	**3.4**	
	64.5	7.3	1.00E-04	0.3	NaCl	**0.5**	
	64.5	7.3	1.00E-04	0.7	NaCl	**5.6**	
Ca^{2+}	64.5	7.3	1.00E-04	0.1	$NaNO_3$	**0.6**	
	64.5	7.3	1.00E-04	0.3	$NaNO_3$	**0.2**	
	64.5	1.2	1.00E-04	0.01	$NaNO_3$	**7.2**	
	64.5	1.2	1.00E-04	0.1	$NaNO_3$	**8.3**	
	64.5	1.2	1.00E-04	0.3	$NaNO_3$	**2.6**	
	64.5	1.2	1.00E-04	0.7	$NaNO_3$	**9.4**	
	64.5	1.2	1.00E-03	0.01	$NaNO_3$	**0.7**	
	64.5	1.2	1.00E-03	0.1	$NaNO_3$	**3.5**	
	64.5	1.2	1.00E-03	0.3	$NaNO_3$	**0.9**	
	64.5	1.2	1.00E-03	0.7	$NaNO_3$	**1**	
	64.5	7.3	1.00E-04	0.01	NaCl	**16.5**	
	64.5	7.3	1.00E-04	0.1	NaCl	**9.7**	
	64.5	7.3	1.00E-04	0.3	NaCl	**1.9**	

Table 5-8, cont.

Metal Ion	SSA (m^2/g)	Solid Conc. (g/L)	Metal Conc. (M)	I.S. (M)	Electrolyte	WSOS/DF	Remarks
	64.5	7.3	1.00E-04	0.7	NaCl	**11.3**	
Sr^{2+}	64.5	7.3	1.00E-04	0.1	$NaNO_3$	**1.8**	
	64.5	7.3	1.00E-04	0.3	$NaNO_3$	**1.2**	
	64.5	0.9	1.00E-04	0.01	$NaNO_3$	**12.5**	
	64.5	0.9	1.00E-04	0.1	$NaNO_3$	**4.1**	
	64.5	0.9	1.00E-04	0.3	$NaNO_3$	**2.4**	
	64.5	0.9	1.00E-04	0.7	$NaNO_3$	**1.9**	
	64.5	8.2	1.00E-04	0.01	NaCl	**17**	
	64.5	8.2	1.00E-04	0.1	NaCl	**1.5**	
	64.5	8.2	1.00E-04	0.3	NaCl	**0.5**	
	64.5	8.2	1.00E-04	0.7	NaCl	**9.3**	
Ba^{2+}	64.5	7.3	1.00E-04	0.1	$NaNO_3$	**1.9**	
	64.5	7.3	1.00E-04	0.3	$NaNO_3$	**1.5**	
	64.5	1.2	7.00E-05	0.01	$NaNO_3$	**4.3**	
	64.5	1.2	7.00E-05	0.1	$NaNO_3$	**5.9**	
	64.5	1.2	7.00E-05	0.3	$NaNO_3$	**3.6**	
	64.5	1.2	7.00E-05	0.7	$NaNO_3$	**13.2**	
	64.5	7.3	1.00E-04	0.01	NaCl	**15**	
	64.5	7.3	1.00E-04	0.1	NaCl	**2.5**	
	64.5	7.3	1.00E-04	0.3	NaCl	**9.5**	
	64.5	8.2	1.00E-04	0.3	NaCl	**9.5**	
	64.5	8.2	1.00E-04	0.7	NaCl	**14.8**	
	50	8.2	1.00E-04	0.1	$NaNO_3$	**16.5**	
	50	6.3	1.00E-04	0.1	$NaNO_3$	**8.8**	
	50	6.3	1.00E-04	0.7	$NaNO_3$+NaCl	**18.2**	
	50	9.4	8.50E-05	0.7	$NaNO_3$	**15.6**	
	50	9.4	8.50E-05	0.7	$RbNO_3$	**3.6**	
	50	9.4	8.50E-05	0.7	$CsNO_3$	**3.5**	
	73	6.2	1.00E-04	0.7	$NaNO_3$	**4.5**	
	73	6.2	1.00E-04	0.7	$NaNO_3$	**4.8**	
	73	6.2	1.00E-04	0.7	NaCl	**6.6**	
	50	9.4	1.00E-04	0.7	NaCl	**10.5**	
Cd	50	1.7	3.50E-05	0.01	$NaNO_3$	**8.4**	Cd only

5.3.2.1. Change of surface/solute ratio

Based on the surface complexes described above, predictions were made for alkaline earth metal ion adsorption on goethite under various solution conditions. Figure 5-4 compares the model predictions to experimental data for Ca^{2+} adsorption at different surface-to-metal loading ratios for two extreme cases of 0.01M and 0.7M ionic strength. As the solute/solid ratio is reduced, it is expected that the fraction of the alkaline earth metal ion removed from solution will decrease. Also, due to the limited availability of surface sites, the proportion of tetradentate surface species also decreases as surface/metal ratio decreases. Note that the abbreviated formula, '4X^_CaOH', represents an outer-sphere tetradentate CaOH surface complex species on the (210) crystal face. The predictions show good agreement with experimental data where the surface/solute ratio is reduced by 1/6 and 1/60 from the original value used for the model calibration (i.e., 1.2 g/L goethite with 10^{-4} M Ca^{2+}, and 1.2 g/L goethite with 10^{-3} M Ca^{2+}, respectively). Note that Ca^{2+} was simply selected as an example; results of other alkaline earth metal ions are presented in Appendix C.

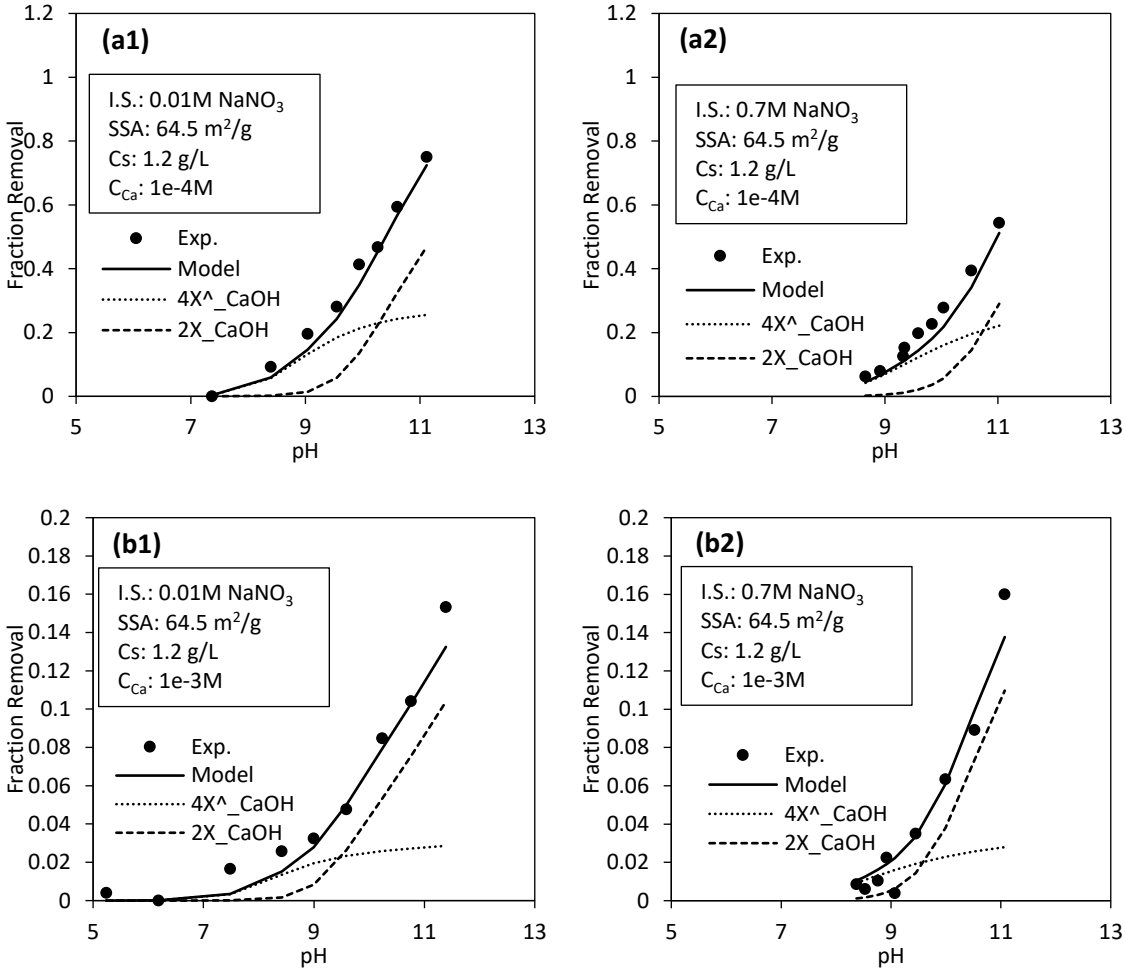

Figure 5-4. Experimental data and model predictions of Ca ion adsorption on the 64.5 m^2/g SSA goethite for different surface-to-metal loadings in 0.01M and 0.7M $NaNO_3$ solutions. (a) solute/solid ratio changed to 1e-4M Ca^{2+} /1.2g/L goethite; (b) ratio changed to 1e-3M Ca^{2+} / 1.2 g/L goethite

5.3.2.2. Intermediate ionic strengths

Predictions were also made for electrolyte concentrations between the two extremes (0.01M and 0.7M) that were used for calibrating the model. Figure 5-5 shows four examples of modeling results: Mg^{2+} and Sr^{2+} adsorption in 0.1M and 0.3M $NaNO_3$

solutions (results for Ca^{2+} and Ba^{2+} are presented in Appendix). The agreement of the model with the experimental data demonstrates that the model is capable of predicting alkaline earth metal ion adsorption over a wide range of $NaNO_3$ concentrations spanning from 0.01M to 0.7M.

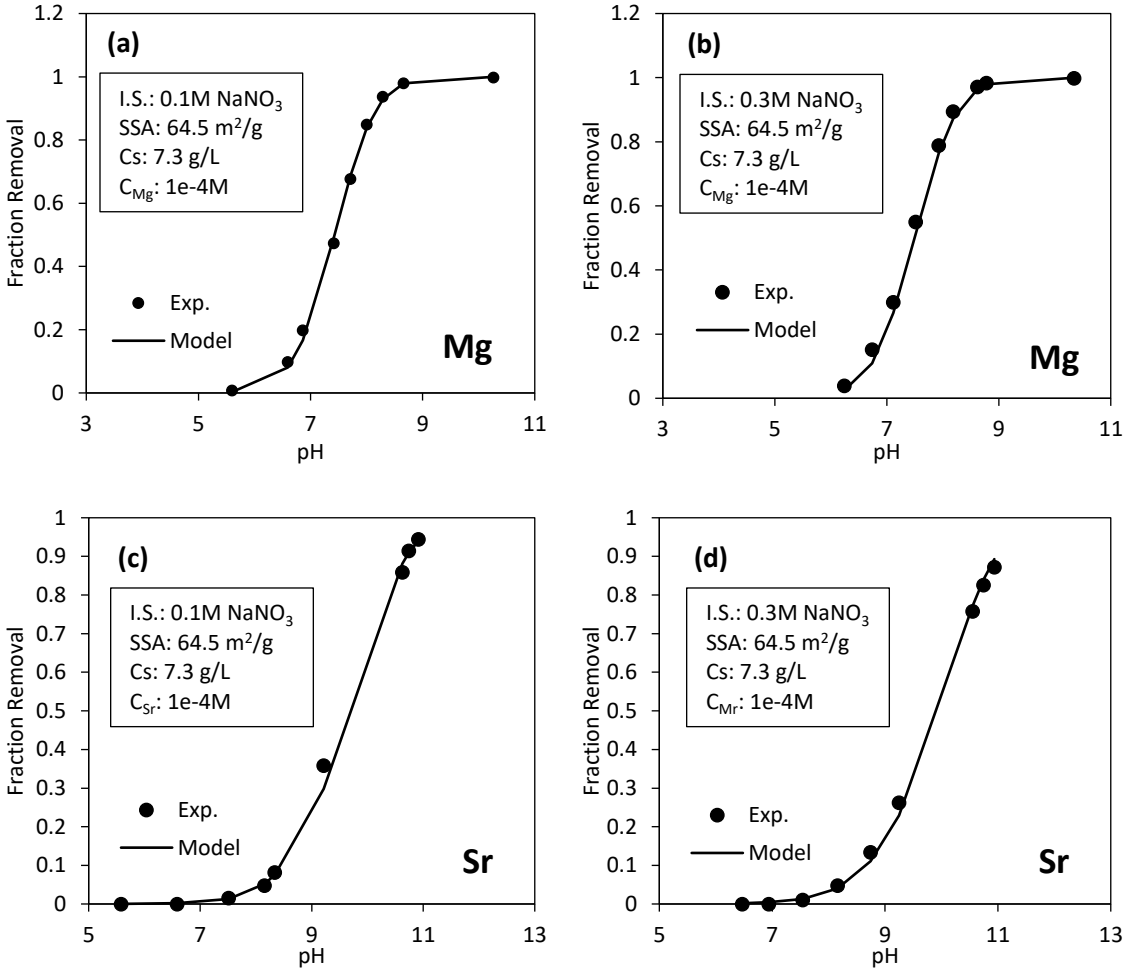

Figure 5-5. Predictions of Mg and Sr adsorption on the 64.5 m^2/g SSA goethite in 0.1M and 0.3M $NaNO_3$ solutions. (a) Mg in 0.1M $NaNO_3$; (b) Mg in 0.3M $NaNO_3$; (c) Sr in 0.1M $NaNO_3$; (d) Sr in 0.3M $NaNO_3$

5.3.2.3. Effect of background electrolytes

Figure 5-6 illustrates the modeling results for Ba^{2+} and Mg^{2+} adsorption on goethite in 0.7M $NaNO_3$ and NaCl solutions. As described in previous chapters, the aqueous complexation of alkaline earth metal ions with NO_3^- ligands reduces the concentration of free metal ions which consequently affects adsorption on goethite. In comparison to $NaNO_3$ solutions, free concentrations of Ba^{2+} are higher for NaCl solutions, whereas for Mg^{2+} the free cation concentration is lower in NaCl solutions. The model accurately predicted the differences in adsorption related to these different solution chemistries. The relatively small difference in Mg^{2+} adsorption between $NaNO_3$ and NaCl solutions is assumed to be due to the higher surface affinity of Mg^{2+} compared to Ba^{2+}.

Model predictions of Ba adsorption in a more complex solution system (i.e., mixture of 0.35M $NaNO_3$ and 0.35M NaCl) were also compared to experimental data in Figure 5-7. Ba^{2+} was specifically selected as the adsorbate due its relatively low affinity to goethite which results in greater impact on adsorption by background electrolytes. The agreement between the model predictions and the experimental data provide further evidence to support the optimized parameter values and selected surface species.

Figure 5-8 displays the model predictions for Ba adsorption in 0.7M $NaNO_3$, $RbNO_3$ and $CsNO_3$ solutions. As explained in the previous chapter, fractional removal of Ba^{2+} at a given pH is highest in $CsNO_3$ solutions and lowest in $NaNO_3$ solutions; this trend is consistent with the trends in the affinity of the monovalent electrolyte cations for goethite which follows $Na^+ > Rb^+ > Cs^+$. The modeling results show that the selected equilibrium constants for the surface complexes of the electrolyte cations enable the model to capture this trend in Ba^{2+} adsorption.

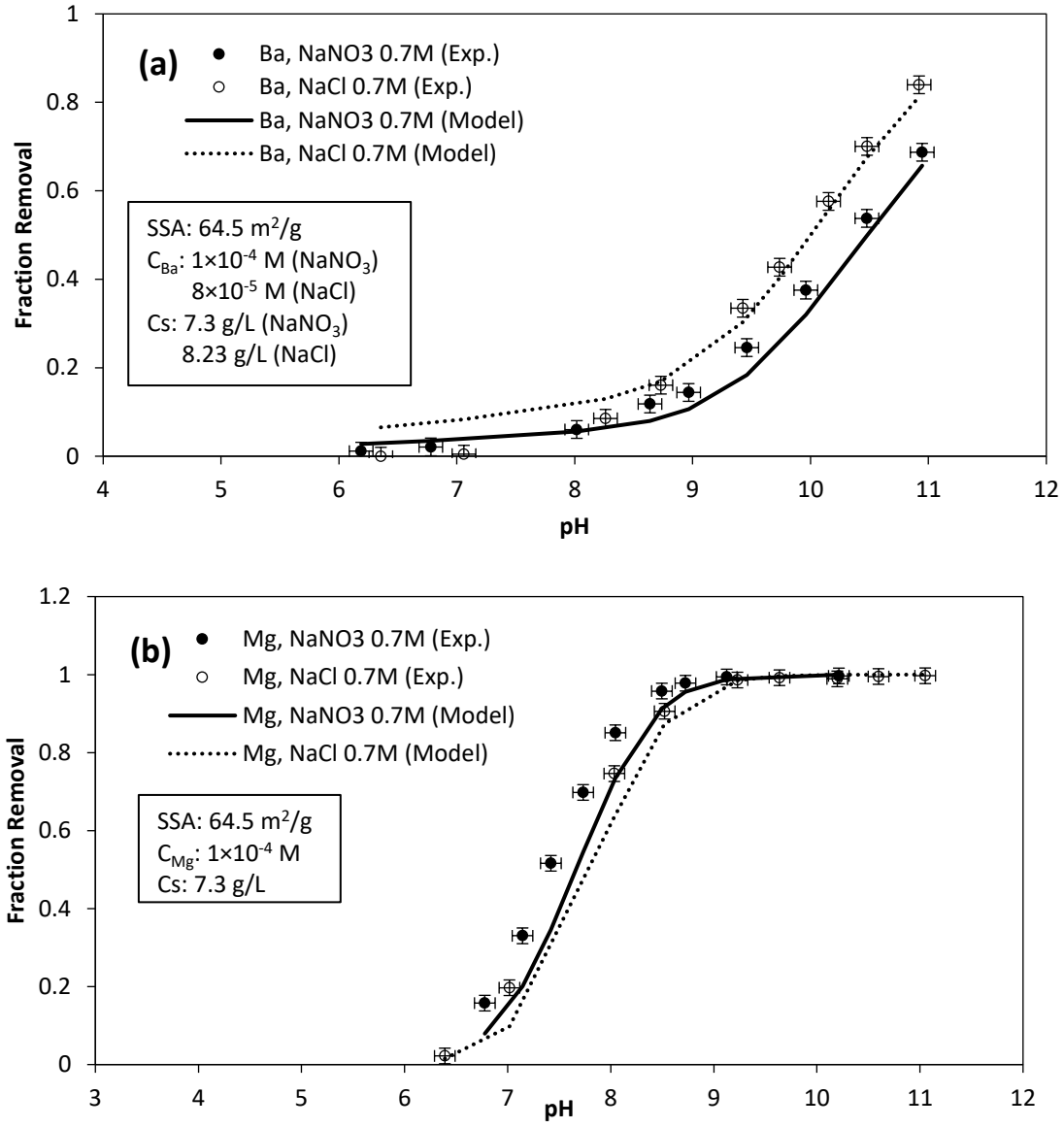

Figure 5-6. Predictions of (a) Ba and (b) Mg ion adsorption on goethite in 0.7M $NaNO_3$ and NaCl solutions

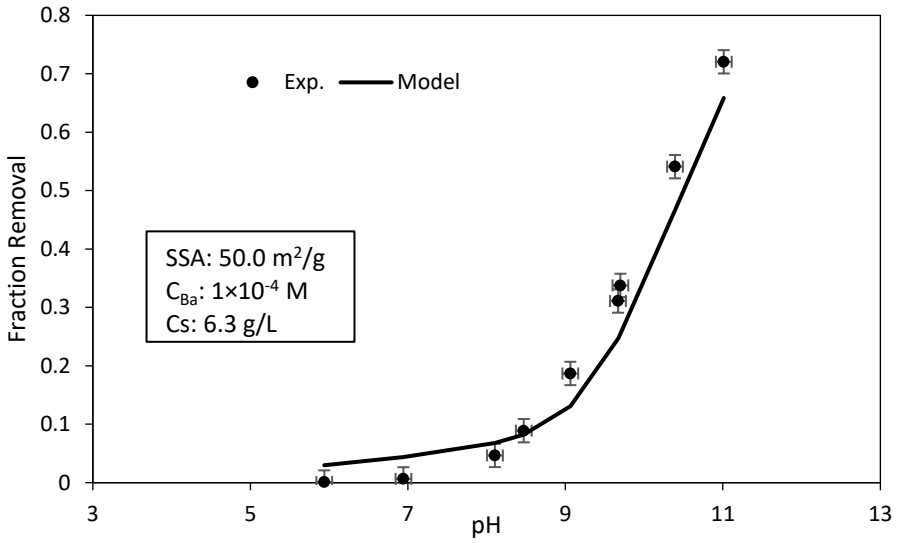

Figure 5-7. Experimental data and model predictions of Ba adsorption in complex electrolyte systems (mixture of 0.35M $NaNO_3$ and 0.35M NaCl)

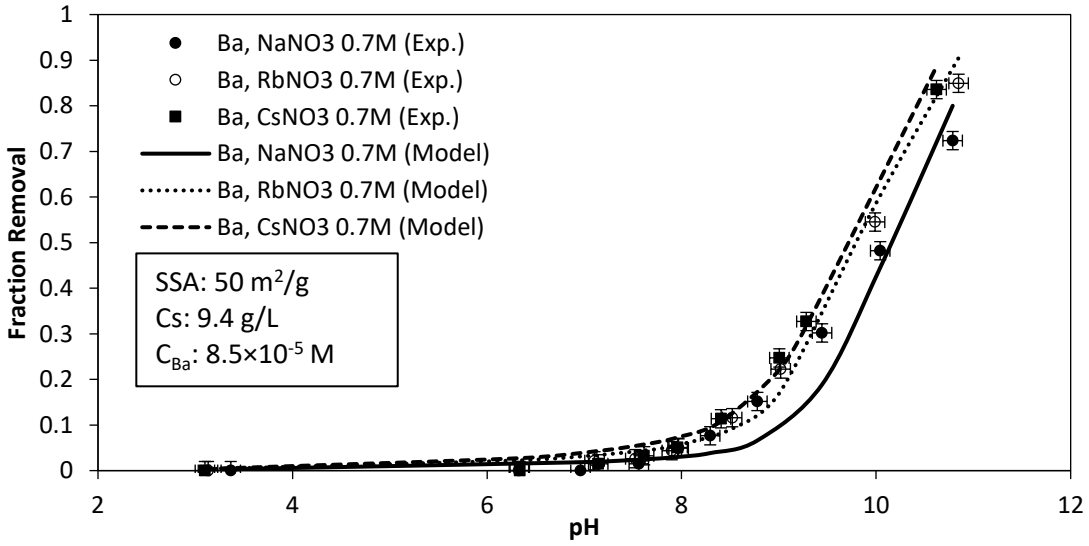

Figure 5-8. Predictions of Ba adsorption on goethite in 0.7M $NaNO_3$, $RbNO_3$ and $CsNO_3$ solutions

5.3.2.4. Different preparations of goethite

The predictions for Ba^{2+} adsorption for three different preparations of goethite (i.e., 50 m^2/g, 64.5 m^2/g, and 73 m^2/g SSA) are shown in Figure 5-9. When the electrolyte concentration and total surface area of goethite in batch reactors are identical, Ba^{2+} adsorption is observed to be greater on lower SSA goethites (50 m^2/g > 64.5 m^2/g > 73 m^2/g SSA). The model predictions show a trend consistent with the experimental results; however, the difference between predictions for the 64.5 m^2/g and 73 m^2/g goethites were very small. The agreement between the simulations for the two goethites (i.e., 64.5 m^2/g and 73 m^2/g SSA) is due to the fact that the estimated densities of surface oxygen groups (i.e., singly-, doubly-, and triply-coordinated sites) on these two goethites were very similar. In fact, the experimental adsorption data of the two goethites are statistically identical when considering the error ranges.

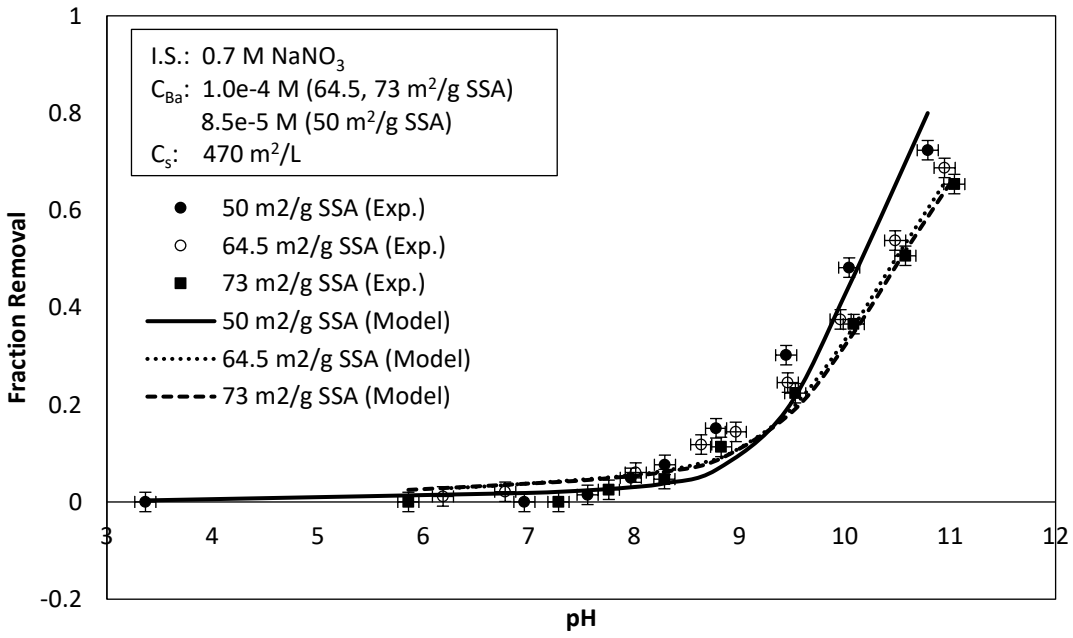

Figure 5-9. Prediction of Ba adsorption for three different goethite preparations (i.e., 50 m^2/g, 64.5 m^2/g and 73 m^2/g)

5.3.2.5. Mg^{2+} and Cd^{2+} bi-solute solution

The model was also tested for bi-solute solutions that contained Mg^{2+} and Cd^{2+} together. Since both metal cations were assumed to adsorb onto goethite as inner-sphere complexes, it was initially expected that the two metal cations would impact the adsorption of each other; due to the relatively high concentration of Mg^{2+} and strong surface affinity of Cd^{2+}. However, experimental results showed that the adsorption of both metal cations were not impacted by the presence of the other over the range of conditions tested. Moreover, the model predictions were also consistent with this result. (see Figure 5-10)

The minimal effect of high concentrations of Mg^{2+} (0.01 mol/L) on Cd^{2+} adsorption is not surprising due to the greater affinity of transition metals such as Cd^{2+} for the goethite surface compared to Mg^{2+}. Indeed, comparisons of the adsorption edges for the two adsorbates shows nearly complete removal of Cd at pH values that are below the adsorption edge for Mg.

The reason for the minimal impact of Cd^{2+} on Mg^{2+} adsorption is presumably due to the system containing a sufficient number of surface sites to accommodate both species without competition. In other words, the number of reactive sites exceeded the total number of Cd^{2+} and Mg^{2+} ions, and thus, both metal cations were able to fully adsorb onto the surface. The calculated surface site concentration of the singly-coordinated oxygen groups on the (210) crystal face, which is the surface site that Mg^{2+} surface complexes were primarily located (approx. 69% of total Mg^{2+}), was 3.86×10^{-4} mol/L which is greater than the total concentration of both metal cations combined (Mg^{2+}: 2.5×10^{-4} mol/L and Cd^{2+}: 3.5×10^{-5} mol/L). Modeling results show that approximately 1/3 – 1/2 of these surface sites are unoccupied by either the metal cation solute or protons throughout the whole pH range tested (i.e., pH 3.6 – 10.4). This result provides some insight regarding the structure of the Mg^{2+} surface complexes. Since the ratio of the reactive surface site concentration

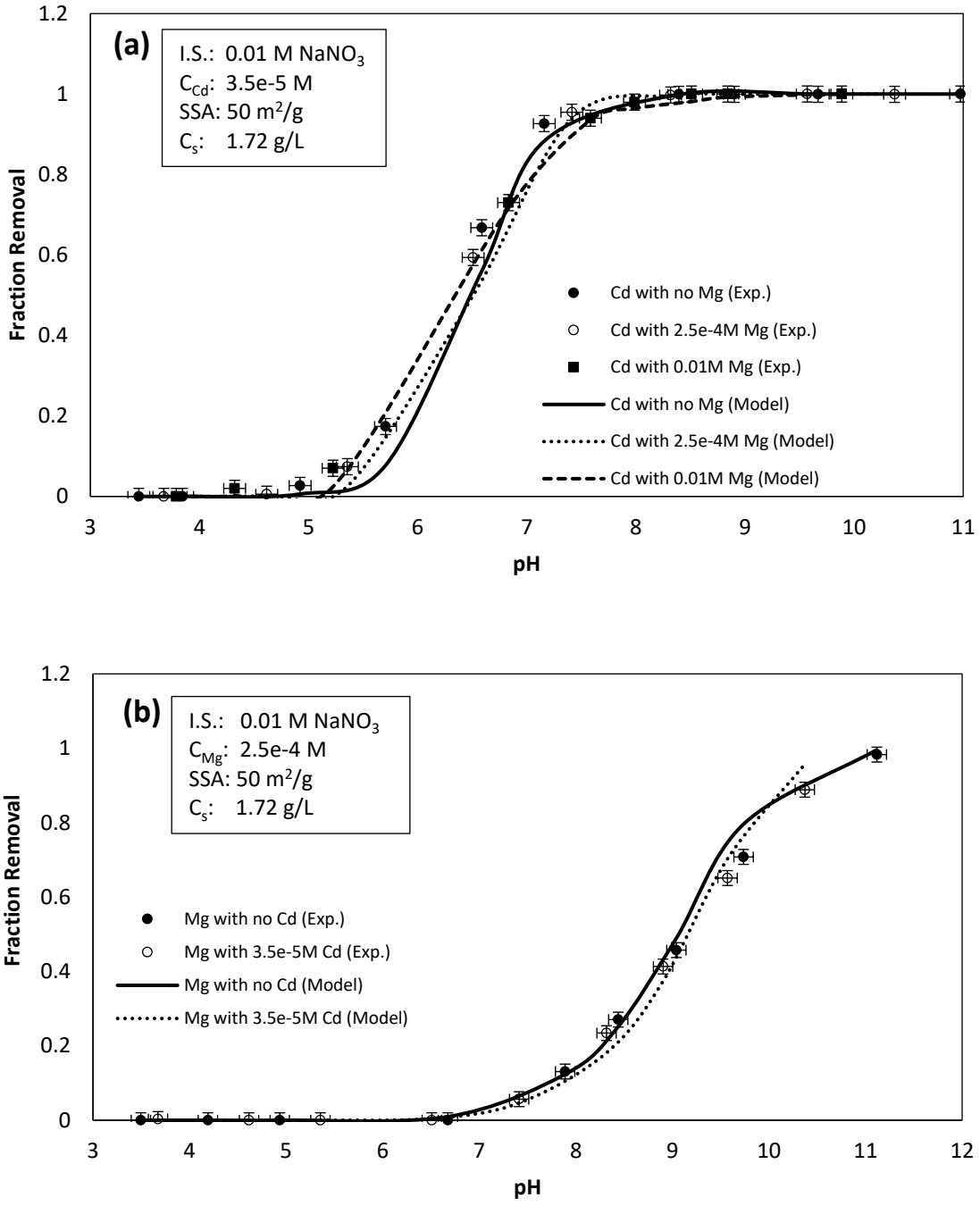

Figure 5-10. Experimental data and model predictions for Mg^{2+} and Cd^{2+} in single and bisolute systems. (a) Fractional removal of Cd^{2+} with three different concentrations of Mg^{2+}, and (b) fractional removal of Mg^{2+} with two different concentrations of Cd^{2+}

over total Mg^{2+} ion concentration is less than two, if the dominant Mg^{2+} surface complexes were combined with more than two surface oxygens of the same type (i.e., bidentate or higher) then there would have been an insufficient number of surface sites available to accommodate both the Mg^{2+} and Cd^{2+}. Thus, the selection of a mono-dentate inner-sphere surface complex for the dominant Mg^{2+} surface species enabled the accurate model prediction of the Mg^{2+} and Cd^{2+} bisolute system studied in this research.

5.3.2.6. Adsorption data from literature

Finally, the calibrated model was used to simulate adsorption data from literature in order to test its capability for predicting alkaline earth metal ion adsorption for different goethite morphologies and in solutions with solute/solid ratios outside the range tested in this study (1.35×10^{-5}– 8.33×10^{-4} $mol_{\text{-solute}}/g_{\text{-solid}}$). Figure 5-11 (a), (b) and (c) show adsorption edge data and model predictions for Mg^{2+}, Ca^{2+}, and Sr^{2+}, respectively, from various studies that used different preparations of goethite. One concern in modeling this data is that the pH_{pzse} of goethite used for the data from Ali and Dzombak (1996) was pH 8.0; a value that suggests the presence of carbonate contamination. Except for the low concentration Ca^{2+} data from Ali and Dzombak (1996), the model provided good fits to the adsorption data found in literature. That the model underpredicted adsorption for the low concentration data is likely due to the reduction in surface charge associated with carbonate sorption in this pH range. For Sr, the model was able to predict sorption for data collected at low solute/solid ratios (i.e., 2.54×10^{-7} – 2.54×10^{-5} $mol_{\text{-Sr}}/g_{\text{-solid}}$). The satisfactory fit of our model predictions to the adsorption data collected from literature indicates that the selected surface complexes and equilibrium constants, along with the approach developed

in Chapter 3 to estimate surface parameters of goethites are capable of predicting alkaline earth metal ion adsorption for a range of solution and surface conditions.

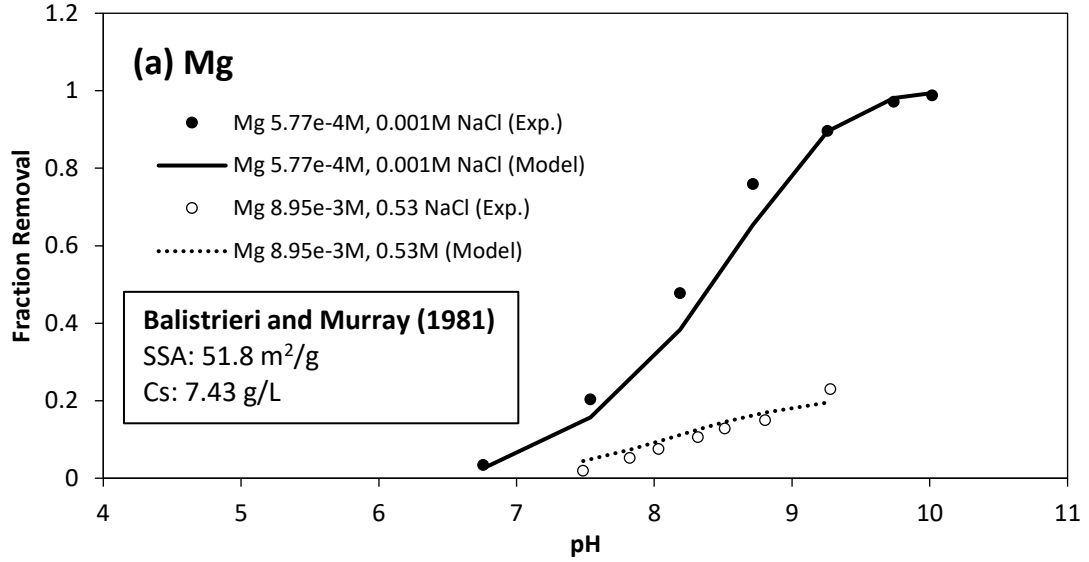

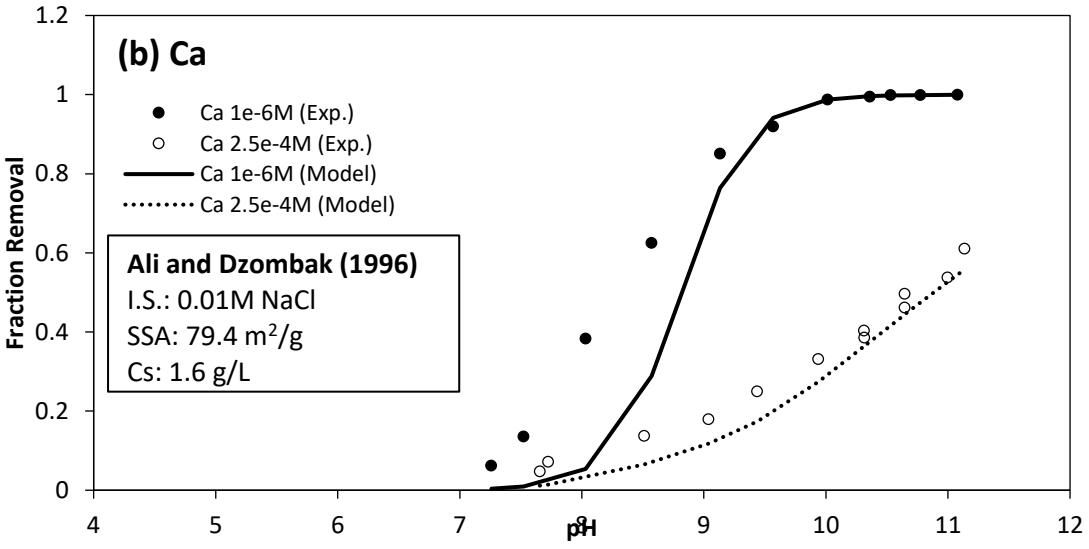

Figure 5-11. Prediction of alkaline earth metal ion adsorption data from literature (a) Mg^{2+}, (b) Ca^{2+}, and (c) Sr^{2+}

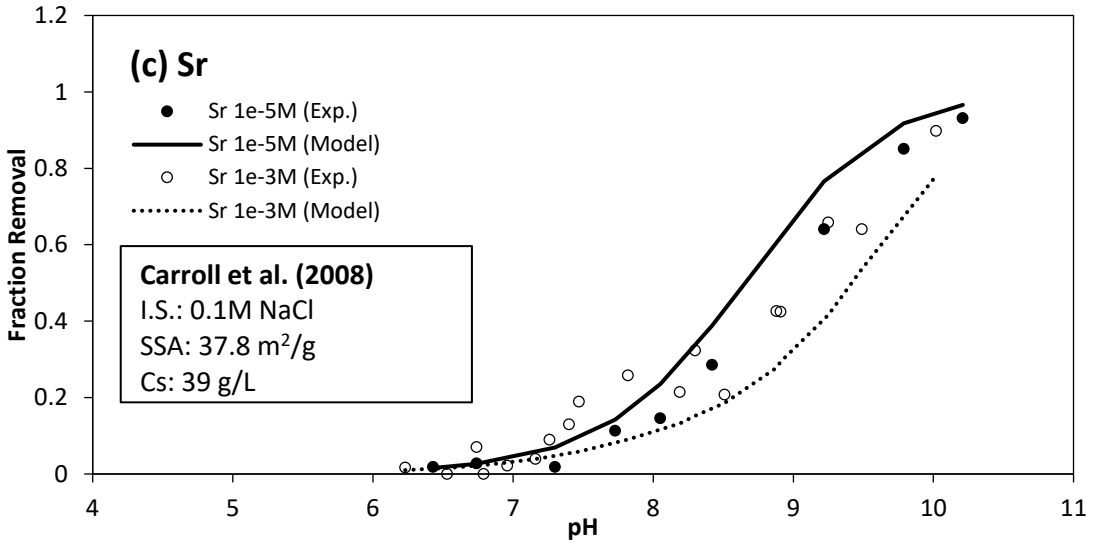

Figure 5-11, cont.

5.4. CONCLUSIONS

The adsorption behavior of alkaline earth metal ions onto goethite and the impact of background electrolytes in solutions containing varying ionic strengths, background electrolytes, and competing adsorbates were accurately simulated with a CD-MUSIC model. Two surface complex species were utilized to model each alkaline earth metal ion and were selected based on spectroscopic, molecular modeling and objective curve fitting of single-solute macroscopic adsorption data. While most of the alkaline earth metal surface complexes formed outer-sphere complexes with the goethite surface, an inner-sphere species was assumed for Mg^{2+}. It must be noted that the data-fitting method does not provide definite evidence of the structure and stoichiometry of surface complexes since multiple combinations of surface species can be used to model adsorption data reasonably well. However, with the surface complex species and equilibrium constants obtained from this study, the calibrated model was able to predict alkaline earth metal ion adsorption over

a wide range of solution and surface conditions; the model predictions encompassed a wide range of pH (5 – 11), solute/solid ratio (1.37×10^{-5} – 8.33×10^{-4} $mol_{-solute}/g_{-solid}$), ionic strengths (0.01M – 0.7M), and background electrolytes (Na^+, Cs^+, Rb^+, Cl^-, NO_3^-). In addition, by combining the relationships between surface parameters and goethite SSA, which were also established as part of this study and described in Chapter 3, the model was able to predict the variation of reactivity between three different preparations of goethite towards Ba^{2+}.

The model was also combined with Cd adsorption model parameters developed by Mangold (2013) [89] to simulate the interaction between Cd^{2+} and Mg^{2+} on the goethite surface. The experimental data and model results showed no competition between the two cations for the solution conditions tested. Finally, several sets of adsorption data from the literature were used to verify the predictability of the model. The results indicate that the model provides reasonable predictions of the data over a wider range of solution conditions.

Chapter 6. Conclusions and Recommendations

6.1. CONCLUSIONS

The variable reactivity of goethite surfaces and the adsorption behavior of alkaline earth metal ions onto goethite in various electrolyte solutions were investigated to achieve the research goal of developing a self-consistent surface complexation model that is capable of predicting ion adsorption over a wide range of surface and solution conditions. The findings from this work are detailed below for each of the objectives set forth in Chapter 1.

Objective 1. Establish an approach to account for the effect of goethite morphology on surface properties and the associated impact of these properties on ion adsorption in a CD-MUSIC model

A new approach to capture the variation of surface reactivity between different morphologies of goethite into a single SCM was developed and tested in this study. By establishing relationships between crystal face contribution (CFC), inner-Helmholtz capacitance, and protonation constants with the specific surface area (SSA) of goethite, modeling parameters for different morphologies of goethite were estimated simply based on their SSA values. The established relationships closely matched trends and values of surface parameters reported in the literature. It was proven that with this approach, a CD-MUSIC model was capable of accurately predicting proton, SeO_3^{2-}, and Cd^{2+} adsorption for a wide range of goethite preparations (i.e., 21 – 105 m^2/g SSA).

Objective 2. Evaluate effects of different background electrolytes on alkaline earth metal ion adsorption onto goethite

Macroscopic adsorption experiments conducted as part of this study show that adsorption of alkaline earth metal (AEM) ions onto goethite can be affected by background electrolytes. Several mono-valent electrolyte cations (Na^+, K^+, Cs^+, Rb^+) and anions (Cl^-, NO_3^-, ClO_4^-) were tested in this study. Alkaline earth metal cations that weakly bind to the surface, such as Ba^{2+}, were more significantly affected by the presence of background electrolytes compared to other AEMs. Experimental results suggested that the electrolyte impact leading to reduced adsorption of AEMs is due to a combination of competitive adsorption and aqueous complexation reactions with electrolyte cations and anions. This indicates that (for at least weakly sorbing ions) background electrolytes should not be assumed to be inert or indifferent, and hence, the effect of electrolytes needs to be identified and characterized in order to obtain proper surface complexation equilibrium constants by experimental adsorption data; experimental results from the current study have shown that electrolyte effects are observable for weakly sorbing ions (i.e., Sr^{2+} and Ba^{2+}) in solutions with background electrolyte concentrations as low as 0.1M.

Objective 3. Utilize a surface complexation model to describe and predict alkaline earth metal ion adsorption onto goethite under a wide range of solution conditions

Finally, the structures of AEM surface complexes were suggested through model calibration with adsorption experimental data. Two surface species were required for each of the four AEM ions tested in this study. This is consistent with numerous studies listed in Table 5-1. While all Ca^{2+}, Sr^{2+} and Ba^{2+} surface complexes were considered outer-sphere, Mg^{2+} adsorption was modeled assuming formation of both inner-sphere and outer-sphere complex species on the goethite surface. The selection of Sr-complexes was

consistent with previous X-ray spectroscopy studies (i.e., Outer-sphere mono- and tetradentate) [70]–[72], [198], and Mg-complexes were also consistent with previous modeling studies [44], [61], [64], [165]. Once calibrated, the CD-MUSC model developed in this research provided accurate predictions of AEM adsorption onto goethite under a variety of solution conditions (i.e., pH 5 – 11, 0.01M – 0.7M ionic strength, various background electrolytes) and on different goethite SSAs with this self-consistent set of model parameters, surface species and equilibrium constants. In addition, model results showed that Mg^{2+} and Cd^{2+}, which both adsorb as inner-sphere complexes onto goethite, do not affect the adsorption of each other. Even at high concentrations of Mg^{2+} (i.e., 0.01 M), the model predicted no effect of Mg^{2+} on Cd^{2+} adsorption (4×10^{-5} M). Also, no impact of Cd^{2+} on Mg^{2+} adsorption was predicted; the predictions in all cases were consistent with the experimental results.

6.2. ENGINEERING IMPLICATIONS

The intellectual merit of this work includes an improved understanding of the variation of surface reactivity resulting from different goethite morphologies, adsorption characteristics of alkaline earth metal ions on metal oxides and the interactions of electrolyte anions and cations with alkaline earth metal ions. The model developed through this study will be the first of its kind that is capable of predicting ion adsorption on a range of different goethites by simply using their SSA values. This feature will greatly enhance the usability of the model since goethite SSA can be obtained relatively easily and with high accuracy. Also, this study provides the most extensive set of adsorption data currently available for alkaline earth metal ions on goethite which covers a vast range of solution conditions (i.e., pH, ionic strength, surface-solute ratio and various electrolytes). The data

helped elucidate the discrete effect of cationic and anionic electrolytes on metal ion adsorption, providing solid evidence to the claim that the commonly used term, indifferent electrolytes, is misleading; especially in high ionic strength solutions and with weakly sorbing ions, such as alkaline earth metal ions

This work potentially enhances our ability to predict the fate and transport of inorganic contaminants in natural and engineered systems. Most immediately, this study can be directly applied to improve the adsorption models of other hazardous metal cations using the same approaches used in this work for cadmium. The approach will also be applicable to adsorbent surfaces other than goethite. The improved predictive capability of these adsorption models may potentially assist engineers in making better decisions, reducing costs, and minimizing risks during a project, especially in cases where high concentrations of electrolytes are present in solutions (i.e., ground waters, produced waters, recycled fracking waters, and wastewaters from soil remediation sites).

The findings of this study may also impact the establishment of the surface complexation modeling (SCM) database. With a modeling approach that links surface properties with the SSA of a mineral, a single set of equilibrium constants for surface complexes can be employed that does not vary with the morphology (or SSA) of goethite.

Knowledge achieved by this study can be particularly useful in designing systems which focus on removing alkaline earth metal ions from waters via adsorption processes. One example of such a system is the precipitation/crystallization process for removal of contaminants or recovery of resources (e.g., phosphorous). The results from this study can help enhance the adsorption capacity of such systems.

Finally, the results from this study can be used to guide the application and formulation of SCMs with fewer parameters. For example, the DLM is frequently used to

describe sorption in practical applications. However, this model does not incorporate background electrolyte adsorption. The results from this research can be used to modify DLM surface complexation parameters for alkaline earth metal ions based on the particular background electrolyte employed.

It is important to note, however, that this study has limitations, especially for direct applications to natural systems. The scope of this study is limited to pure synthetic goethite systems. Therefore, the impact of other factors that may potentially affect the adsorption reaction of ions in natural water and soil has not been investigated; these other factors may include, but are not limited to, the presence of natural organic matter (NOM), heterogeneity of soil minerals, weathering of goethite particles, and microbiological activity. Among these factors, NOMs are particularly important in metal cation adsorption modeling since they are typically negatively charged in natural waters and may adsorb onto minerals, thereby altering the apparent surface reactivity of minerals. However, several researchers have demonstrated that the incorporation of NOM into SCMs is possible by determining the equilibrium constants of the adsorption reaction between minerals and NOM, and also, metal cations and NOM [66], [68], [216]. By using the method set forth in these previous studies, the predictive capability of the CD-MUSIC model used in the current study may be further enhanced toward ion adsorption in NOM containing environments.

6.3. Recommendations for Future Work

The current study can be extended in many directions. A couple of examples are suggested and discussed below.

1. Applying similar approach to other metal oxides

Although the scope of this study was limited to goethite, the approach used for this study can be applied to other metal oxides. The well-crystalized structure of goethite has enabled establishment of relationships between surface parameters and SSA. Similarly, other minerals that have well-defined crystal structures may be able to link surface properties to readily measurable parameters. Establishing such relationships between surface properties will result in reducing the number of required parameters for modeling ion adsorption to the mineral surface and will eventually extend the predictive capability of SCMs to a wide range of different mineral morphologies. It will also be meaningful to develop approaches to capture the variable surface reactivities of amorphous metal oxides. However, in such cases, other measures (e.g., site densities, oxygen-metal ion ratio) would be required to characterize and identify characteristics of the target metal oxide mineral that impact surface complexation parameters.

It will be also important to investigate other mineral surfaces to identify the effect of electrolytes on AEM adsorption. Since the impact of background electrolyte cations to AEM adsorption are related to the electrolyte's relative affinity to the goethite surface, it is expected that the degree of and trend for impacts of electrolytes can vary among different metal oxide surfaces. As an example, the affinity trends of monovalent electrolyte cations (i.e., Na^+, K^+, Cs^+, Rb^+) are flipped between high and low dielectric constant minerals as documented in previous studies [51]. Since, goethite is considered a low dielectric constant mineral, future research may focus on high dielectric constant minerals such as magnetite (Fe_3O_4), rutile (α-TiO_2), and manganese oxide (α-MnO_2) to contrast the difference in electrolyte effects on AEM adsorption.

2. Assessing the validity of simpler SCMs

The current study has proven that the CD-MUSIC model parameterized in this work was capable of simulating subtle differences in proton and ion reactivity between different goethite preparations as well as difference in Mg^{2+} and Ba^{2+} adsorption for a range of background electrolyte solutions. The modeling results demonstrate that the relatively large number of required parameters associated with the complexity of the CD-MUSIC model, was beneficial for making such accurate predictions; however, the level of accuracy required in practical situations may not warrant this degree of complexity. In fact, simple models (e.g., DLM and CCM) are generally preferred over complicated models in practical applications given that they provide a suitable level of accuracy for the purpose. Simple models are favored because they are easier to use and require less information about the target system. Therefore, it will be helpful to engineers if the range of conditions where these simpler models provide accurate predictions are pre-determined. The CD-MUSIC developed in the current study can be applied to assess the appropriate range of conditions by employing a 'top-down' approach, in which a more robust model that can accurately predict adsorption over an extensive range of system conditions is used to evaluate the applicability of simpler models over ranges of conditions. Ideally, model results should be compared with data from experiments performed under conditions similar to the application system of interest in order to assess its accuracy. But in reality, these experimental data are rarely available or are limited in scope. Therefore, the 'top-down' approach can serve as a viable alternative for such situations.

APPENDICES

APPENDIX A. EXAMPLE OF FITEQL 4.0 INPUT FILE

Input files for FITEQL 4.0 can be generated by either the Windows Pre-Processor (i.e., GUI interface developed as a Windows application) or the Notepad application. Tableaux of the surface complexation reactions, experimental data, surface site concentrations, surface parameters, charge distribution values, solid concentration, capacitance and SSA information are included in the input file, which setups the SCM. Below is a screen capture image of an FITEQL 4.0 input file.

```
': PROGRAM: FITEQL Version 4.0
': FILENAME: C:\FITEQL4\FITDATA\NEWMYD~1\BA\BAT4607N.F40
': PATH: C:\FITEQL4\FITDATA\NEWMYD~1\BA\
': DESCRIPTION: CD-MUSIC Ba on goethite
'Alumina, Triple Layer, from FITEQL 2.0
     0
     0
     1
     0
     0
    30
    11     1     1    24     1     1
   170 Activity     -1.000  7.000E-01
   811 XOH          -4.000  2.069E-03
   813 ZO           -4.000  2.069E-03
   814 X^OH         -4.000  7.890E-04
   812 Y^OH         -4.000  3.945E-04
   160 PSI(0)       -1.000  0.000E+00
   161 PSI(beta)    -0.500  0.000E+00
   162 PSI(d)       -0.200  0.000E+00
    30 Na[+]        -1.000  7.000E-01
    31 NO3[-]       -1.000  7.000E-01
   200 Ba[+2]       -4.000  1.000E-04
   220 Ba(ads)       0.000  0.000E+00
    50 H[+]          0.000  0.000E+00

    50 H[+]          0.000   50    1
   100 OH[-]       -13.997  170   -2  50   -1
    30 Na[+]         0.000   30    1
    31 NO3[-]        0.000   31    1
    32 NaOH(aq)    -13.897   30    1  50   -1
    33 NaNO3(aq)    -0.550  170    2  30    1  31    1
   200 Ba[+2]        0.000  200    1
   201 BaOH+       -13.357  170    2 200    1  50   -1
   206 BaNO3+        0.700  170    4  31    1 200    1
   811 XOH           0.000  811    1
     2 XOH2          8.500  811    1 160    1  50    1
     3 XOH2_NO3      8.000  811    1 160    1 161   -1  31    1  50    1
     4 XOH_Na        0.100  811    1 161    1  30    1
   813 ZO            0.000  813    1
    20 ZOH          11.700  813    1 160    1  50    1
    21 ZOH_NO3      11.200  813    1 160    1 161   -1  31    1  50    1
    22 ZO_Na         0.100  813    1 161    1  30    1
   814 X^OH          0.000  814    1
    10 X^OH2         8.500  814    1 160    1  50    1
    11 X^OH2_NO3     8.000  814    1 160    1 161   -1  31    1  50    1
    12 X^OH_Na       0.100  814    1 161    1  30    1
   812 Y^OH          0.000  812    1
   220 2X_Ba         5.538  811    2 161    2 200    1 220    1
   221 4X^_BaOH      3.713  814    4 161    1 200    1 220    1  50   -1
```

General description of file

Concentrations of surface sites, electrolytes, sorbing ions

Tableau of the surface complexation reactions

```
  50 H[+]          170    0.500
 100 OH[-]         170    0.500
  30 Na[+]         170    0.500
  31 NO3[-]        170    0.500
  32 NaOH(aq)
  33 NaNO3(aq)     170    0
 200 Ba[+2]        170    2
 201 BaOH+         170    0.500
 206 BaNO3+        170    0.500
 811 XOH           160   -0.500
   2 XOH2          160    0.500
   3 XOH2_NO3      160    0.500
   4 XOH_Na        160   -0.500
 813 ZO            160   -0.500
  20 ZOH           160    0.500
  21 ZOH_NO3       160    0.500
  22 ZO_Na         160   -0.500
 814 X^OH          160   -0.500
  10 X^OH2         160    0.500
  11 X^OH2_NO3     160    0.500
  12 X^OH_Na       160   -0.500
 812 Y^OH
 220 2X_Ba         160   -1
 221 4X^_BaOH      160   -2

   4  73.000000   6.200000   0.970000   0.970000
0.700000   1.000000
```

Solid information

```
   0     0     0
   0    '* NDIS

   1     9
   T          logX
   220        50
'*   Ba(ads)     H[+]
  1  0.000E+00  -5.337000
  2  0.000E+00  -7.187000
  3  2.845E-06  -8.018000
  4  7.446E-06  -8.544000
  5  1.434E-05  -8.925000
  6  2.367E-05  -9.461000
  7  3.915E-05 -10.057000
  8  4.945E-05 -10.419000
  9  6.584E-05 -10.994000
```

Experimental data

```
   2     1     0     '* NST, NSX, KUWSOS
200  0.0100000  0.0000010     '* ST for Component: Ba[+2]     (REL, ABS)
220  0.0100000  0.0000010     '* ST for Component: Ba(ads)    (REL, ABS)
220  5.000E-02  0.000E+00     '* SX for Component: Ba(ads)    (REL, ABS)
```

Error description

APPENDIX B. CODE USED FOR AUTOMATED OPTIMIZATION OF LOG K VALUES OF ALKALINE EARTH METAL ION ADSORPTION

An automated program was developed and used to assist the iterative optimization of log K values. AHK language was used for the coding and a script generator (Pulover's Macro Creator v.5.05) was used for the execution of the developed program. The code is consisted of two modules, 1) an optimization module which runs the FITEQL 4.0 to find the log K value that returns the lowest WSOS/DF of a given surface species, and 2) a scanning module which executes iterative run of the model to scan and record the modeling results by sequentially inputting different log K values for a given surface species. It should be noted that, for an unknown technical reason, the code did not operate properly (i.e., crash or return error) when executed outside the script generator. The codes for each module are as below.

// Optimization Module //

```
IfWinExist, ahk_class SALFRAME
{
   WinActivate, ahk_class SALFRAME
   Sleep, 10
   WinWaitActive, ahk_class SALFRAME, , 3
   Sleep, 10
}
Else
{
   MsgBox, 0, ,
   (LTrim
   ERROR!
   OpenOffice does not exist
   )
   Goto, EndRun
}
Send, {f5}
WinWaitActive, Navigator ahk_class SALSUBFRAME
Sleep, 10
Send, {del}{del}B{tab}7{enter}{f5}
WinWaitClose, Navigator ahk_class SALSUBFRAME
Sleep, 10
clipboard := ""
```

```
Send, ^c
ClipWait
In_file := clipboard
clipboard := ""
Send, {down}^c
ClipWait
Out_file := clipboard
StringReplace, Out_file, Out_file, `n, , a
StringReplace, Out_file, Out_file, `r, , a
Num_array := Array(211, 212, 213, 215, 216, 217, 221, 222, 223, 224, 225, 226, 227, 228, 241, 242, 243, 244, 245,
246, 247, 248, 611, 612, 613, 615, 616, 617, 621, 622, 623, 624, 625, 626, 627, 628, 641, 642, 643, 644, 645, 646, 647,
648)
Species_array := Array("X_Sr", "Z_Sr", "X)_Sr", "X_SrOH", "Z_SrOH", "X)_SrOH", "2X_Sr", "2Z_Sr", "2X)_Sr",
"X_Sr_Z", "2X_SrOH", "2Z_SrOH", "2X)_SrOH", "X_SrOH_Z", "4X_Sr", "4Z_Sr", "4X)_Sr", "2X_Sr_2Z",
"4X_SrOH", "4Z_SrOH", "4X)_SrOH", "2X_SrOH_2Z", "X.Sr", "Z.Sr", "X).Sr", "X.SrOH", "Z.SrOH", "X).SrOH",
"2X.Sr", "2Z.Sr", "2X).Sr", "X.Sr.Z", "2X.SrOH", "2Z.SrOH", "2X).SrOH", "X.SrOH.Z", "4X.Sr", "4Z.Sr", "4X).Sr",
"2X.Sr.2Z", "4X.SrOH", "4Z.SrOH", "4X).SrOH", "2X.SrOH.2Z")
Dentate_array := Array(1, 1, 1, 1, 1, 1, 2, 2, 2, 2, 2, 2, 2, 2, 4, 4, 4, 4, 4, 4, 4, 4, 1, 1, 1, 1, 1, 1, 2, 2, 2, 2, 2, 2, 2, 2, 4, 4,
4, 4, 4, 4, 4, 4)
Combo1_LoopNum := 0  ; Normaly starts at LoopNum=0
LoopNum := 0
BigLoopBeginning:
Combo1_LoopNum += 1
If Combo1_LoopNum <= 44
{
   Combo2_LoopNum := Combo1_LoopNum + 1  ; Normaly starts at LoopNum=0
   SmallLoopBeginning:
   LoopNum += 1
   WinActivate, ahk_class ThunderForm
   Sleep, 10
   WinWaitActive, ahk_class ThunderForm
   Sleep, 10
   Send, ^o
   Send, %in_file%
   Send, {enter}
   Sleep, 100
   WinWaitActive, ahk_class ThunderForm
   Sleep, 10
   If Combo2_LoopNum <= 44
   {
      Combo1_Num := Num_array[%Combo1_LoopNum%]
      Combo1_Species := Species_array[%Combo1_LoopNum%]
      Combo1_Dentate := Dentate_array[%Combo1_LoopNum%]
      Combo2_Num := Num_array[%Combo2_LoopNum%]
      Combo2_Species := Species_array[%Combo2_LoopNum%]
      Combo2_Dentate := Dentate_array[%Combo2_LoopNum%]
      WinActivate, ahk_class ThunderForm
      Sleep, 10
      WinWaitActive, ahk_class ThunderForm
      Sleep, 10
      Sleep, 100
      Send, ^t
      WinWait, FIT-TEMP - Notepad ahk_class Notepad
```

```
Sleep, 10
WinWaitActive, FIT-TEMP - Notepad ahk_class Notepad
Sleep, 10
Send, ^f
WinWait, Find ahk_class #32770
Sleep, 10
WinWaitActive, Find ahk_class #32770
Sleep, 10
SendRaw,      0    '* NDIS
Send, {enter}{esc}
Send, {right}+{up}+{up}+{up}{del}{enter}
Send, 1{tab}0{tab}0{enter}%Combo1_Num%{enter}     0    '* NDIS{enter}
Send, ^s
Sleep, 333
WinClose, FIT-TEMP - Notepad ahk_class Notepad
Sleep, 100
Sleep, 333
IfWinExist, Loading data file ahk_class #32770
{
   WinActivate, ahk_class #32770
   Sleep, 100
   Send, {enter}
   IfWinExist, ahk_class #32770
   {
      WinActivate, ahk_class #32770
      Sleep, 100
      Send, {enter}
   }
   Goto, SmallLoopBeginning
}
WinWaitActive, Windows Pre-Processor ahk_class ThunderForm
Sleep, 100
Send, ^r
WinWait, C:\FITEQL4\FITEQL4.EXE ahk_class ConsoleWindowClass
Sleep, 10
WinWaitClose, C:\FITEQL4\FITEQL4.EXE ahk_class ConsoleWindowClass, , 15
Sleep, 10
IfWinExist, C:\FITEQL4\FITEQL4.EXE ahk_class ConsoleWindowClass
{
   WinActivate, C:\FITEQL4\FITEQL4.EXE ahk_class ConsoleWindowClass
   Sleep, 10
   Send, {enter}
   Sleep, 333
}
WinWaitActive, Windows  Pre-Processor ahk_class #32770
Sleep, 10
Send, {enter}
WinWaitClose, Windows  Pre-Processor ahk_class #32770
Sleep, 10
WinWaitActive, Windows Pre-Processor ahk_class ThunderForm
Sleep, 10
Send, ^v
WinWait, ahk_class Notepad
```

```
Sleep, 10
WinWaitActive, ahk_class Notepad
Sleep, 10
Send, ^f
WinWaitActive, Find ahk_class #32770
Sleep, 10
SendRaw, Converged ****
Send, {enter}
Send, {esc}
WinWaitActive, ahk_class Notepad, , 1
Sleep, 10
IfWinExist, ahk_class #32770
{
   K1_opt_fit := "Overflow"
   wsos1_opt := "Overflow"
   Send, {esc}
   WinWaitClose, ahk_class #32770
   Sleep, 10
   WinWaitActive, ahk_class Notepad
   Sleep, 10
   Goto, FinishRead1
}
Send, ^{right}^{right}^+{right}
clipboard := ""
Send, ^c
ClipWait
K1_opt_fit := clipboard
Send, {left}{right}^+{right}
clipboard := ""
Send, ^c
ClipWait
wsos1_opt := clipboard
FinishRead1:
WinClose, ahk_class Notepad
Sleep, 100
WinWaitClose, ahk_class Notepad
Sleep, 100
WinActivate, ahk_class ThunderForm
Sleep, 10
WinWaitActive, ahk_class ThunderForm
Sleep, 10
Sleep, 100
Send, ^t
WinWait, FIT-TEMP - Notepad ahk_class Notepad
Sleep, 10
WinWaitActive, FIT-TEMP - Notepad ahk_class Notepad
Sleep, 10
Send, ^f
WinWait, Find ahk_class #32770
Sleep, 10
WinWaitActive, Find ahk_class #32770
Sleep, 10
SendRaw,      0    '* NDIS
```

```
Send, {enter}{esc}
Send, {right}+{up}+{up}+{up}{del}{enter}
Send, 1{tab}0{tab}0{enter}%Combo2_Num%{enter}     0    '* NDIS{enter}
Send, ^s
Sleep, 333
WinClose, FIT-TEMP - Notepad ahk_class Notepad
Sleep, 100
Sleep, 333
IfWinExist, Loading data file ahk_class #32770
{
   WinActivate, ahk_class #32770
   Sleep, 100
   Send, {enter}
   IfWinExist, ahk_class #32770
   {
      WinActivate, ahk_class #32770
      Sleep, 100
      Send, {enter}
   }
   Goto, SmallLoopBeginning
}
WinWaitActive, Windows Pre-Processor ahk_class ThunderForm
Sleep, 100
Send, ^r
WinWait, C:\FITEQL4\FITEQL4.EXE ahk_class ConsoleWindowClass
Sleep, 10
WinWaitClose, C:\FITEQL4\FITEQL4.EXE ahk_class ConsoleWindowClass, , 15
Sleep, 10
IfWinExist, C:\FITEQL4\FITEQL4.EXE ahk_class ConsoleWindowClass
{
   WinActivate, C:\FITEQL4\FITEQL4.EXE ahk_class ConsoleWindowClass
   Sleep, 10
   Send, {enter}
   Sleep, 333
}
WinWaitActive, Windows  Pre-Processor ahk_class #32770
Sleep, 10
Send, {enter}
WinWaitClose, Windows  Pre-Processor ahk_class #32770
Sleep, 10
WinWaitActive, Windows Pre-Processor ahk_class ThunderForm
Sleep, 10
Send, ^v
WinWait, ahk_class Notepad
Sleep, 10
WinWaitActive, ahk_class Notepad
Sleep, 10
Send, ^f
WinWaitActive, Find ahk_class #32770
Sleep, 10
SendRaw, Converged ****
Send, {enter}
Send, {esc}
```

```
WinWaitActive, ahk_class Notepad, , 1
Sleep, 10
IfWinExist, ahk_class #32770
{
   K2_opt_fit := "Overflow"
   wsos2_opt := "Overflow"
   Send, {esc}
   WinWaitClose, ahk_class #32770
   Sleep, 10
   WinWaitActive, ahk_class Notepad
   Sleep, 10
   Goto, FinishRead2
}
Send, ^{right}^{right}^+{right}
clipboard := ""
Send, ^c
ClipWait
K2_opt_fit := clipboard
Send, {left}{right}^+{right}
clipboard := ""
Send, ^c
ClipWait
wsos2_opt := clipboard
FinishRead2:
WinClose, ahk_class Notepad
Sleep, 100
WinWaitClose, ahk_class Notepad
Sleep, 100
WinActivate, ahk_class SALFRAME
Sleep, 100
WinWaitActive, ahk_class SALFRAME
Sleep, 100
If LoopNum = 1
{
   Send, {f5}
   WinWaitActive, Navigator ahk_class SALSUBFRAME
   Sleep, 10
   Send, {del}{del}b{tab}25{enter}{f5}
   Sleep, 10
   WinWaitClose, Navigator ahk_class SALSUBFRAME
   Sleep, 10
}
Else
{
   Send, {down}{down}{down}
}
Send, %Combo1_Num%{tab}
Sleep, 50
Send, %Combo2_Num%{down}{left}
Sleep, 50
Send, %Combo1_Species%{tab}
Sleep, 50
Send, %Combo2_Species%{down}{left}
```

```
      Sleep, 50
      Send, %K1_opt_fit%{tab}
      Sleep, 50
      Send, %K2_opt_fit%{down}{left}
      Sleep, 50
      Send, %wsos1_opt%{tab}
      Sleep, 50
      Send, %wsos2_opt%{down}{left}
      Sleep, 50
      Goto, StartScan
      OptReturn:
      Combo2_LoopNum += 1
      Goto, SmallLoopBeginning
   }
   Goto, BigLoopBeginning
}
MsgBox, 0, , Run complete
```

// Scanning Module //

```
StartScan:
Result := 0
LowRange := 2
HighRange := 0.5
MaxError := 15
Increment_criteria1 := 30
Increment_criteria2 := 60
K1_initial := K1_opt_fit - LowRange
K1_end := K1_opt_fit + HighRange
K1 := K1_initial
K2_initial := K2_opt_fit - LowRange
K2_end := K2_opt_fit + HighRange
Loop, 2
{
   Send, {down}
   Sleep, 20
}
WinActivate, ahk_class ThunderForm
Sleep, 10
WinWaitActive, ahk_class ThunderForm
Sleep, 10
Send, ^o
Send, %In_file%
Send, {enter}
Sleep, 333
WinWaitActive, ahk_class ThunderForm
Sleep, 10
Send, {ctrl down}t{ctrl up}
Sleep, 50
WinWait, FIT-TEMP - Notepad ahk_class Notepad
```

```
Sleep, 10
WinWaitActive, FIT-TEMP - Notepad ahk_class Notepad
Sleep, 10
K1_Loop:
Prev_Result := 10000
Min_Result := 0
If K1 <= %K1_end%
{
   Send, ^f
   WinWait, Find ahk_class #32770
   Sleep, 10
   WinWaitActive, Find ahk_class #32770
   Sleep, 10
   Send, %Combo1_Num%{space}
   Sleep, 30
   Send, %Combo1_species%
   Sleep, 30
   Send, {enter}{esc}
   Sleep, 30
   Send, ^{right}^{left}^+{right}
   Sleep, 20
   Send, %K1%{space}{space}
   Sleep, 30
   K2 := K2_initial
   K2_Loop:
   If K2 <= %K2_end%
   {
      Send, ^f
      WinWait, Find ahk_class #32770
      Sleep, 10
      WinWaitActive, Find ahk_class #32770
      Sleep, 10
      Send, %Combo2_Num%
      Sleep, 20
      Send, %Combo2_species%
      Sleep, 20
      Send, {enter}{esc}
      Sleep, 20
      Send, ^{right}^{left}^+{right}
      Sleep, 20
      Send, %K2%{space}{space}
      Sleep, 20
      Send, ^s
      Sleep, 100
      WinClose, FIT-TEMP - Notepad ahk_class Notepad
      Sleep, 10
      WinWaitClose, FIT-TEMP - Notepad ahk_class Notepad, , 5
      Sleep, 10
      WinActivate, Windows Pre-Processor ahk_class ThunderForm
      Sleep, 10
      WinWaitActive, Windows Pre-Processor ahk_class ThunderForm, , 5
      Sleep, 10
      Send, {ctrl down}r{ctrl up}
```

```
WinWait, C:\FITEQL4\FITEQL4.EXE ahk_class ConsoleWindowClass, , 5
Sleep, 10
WinWaitClose, C:\FITEQL4\FITEQL4.EXE ahk_class ConsoleWindowClass, , 5
Sleep, 10
IfWinExist, C:\FITEQL4\FITEQL4.EXE ahk_class ConsoleWindowClass
{
   Send, {enter}
   Sleep, 333
}
WinWait, Windows  Pre-Processor ahk_class #32770, , 5
Sleep, 10
WinActivate, Windows  Pre-Processor ahk_class #32770
Sleep, 10
Send, {enter}
Sleep, 100
IfWinExist, Windows  Pre-Processor ahk_class #32770
{
   Loop
   {
      CoordMode, Pixel, Window
      ImageSearch, FoundX, FoundY, -290, -121, 485, 245, C:\Documents and Settings\IEUser\Application
Data\MacroCreator\Screenshots\Screen_20170114214344.png
      If ErrorLevel = 0
            Click, %FoundX%, %FoundY% Left, 1
   }
   Until ErrorLevel = 0
}
Sleep, 100
FileReadLine, Result, %Out_File%, 6
FileReadLine, Result, %Out_File%, 6
Sleep, 50
If Result <= %MaxError%
{
   WinActivate, ahk_class SALFRAME
   Sleep, 10
   WinWaitActive, ahk_class SALFRAME
   Sleep, 10
   Send, %K1%
   Send, {tab}
   Send, %K2%
   Send, {tab}
   Sleep, 20
   Send, %Result%
   Sleep, 60
   Sleep, 50
   Send, {tab}
   Sleep, 30
   Send, {enter}
   Sleep, 30
}
If Result >= %Prev_Result%
{
   If Result >= %MaxError%
```

```
        {
          WinActivate, ahk_class ThunderForm
          Sleep, 10
          WinWaitActive, ahk_class ThunderForm
          Sleep, 10
          Sleep, 100
          Send, ^t
          WinWait, FIT-TEMP - Notepad ahk_class Notepad
          Sleep, 10
          WinWaitActive, FIT-TEMP - Notepad ahk_class Notepad
          Sleep, 10
          Goto, After_K2_Loop
        }
        Goto, Override_prev_result
      }
      Min_Result := Result
      Override_prev_result:
      Prev_Result := Result
      WinActivate, ahk_class ThunderForm
      Sleep, 10
      WinWaitActive, ahk_class ThunderForm
      Sleep, 10
      Sleep, 100
      Send, ^t
      WinWait, FIT-TEMP - Notepad ahk_class Notepad
      Sleep, 10
      WinWaitActive, FIT-TEMP - Notepad ahk_class Notepad
      Sleep, 10
      K2 += 0.1
      If Result >= %increment_criteria1%
      {
        K2 += 0.1
        If Result >= %increment_criteria2%
        {
          K2 += 0.2
        }
      }
      Goto, K2_Loop
    }
    After_K2_Loop:
    K1 += 0.1
    If Min_Result >= %increment_criteria1%
    {
      K1 += 0.1
      If Min_Result >= %increment_criteria2%
      {
        K1 += 0.2
      }
    }
    Goto, K1_Loop
}
WinClose, FIT-TEMP - Notepad ahk_class Notepad
Sleep, 10
```

```
WinWaitClose, FIT-TEMP - Notepad ahk_class Notepad
Sleep, 10
Goto, OptReturn
```

APPENDIX C. ADDITIONAL PLOTS OF MODEL PREDICTIONS FOR ALKALINE EARTH METAL ION ADSORPTION

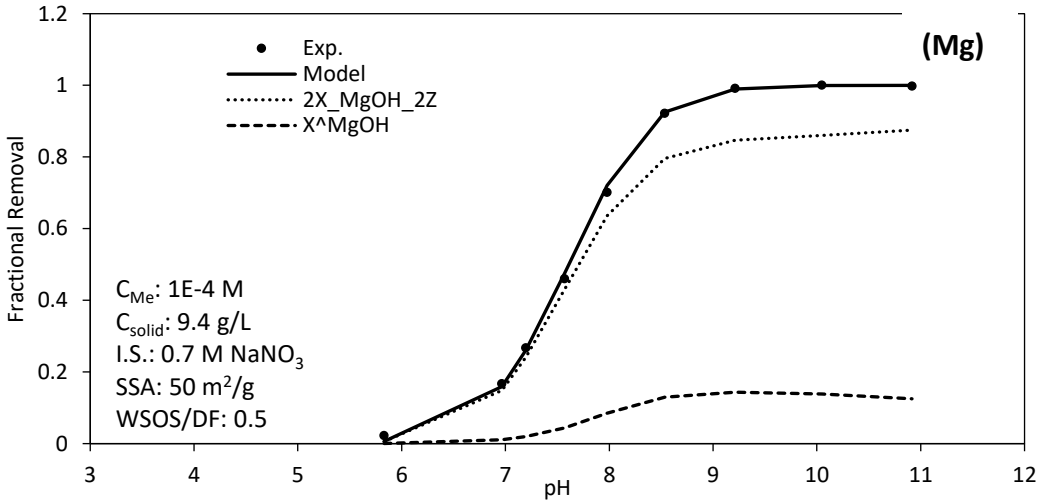

Figure C- 1. Experimental data and model predictions of Mg adsorption on 50 m^2/g SSA goethite in 0.7 M $NaNO_3$ solution (C_{Me}: 1e-4 M, C_{solid}: 9.4 g/L)

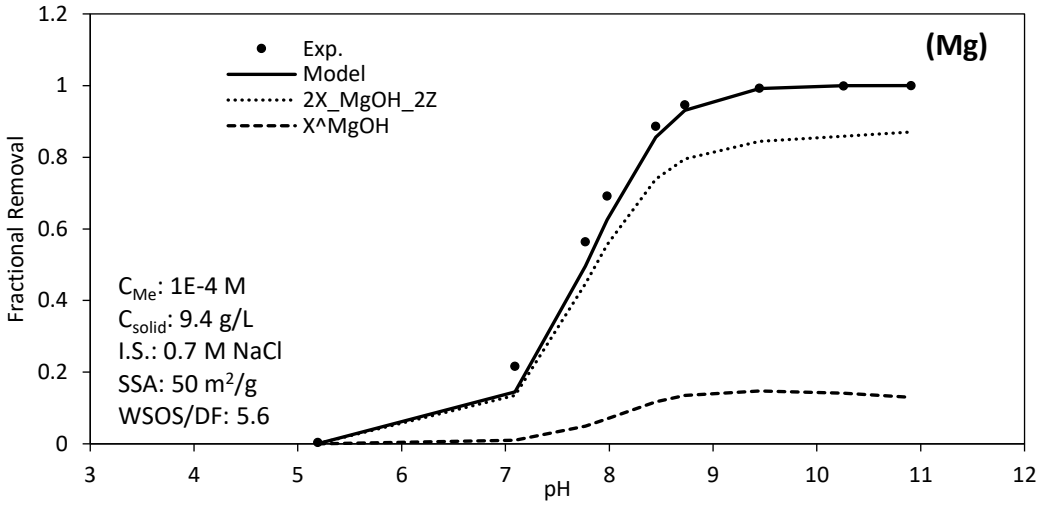

Figure C- 2. Experimental data and model predictions of Mg adsorption on 50 m^2/g SSA goethite in 0.7 M NaCl solution (C_{Me}: 1e-4 M, C_{solid}: 9.4 g/L)

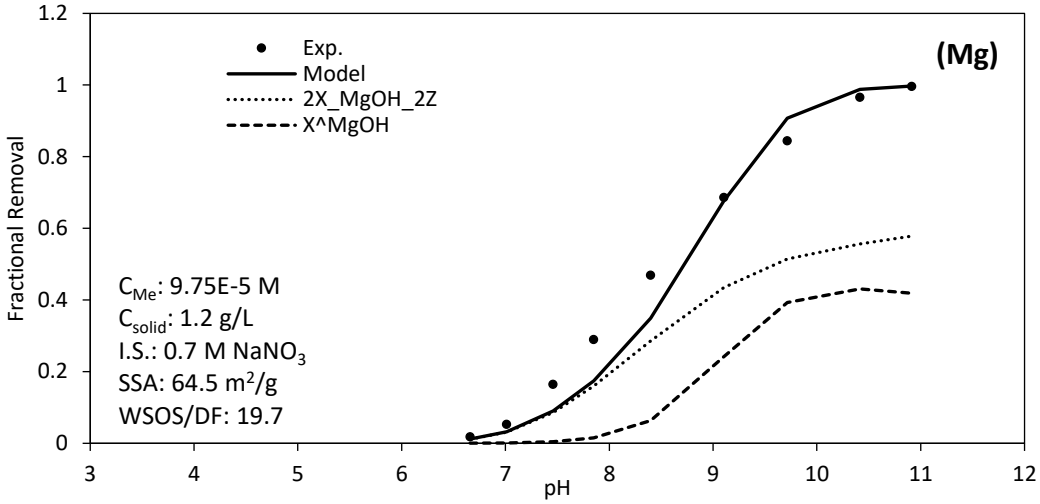

Figure C- 3. Experimental data and model predictions of Mg adsorption on 64.5 m^2/g SSA goethite in 0.7 M $NaNO_3$ solution (C_{Me}: 9.75e-5 M, C_{solid}: 1.2 g/L)

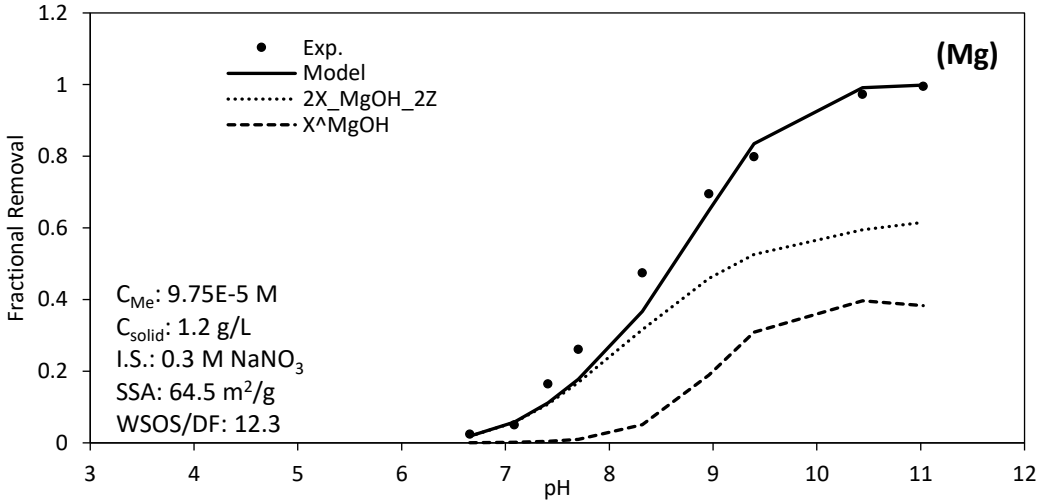

Figure C- 4. Experimental data and model predictions of Mg adsorption on 64.5 m^2/g SSA goethite in 0.3 M $NaNO_3$ solution (C_{Me}: 9.75e-5 M, C_{solid}: 1.2 g/L)

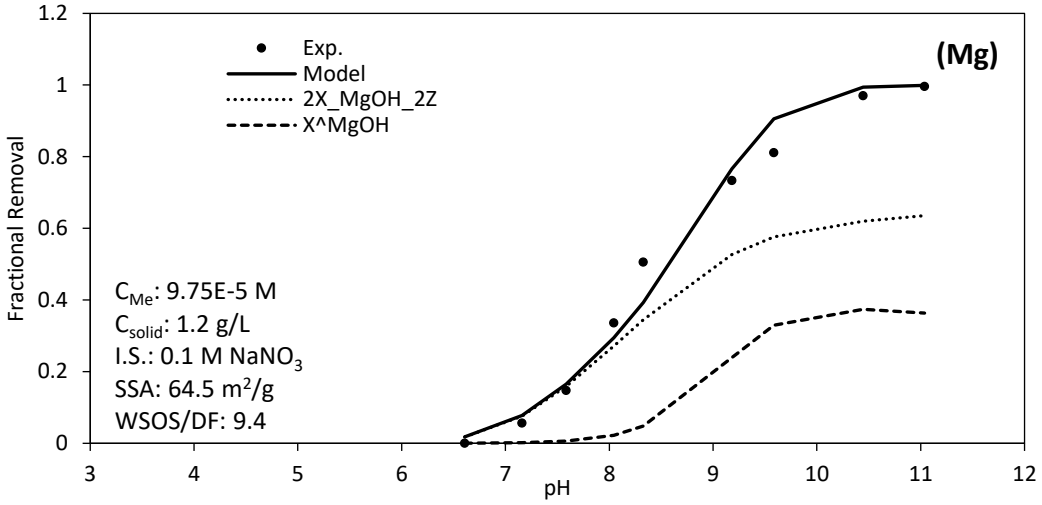

Figure C- 5. Experimental data and model predictions of Mg adsorption on 64.5 m^2/g SSA goethite in 0.1 M $NaNO_3$ solution (C_{Me}: 9.75e-5 M, C_{solid}: 1.2 g/L)

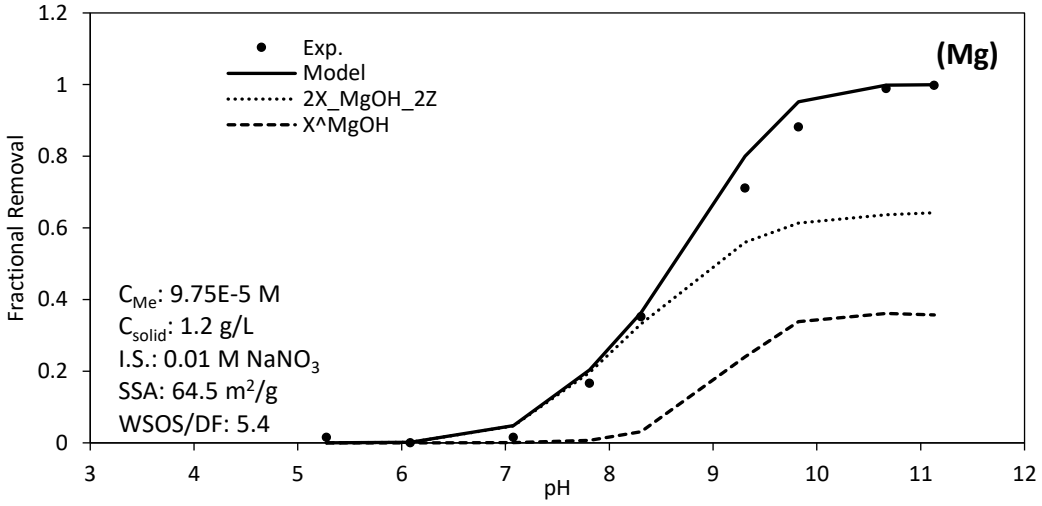

Figure C- 6. Experimental data and model predictions of Mg adsorption on 64.5 m^2/g SSA goethite in 0.01 M $NaNO_3$ solution (C_{Me}: 9.75e-5 M, C_{solid}: 1.2 g/L)

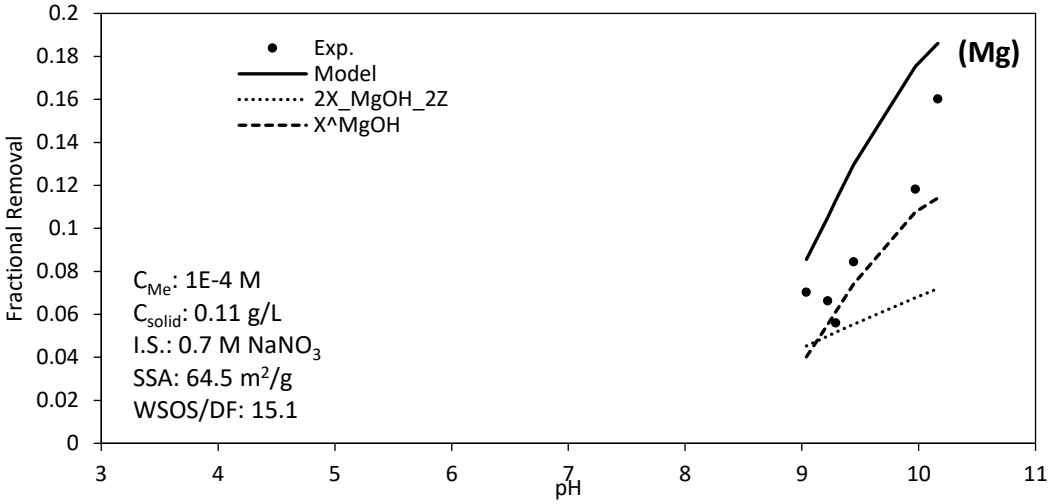

Figure C- 7. Experimental data and model predictions of Mg adsorption on 64.5 m^2/g SSA goethite in 0.7 M $NaNO_3$ solution (C_{Me}: 1e-4 M, C_{solid}: 0.11 g/L)

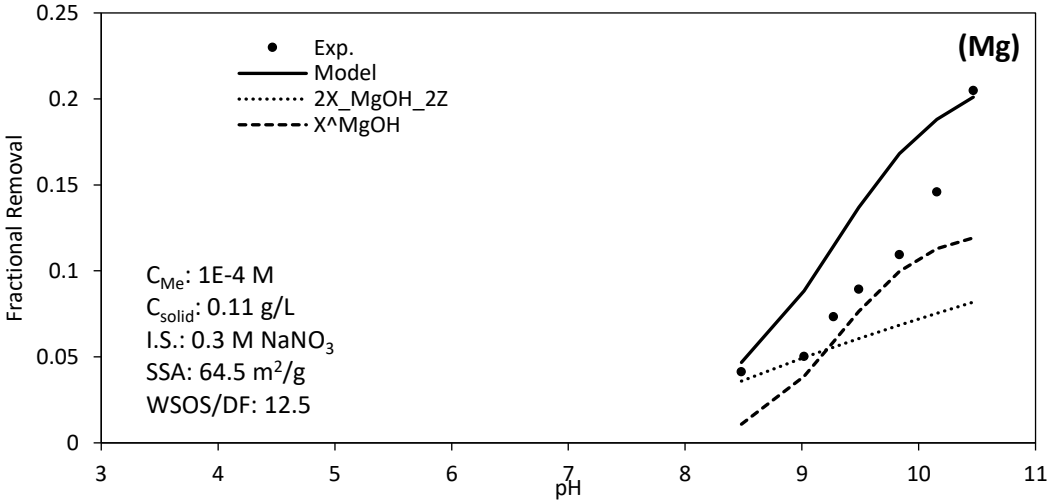

Figure C- 8. Experimental data and model predictions of Mg adsorption on 64.5 m^2/g SSA goethite in 0.3 M $NaNO_3$ solution (C_{Me}: 1e-4 M, C_{solid}: 0.11 g/L)

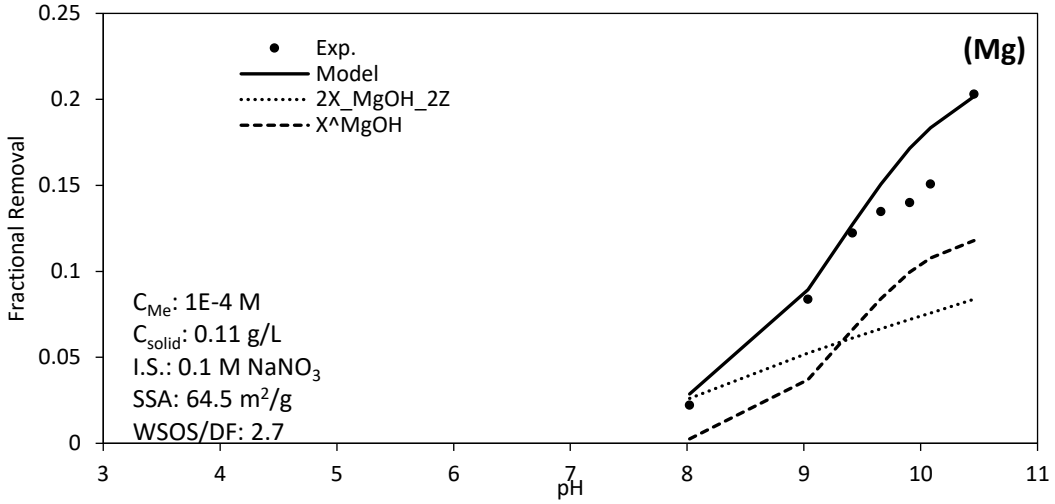

Figure C- 9. Experimental data and model predictions of Mg adsorption on 64.5 m^2/g SSA goethite in 0.1 M $NaNO_3$ solution (C_{Me}: 1e-4 M, C_{solid}: 0.11 g/L)

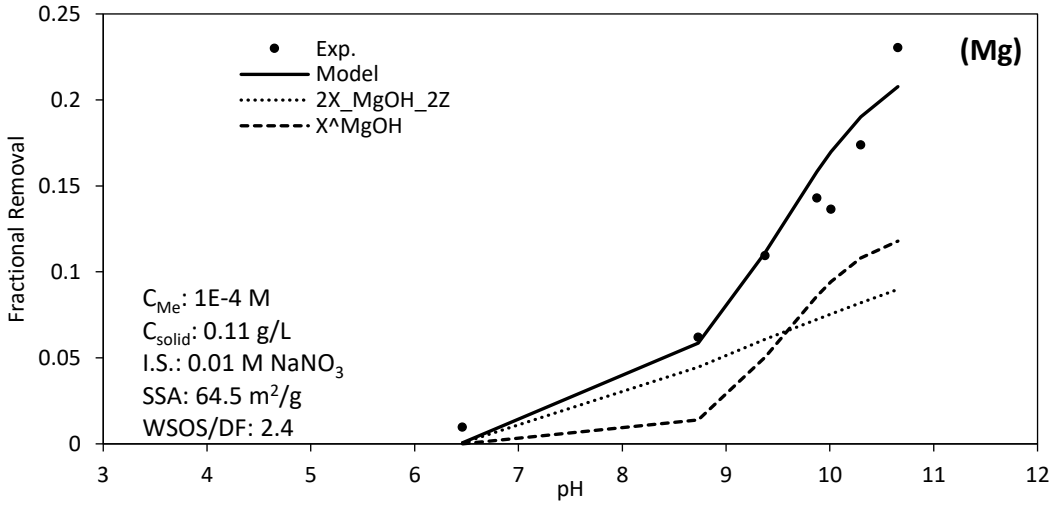

Figure C- 10. Experimental data and model predictions of Mg adsorption on 64.5 m^2/g SSA goethite in 0.01 M $NaNO_3$ solution (C_{Me}: 1e-4 M, C_{solid}: 0.11 g/L)

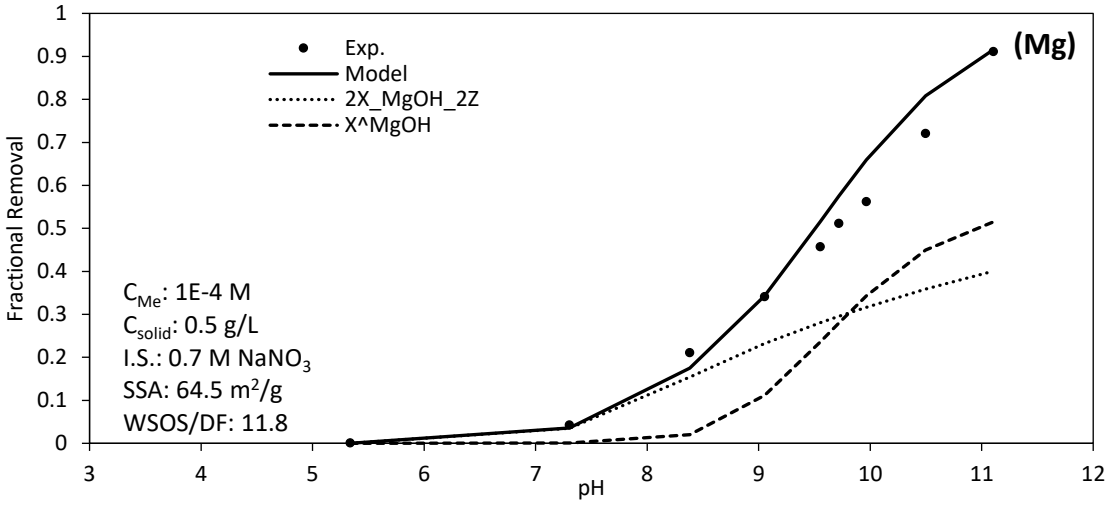

Figure C- 11. Experimental data and model predictions of Mg adsorption on 64.5 m^2/g SSA goethite in 0.7 M $NaNO_3$ solution (C_{Me}: 1e-4 M, C_{solid}: 0.5 g/L)

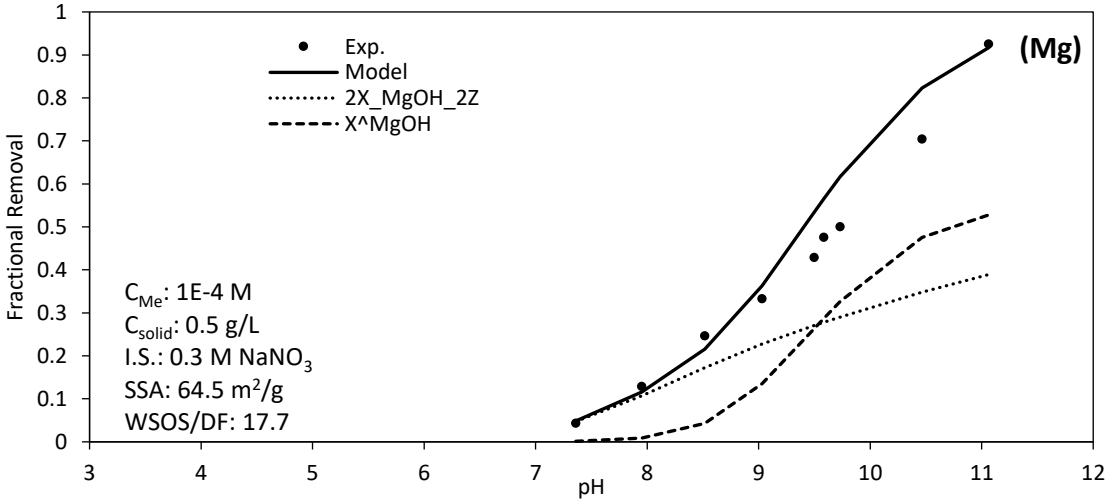

Figure C- 12. Experimental data and model predictions of Mg adsorption on 64.5 m^2/g SSA goethite in 0.3 M $NaNO_3$ solution (C_{Me}: 1e-4 M, C_{solid}: 0.5 g/L)

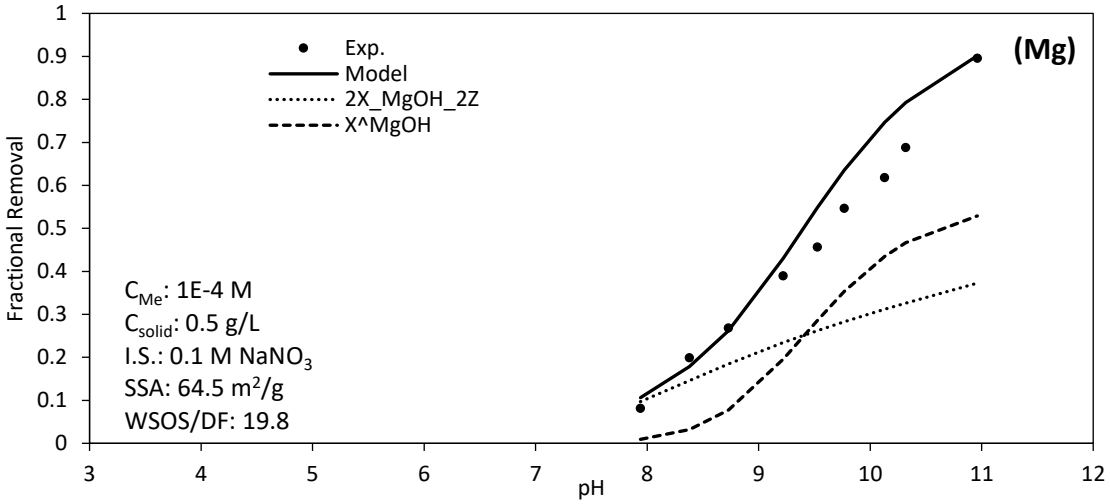

Figure C- 13. Experimental data and model predictions of Mg adsorption on 64.5 m^2/g SSA goethite in 0.1 M $NaNO_3$ solution (C_{Me}: 1e-4 M, C_{solid}: 0.5 g/L)

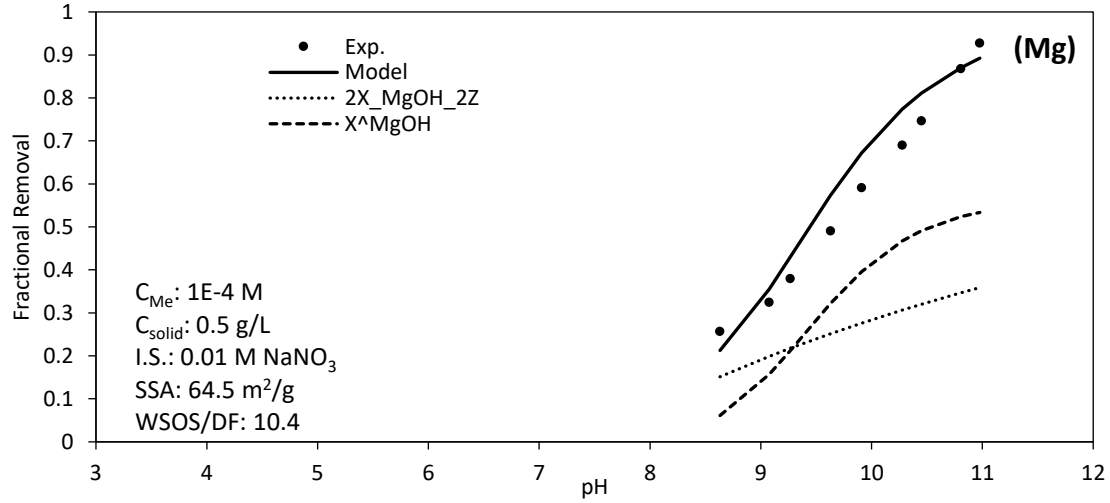

Figure C- 14. Experimental data and model predictions of Mg adsorption on 64.5 m^2/g SSA goethite in 0.01 M $NaNO_3$ solution (C_{Me}: 1e-4 M, C_{solid}: 0.5 g/L)

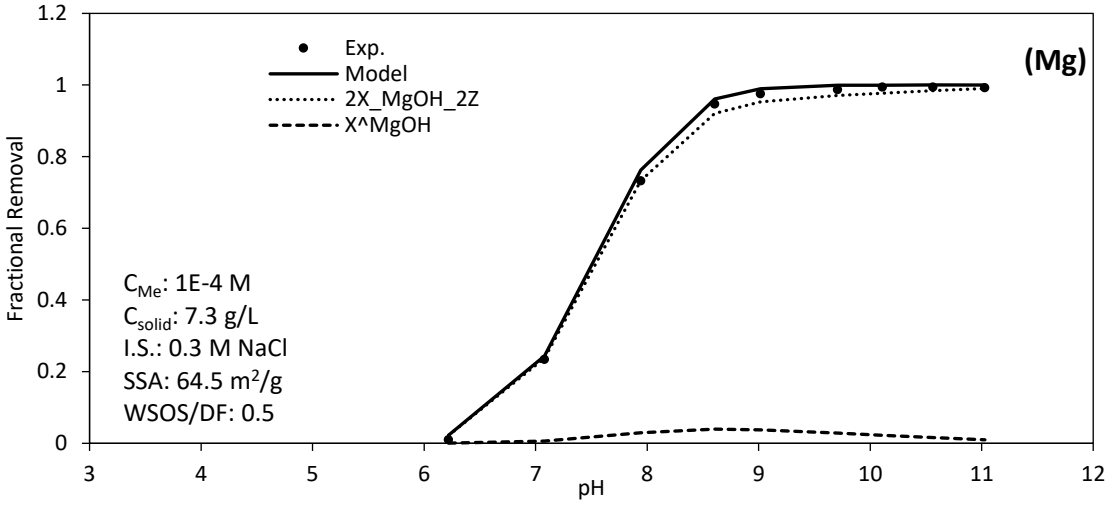

Figure C- 15. Experimental data and model predictions of Mg adsorption on 64.5 m^2/g SSA goethite in 0.3 M NaCl solution (C_{Me}: 1e-4 M, C_{solid}: 7.3 g/L)

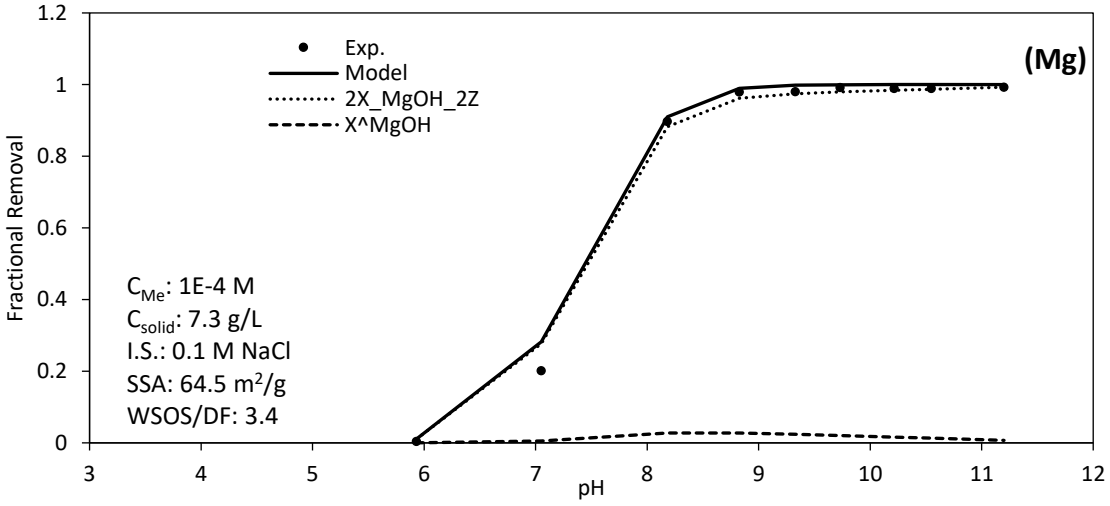

Figure C- 16. Experimental data and model predictions of Mg adsorption on 64.5 m^2/g SSA goethite in 0.1 M NaCl solution (C_{Me}: 1e-4 M, C_{solid}: 7.3 g/L)

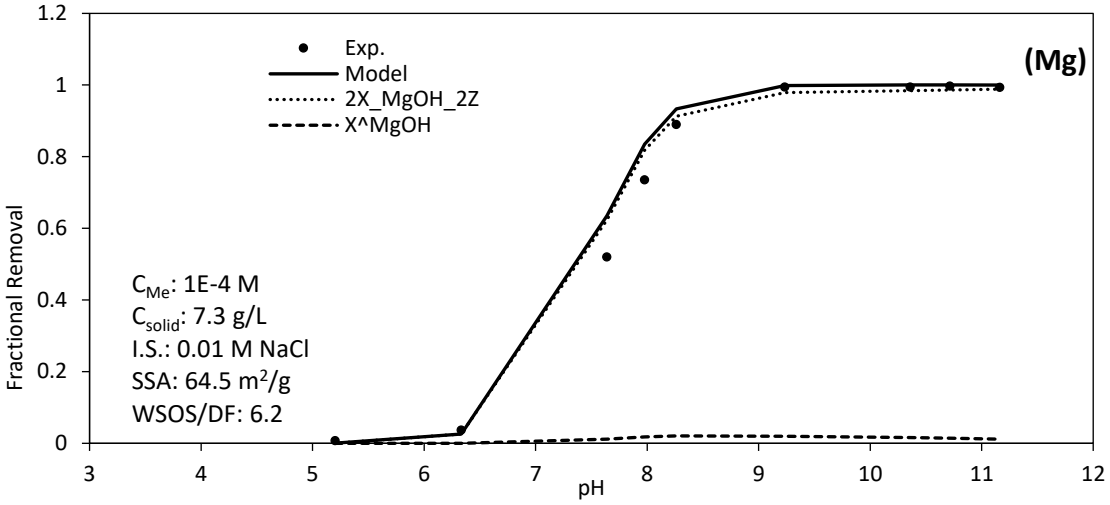

Figure C- 17. Experimental data and model predictions of Mg adsorption on 64.5 m^2/g SSA goethite in 0.01 M NaCl solution (C_{Me}: 1e-4 M, C_{solid}: 7.3 g/L)

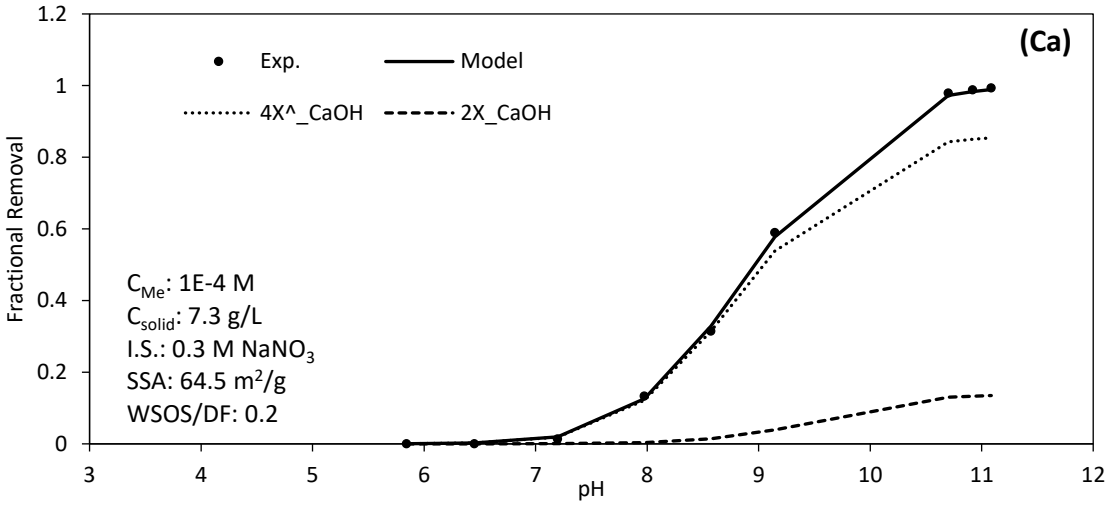

Figure C- 18. Experimental data and model predictions of Ca adsorption on 64.5 m^2/g SSA goethite in 0.3 M $NaNO_3$ solution (C_{Me}: 1e-4 M, C_{solid}: 7.3 g/L)

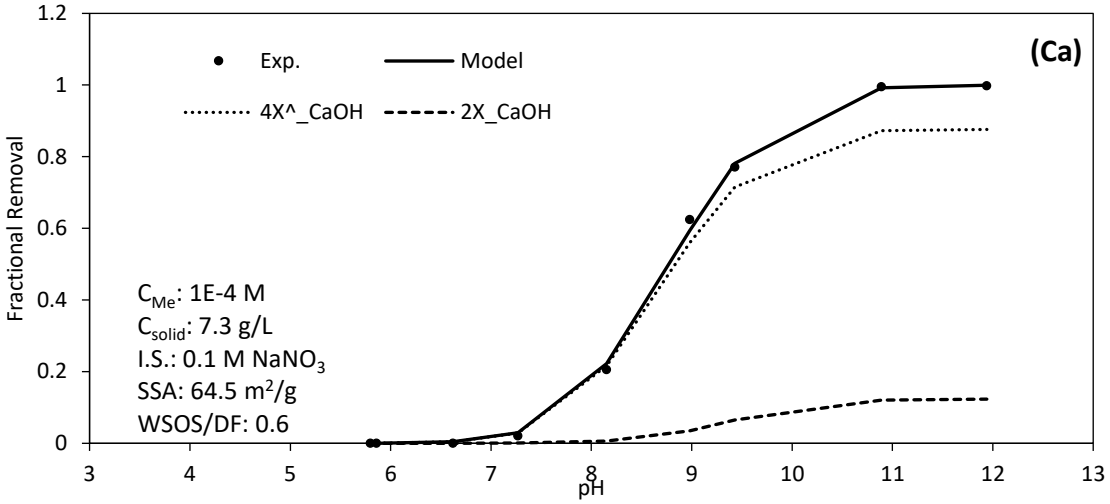

Figure C- 19. Experimental data and model predictions of Ca adsorption on 64.5 m^2/g SSA goethite in 0.1 M $NaNO_3$ solution (C_{Me}: 1e-4 M, C_{solid}: 7.3 g/L)

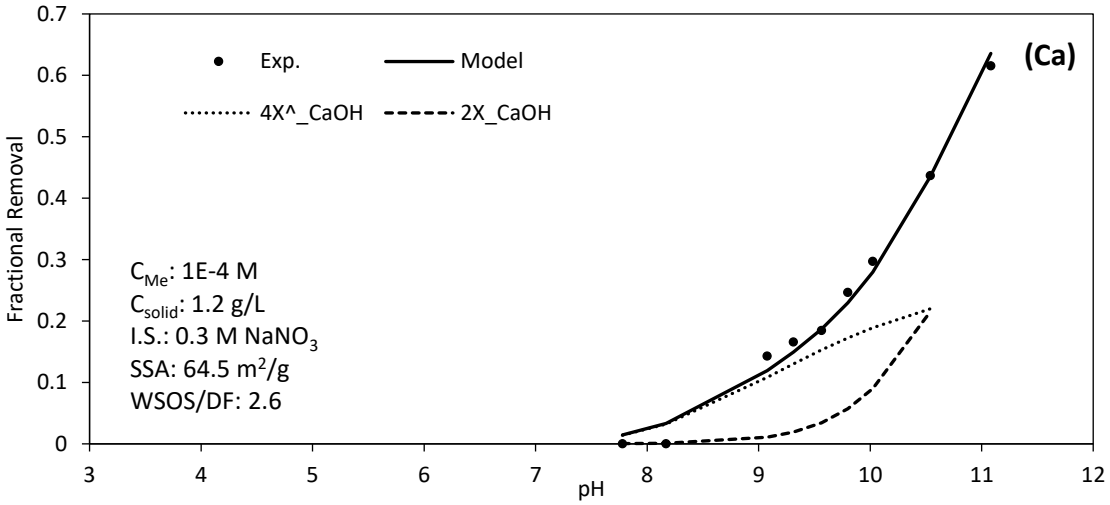

Figure C- 20. Experimental data and model predictions of Ca adsorption on 64.5 m^2/g SSA goethite in 0.3 M $NaNO_3$ solution (C_{Me}: 1e-4 M, C_{solid}: 1.2 g/L)

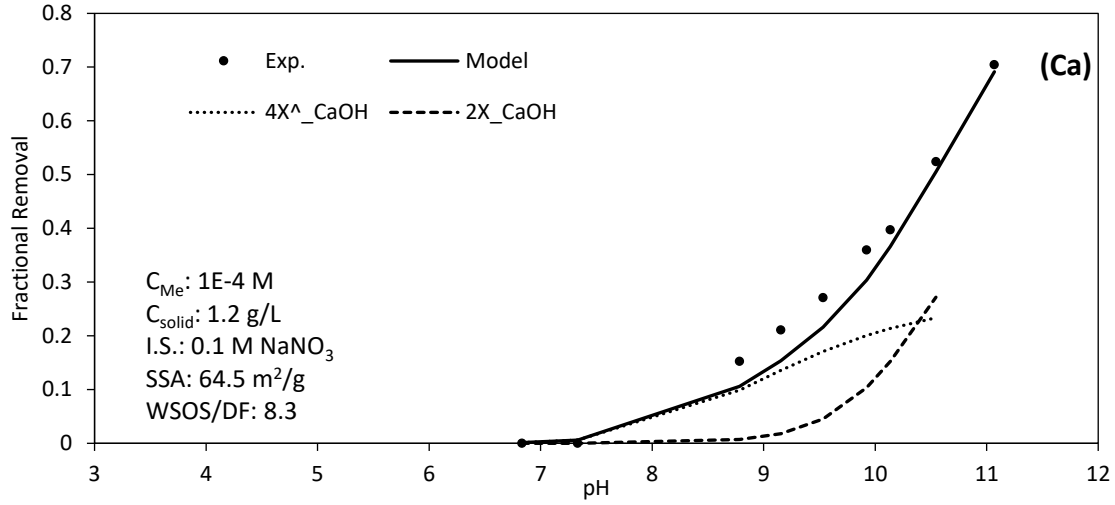

Figure C- 21. Experimental data and model predictions of Ca adsorption on 64.5 m^2/g SSA goethite in 0.1 M $NaNO_3$ solution (C_{Me}: 1e-4 M, C_{solid}: 1.2 g/L)

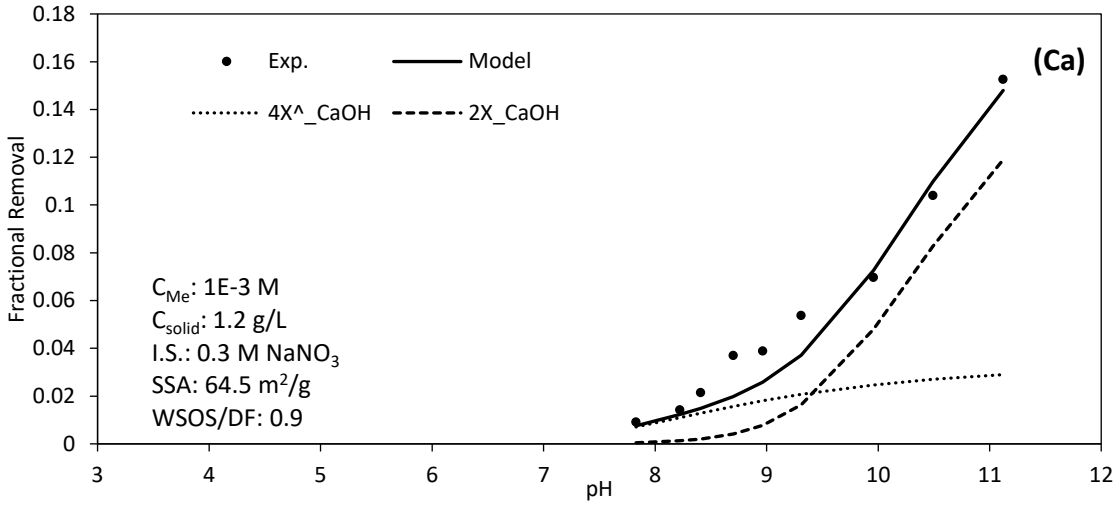

Figure C- 22. Experimental data and model predictions of Ca adsorption on 64.5 m^2/g SSA goethite in 0.3 M $NaNO_3$ solution (C_{Me}: 1e-3 M, C_{solid}: 1.2 g/L)

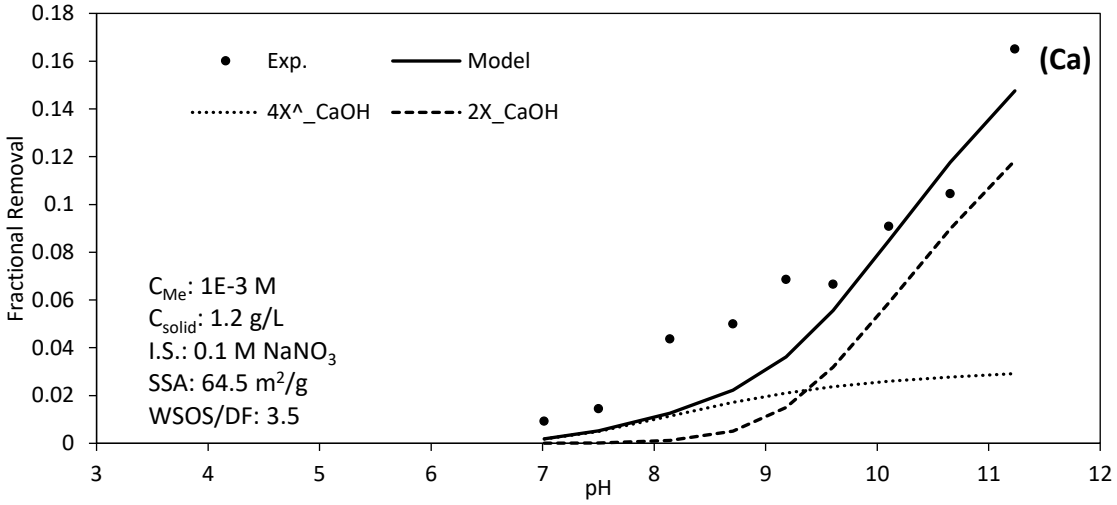

Figure C- 23. Experimental data and model predictions of Ca adsorption on 64.5 m^2/g SSA goethite in 0.1 M $NaNO_3$ solution (C_{Me}: 1e-3 M, C_{solid}: 1.2 g/L)

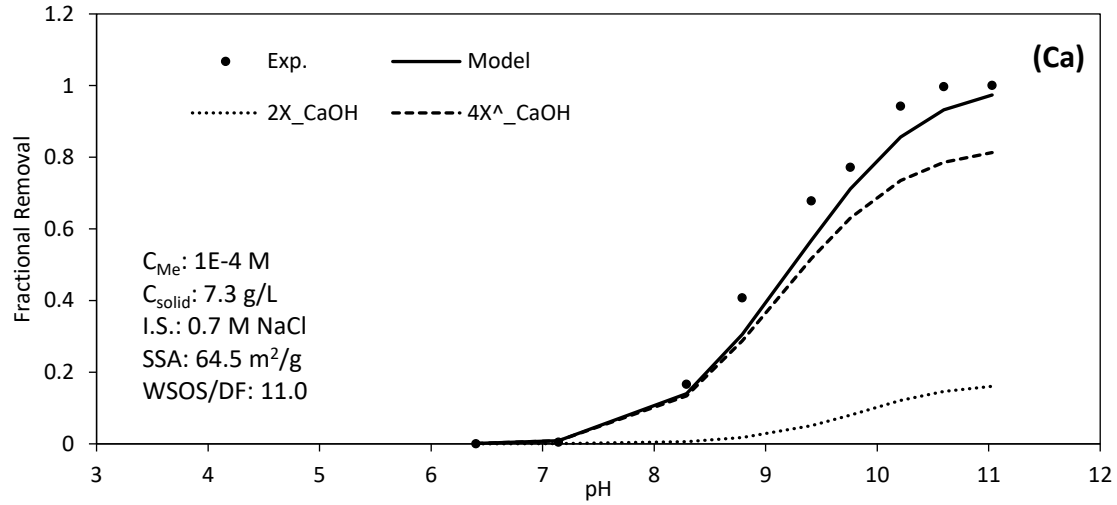

Figure C- 24. Experimental data and model predictions of Ca adsorption on 64.5 m^2/g SSA goethite in 0.7 M NaCl solution (C_{Me}: 1e-4 M, C_{solid}: 7.3 g/L)

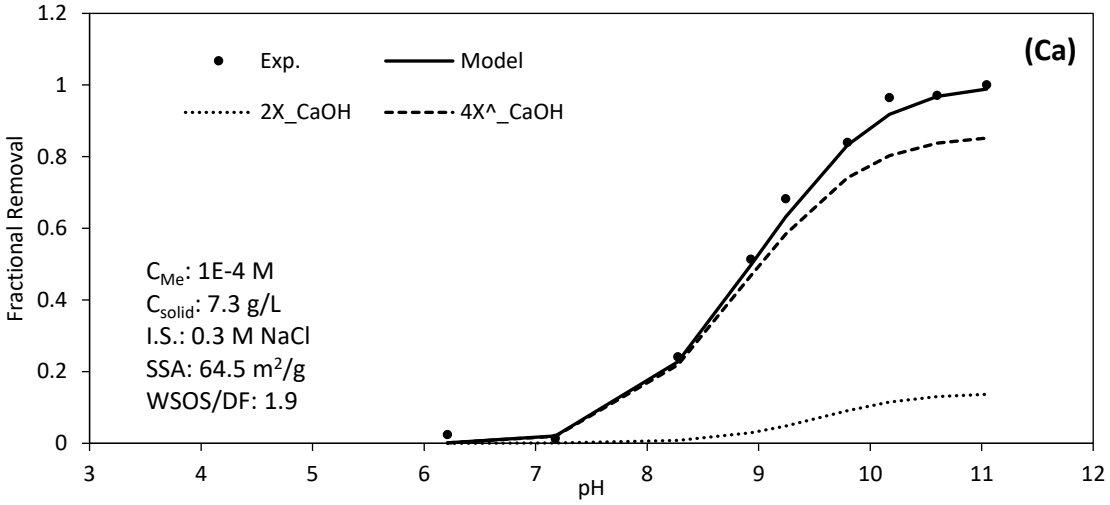

Figure C- 25. Experimental data and model predictions of Ca adsorption on 64.5 m^2/g SSA goethite in 0.3 M NaCl solution (C_{Me}: 1e-4 M, C_{solid}: 7.3 g/L)

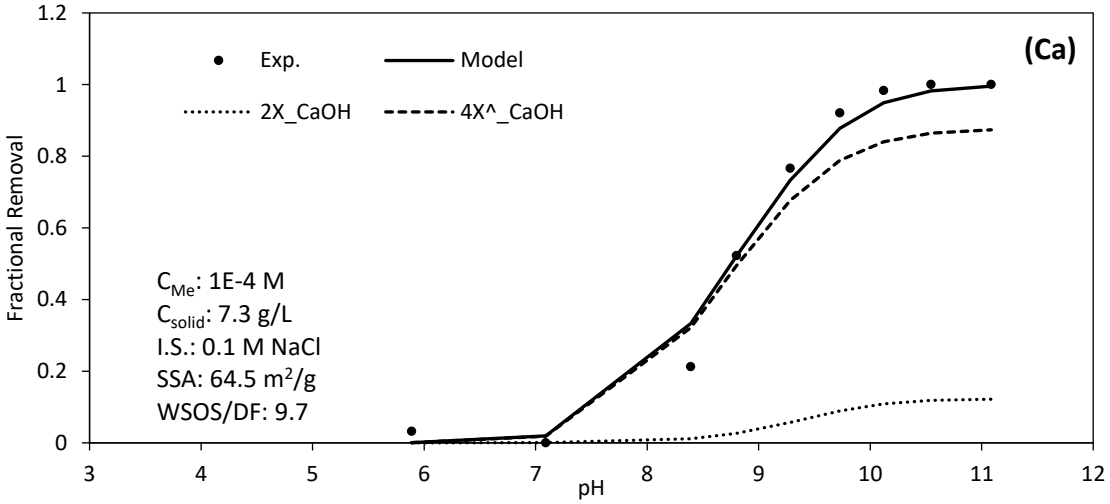

Figure C- 26. Experimental data and model predictions of Ca adsorption on 64.5 m^2/g SSA goethite in 0.1 M NaCl solution (C_{Me}: 1e-4 M, C_{solid}: 7.3 g/L)

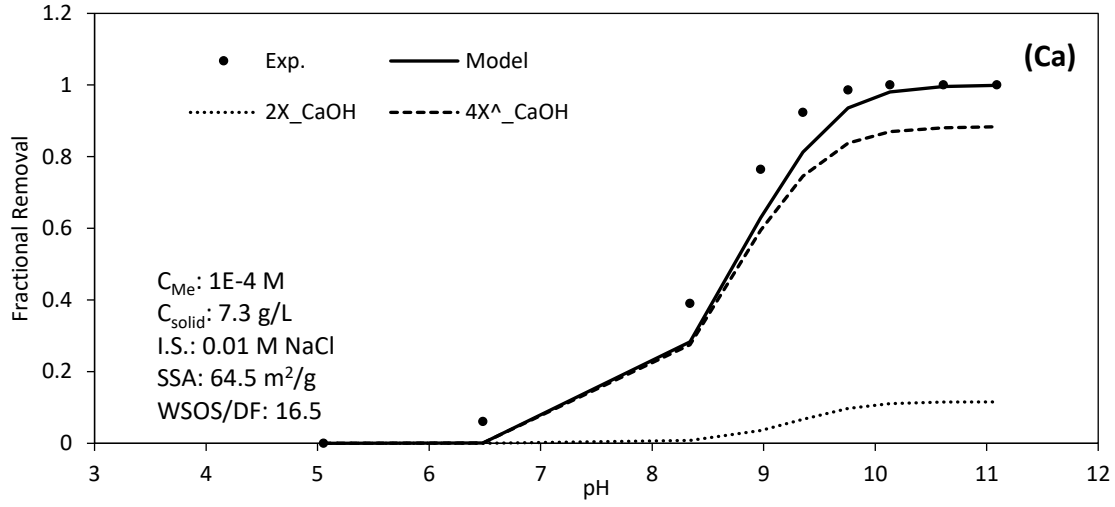

Figure C- 27. Experimental data and model predictions of Ca adsorption on 64.5 m^2/g SSA goethite in 0.01 M NaCl solution (C_{Me}: 1e-4 M, C_{solid}: 7.3 g/L)

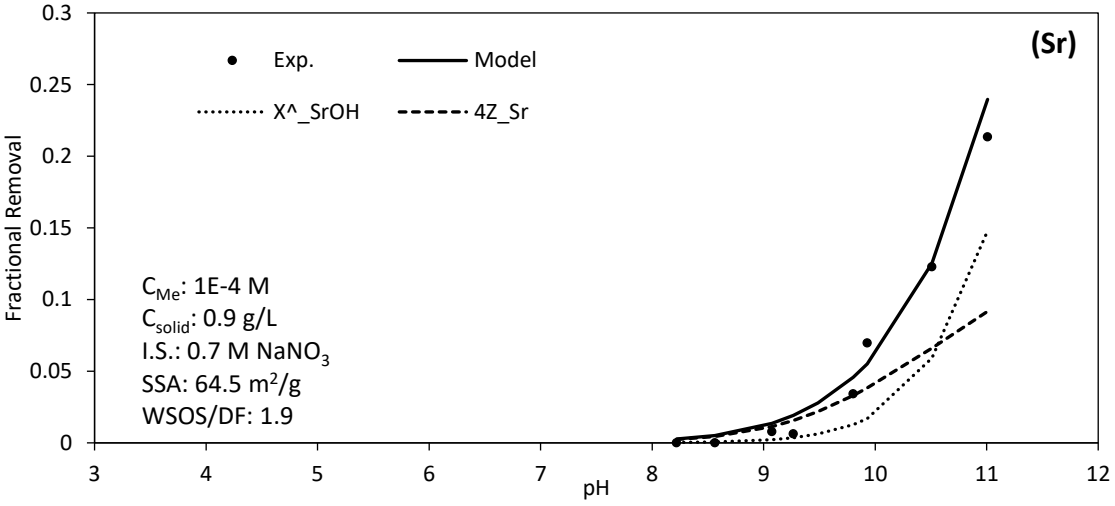

Figure C- 28. Experimental data and model predictions of Sr adsorption on 64.5 m^2/g SSA goethite in 0.7 M $NaNO_3$ solution (C_{Me}: 1e-4 M, C_{solid}: 0.9 g/L)

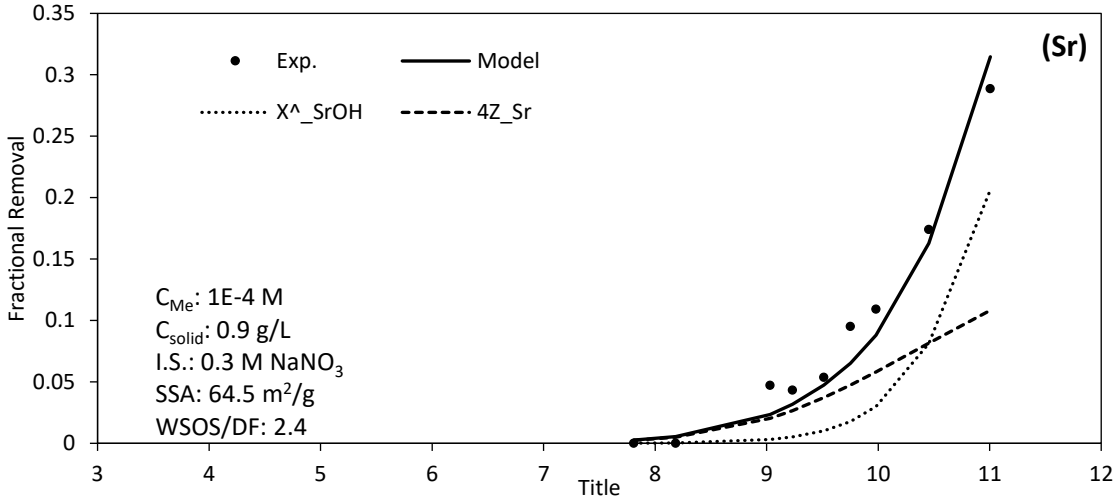

Figure C- 29. Experimental data and model predictions of Sr adsorption on 64.5 m^2/g SSA goethite in 0.3 M $NaNO_3$ solution (C_{Me}: 1e-4 M, C_{solid}: 0.9 g/L)

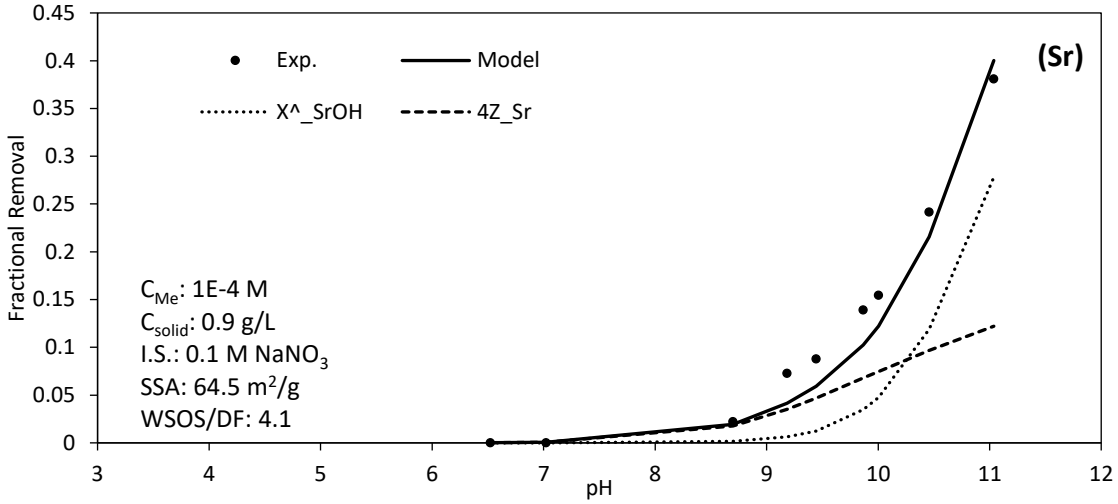

Figure C- 30. Experimental data and model predictions of Sr adsorption on 64.5 m^2/g SSA goethite in 0.1 M $NaNO_3$ solution (C_{Me}: 1e-4 M, C_{solid}: 0.9 g/L)

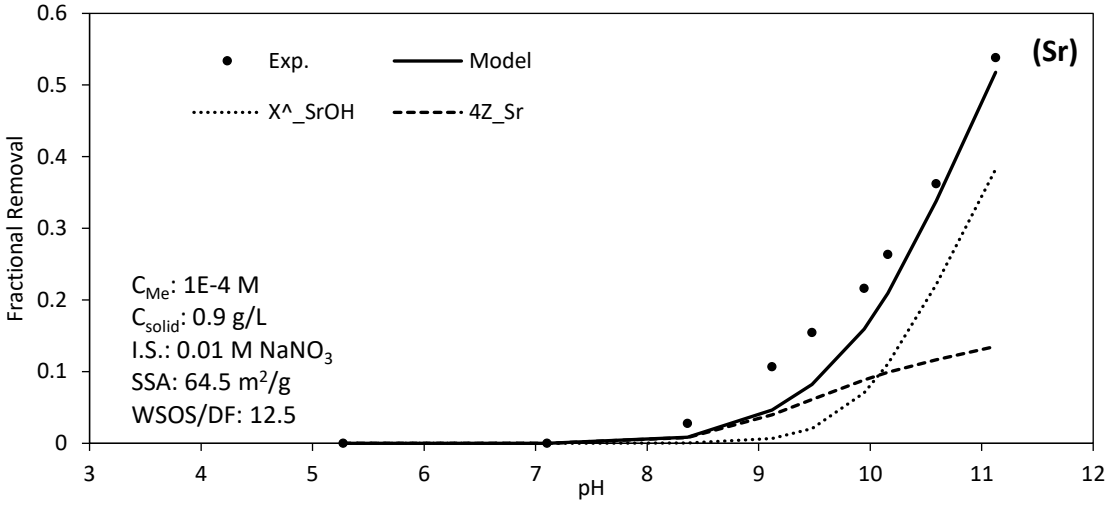

Figure C- 31. Experimental data and model predictions of Sr adsorption on 64.5 m^2/g SSA goethite in 0.01 M $NaNO_3$ solution (C_{Me}: 1e-4 M, C_{solid}: 0.9 g/L)

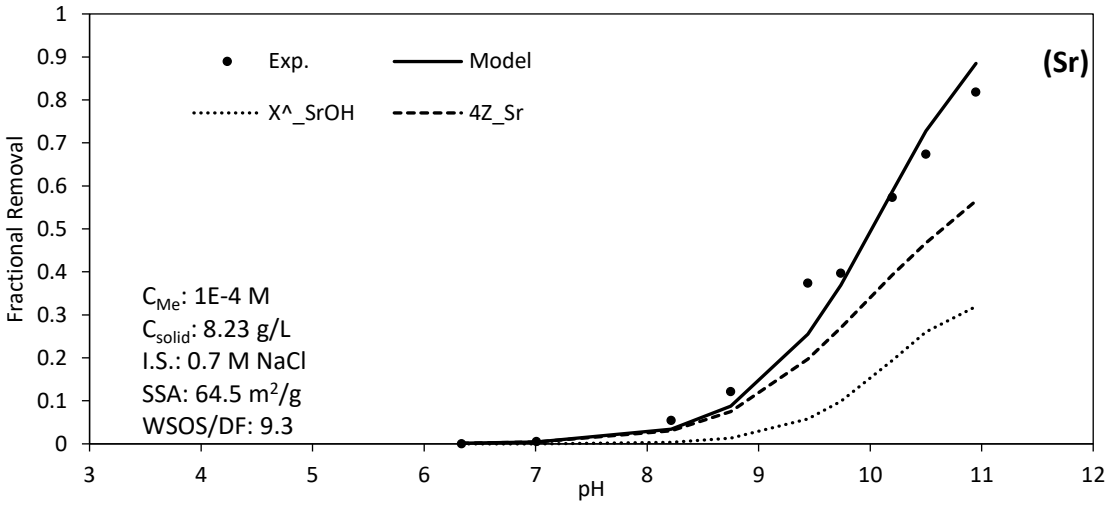

Figure C- 32. Experimental data and model predictions of Sr adsorption on 64.5 m^2/g SSA goethite in 0.7 M NaCl solution (C_{Me}: 1e-4 M, C_{solid}: 8.23 g/L)

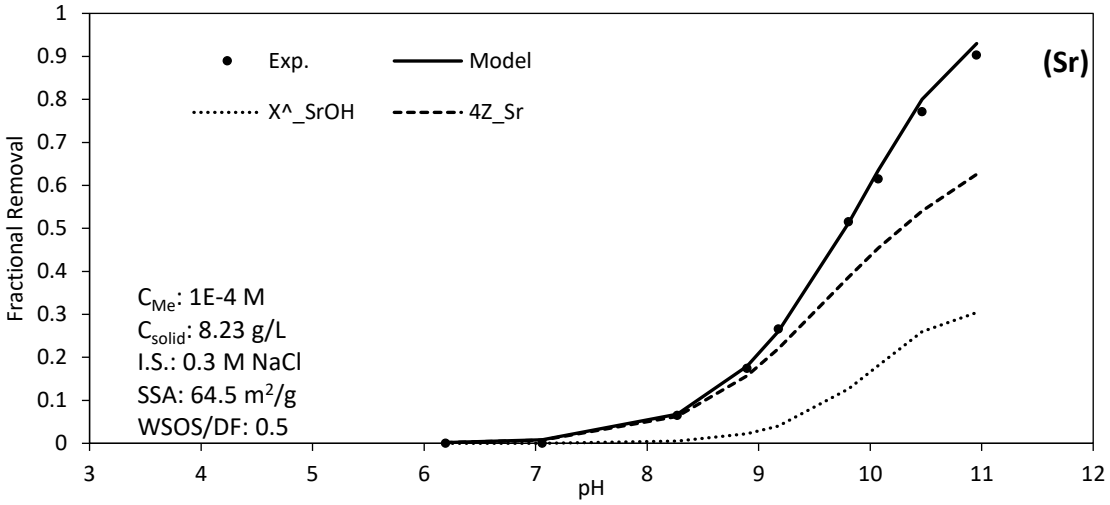

Figure C- 33. Experimental data and model predictions of Sr adsorption on 64.5 m^2/g SSA goethite in 0.3 M NaCl solution (C_{Me}: 1e-4 M, C_{solid}: 8.23 g/L)

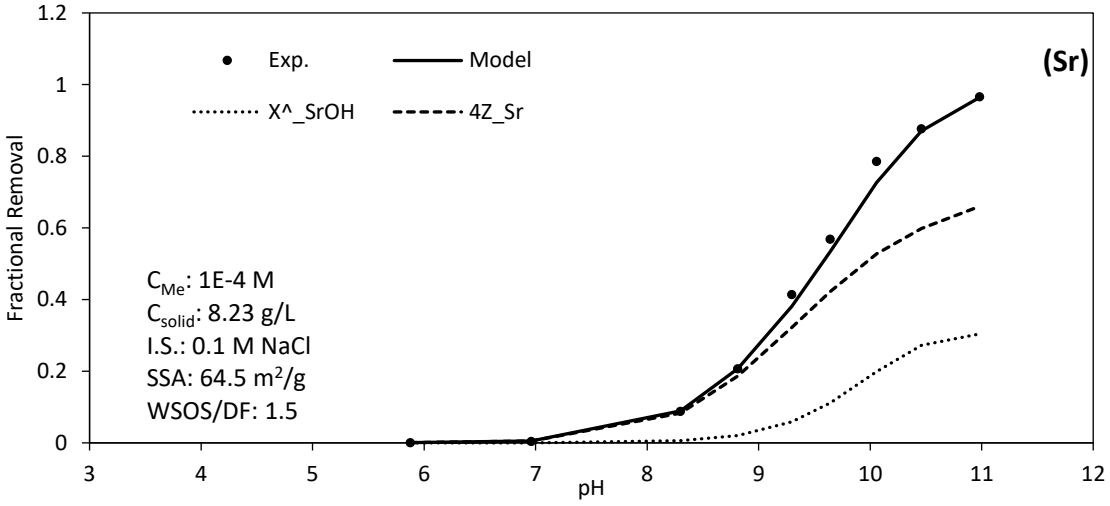

Figure C- 34. Experimental data and model predictions of Sr adsorption on 64.5 m^2/g SSA goethite in 0.1 M NaCl solution (C_{Me}: 1e-4 M, C_{solid}: 8.23 g/L)

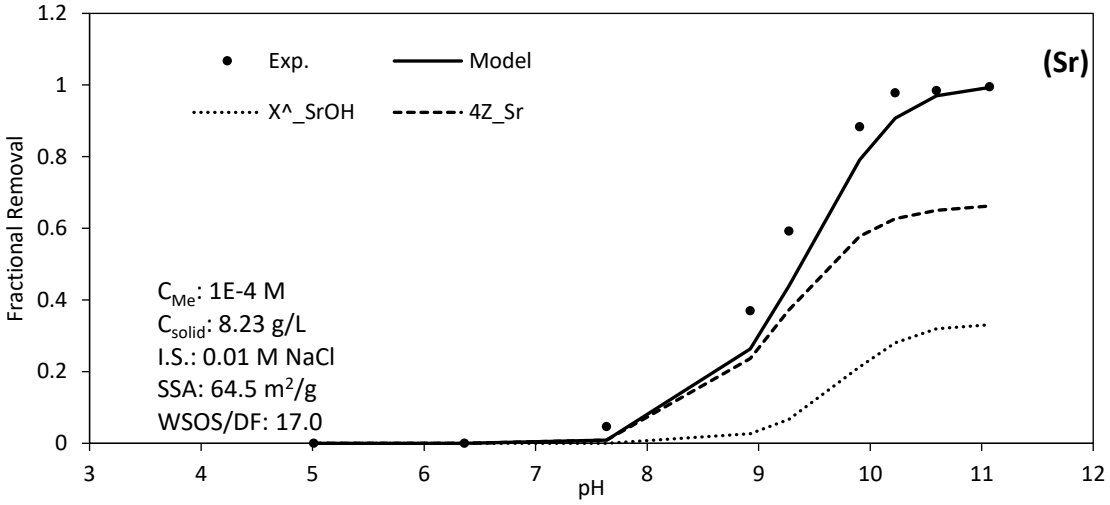

Figure C- 35. Experimental data and model predictions of Sr adsorption on 64.5 m^2/g SSA goethite in 0.01 M NaCl solution (C_{Me}: 1e-4 M, C_{solid}: 8.23 g/L)

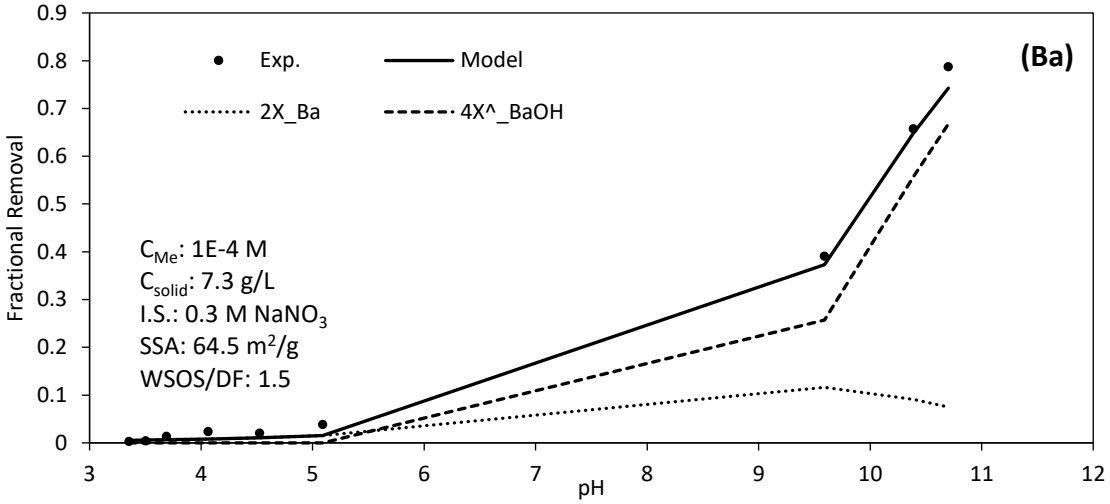

Figure C- 36. Experimental data and model predictions of Ba adsorption on 64.5 m^2/g SSA goethite in 0.3 M $NaNO_3$ solution (C_{Me}: 1e-4 M, C_{solid}: 7.3 g/L)

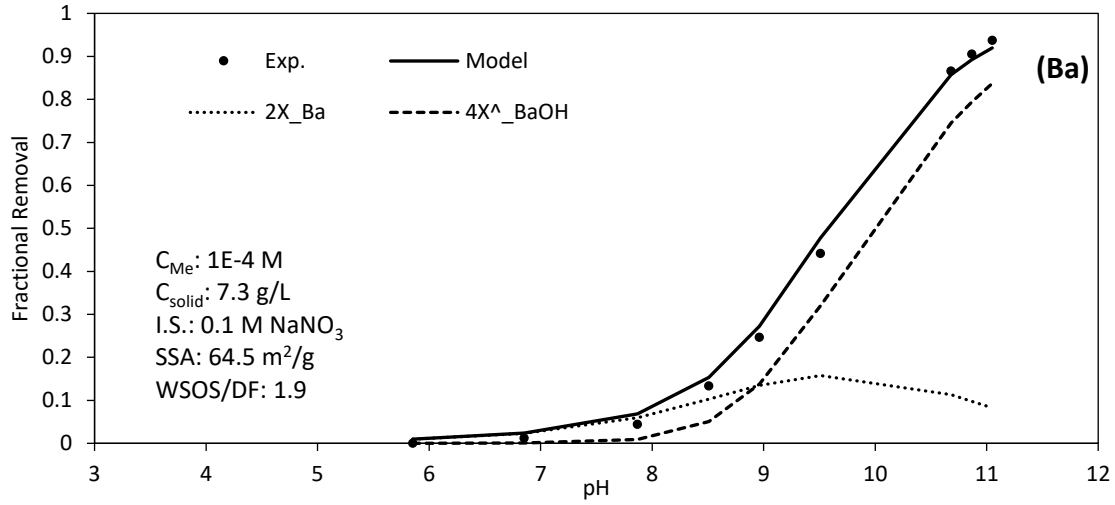

Figure C- 37. Experimental data and model predictions of Ba adsorption on 64.5 m^2/g SSA goethite in 0.1 M $NaNO_3$ solution (C_{Me}: 1e-4 M, C_{solid}: 7.3 g/L)

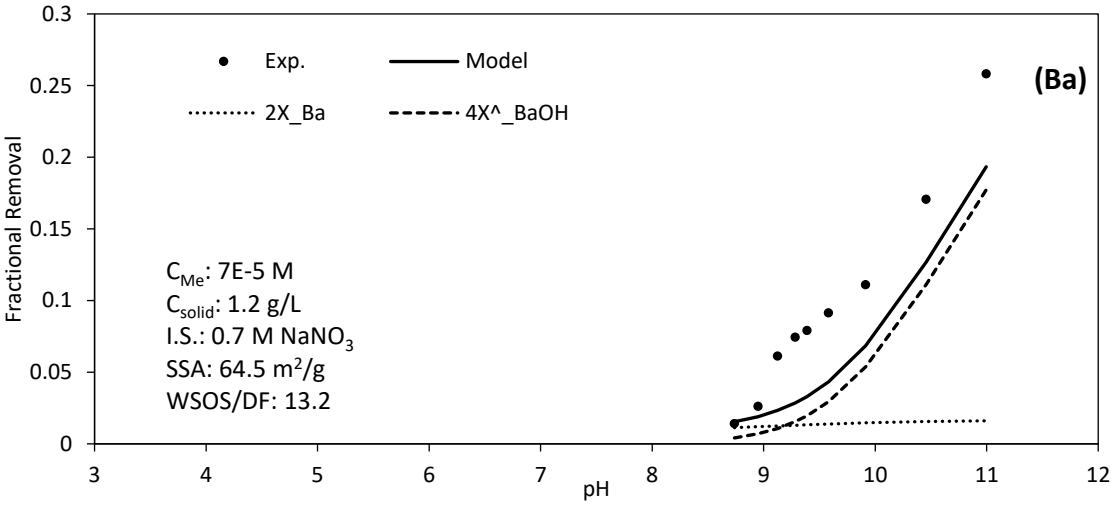

Figure C- 38. Experimental data and model predictions of Ba adsorption on 64.5 m^2/g SSA goethite in 0.7 M $NaNO_3$ solution (C_{Me}: 7e-5 M, C_{solid}: 1.2 g/L)

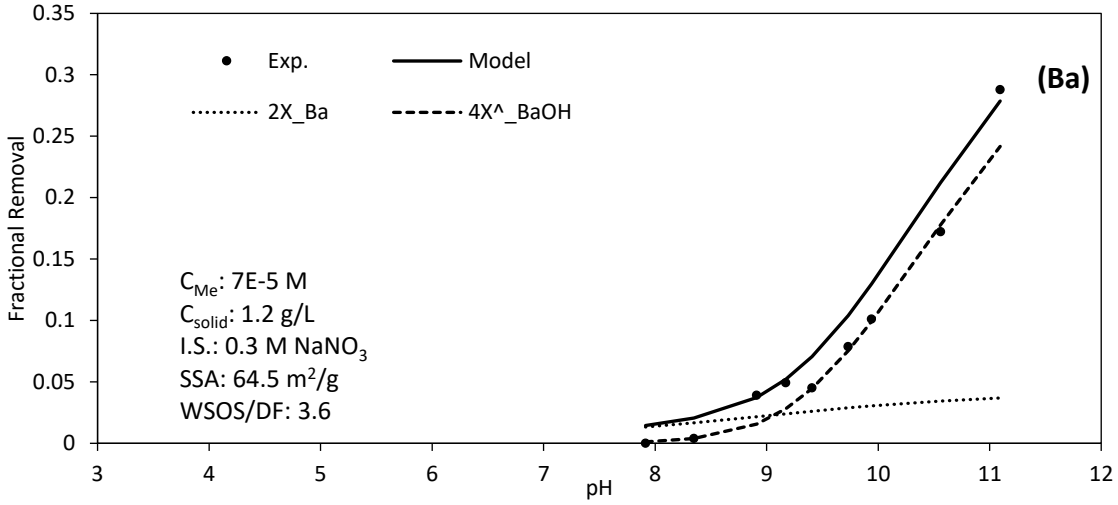

Figure C- 39. Experimental data and model predictions of Ba adsorption on 64.5 m^2/g SSA goethite in 0.3 M $NaNO_3$ solution (C_{Me}: 7e-5 M, C_{solid}: 1.2 g/L)

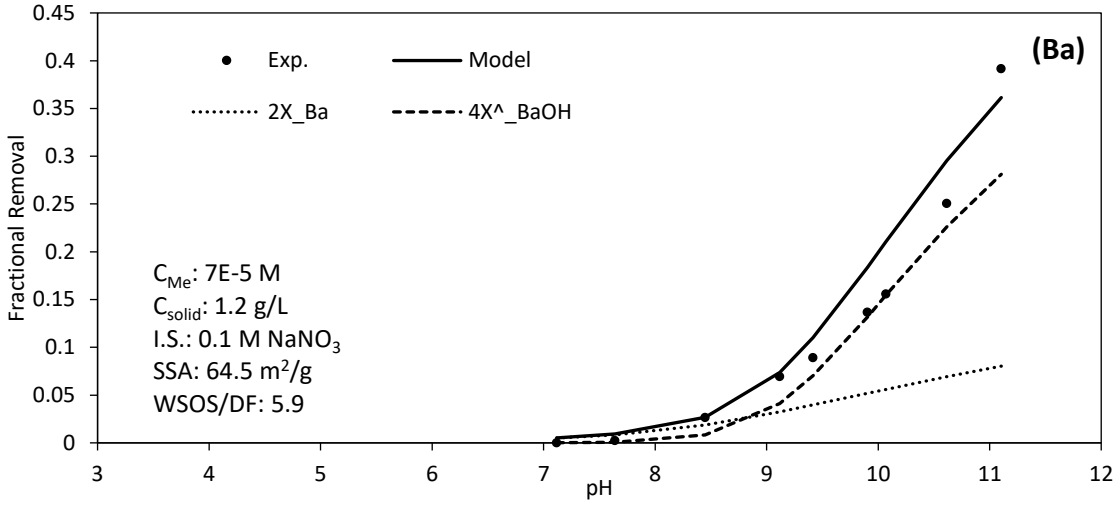

Figure C- 40. Experimental data and model predictions of Ba adsorption on 64.5 m^2/g SSA goethite in 0.1 M $NaNO_3$ solution (C_{Me}: 7e-5 M, C_{solid}: 1.2 g/L)

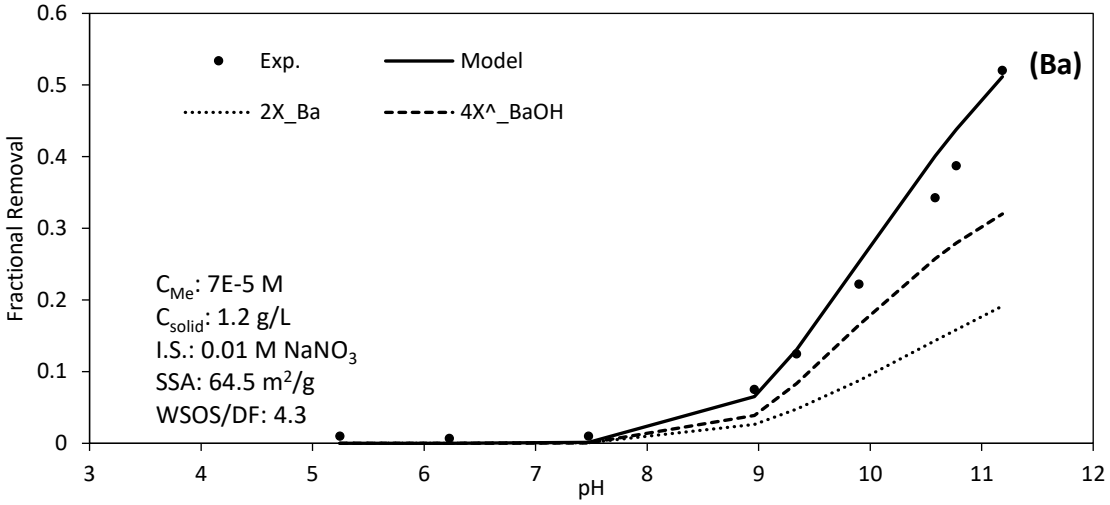

Figure C- 41. Experimental data and model predictions of Ba adsorption on 64.5 m^2/g SSA goethite in 0.01 M $NaNO_3$ solution (C_{Me}: 7e-5 M, C_{solid}: 1.2 g/L)

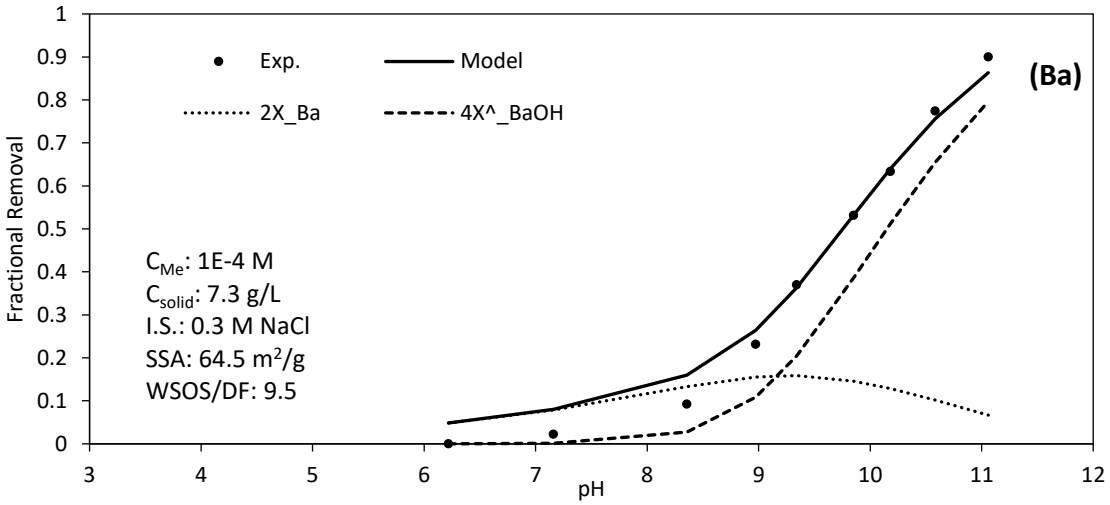

Figure C- 42. Experimental data and model predictions of Ba adsorption on 64.5 m^2/g SSA goethite in 0.3 M NaCl solution (C_{Me}: 1e-4 M, C_{solid}: 7.3 g/L)

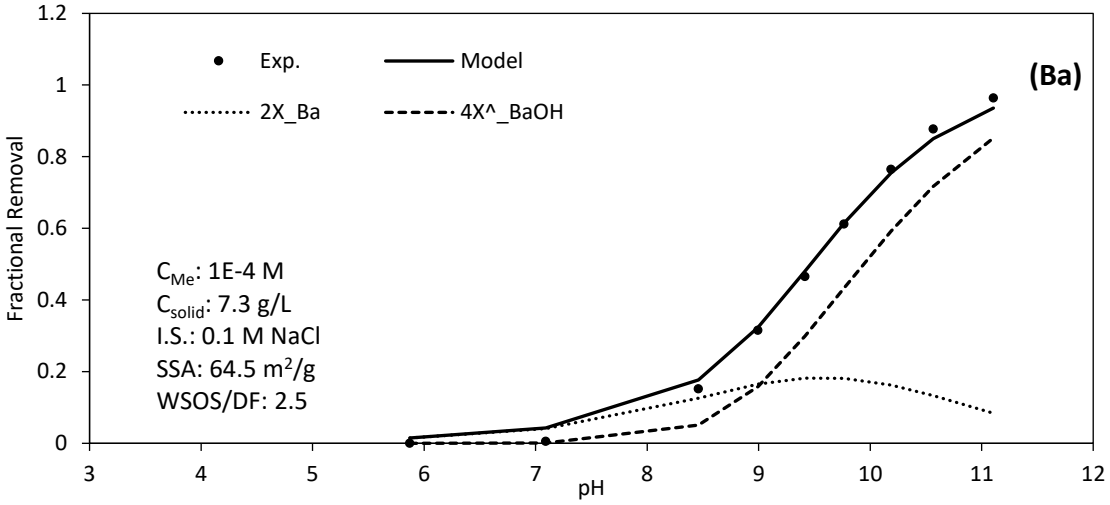

Figure C- 43. Experimental data and model predictions of Ba adsorption on 64.5 m^2/g SSA goethite in 0.1 M NaCl solution (C_{Me}: 1e-4 M, C_{solid}: 7.3 g/L)

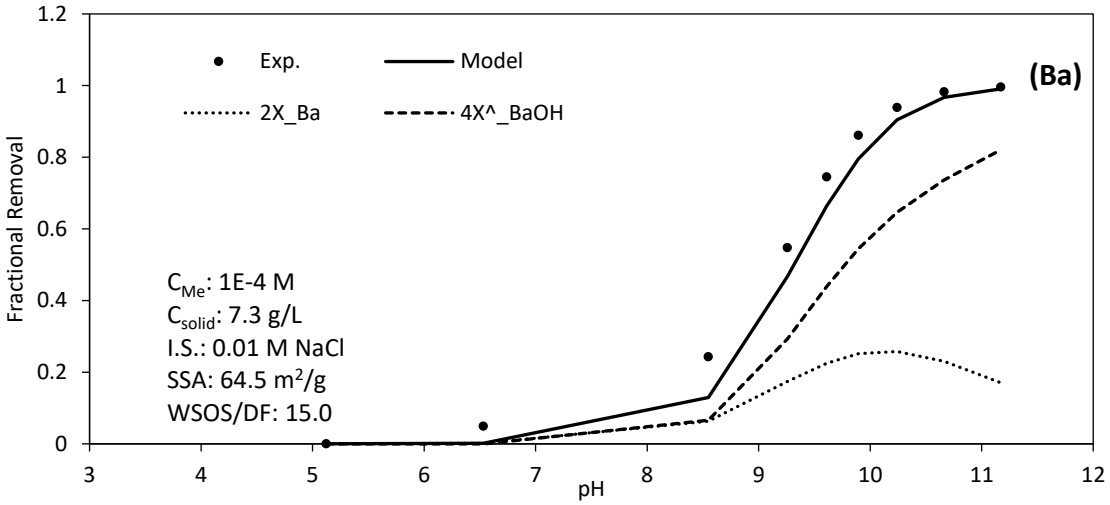

Figure C- 44. Experimental data and model predictions of Ba adsorption on 64.5 m^2/g SSA goethite in 0.01 M NaCl solution (C_{Me}: 1e-4 M, C_{solid}: 7.3 g/L)

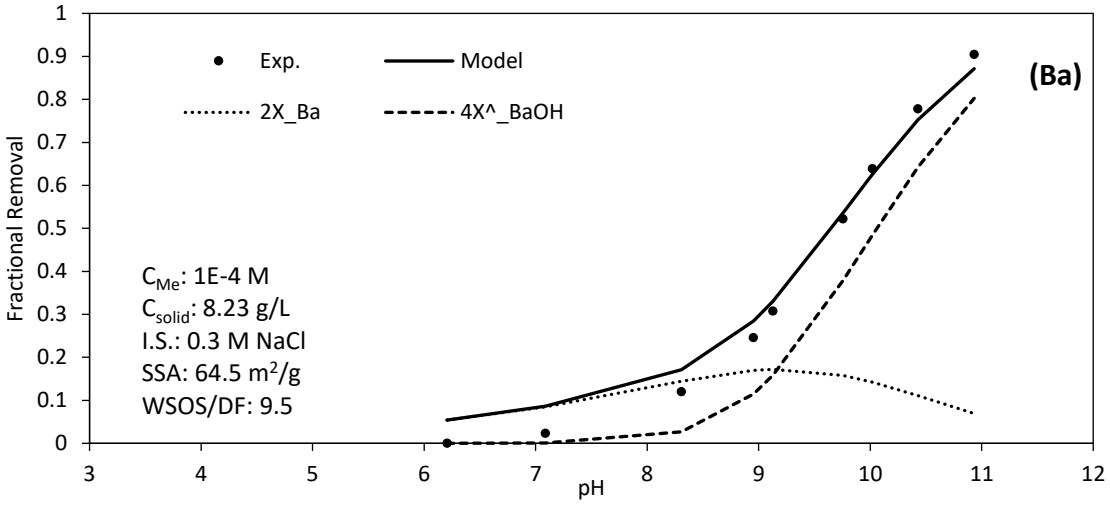

Figure C- 45. Experimental data and model predictions of Ba adsorption on 64.5 m^2/g SSA goethite in 0.3 M NaCl solution (C_{Me}: 1e-4 M, C_{solid}: 8.23 g/L)

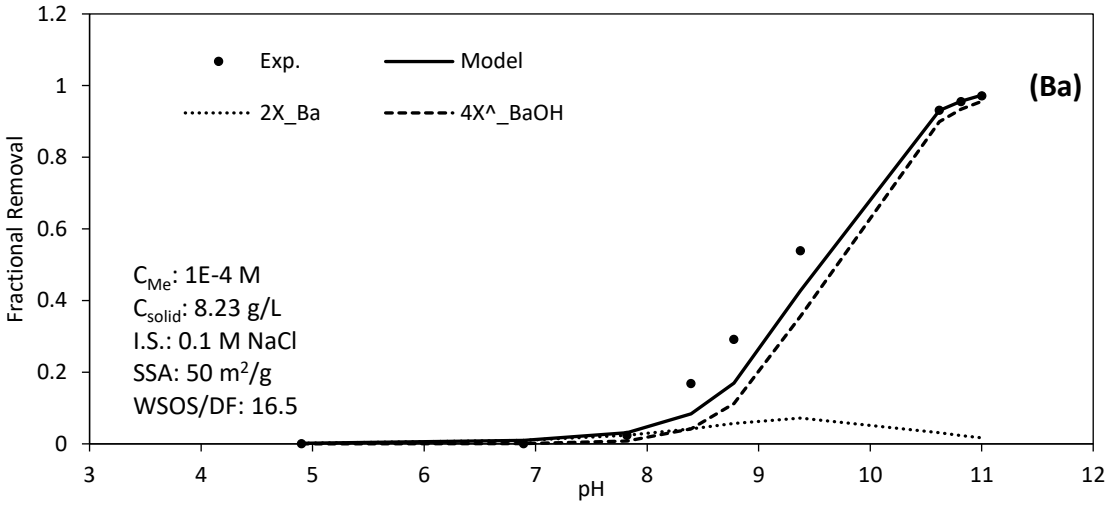

Figure C- 46. Experimental data and model predictions of Ba adsorption on 50 m^2/g SSA goethite in 0.1 M NaCl solution (C_{Me}: 1e-4 M, C_{solid}: 8.23 g/L)

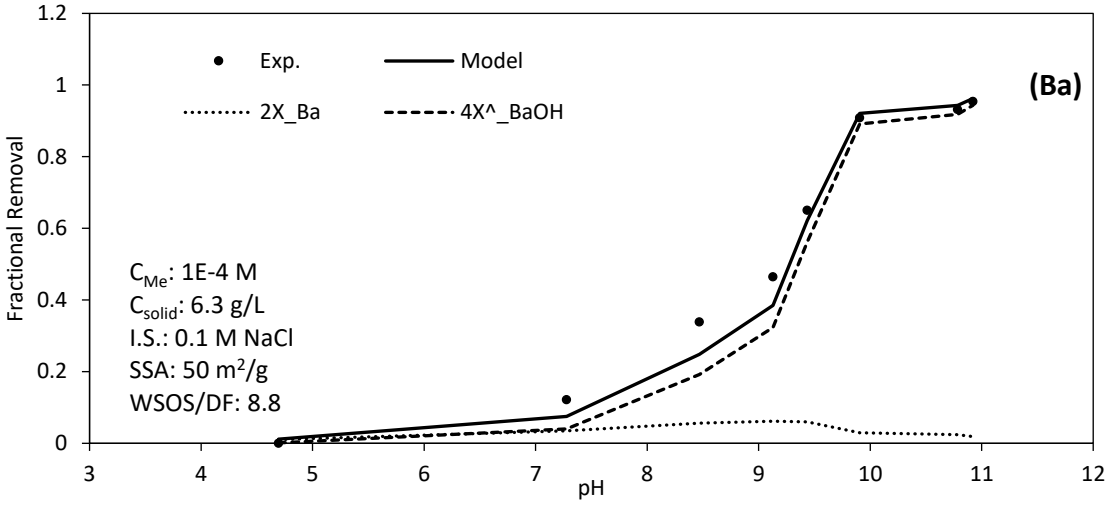

Figure C- 47. Experimental data and model predictions of Ba adsorption on 50 m^2/g SSA goethite in 0.1 M NaCl solution (C_{Me}: 1e-4 M, C_{solid}: 6.3 g/L)

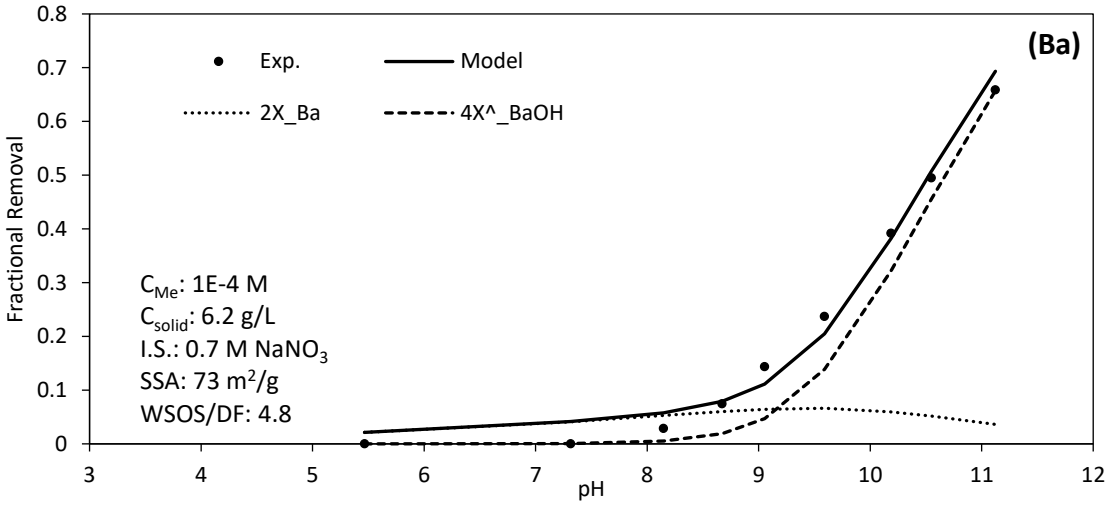

Figure C- 48. Experimental data and model predictions of Ba adsorption on 73 m^2/g SSA goethite in 0.7 M $NaNO_3$ solution (C_{Me}: 1e-4 M, C_{solid}: 6.2 g/L)

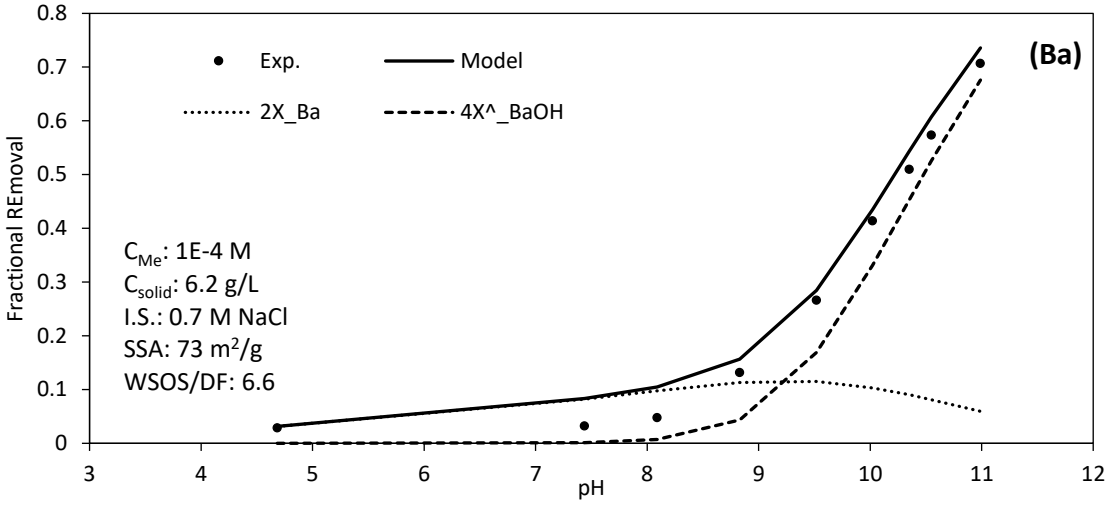

Figure C- 49. Experimental data and model predictions of Ba adsorption on 73 m^2/g SSA goethite in 0.7 M NaCl solution (C_{Me}: 1e-4 M, C_{solid}: 6.2 g/L)

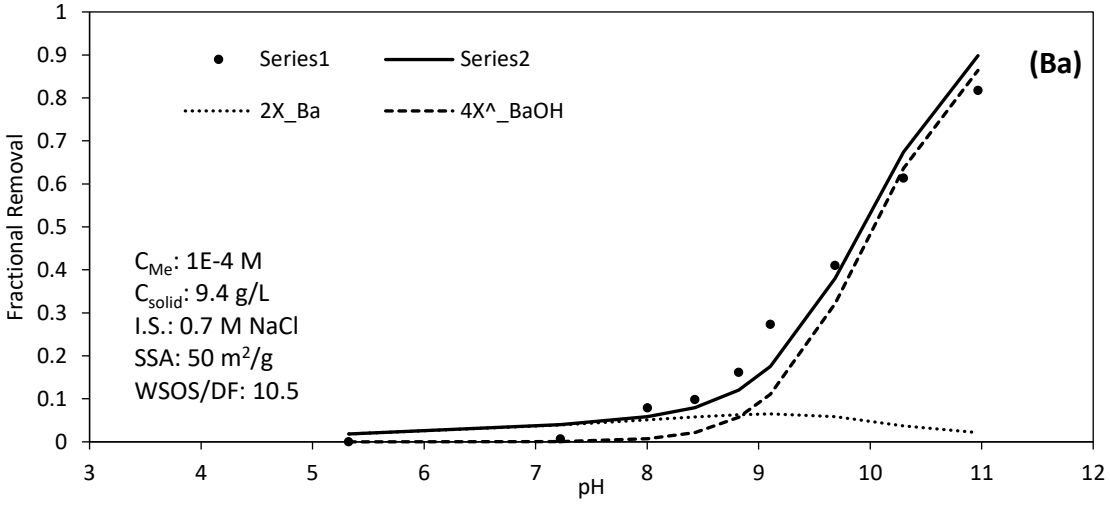

Figure C- 50. Experimental data and model predictions of Ba adsorption on 50 m^2/g SSA goethite in 0.7 M NaCl solution (C_{Me}: 1e-4 M, C_{solid}: 9.4 g/L)

REFERENCES

[1] U. Schwertmann and R. M. Taylor, “Iron oxides,” *Miner. soil Environ.*, no. mineralsinsoile, pp. 379–438, 1989.

[2] R. M. Cornell and U. Schwertmann, *The iron oxide*. New York: VCH, 1996.

[3] L. Donald, “Aqueous environmental geochemistry.” Upper Saddle River, NJ: Prentice Hall, 1997.

[4] D. A. Dzombak and F. M. M. Morel, “Adsorption of inorganic pollutants in aquatic systems,” *J. Hydraul. Eng.*, vol. 113, no. 4, pp. 430–475, 1987.

[5] W. Stumm and J. J. Morgan, *Aquatic chemistry: an introduction emphasizing chemical equilibria in natural waters*. John Wiley, 1981.

[6] H. Freundlich, “Über die adsorption in lösungen,” *Zeitschrift für Phys. Chemie*, vol. 57, no. 1, pp. 385–470, 1907.

[7] I. Langmuir, “The adsorption of gases on plane surfaces of glass, mica and platinum.,” *J. Am. Chem. Soc.*, vol. 40, no. 9, pp. 1361–1403, 1918.

[8] H. W. Kerr, “Nature of base exchange and soil acidity,” *J. Am. Soc. Agron.*, 1928.

[9] E. N. Gapon, “Theory of exchange adsorption in soils,” *J Gen Chem*, vol. 3, no. 2, pp. 144–152, 1933.

[10] M. J. Tempkin and V. Pyzhev, “Heavy metals removal and isotherms study,” *Acta Physiochim URSS*, vol. 12, pp. 217–222, 1940.

[11] Mm. Dubinin, “The potential theory of adsorption of gases and vapors for adsorbents with energetically nonuniform surfaces.,” *Chem. Rev.*, vol. 60, no. 2, pp. 235–241, 1960.

[12] W. Stumm, C.-P. Huang, and S. R. Jenkins, “Specific chemical interaction affecting stability of dispersed systems,” *Croat. Chem. Acta*, vol. 42, no. 2, p. 223, 1970.

[13] I. C. R. Holford, R. W. M. Wedderburn, and G. E. G. Mattingly, “A Langmuir

two-surface equation as a model for phosphate adsorption by soils," *Eur. J. Soil Sci.*, vol. 25, no. 2, pp. 242–255, 1974.

[14] T. Hiemstra, W. H. van Riemsdijk, and G. H. Bolt, "Multisite proton adsorption modeling at the solid/solution interface of (hydr) oxides: A new approach: I. Model description and evaluation of intrinsic reaction constants," *J. Colloid Interface Sci.*, vol. 133, no. 1, pp. 91–104, 1989.

[15] K. F. Hayes, G. Redden, W. Ela, and J. O. Leckie, "Surface complexation models: An evaluation of model parameter estimation using FITEQL and oxide mineral titration data," *J. Colloid Interface Sci.*, vol. 142, no. 2, pp. 448–469, 1991.

[16] W. Stumm, H. Hohl, and F. Dalang, "Interaction of metal-ions with hydrous oxide surfaces," *Croat. Chem. Acta*, vol. 48, no. 4, pp. 491–504, 1976.

[17] P. W. Schindler, "Grenzflächenchemie oxidischer Mineralien," *Oester. Chem. Z*, vol. 86, pp. 141–147, 1985.

[18] D. A. Dzombak and F. M. M. Morel, *Surface complexation modeling: hydrous ferric oxide*. New York: John Wiley & Sons, 1990.

[19] J. A. Davis and D. B. Kent, "Surface complexation modeling in aqueous geochemistry," *Rev. Mineral. Geochemistry*, vol. 23, no. 1, pp. 177–260, 1990.

[20] D. L. Dugger, J. H. Stanton, B. N. Irby, B. L. McConnell, W. W. Cummings, and R. W. Maatman, "The Exchange of Twenty Metal Ions with the Weakly Acidic Silanol Group of Silica Gel1, 2," *J. Phys. Chem.*, vol. 68, no. 4, pp. 757–760, 1964.

[21] P. W. Schindler, B. Fürst, R. Dick, and P. U. Wolf, "Ligand properties of surface silanol groups. I. surface complex formation with Fe3+, Cu2+, Cd2+, and Pb2+," *J. Colloid Interface Sci.*, vol. 55, no. 2, pp. 469–475, 1976.

[22] W. Stumm, R. Kummert, and L. Sigg, "A ligand-exchange model for the adsorption of inorganic and organic-ligands at hydrous oxide interfaces," *Croat. Chem. acta*, vol. 53, no. 2, pp. 291–312, 1980.

[23] G. Sposito, *The Surface Chemistry of Solids*. Oxford university press, 1984.

[24] Z. Wang and D. E. Giammar, “Mass Action Expressions for Bidentate Adsorption in Surface Complexation Modeling: Theory and Practice,” *Environ. Sci. Technol.*, vol. 47, no. 2, pp. 3982–3996, 2013.

[25] P. L. Brezonik and W. A. Arnold, “Water chemistry: Fifty years of change and progress.” ACS Publications, 2012.

[26] C. Koretsky, “The significance of surface complexation reactions in hydrologic systems: a geochemist’s perspective,” *J. Hydrol.*, vol. 230, no. 3, pp. 127–171, 2000.

[27] R. Atkinson, A. M. Posner, and J. P. Quirk, “Adsorption of potential-determining ions at the ferric oxide-aqueous electrolyte interface,” *J. Phys. Chem.*, vol. 71, no. 3, pp. 550–558, 1967.

[28] R. Strauss, G. W. Brummer, and N. J. Barrow, “Effects of crystallinity of goethite: II. Rates of sorption and desorption of phosphate,” *Eur. J. Soil Sci.*, vol. 48, no. March, pp. 101–1, 1997.

[29] P. Zarzycki, S. Kerisit, and K. M. Rosso, “Molecular Dynamics Study of Fe(II) Adsorption, Electron Exchange, and Mobility at Goethite (α-FeOOH) Surfaces,” *J. Phys. Chem. C*, vol. 119, no. 6, pp. 3111–3123, 2015.

[30] J. M. Bigham, R. W. Fitzpatrick, D. G. Schulze, and J. B. Dixon, “Iron oxides.,” *Soil Mineral. with Environ. Appl.*, pp. 323–366, 2002.

[31] M. Villalobos, M. a Trotz, and J. O. Leckie, “Variability in goethite surface site density: evidence from proton and carbonate sorption,” *J. Colloid Interface Sci.*, vol. 268, no. 2, pp. 273–287, Dec. 2003.

[32] J. Rakovan, U. Becker, and M. F. Hochella, “Aspects of goethite surface microtopography, structure, chemistry, and reactivity,” *Am. Mineral.*, vol. 84, no. 5–6, pp. 884–894, 1999.

[33] F. Gaboriaud and J.-J. Ehrhardt, “Effects of different crystal faces on the surface charge of colloidal goethite (a-FeOOH) particles: An experimental and modeling study,” *Geochim. Cosmochim. Acta*, vol. 67, no. 5, pp. 967–983, 2003.

[34] M. Villalobos, M. a Trotz, and J. O. Leckie, “Surface complexation modeling of carbonate effects on the adsorption of Cr(VI), Pb(II), and U(VI) on goethite.,”

Environ. Sci. Technol., vol. 35, no. 19, pp. 3849–56, Oct. 2001.

[35] A. Navrotsky, L. Mazeina, and J. Majzlan, "Size-driven structural and thermodynamic complexity in iron oxides," *Science (80-.).*, vol. 319, no. 5870, pp. 1635–1638, 2008.

[36] H. Liu, T. Chen, and R. L. Frost, "An overview of the role of goethite surfaces in the environment.," *Chemosphere*, vol. 103, pp. 1–11, May 2014.

[37] M. Kosmulski, "pH-dependent surface charging and points of zero charge II. Update.," *J. Colloid Interface Sci.*, vol. 275, no. 1, pp. 214–24, Jul. 2004.

[38] E. Goli, R. Rahnemaie, T. Hiemstra, and M. J. Malakouti, "The interaction of boron with goethite: Experiments and CD-MUSIC modeling," *Chemosphere*, vol. 82, no. 10, pp. 1475–1481, 2011.

[39] K. Kaneko and K. Inouye, "The mechanism of chemisorption of SO2 on iron (III) hydroxide oxides," *Corros. Sci.*, vol. 21, no. 9–10, pp. 639–646, 1981.

[40] J. Baltrusaitis, D. M. Cwiertny, and V. H. Grassian, "Adsorption of sulfur dioxide on hematite and goethite particle surfaces," *Phys. Chem. Chem. Phys.*, vol. 9, no. 41, p. 5542, 2007.

[41] D. V. Nguyen, J. Kynicky, P. Ambrozova, and V. Adam, "Microwave-Assisted Synthesis of Goethite Nanoparticles Used for Removal of Cr(VI) from Aqueous Solution," *Materials* , vol. 10, no. 7. 2017.

[42] L. S. Balistrieri and J. W. Murray, "The adsorption of Cu, Pb, Zn, and Cd on goethite from major ion seawater," *Geochim. Cosmochim. Acta*, vol. 46, no. 1255, 1982.

[43] M. Villalobos and A. Pérez-Gallegos, "Goethite surface reactivity: A macroscopic investigation unifying proton, chromate, carbonate, and lead(II) adsorption," *J. Colloid Interface Sci.*, vol. 326, no. 2, pp. 307–323, 2008.

[44] D. A. Sverjensky, "Prediction of the speciation of alkaline earths adsorbed on mineral surfaces in salt solutions," *Geochim. Cosmochim. Acta*, vol. 70, no. 10, pp. 2427–2453, May 2006.

[45] C. E. Cowan, J. M. Zachara, and C. T. Resch, “Cadmium adsorption on iron oxides in the presence of alkaline-earth elements,” *Environ. Sci. Technol.*, vol. 25, no. 3, pp. 437–446, 1991.

[46] U. Schwertmann, P. Cambier, and E. Murad, “Properties of goethites of varying crystallinity,” *Clays Clay Miner.*, vol. 33, no. 5, pp. 369–378, 1985.

[47] M. Kosmulski, S. Durand-Vidal, E. Maczka, and J. B. Rosenholm, “Morphology of synthetic goethite particles.,” *J. Colloid Interface Sci.*, vol. 271, no. 2, pp. 261–9, Mar. 2004.

[48] J.-F. Boily, J. Lützenkirchen, O. Balmes, J. Beattie, and S. Sjöberg, “Modeling proton binding at the goethite (a -FeOOH)– water interface,” *Colloids Surfaces A Physicochem. Eng. Asp.*, vol. 179, pp. 11–27, 2001.

[49] J. Lützenkirchen, J.-F. Boily, L. Gunneriusson, L. Lövgren, and S. Sjöberg, “Protonation of different goethite surfaces-Unified models for NaNO3 and NaCl media,” *J. Colloid Interface Sci.*, vol. 317, no. 1, pp. 155–165, 2008.

[50] R. Rahnemaie, T. Hiemstra, and W. H. van Riemsdijk, “A new surface structural approach to ion adsorption: Tracing the location of electrolyte ions,” *J. Colloid Interface Sci.*, vol. 293, pp. 312–321, 2006.

[51] D. A. Sverjensky, “Prediction of surface charge on oxides in salt solutions: Revisions for 1:1 (M+L−) electrolytes,” *Geochim. Cosmochim. Acta*, vol. 69, no. 2, pp. 225–257, Jan. 2005.

[52] P. Venema, *Charging and ion adsorption behaviour of different iron (hydr) oxides*. Landbouwuniversiteit Wageningen, 1997.

[53] T. Hiemstra, J. C. M. De Wit, and W. H. van Riemsdijk, “Multisite proton adsorption at the soil/solution interface of (Hydr) oxides: a new approach. II: Application to various important (Hydr) oxides,” *J. Colloid Interface Sci.*, vol. 133, no. 1, pp. 105–117, 1989.

[54] C. N. Durfor and E. Becker, “Geological Survey Water-Supply Paper 1812,” Washington D.C., 1964.

[55] D. K. Todd and L. W. Mays, “Groundwater hydrology,” 1980.

[56] E. Tipping, “Modeling the competition between alkaline earth cations and trace metal species for binding by humic substances,” *Environ. Sci. Technol.*, vol. 27, no. 3, pp. 520–529, 1993.

[57] R. Mandal *et al.*, “Competition of Ca(II) and Mg(II) with Ni(II) for binding by a well-characterized fulvic acid in model solutions,” *Environ. Sci. Technol.*, vol. 34, no. 11, pp. 2201–2208, 2000.

[58] T. Harter, “Groundwater Quality and Groundwater Pollution,” 2003.

[59] L. Candela and I. Morell, “Basic Chemical Principles of Groundwater,” in *Groundwater*, vol. II, L. Silveira and E. J. Usunoff, Eds. EOLSS Publications, 2009, pp. 43–54.

[60] K. B. Gregory, R. D. Vidic, and D. a. Dzombak, “Water management challenges associated with the production of shale gas by hydraulic fracturing,” *Elements*, vol. 7, pp. 181–186, 2011.

[61] M. Stachowicz, T. Hiemstra, and W. H. van Riemsdijk, “Multi-competitive interaction of As(III) and As(V) oxyanions with Ca(2+), Mg(2+), PO(3-)(4), and CO(2-)(3) ions on goethite.,” *J. Colloid Interface Sci.*, vol. 320, no. 2, pp. 400–14, Apr. 2008.

[62] J. I. Drever, “The Geochemistry of Natural Waters: Surface and Groundwater Environments, 436 pp.” Prentice Hall, Upper Saddle River, NJ, 1997.

[63] M. Sajih *et al.*, “Adsorption of radium and barium on goethite and ferrihydrite: A kinetic and surface complexation modelling study,” *Geochim. Cosmochim. Acta*, vol. 146, pp. 150–163, Dec. 2014.

[64] R. Rahnemaie, T. Hiemstra, and W. H. van Riemsdijk, “Inner- and outer-sphere complexation of ions at the goethite-solution interface.,” *J. Colloid Interface Sci.*, vol. 297, no. 2, pp. 379–388, May 2006.

[65] R. P. J. J. Rietra, T. Hiemstra, and W. H. van Riemsdijk, “Interaction between calcium and phosphate adsorption on goethite.,” *Environ. Sci. Technol.*, vol. 35, no. 16, pp. 3369–74, Aug. 2001.

[66] L. P. Weng, W. H. van Riemsdijk, and T. Hiemstra, “Cu2+ and Ca2+adsorption to goethite in the presence of fulvic acids,” *Geochim. Cosmochim. Acta*, vol. 72, no.

24, pp. 5857–5870, 2008.

[67] M. a. Ali and D. a. Dzombak, “Effects of simple organic acids on sorption of Cu2+ and Ca2+ on goethite,” *Geochim. Cosmochim. Acta*, vol. 60, no. 2, pp. 291–304, 1996.

[68] L. P. Weng, L. K. Koopal, T. Hiemstra, J. C. L. Meeussen, and W. H. van Riemsdijk, “Interactions of calcium and fulvic acid at the goethite-water interface,” *Geochim. Cosmochim. Acta*, vol. 69, no. 2, pp. 325–339, 2005.

[69] C. R. Collins, D. M. Sherman, and K. V. Ragnarsdöttir, “The adsorption mechanism of Sr2+ on the surface of goethite,” *Radiochim. Acta*, vol. 81, no. 4, pp. 201–206, 1998.

[70] N. Sahai, S. A. Carroll, S. K. Roberts, and P. A. O’Day, “X-Ray Absorption Spectroscopy of Strontium(II) Coordination: II. Sorption and Precipitation at Kaolinite, Amorphous Silica, and Goethite Surfaces,” *J. Colloid Interface Sci.*, vol. 222, no. 2, pp. 198–212, Feb. 2000.

[71] K. F. Hayes and L. E. Katz, “Application of X-ray absorption spectroscopy for surface complexation modeling of metal ion sorption,” in *Physics and chemistry of mineral surfaces*, CRC Press: Boca Raton, FL, 1996, pp. 147–223.

[72] S. A. Carroll, S. K. Roberts, L. J. Criscenti, and P. A. O’Day, “Surface complexation model for strontium sorption to amorphous silica and goethite.,” *Geochem. Trans.*, vol. 9, p. 2, Jan. 2008.

[73] L. E. Katz, L. J. Criscenti, C. Chen, J. P. Larentzos, and H. M. Liljestrand, “Temperature effects on alkaline earth metal ions adsorption on gibbsite: approaches from macroscopic sorption experiments and molecular dynamics simulations.,” *J. Colloid Interface Sci.*, vol. 399, pp. 68–76, Jun. 2013.

[74] C.-C. Chen, M. L. Coleman, and L. E. Katz, “Bridging the Gap between Macroscopic and Spectroscopic Studies of Metal Ion Sorption at the Oxide/Water Interface: Sr(II), Co(II), and Pb(II) Sorption to Quartz,” *Environ. Sci. Technol.*, vol. 40, no. 1, pp. 142–148, Jan. 2006.

[75] P. Fenter, L. Cheng, S. Rihs, M. L. Machesky, M. J. Bedzyk, and N. C. Sturchio, “Electrical Double-Layer Structure at the Rutile-Water Interface as Observed in Situ with Small-Period X-Ray Standing Waves.,” *J. Colloid Interface Sci.*, vol.

225, pp. 154–165, 2000.

[76] M. L. Machesky *et al.*, “Comparison of cation adsorption by isostructural rutile and cassiterite.,” *Langmuir*, vol. 27, no. 8, pp. 4585–93, Apr. 2011.

[77] Z. Zhang *et al.*, “Ion adsorption at the rutile-water interface: Linking molecular and macroscopic properties,” *Langmuir*, vol. 20, no. 5, pp. 4954–4969, 2004.

[78] M. Předota, Z. Zhang, P. Fenter, D. J. Esolowski, and P. T. Cummings, “Electric double layer at the rutile (110) surface. 2. Adsorption of ions from molecular dynamics and X-ray experiments,” *J. Phys. Chem. B*, vol. 108, no. 32, pp. 12061–12072, 2004.

[79] M. K. Ridley, T. Hiemstra, W. H. van Riemsdijk, and M. L. Machesky, “Inner-sphere complexation of cations at the rutile–water interface: A concise surface structural interpretation with the CD and MUSIC model,” *Geochim. Cosmochim. Acta*, vol. 73, no. 7, pp. 1841–1856, Apr. 2009.

[80] C.-C. Chen and K. F. Hayes, “X-ray absorption spectroscopy investigation of aqueous Co (II) and Sr (II) sorption at clay–water interfaces,” *Geochim. Cosmochim. Acta*, vol. 63, no. 19, pp. 3205–3215, 1999.

[81] R. H. Parkman, J. M. Charnock, F. R. Livens, and D. J. Vaughan, “A study of the interaction of strontium ions in aqueous solution with the surfaces of calcite and kaolinite,” *Geochim. Cosmochim. Acta*, vol. 62, no. 9, pp. 1481–1492, 1998.

[82] P. Venema, T. Hiemstra, and W. H. van Riemsdijk, “Multisite Adsorption of Cadmium on Goethite,” *J. Colloid Interface Sci.*, vol. 183, pp. 515–27, 1996.

[83] T. Hiemstra and W. H. van Riemsdijk, “A Surface Structural Approach to Ion Adsorption: The Charge Distribution (CD) Model,” *J. Colloid Interface Sci.*, vol. 179, no. 2, pp. 488–508, 1996.

[84] C. J. Tadanier and M. J. Eick, “Formulating the Charge-distribution Multisite Surface Complexation Model,” *Soil Sci. Soc. Am. J.*, vol. 66, no. 5, pp. 1505–1517, 2002.

[85] G. H. Bolt and W. H. van Riemsdijk, “Ion adsorption on inorganic variable charge constituents,” in *Soil Chemistry Part B*, Second., G.H. Bolt, Ed. Amsterdam: Elsevier, 1982, pp. 459–504.

[86] F. M. M. Morel and J. G. Hering, *Principles and applications of aquatic chemistry*. John Wiley & Sons, 1993.

[87] J. C. Westall, "Chemical Equilibrium Including Adsorption on Charged Surfaces," in *Particulates in Water*, vol. 189, AMERICAN CHEMICAL SOCIETY, 1980, pp. 2–33.

[88] S. Goldberg, "Adsorption Models Incorporated into Chemical Equilibrium Models," in *Chemical Equilibrium and Reaction Models*, 1995, pp. 75–95.

[89] J. E. Mangold, "Predicting Ion Adsorption onto the Iron Hydroxide Goethite in Single and Multi- Solute Systems," University of Texas at Austin, 2013.

[90] J. C. Westall, "Reactions at the oxide-solution interface: Chemical and electrostatic models," in *Geochemical processes at mineral surfaces*, vol. 323, American Chemical Society Washington, DC, 1986, pp. 54–78.

[91] J. C. Westall, *FITEQL: A computer program for determination of chemical equilibrium constants from experimental data*. Department of Chemistry, Oregon State University, 1982.

[92] B. D. Honeyman and J. O. Leckie, "Macroscopic Partitioning Coefficients for Metal Ion Adsorption," in *Geochemical Processes at Mineral Surfaces*, vol. 323, American Chemical Society, 1987, pp. 162-190 SE–9.

[93] J. A. Davis and D. B. Kent, "Waste Isolation Pilot Plant Compliance Certification Application Reference 583," *Rev. Mineral. Geochemistry*, vol. 23, pp. 177–260, 1990.

[94] J. A. Davis, D. B. Kent, B. A. Rea, A. S. Maest, and S. P. Garabedian, "Influence of redox environment and aqueous speciation on metal transport in groundwater: Preliminary results of tracer injection studies," *Met. Groundwater, Chelsea, MI, Lewis Publ.*, pp. 223–273, 1993.

[95] B. D. Honeyman and P. H. Santschi, "Metals in aquatic systems.," *Environ. Sci. Technol.*, vol. 22, no. 8, pp. 862–871, 1988.

[96] D. B. Kent, V. S. Tripathi, N. B. Ball, J. O. Leckie, and M. D. Siegel, "Surface-complexation modeling of radionuclide adsorption in subsurface environments," Stanford Univ., CA (USA). Dept. of Civil Engineering; Sandia National Labs.,

Albuquerque, NM (USA), 1988.

[97] J. Lützenkirchen *et al.*, “Treatment of multi-dentate surface complexes and diffuse layer implementation in various speciation codes,” *Appl. Geochemistry*, vol. 55, pp. 128–137, 2015.

[98] R. P. J. J. Rietra, T. Hiemstra, and W. H. van Riemsdijk, “Electrolyte Anion Affinity and Its Effect on Oxyanion Adsorption on Goethite.,” *J. Colloid Interface Sci.*, vol. 229, pp. 199–206, 2000.

[99] J. C. Westall and H. Hohl, “A comparison of electrostatic models for the oxide/solution interface,” *Adv. Colloid Interface Sci.*, vol. 12, no. 4, pp. 265–294, 1980.

[100] L. E. Wangen and J. M. Williams, “Control by alkaline neutralization of trace elements in acidic coal cleaning waste leachates,” *J. (Water Pollut. Control Fed.*, vol. 54, no. 9, pp. 1302–1310, 1982.

[101] S. Goldberg and G. Sposito, “A Chemical Model of Phosphate Adsorption by Soils: I. Reference Oxide Minerals1,” *Soil Sci. Soc. Am. J.*, vol. 48, no. 4, p. 772, 1984.

[102] M. Ochs *et al.*, “Use of thermodynamic sorption models to derive radionuclide Kd values for performance assessment: Selected results and recommendations of the NEA sorption project,” *Radiochim. Acta*, vol. 94, no. 9–11, pp. 779–785, 2006.

[103] M. M. Benjamin, “Modeling the mass-action expression for bidentate adsorption,” *Environ. Sci. Technol.*, vol. 36, no. 3, pp. 307–313, 2002.

[104] P. Venema, T. Hiemstra, and W. H. van Riemsdijk, “Comparison of Different Site Binding Models for Cation Sorption: Description of pH Dependency, Salt Dependency, and Cation–Proton Exchange,” *J. Colloid Interface Sci.*, vol. 181, pp. 45–59, 1996.

[105] H. Hohl and W. Stumm, “Interaction of Pb2+ with hydrous γ-Al2O3,” *J. Colloid Interface Sci.*, vol. 55, no. 2, pp. 281–288, 1976.

[106] P. von Schindler and H. R. Kamber, “Die acidität von silanolgruppen. Vorläufige mitteillung,” *Helv. Chim. Acta*, vol. 51, no. 7, pp. 1781–1786, 1968.

[107] P. W. Schindler and H. Gamsjäger, “Acid—base reactions of the TiO 2 (Anatase)—water interface and the point of zero charge of TiO 2 suspensions,” *Colloid Polym. Sci.*, vol. 250, no. 7, pp. 759–763, 1972.

[108] D. E. Yates, S. Levine, and T. W. Healy, “Site-binding Model of the Electrical Double Layer at the Oxide / Water Interface,” *J. Chem. Soc. Faraday Trans. 1 Phys. Chem. Condens. Phases*, vol. 70, pp. 1807–1818, 1974.

[109] M. Gouy, “Sur la constitution de la charge électrique à la surface d’un électrolyte,” *J. Phys. Théorique Appliquée*, vol. 9, pp. 457–468, 1910.

[110] D. L. Chapman, “LI. A contribution to the theory of electrocapillarity,” *Philos. Mag. Ser. 6*, vol. 25, pp. 475–481, 1913.

[111] S. Srinivasan, “Electrode / Electrolyte Interfaces: Structure and Kinetics of Charge Transfer,” in *Fuel Cells: From Fundamentals to Applications*, Springer US, 2006, pp. 27–92.

[112] M. M. Benjamin and J. O. Leckie, “Multiple-site adsorption of Cd, Cu, Zn, and Pb on amorphous iron oxyhydroxide,” *J. Colloid Interface Sci.*, vol. 79, no. 1, pp. 209–221, 1981.

[113] K. J. Farley, D. A. Dzombak, and F. M. M. Morel, “A surface precipitation model for the sorption of cations on metal oxides,” *J. Colloid Interface Sci.*, vol. 106, no. 1, pp. 226–242, 1985.

[114] J. A. Davis, R. O. James, and J. O. Leckie, “Surface ionization and complexation at the oxide/water interface: I. Computation of electrical double layer properties in simple electrolytes,” *J. Colloid Interface Sci.*, vol. 63, no. 3, pp. 480–499, 1978.

[115] T. Hiemstra, P. Venema, and W. H. van Riemsdijk, “Intrinsic Proton Affinity of Reactive Surface Groups of Metal (Hydr)oxides: The Bond Valence Principle,” *J. Colloid Interface Sci.*, vol. 184, pp. 680–92, 1996.

[116] C. Salazar-Camacho and M. Villalobos, “Goethite surface reactivity: III. Unifying arsenate adsorption behavior through a variable crystal face – Site density model,” *Geochim. Cosmochim. Acta*, vol. 74, no. 8, pp. 2257–2280, 2010.

[117] R. M. Cornell and U. Schwertmann, *The iron minerals: Structure, properties, reactions, occurrence and uses*. VCH, Weinheim, 1996.

[118] M. Villalobos, M. a. Cheney, and J. Alcaraz-Cienfuegos, “Goethite surface reactivity: II. A microscopic site-density model that describes its surface area-normalized variability,” *J. Colloid Interface Sci.*, vol. 336, no. 2, pp. 412–422, 2009.

[119] B. Prélot *et al.*, “Morphology and surface heterogeneities in synthetic goethites,” *J. Colloid Interface Sci.*, vol. 261, no. 2, pp. 244–254, 2003.

[120] J. Lützenkirchen, J.-F. Boily, L. Lövgren, and S. Sjöberg, “Limitations of the potentiometric titration technique in determining the proton active site density of goethite surfaces,” *Geochim. Cosmochim. Acta*, vol. 66, no. 19, pp. 3389–3396, 2002.

[121] T. Hiemstra and W. H. van Riemsdijk, “Physical chemical interpretation of primary charging behaviour of metal (hydr) oxides,” *Colloids and surfaces*, vol. 59, pp. 7–25, 1991.

[122] T. Hiemstra and W. H. van Riemsdijk, “On the relationship between charge distribution, surface hydration, and the structure of the interface of metal hydroxides,” *J. Colloid Interface Sci.*, vol. 301, pp. 1–18, 2006.

[123] A. van Geen, A. P. Robertson, and J. O. Leckie, “Complexation of carbonate species at the goethite surface: Implications for adsorption of metal ions in natural waters,” *Geochim. Cosmochim. Acta*, vol. 58, no. 9, pp. 2073–2086, May 1994.

[124] G. A. Waychunas, C. S. Kim, and J. F. Banfield, “Nanoparticulate iron oxide minerals in soils and sediments: Unique properties and contaminant scavenging mechanisms,” *J. Nanoparticle Res.*, vol. 7, no. 4–5, pp. 409–433, 2005.

[125] J. E. Mangold, C. M. Park, H. M. Liljestrand, and L. E. Katz, “Surface complexation modeling of Hg(II) adsorption at the goethite/water interface using the Charge Distribution Multi-Site Complexation (CD-MUSIC) model,” *J. Colloid Interface Sci.*, vol. 418, no. 2014, pp. 147–161, 2014.

[126] K. J. T. Livi *et al.*, “Crystal Face Distributions and Surface Site Densities of Two Synthetic Goethites: Implications for Adsorption Capacities as a Function of Particle Size,” *Langmuir*, vol. 33, no. 36, pp. 8924–8932, 2017.

[127] A. Vieira, “Surface complexation modeling of Pb (II), Cd (II) and Se (IV) onto iron hydroxides in single and bisolute systems,” University of Texas at Austin,

2007.

[128] V. Barron and J. Torrent, “Surface Hydroxyl Configuration of Various Crystal Faces of Hematite and Goethite,” *J. Colloid Interface Sci.*, vol. 177, no. 2, pp. 407–410, 1996.

[129] A. Manceau and L. Charlet, “The mechanism of selenate adsorption on goethite and hydrous ferric oxide,” *J. Colloid Interface Sci.*, vol. 168, no. 1, pp. 87–93, 1994.

[130] L. Spadini, A. Manceau, P. W. Schindler, and L. Charlet, “Structure and Stability of Cd2+ Surface Complexes on Ferric Oxides: 1. Results from EXAFS Spectroscopy,” *J. Colloid Interface Sci.*, vol. 168, pp. 73–86, 1994.

[131] S. R. Randall, D. M. Sherman, K. V. Ragnarsdöttir, and C. R. Collins, “The mechanism of cadmium surface complexation on iron oxyhydroxide minerals,” *Geochim. Cosmochim. Acta*, vol. 63, no. 19–20, pp. 2971–2987, 1999.

[132] J. D. Ostergren, G. E. J. Brown, G. A. Parks, and P. Persson, “Inorganic ligand effects on Pb (II) sorption to goethite (α-FeOOH): II. Sulfate,” *J. Colloid Interface Sci.*, vol. 225, no. 2, pp. 483–493, 2000.

[133] H. Arnold, “International Tables for Crystallography, Vol. A, edited by Th. Hahn, Section 5.” Dordrecht: Kluwer Academic Publishers, 1996.

[134] U. Schwertmann, “The double dehydroxylation peak of goethite,” *Thermochim. Acta*, vol. 78, no. 1, pp. 39–46, 1984.

[135] U. Schwertmann and R. M. Cornell, “Iron oxides in the laboratory,” 1991.

[136] R. M. Cornell, A. M. Posner, and J. P. Quirk, “Crystal morphology and the dissolution of goethite,” *J. Inorg. Nucl. Chem.*, vol. 36, no. 9, pp. 1937–1946, 1974.

[137] E. D. Sone, S. Weiner, and L. Addadi, “Morphology of goethite crystals in developing limpet teeth: Assessing biological control over mineral formation,” *Cryst. Growth Des.*, vol. 5, no. 6, pp. 2131–2138, 2005.

[138] C. Colombo, V. Barrón, and J. Torrent, “Phosphate adsorption and desorption in

relation to morphology and crystal properties of synthetic hematites," *Geochim. Cosmochim. Acta*, vol. 58, no. 4, pp. 1261–1269, 1994.

[139] P. G. Weidler, T. Schwinn, and H. E. Gaub, "Vicinal faces on synthetic goethite observed by atomic force microscopy," *Clays Clay Miner.*, vol. 44, no. 4, pp. 437–442, 1996.

[140] P. G. Weidler, S. J. Hug, T. P. Wetche, and T. Hiemstra, "Determination of growth rates of (100) and (110) faces of synthetic goethite by scanning force microscopy," *Geochim. Cosmochim. Acta*, vol. 62, no. 21, pp. 3407–3412, 1998.

[141] H. Von Helmholtz, "Studien über electrische Grenzschichten," *Ann. Phys.*, vol. 243, no. 7, pp. 337–382, 1879.

[142] D. A. Sverjensky, "Interpretation and prediction of triple-layer model capacitances and the structure of the oxide-electrolyte-water interface," *Geochim. Cosmochim. Acta*, vol. 65, no. 21, pp. 3643–3655, 2001.

[143] J.-F. Boily, "The variable capacitance model: A strategy for treating contrasting charge-neutralizing capabilities of counterions at the mineral/water interface," *Langmuir*, vol. 30, no. 8, pp. 2009–2018, 2014.

[144] S. Levine, "Adsorption isotherms in the electric double layer and the discreteness-of-charge effect," *J. Colloid Interface Sci.*, vol. 37, no. 3, pp. 619–634, 1971.

[145] J. H. A. Pieper and D. A. De Vooys, "Direct measurement of the double layer capacity at the silver iodide-aqueous electrolyte interface," *J. Electroanal. Chem. Interfacial Electrochem.*, vol. 53, pp. 243–252, 1974.

[146] T. Hiemstra, R. P. J. J. Rietra, and W. H. van Riemsdijk, "Surface Complexation of Selenite on Goethite: MO/DFT Geometry and Charge Distribution," *Croat. Chem. Acta*, vol. 80, no. 2007, pp. 313–324, 2007.

[147] R. Rahnemaie, T. Hiemstra, and W. H. van Riemsdijk, "Carbonate adsorption on goethite in competition with phosphate.," *J. Colloid Interface Sci.*, vol. 315, no. 2, pp. 415–25, Nov. 2007.

[148] R. Rahnemaie, T. Hiemstra, and W. H. van Riemsdijk, "Geometry, charge distribution, and surface speciation of phosphate on goethite," *Langmuir*, vol. 23, no. 7, pp. 3680–3689, 2007.

[149] T. Hiemstra, M. O. Barnett, and W. H. van Riemsdijk, “Interaction of silicic acid with goethite,” *J. Colloid Interface Sci.*, vol. 310, no. 1, pp. 8–17, 2007.

[150] R. G. Gast, “Surface and colloid chemistry,” *Miner. soil Environ.*, pp. 27–73, 1977.

[151] K. Leung and L. J. Criscenti, “Predicting the acidity constant of a goethite hydroxyl group from first principles,” *J. Phys. Condens. Matter*, vol. 24, no. 12, p. 124105, 2012.

[152] G. A. Parks and P. L. DeBruyn, “The Zero Point of Charge of Oxides1,” *J. Phys. Chem.*, vol. 66, no. 6, pp. 967–973, 1962.

[153] R. O. James and G. A. Parks, “Characterization of aqueous colloids by their electrical double-layer and intrinsic surface chemical properties,” in *Surface and colloid science*, Springer, 1982, pp. 119–216.

[154] D. Vasudevan and A. T. Stone, “Adsorption of 4-nitrocatechol, 4-nitro-2-aminophenol, and 4-nitro-1, 2-phenylenediamine at the metal (hydr) oxide/water interface: Effect of metal (hydr) oxide properties,” *J. Colloid Interface Sci.*, vol. 202, no. 1, pp. 1–19, 1998.

[155] T. Hiemstra and W. H. van Riemsdijk, “A surface structural model for ferrihydrite I: Sites related to primary charge, molar mass, and mass density,” *Geochim. Cosmochim. Acta*, vol. 73, no. 15, pp. 4423–4436, 2009.

[156] P. Venema, T. Hiemstra, and P. G. Weidler, “Intrinsic proton affinity of reactive surface groups of metal (hydr) oxides: Application to iron (hydr) oxides,” *J. Colloid Interface Sci.*, vol. 198, no. 198, pp. 282–295, 1998.

[157] J. R. Rustad, A. R. Felmy, and B. P. Hay, “Molecular statics calculations of proton binding to goethite surfaces: A new approach to estimation of stability constants for multisite surface complexation models,” *Geochim. Cosmochim. Acta*, vol. 60, no. 9, pp. 1563–1576, 1996.

[158] J. R. Rustad, A. R. Felmy, and B. P. Hay, “Molecular statics calculations for iron oxide and oxyhydroxide minerals: Toward a flexible model of the reactive mineral-water interface,” *Geochim. Cosmochim. Acta*, vol. 60, no. 9, pp. 1553–1562, 1996.

[159] E. Wasserman, J. R. Rustad, and A. R. Felmy, “Molecular modeling of the surface charging of hematite: I. The calculation of proton affinities and acidities on a surface,” *Surf. Sci.*, vol. 424, no. 1, pp. 19–27, 1999.

[160] J. A. Tossell and N. Sahai, “Calculating the acidity of silanols and related oxyacids in aqueous solution,” *Geochim. Cosmochim. Acta*, vol. 64, no. 24, pp. 4097–4113, 2000.

[161] J. R. Rustad, “Molecular models of surface relaxation, hydroxylation, and surface charging at oxide-water interfaces,” *Rev. Mineral. Geochemistry*, vol. 42, no. 1, pp. 169–198, 2001.

[162] B. R. Bickmore, K. M. Rosso, K. L. Nagy, R. T. Cygan, and C. J. Tadanier, “Ab initio determination of edge surface structures for dioctahedral 2: 1 phyllosilicates: implications for acid-base for reactivity,” *Clays Clay Miner.*, vol. 51, no. 4, pp. 359–371, 2003.

[163] B. R. Bickmore, C. J. Tadanier, K. M. Rosso, W. D. Monn, and D. L. Eggett, “Bond-valence methods for pKa prediction: Critical reanalysis and a new approach,” *Geochim. Cosmochim. Acta*, vol. 68, no. 9, pp. 2025–2042, 2004.

[164] J.-F. Boily, “Water Structure and Hydrogen Bonding at Goethite / Water Interfaces : Implications for Proton Affinities,” *J. Phys. Chem. C*, vol. 116, no. 7, pp. 4714–4724, 2012.

[165] M. Talebi Atouei, R. Rahnemaie, E. Goli Kalanpa, and M. H. Davoodi, “Competitive adsorption of magnesium and calcium with phosphate at the goethite water interface: Kinetics, equilibrium and CD-MUSIC modeling,” *Chem. Geol.*, vol. 437, pp. 19–29, 2016.

[166] D. Peak, R. Ford, and D. L. Sparks, “An in Situ ATR-FTIR Investigation of Sulfate Bonding Mechanisms on Goethite.,” *J. Colloid Interface Sci.*, vol. 218, no. 1, pp. 289–299, Oct. 1999.

[167] J. R. Rustad and J.-F. Boily, “Density functional calculation of the infrared spectrum of surface hydroxyl groups on goethite (α-FeOOH),” *Am. Mineral.*, vol. 95, no. 2–3, pp. 414–417, 2010.

[168] T. Hiemstra and W. H. van Riemsdijk, “Surface structural ion adsorption modeling of competitive binding of oxyanions by metal (hydr) oxides,” *J. Colloid Interface*

Sci., vol. 210, no. 1, pp. 182–193, 1999.

[169] T. Hiemstra and W. H. van Riemsdijk, "Fluoride Adsorption on Goethite in Relation to Different Types of Surface Sites.," *J. Colloid Interface Sci.*, vol. 225, no. 1, pp. 94–104, 2000.

[170] T. Hiemstra, W. H. van Riemsdijk, and K. U. Ulrich, "A surface structural model for ferrihydrite II: Adsorption of uranyl and carbonate," *Geochim. Cosmochim. Acta*, vol. 73, no. 15, pp. 4437–4451, 2009.

[171] D. E. Yates, "The structure of the oxide/aqueous electrolyte interface," University of Melbourne, Australia, 1975.

[172] H. Wijnja and C. P. Schulthess, "ATR–FTIR and DRIFT spectroscopy of carbonate species at the aged γ-Al 2 O 3/water interface," *Spectrochim. Acta Part A Mol. Biomol. Spectrosc.*, vol. 55, no. 4, pp. 861–872, 1999.

[173] A. E. Martell, R. M. Smith, and R. J. Motekaitis, "NIST critically selected stability constants of metal complexes," *NIST Stand. Ref. database*, vol. 46, no. 6.0, 2004.

[174] A. T. Lima, A. B. Ribeiro, J. M. Rodríguez-Maroto, E. P. Mateus, A. M. Castro, and L. M. Ottosen, "Experimental and modeling of the electrodialytic and dialytic treatment of a fly ash containing Cd, Cu and Pb," *J. Appl. Electrochem.*, vol. 40, no. 9, pp. 1689–1697, 2010.

[175] K. F. Hayes, A. L. Roe, G. E. J. Brown, and K. O. Hodgson, "In situ X-ray absorption study of surface complexes: Selenium oxyanions on α-FeOOH," *Science (80-.).*, vol. 238, no. 4828, pp. 783–786, 1987.

[176] R. H. Parkman, J. M. Charnock, N. D. Bryan, F. R. Livens, and D. J. Vaughan, "Reactions of copper and cadmium ions in aqueous solution with goethite, lepidocrocite, mackinawite, and pyrite," *Am. Mineral.*, vol. 84, no. 3, pp. 407–419, 1999.

[177] P. Zhang and D. L. Sparks, "Kinetics of Selenate and Selenite Adsorption/Desorption at the Goethite/Water Interface," *Environ. Sci. Technol.*, vol. 24, no. 12, pp. 1848–1856, 1990.

[178] A. L. Herbelin and J. C. Westall, "FITEQL 4.0 User's Manual," *Dept Chem. Oregon State Univ.*, 1999.

[179] J. R. Rustad and A. R. Felmy, “The influence of edge sites on the development of surface charge on goethite nanoparticles: A molecular dynamics investigation,” *Geochim. Cosmochim. Acta*, vol. 69, no. 6, pp. 1405–1411, 2005.

[180] A. Rohatgi, “WebPlotDigitizer.” http://arohatgi.info/WebPlotDigitizer, Austin, Texas, USA, 2017.

[181] J. P. Gustafsson, “Visual MINTEQ version 3.0 beta. Royal Institute of technology, department of Land and Water Resources Engineering, Stockholm, Sweden.” 2010.

[182] J. N. Butler, *Ionic equilibrium: solubility and pH calculations*. John Wiley & Sons, 1998.

[183] F. J. Hingston, R. J. Atkinson, A. M. Posner, and J. P. Quirk, “Specific absorption of anions on goethite,” *Int Soc Soil Sci Trans*, 1968.

[184] L. Sigg and W. Stumm, “The interaction of anions and weak acids with the hydrous goethite (α-FeOOH) surface,” *Colloids and surfaces*, vol. 2, no. 2, pp. 101–117, 1981.

[185] T. Hiemstra and W. H. van Riemsdijk, “Adsorption and surface oxidation of Fe(II) on metal (hydr)oxides,” *Geochim. Cosmochim. Acta*, vol. 71, no. 24, pp. 5913–5933, 2007.

[186] P. Venema, T. Hiemstra, and W. H. van Riemsdijk, “Interaction of Cadmium with Phosphate on Goethite,” *J. Colloid Interface Sci.*, vol. 192, no. 1, pp. 94–103, 1997.

[187] R. P. J. J. Rietra, T. Hiemstra, and W. H. van Riemsdijk, “Sulfate Adsorption on Goethite.,” *J. Colloid Interface Sci.*, vol. 218, pp. 511–521, 1999.

[188] J. P. Gustafsson, “FITEQLC: Implementation of CD-MUSIC in FITEQL 4.0,” *Land and Water Resources Engineering. Royal Institute of Technology (KTH)*, 2003. .

[189] U. Hoins, L. Charlet, and H. Sticher, “Ligand effect on the adsorption of heavy metals : The Sulfate - Cadmium - Goethite Case,” *Water. Air. Soil Pollut.*, vol. 68, pp. 241–255, 1993.

[190] M. J. Angove, J. D. Wells, and B. B. Johnson, “The influence of temperature on the adsorption of cadmium (II) and cobalt (II) on goethite,” *J. Colloid Interface Sci.*, vol. 211, no. 2, pp. 281–290, 1999.

[191] M. Villalobos and J. O. Leckie, “Surface Complexation Modeling and FTIR Study of Carbonate Adsorption to Goethite.,” *J. Colloid Interface Sci.*, vol. 235, no. 1, pp. 15–32, Mar. 2001.

[192] T. L. Theis, R. Iyer, and L. W. Kaul, “Kinetic Studies of Cadmium and Ferricyanide Adsorption on Goethite,” *Environ. Sci. Technol.*, vol. 22, no. 9, pp. 1013–1017, 1988.

[193] D. A. Dzombak and F. M. M. Morel, “Sorption of cadmium on hydrous ferric oxide at high sorbate/sorbent ratios: Equilibrium, kinetics, and modeling,” *J. Colloid Interface Sci.*, vol. 112, no. 2, pp. 588–598, 1986.

[194] M. M. Benjamin, “Effects of competing metals and complexing ligands on trace metal adsorption at the oxide/solution interface,” Stanford University, 1978.

[195] D. G. Lumsdon and L. J. Evans, “Surface complexation model parameters for goethite (α-FeOOH),” *J. Colloid Interface Sci.*, vol. 164, pp. 119–125, 1994.

[196] M. Villalobos and J. O. Leckie, “Carbonate adsorption on goethite under closed and open CO 2 conditions,” *Geochim. Cosmochim. Acta*, vol. 64, no. 22, pp. 3787–3802, 2000.

[197] P. Persson and L. Lövgren, “Potentiometric and spectroscopic studies of sulfate complexation at the goethite-water interface,” *Geochim. Cosmochim. Acta*, vol. 60, no. 15, pp. 2789–2799, 1996.

[198] A. J. Fuller, S. Shaw, C. L. Peacock, D. Trivedi, and I. T. Burke, “EXAFS Study of Sr sorption to Illite, Goethite, Chlorite, and Mixed Sediment under Hyperalkaline Conditions,” *Langmuir*, vol. 32, no. 12, pp. 2937–2946, 2016.

[199] S. A. Khan and M. A. Khan, “Sorption of strontium on bentonite,” *Waste Manag.*, vol. 15, no. 8, pp. 641–650, 1995.

[200] B. Hu, W. Cheng, H. Zhang, and G. Sheng, “Sorption of radionickel to goethite: effect of water quality parameters and temperature,” *J. Radioanal. Nucl. Chem.*, vol. 285, no. 2, pp. 389–398, 2010.

[201] L. Clausen and I. Fabricius, “BET Measurements: Outgassing of Minerals.,” *J. Colloid Interface Sci.*, vol. 227, no. 1, pp. 7–15, Jul. 2000.

[202] J. W. Bowden, S. Nagarajah, N. J. Barrow, A. M. Posner, and J. P. Quirk, “Describing the adsorption of phosphate, citrate and selenite on a variable-charge mineral surface,” *Soil Res.*, vol. 18, no. 1, pp. 49–60, 1980.

[203] W. Zeltner and M. A. Anderson, “Surface charge development at the goethite/aqueous solution interface: effects of CO2 adsorption,” *Langmuir*, no. 14, pp. 469–474, 1988.

[204] J. W. Tonkin, L. S. Balistrieri, and J. W. Murray, “Modeling sorption of divalent metal cations on hydrous manganese oxide using the diffuse double layer model,” *Appl. Geochemistry*, vol. 19, no. 1, pp. 29–53, Jan. 2004.

[205] A. Breeuwsma and J. Lyklema, “Physical and chemical adsorption of ions in the electrical double layer on hematite (α-Fe 2 O 3),” *J. Colloid Interface Sci.*, vol. 43, no. 2, pp. 437–448, 1973.

[206] M. K. Ridley, M. L. Machesky, D. J. Wesolowski, and D. A. Palmer, “Calcium adsorption at the rutile-water interface: A potentiometric study in NaCl media to 250 C,” *Geochim. Cosmochim. Acta*, vol. 63, no. 19, pp. 3087–3096, 1999.

[207] L. J. Criscenti and D. A. Sverjensky, “The role of electrolyte anions (ClO 4-, NO 3-, and Cl-) in divalent metal (M 2+) adsorption on oxide and hydroxide surfaces in salt solutions,” *Am. J. Sci.*, vol. 299, no. 10, pp. 828–899, 1999.

[208] I. Pochard, R. Denoyel, P. Couchot, and A. Foissy, “Adsorption of Barium and Calcium Chloride onto Negatively Charged α-Fe2O3 Particles,” *J. Colloid Interface Sci.*, vol. 255, no. 1, pp. 27–35, 2002.

[209] M. K. Ridley, M. L. Machesky, D. J. Wesolowski, and D. A. Palmer, “Modeling the surface complexation of calcium at the rutile-water interface to 250°C,” *Geochim. Cosmochim. Acta*, vol. 68, no. 2, pp. 239–251, 2004.

[210] M. Předota and L. Vlček, “Comment on parts 1 and 2 of the series ‘electric double layer at the rutile (110) surface,’” *J. Phys. Chem. B*, vol. 111, no. 5, pp. 1245–1247, 2007.

[211] L. Pauling, “The principles determining the structure of complex ionic crystals,” *J.*

Am. Chem. Soc., vol. 51, no. 4, pp. 1010–1026, 1929.

[212] J. C. Westall and F. M. M. Morel, "FITEQL: A general algorithm for the determination of metal-ligand complex stability constants from experimental data," *Tech. Note*, vol. 19, 1977.

[213] C. Mallett and S. Gray, "AutoHotkey," 2003. [Online]. Available: https://autohotkey.com/.

[214] L. S. Balistrieri and J. W. Murray, "The surface chemistry of goethite (alpha FeOOH) in major ion seawater," *Am. J. Sci.*, 1981.

[215] S. Kerisit, E. S. Ilton, and S. C. Parker, "Molecular dynamics simulations of electrolyte solutions at the (100) goethite surface," *J. Phys. Chem. B*, vol. 110, no. 41, pp. 20491–20501, 2006.

[216] L. P. Weng, W. H. van Riemsdijk, and T. Hiemstra, "Factors Controlling Phosphate Interaction with Iron Oxides," *J. Environ. Qual.*, vol. 41, no. 3, p. 628, 2012.